UNIVERSITÀ DEGLI STUDI DELL'INSUBRIA

PhD Program in Chemical and Environmental Sciences (XXXVIII Cycle)

STUDY OF THE IMPACT OF CLIMATE CHANGE ON VEGETATION IN TEMPERATE FORESTS AND TUNDRA

PhD Thesis

Supervisor: **Prof. Cannone Nicoletta**

Candidate: **Ilaria Bonfanti**

Index

INTRODUCTION

Introduction

Warming of the climate system has been defined, by the IPCC 2021, as unequivocal and that many of the changes observed, since the 1950s, are unprecedented over decades to millennia. Each of the last four decades has been successively warmer than any preceding decade since 1850. It has been observed that the temperature increase is not uniform across the planet, in fact the most sensitive and vulnerable environments to climatic warming are the boreal regimes, arctic regions, and high mountains (Walther et al., 2002; Cannone et al., 2007; IPCC, 2014; IPCC, 2021).

Climate change is increasing the frequency and magnitude of extreme weather events, accompanied by anomalies of temperature and precipitation, for example heat waves and summer droughts, which, could exert relevant impacts on ecosystems, especially on vegetation (Min et al., 2011; Coumou and Rahmstorf, 2012; Russo et al., 2014; IPCC 2021).

Increasing drought stress could alter the composition, structure, and function of terrestrial ecosystems (Huang et al., 2018) and affect his sequestration capacity of carbon from the atmosphere (Anderegg et al., 2015; Schwalm et al. 2017) and could intensify positive climate feedback, leading to even greater warming (Stark et al., 2016; Szejner et al., 2020).

Heat waves and prolonged drought events are typically associated with declines in vegetation productivity due to water stress on ecosystem metabolism (Leuzingeretal.,2005; Schwalm et al.,2012; Eamus et al., 2013; Ivits et al., 2014; Huang et al., 2017; Huang et al., 2018), making it more susceptible to other biotic and abiotic stress factors. This increased vulnerability leads to higher tree mortality, wildfire risks, and loss of biodiversity (Seidl et al., 2017; Gharun et al., 2024).

Particularly, drought can have a ‘legacy effect’ on ecosystems (Gutschick and Bassirirad, 2003; Walter et al., 2013; Anderegg et al., 2015; Camarero et al., 2015; Frank et al.,2015; Huang et al., 2018) and reduce their capacity on carbon sequestration in the following years (Ciais et al., 2005; Descals et al., 2023). Legacy effect is defined as the lag in recovery that has effects on vegetation performance (Gutschick and Bassirirad, 2003; Huang et al., 2018). Their recovery capacity depends on multiple factors including: the severity and frequency of climate extremes (e.g., maximum temperatures reached during a heat wave), post-event weather conditions, site variables (topography, soil depth and texture), stand structure and composition or functional traits enhancing resilience (Anderegg et al., 2015; Rita et al., 2020). For example, frequent heat

waves or droughts, associated with their legacy effects, limit recovery capacity and affect growth resilience (Ingrisch and Bahn, 2018; Kannenberg et al., 2020; Schwarz et al., 2020; Serra-Maluquer et al., 2021). The timing of the extreme climate event with respect to principal tree phenological phases (bud burst, leaf flushing, tree-ring formation) is a critical factor determining damage.

Lower drought resilience tends to result in a higher risk of mortality in the event of future droughts (Klein et al., 2018; Trugman et al., 2018; DeSoto et al., 2020), in fact over the past 30 years, drought and heat-related mortality have been reported on every wooded continent (Allen et al. 2010; Eamus et al., 2013). Tree death can be related with different biotic (stem size, stand conditions, tree species and pathogens) and abiotic factors (storms, precipitation, topographic features, edaphic conditions and disturbance history) and is usually due to stem breakage or uprooting caused by wind-throw or standing death caused by root and butt diseases (McCarthy, 2001; Rubio-Cuadrado et al., 2018).

Also, the shift in timing of vegetation phenology is a bio-indicator of climate change (Peñuelas et al., 2001; Ibáñez et al., 2010; Xie et al., 2015). While numerous research has concentrated on the spring season, typically driven by temperature (Zhang et al., 2024), influences of climate change on autumn leaf senescence received less attention and it's more complex due to the multitude of influencing factors (Gallinat et al., 2015; Liu et al., 2016; Zhang et al., 2024). Previous studies observed that environmental variables like temperature, precipitation, and solar radiation could be responsible for variations in fall phenology (Keskitalo et al., 2005; Piao et al., 2006; Kong et al., 2016; Liu et al., 2016a; Liu et al., 2016b; Zu et al., 2018), but the correlations are still not clear (Garcı´a-Plazaola et al., 2003; Richardson et al., 2013; Zohner et al., 2023).

Plant responses to drought could be studied by several approaches. One strategy could be to examine water and carbon processes, such as tree ring width, wood anatomical traits and intrinsic water use efficiency (iWUE**)** assessed by carbon isotope discrimination (Ponton et al., 2001; Olano et al., 2014; Pellizzari et al., 2016; Cailleret et al., 2017; Puchi et al., 2021; Camarero et al., 2023; Zhang et al., 2025). The traits of the vessels affect plant hydraulic performance (Wheeler et al., 2005; Zhang et al., 2025), and they could be used as a proxy of theoretical specific hydraulic conductivity (Tyree & Ewers, 1991; Poorter et al., 2010; Schuldt et al., 2016; Zhang et al.,2025). The iWUE is an indicator of leaf water loss in plants due to transpiration and it's important for determining water exchange between terrestrial ecosystems and the atmosphere. (Seibt et al., 2008). The isotopic composition of carbon in tree rings ($\delta^{13}C$) is widely used to derive iWUE, because it provides information on the ratio between the

photosynthesis rate and the stomatal conductance rate, which is linked to the intercellular (Ci) and atmospheric (Ca) concentrations of CO_2 (Saurer et al., 2004; Battipaglia et al., 2010; Pellizzari et al., 2016; Diao et al., 2023; Zhang et al., 2025). For example, lower stomatal conductance leads to a decrease in Ci/Ca ratios and consequently to an increase in iWUE and $\delta^{13}C$ in tree rings.

Another method is the study of the land surface phenology from remote sensing observations at high resolution. The seasonality of vegetation is often studied using time series of vegetation indices such as the normalized difference vegetation index (NDVI) (Yang et al., 2022; Descals et al., 2023). Structural indices such as NDVI are highly dependent on changes in the near-infrared spectrum and therefore reflect seasonal changes in leaf biomass.

The first part of this thesis is focused on the impacts of extreme drought combined with long-lasting heat waves of 2022 in three areas located in Northern of Italy across an elevation gradient, from the Po plain to the Alps.

The year 2022 in Europe was characterized by hottest and driest year on record, with the summer of that year being the warmest summer ever recorded, with nine consecutive months with almost no precipitation, and winter 2022-2023 remained relatively dry (Toreti et al., 2023; Knutzen et al., 2025). Compound drought and heat-wave conditions in 2022 caused widespread crop damage, water shortages, and wildfires across Europe (Gharun et al., 2024).

The most affected regions were France, Italy, and the Iberian Peninsula, where extreme droughts lasted from May to August and temperatures rose by more than 2.5°C above the seasonal means (Tripathy and Mishra, 2023; Gharun et al., 2024).

However, the impact of the extreme year 2022 was not uniform across Europe, with the highest impacts detected in central Europe and the lowest in the alpine regions, suggesting different sensitivity due to the effect of elevation or the adaptation to historical drought exposure (e.g., Knutzen et al., 2025). In the southern region, the thinning of deciduous tree canopy cover was particularly pronounced in Italy and Spain. This indicates that even regions well adapted to drought conditions have experienced unprecedented stress during these years (Knutzen et al., 2025). While the Alpine zone exhibited minimal impact. This limited impact can be attributed to the higher altitudes, which may provide mitigating effects such as cooler temperatures or reduced evapotranspiration, potentially protecting the area from extreme drought conditions. However, it should be noted that mountain forests are under pressure from the effects of climate change, due to their temperature limitations and high exposure to warming (Albrich et al., 2020; Knutzen et al., 2025).

European forests are extremely vulnerable to the combined effects of increased heat and drought, which threaten even ecosystems currently considered resilient. This vulnerability is likely to increase, with serious consequences such as increased tree mortality, changes in species composition, increased risk of insect infestations and wildfires, and decreased forest productivity and carbon sequestration.

A comprehensive and collaborative approach is essential to effectively address the complex challenges posed by recurring heat waves and droughts. The development of adaptive management techniques and climate-resilient forestry strategies requires the combined efforts of researchers, policymakers and forest managers. The integration of forest management, climate change adaptation and global greenhouse gas reduction strategies is critical to mitigating future environmental impacts and providing greater ecological and social stability (Knutzen et al., 2025).

The second part of the thesis has been realized in the Alaskan Arctic tundra, at the Toolik Lake Field Station, in the upper Kuparuk River region, as part of the InsubrePolar project, funded by the University of Insubria and carried out in collaboration with the University of Alaska Fairbanks (UAF).

The Arctic is one of the areas extremely sensitive and vulnerable to the recent climate change, where impacts on both abiotic (e.g., permafrost degradation, ground temperature increase, loss of seasonal snow cover, and change in soil Carbon stocks, biogeochemical cycles, and ground hydrology) and biotic components of the ecosystems, such as the phenology of organisms, the range and distribution of species, the composition, and dynamics of communities, are significant and extensive (Walther et al., 2002; Cannone et al., 2007; Oberbauer et al., 2013; Overland and Wang, 2013; Christensen 2014; Lund et al., 2014; IPCC, 2014; Kwok and Cunningham 2015; Bhatt et al., 2017; Comiso et al., 2017; Brown et al 2018; Zhang et al., 2018; Box et al., 2019; IPCC, 2021).

Arctic regions are estimated to store 1,100-1,500 Pg of Carbon within permafrost (Hugelius et al., 2014), and its thawing could release in atmosphere significant amounts of carbon (CO_2 and CH_4) that could have positive feedback on climate change (Schaefer et al., 2014). In particular, each molecule of CH_4 has 28-34 times potential of global warming compared to a molecule of CO_2 (Myhre et al., 2013).

The production of CH_4 (methanogenesis), takes place in soils because of the decomposition of organic matter. This process is carried out by specialized anaerobic microorganisms, known as methanogens, which are typically found in wetlands and other inland water environments

(Christensen et al., 2015; Nzotungicimpaye and Zickfeld, 2017). Vegetation type plays a key role in CH_4 dynamics (production, consumption and transport) (Joabsson et al., 1999; Ström et al., 2003). Methanogenesis can be inhibited and the oxidation of CH_4 to CO_2 can be promoted when roots release oxygen into the rhizosphere (Chanton and Dacey, 1991; Watson et al., 1997; Frenzel, 2000; Ström et al., 2003). At the same time, CH_4 transported through the aerenchyma bypasses oxidation, as it conducted directly from the anoxic zone to the atmosphere without passing through the oxic layer of the peat (Frenzel and Rudolph, 1998; Bellisario et al., 1999; Ström et al., 2003). According to Ström et al. (2003), the amount of labile carbon depends on plant species and photosynthetic rates, and the production of CH_4 is linked to the quality of substrate and the root exudation of labile carbon. Changes in vascular plant composition, induced by climate change, may have consequences for substrate quality, carbon cycling and CH_4 emissions in Arctic ecosystems.

The aim of the InsubrePolar project is the assessment of CH_4 emissions in relation to climatic and environmental conditions, in three different vegetation communities: dry heath tundra, moist acidic tussock-tundra and wet meadow tundra (Euskirchen et al., 2012; Kade et al., 2012), with a particular focus on the end of vegetation period (fall to winter), characterized by high methane emissions, but few information are available in literature (e.g. Howard et al., 2020; Kim et al., 2007). To better understand the vegetation dynamics and the relation with fluxes, a phytosociological map of the area was made merging field surveys with UAS imagery.

Climate change is severely impacting terrestrial ecosystems, from European forests subjected to unprecedented drought and heat events to Arctic tundra ecosystems experiencing rapid transformations. Both regions, although ecologically distinct, illustrate the vulnerability of vegetation to extreme climatic conditions and the domino effect on the structure, function and biogeochemical cycles of ecosystems. The increasing frequency and intensity of droughts represent a serious risk to forest resilience, carbon sequestration and biodiversity in Europe. Similarly, the Arctic is a critical area in the global climate system, where permafrost degradation and changes in vegetation can increase greenhouse gas emissions, amplifying climate feedback. It is therefore important and urgent to integrate long-term monitoring, interdisciplinary research and mitigation strategies to ensure the survival and preservation of ecosystems, which are extremely susceptible to climate change.

This thesis aims to assess how climate warming and extreme climatic events influence the structure, functioning and carbon-related processes of terrestrial ecosystems across contrasting biomes (temperate deciduous forests and Arctic tundra):

1. Quantify the effects of the 2022 compound drought–heatwave event on vegetation phenology, productivity and canopy dynamics along a lowland–alpine gradient in northern Italy through high-resolution remote sensing.

2. Evaluate species-specific growth responses and wood-anatomical adjustments to extreme heat stress, integrating dendrochronology, carbon isotope discrimination ($\delta^{13}C$) and functional xylem traits.

3. Investigate spatial and seasonal variability of CH_4 fluxes in Arctic tundra, identifying the biotic and abiotic drivers regulating CH_4 production, oxidation and plant-mediated transport across vegetation types.

4. Provide a high-resolution phytosociological and physiognomic vegetation map of the Toolik Lake region to establish a baseline for detecting ongoing and future Arctic vegetation shifts.

References

Albrich, K., Rammer, W., and Seidl, R.: Climate change causes critical transitions and irreversible alterations of mountain forests, Glob. Change Biol., 26, 4013–4027, https://doi.org/10.1111/gcb.15118, 2020.

Allen, C.D., Breshears, D.D., McDowell, N.G., 2015. On underestimation of global vulnerability to tree mortality and forest die-off from hotter drought in the Anthropocene. Ecosphere 6, 1–55. 9.1 (2023): 76-89.

Anderegg, W.R.L., Schwalm, C., Biondi, F., et al., 2015. Pervasive drought legacies in forest ecosystems and their implications for carbon cycle models. Science 349, 528–532

Battipaglia, G., De Micco, V., Brand, W. A., Linke, P., Aronne, G., Saurer, M., & Cherubini, P. (2010). Variations of vessel diameter and δ13C in false rings of Arbutus unedo L. reflect different environmental conditions. New Phytologist, 188, 1099–1112.

Bhatt, U. S., Walker, D. A., Raynolds, M. K., Bieniek, P. A., Epstein, H. E., Comiso, J. C., ... & Zhang, J. (2017). Changing seasonality of panarctic tundra vegetation in relationship to climatic variables. Environmental Research Letters, 12(5), 055003

Box, J. E., Colgan, W. T., Christensen, T. R., Schmidt, N. M., Lund, M., Parmentier, F.-J. W., Brown, R., Bhatt, U. S., Euskirchen, E. S., Romanovsky, V. E., Walsh, J. E., Overland, J. E., Wang, M., Corell, R. W., Meier, W. N., Wouters, B., Mernild, S., Mård, J., Pawlak, J., & Olsen, M. S. (2019). Key indicators of Arctic climate change: 1971–2017. Environmental Research Letters, 14(4), 045010. https://doi.org/10.1088/1748-9326/aafc1b

Brown, R., Barrette, C., Brown, L., Chaumont, D., Grenier, P., Howell, S., & Sharp, M. (2018). Climate variability, trends and projected change. From Science to Policy in the Eastern Canadian Arctic: An Integrated Regional Impact Study (IRIS) of Climate Change and Moderization. ArcticNet, Quebec City, 560 pp, 55.

Cailleret, M., Jansen, S., Robert, E. M. R., Desoto, L., Aakala, T., Antos, J. A., Beikircher, B., Bigler, C., Bugmann, H., Caccianiga, M., Čada, V., Camarero, J. J., Cherubini, P., Cochard, H., Coyea, M. R., Čufar, K., Das, A. J., Davi, H., Delzon, S., & Martínez-Vilalta, J. (2017). A synthesis of radial growth patterns preceding tree mortality. Global Change Biology, 23, 1675–1690. Puchi, P. F., Camarero, J. J., Battipaglia, G., & Carrer, M. (2021). Retrospective analysis of wood anatomical traits and tree- ring isotopes suggests site- specific mechanisms triggering Araucaria araucana drought- induced dieback. Global Change Biology, 27, 6394–6408.

Camarero, J., Franquesa, M., Sangüesa-Barreda, G., 2015. Timing of Drought Triggers Distinct Growth Responses in Holm Oak: Implications to Predict Warming-Induced Forest Defoliation and Growth Decline. Forests 6, 1576–1597. https://doi.org/10.3390/f6051576

Camarero, J.J., Colangelo, M., Rodríguez-González, P.M., 2023. Tree growth, wood anatomy and carbon and oxygen isotopes responses to drought in Mediterranean riparian forests. Forest Ecology and Management 529, 120710. https://doi.org/10.1016/j.foreco.2022.120710

Cannone, N., Sgorbati, S., Guglielmin, M., 2007. Unexpected impacts of climate change on alpine vegetation. Frontiers in Ecology and the Environment 5, 360–364. https://doi.org/10.1890/1540-9295(2007)5[360:UIOCCO]2.0.CO;2

Chanton JP, Dacey JWH (1991) Effects of vegetation on methane flux, reservoirs, and carbon isotopic composition. In: Trace Gas Emissions by Plants (eds Sharkey TD, Holland EA, Mooney HA), pp. 65–92. Academic Press, San Diego.

Christensen TR, van Huissteden K, Sachs T. Natural terrestrial methane sources in the Arctic. AMAPAssessment 2015: Methane as an Arctic climate forcer. Oslo, Norway: Arctic Monitoring and Assessment Programme (AMAP); 2015. p. 15–26.

Christensen, T. R., Arora, V. K., Gauss, M., Höglund-Isaksson, L., & Parmentier, F. J. W. (2019). Tracing the climate signal: mitigation of anthropogenic methane emissions can outweigh a large Arctic natural emission increase. Scientific reports, 9(1), 1146.

Ciais, P., Reichstein, M., Viovy, N., Granier, A., Ogee, J., Allard, V. et al. (2005) Europe-wide reduction in primary productivity caused by the heat and drought in 2003. Nature, 437(7058), 529–533.

Comiso, J. C., Meier, W. N., & Gersten, R. (2017). Variability and trends in the Arctic Sea ice cover: Results from different techniques. Journal of Geophysical Research: Oceans, 122(8), 6883-6900.

Coumou, D, and Rahmstorf, S. 2012. A decade of weather extremes. Nature Climate Change 2.7: 491-496.

Descals, A., et al. 2023. Widespread drought-induced leaf shedding and legacy effects on productivity in European deciduous forests. Remote Sensing in Ecology and Conservation 9.1 (2023): 76-89.

DeSoto, L., Cailleret, M., Sterck, F., Jansen, S., Kramer, K., Robert, E. M. R., Aakala, T., Amoroso, M. M., Bigler, C., Camarero, J. J., Čufar, K., Gea- Izquierdo, G., Gillner, S., Haavik, L. J., Hereş, A.- M., Kane, J. M., Kharuk, V. I., Kitzberger, T., Klein, T., & Martínez- Vilalta, J. (2020). Low growth resilience to drought is related to future mortality risk in trees. Nature Communications, 11, 545.

Eamus, D., Boulain, N., Cleverly, J., & Breshears, D. D. (2013). Global change-type drought-induced tree mortality: vapor pressure deficit is more important than temperature per se in causing decline in tree health. Ecology and Evolution, 3, 2711–2729.

Euskirchen, E. S., Bret-Harte, M. S., Scott, G. J., Edgar, C., Shaver, G. R., (2012). Seasonal patterns of carbon dioxide and water fluxes in three representative tundra ecosystems in northern Alaska. Ecosphere, 3(1), 1–19. https://doi.org/10.1890/ES11-00202.1

Frank, D., Reichstein, M., Bahn, M., Thonicke, K., Frank, D., Mahecha, M. D., ...Zscheischler, J. (2015). Effects of climate extremes on the terres trial carbon cycle: Concepts, processes and potential future impacts. Global Change Biology, 21, 2861. https://doi.org/10.1111/gcb.12916

Frenzel P (2000) Plant-associated methane oxidation in rice fields and wetlands. In: Vol. 16 (ed. Schink B), pp. 85–114. Kluwer, New York.

Gallinat, A.S., Primack, R.B., Wagner, D.L., 2015. Autumn, the neglected season in climate change research. Trends Ecol. Evol. 30, 169–176. https://doi.org/10.1016/j.tree.2015.01.004

García-Plazaola, J. I., A. Hernández, and J. M. Becerril. "Antioxidant and pigment composition during autumnal leaf senescence in woody deciduous species differing in their ecological traits." Plant Biology 5.05 (2003): 557-566.

Gharun, M., Shekhar, A., Xiao, J., Li, X., Buchmann, N., 2024. Effect of the 2022 summer drought across forest types in Europe. Biogeosciences 21, 5481–5494. https://doi.org/10.5194/bg-21-5481-2024

Gutschick, V. P., & Bassirirad, H. (2003). Extreme events as shaping phys iology, ecology, and evolution of plants: Toward a unified definition and evaluation of their consequences. New Phytologist, 160, 21–42. https://doi.org/10.1046/j.1469-8137.2003.00866.x

Howard, D., Agnan, Y., Helmig, D., Yang, Y., & Obrist, D. (2020). Environmental controls on ecosystem-scale cold-season methane and carbon dioxide fluxes in an Arctic tundra ecosystem. Biogeosciences, 17(15), 4025–4042. https://doi.org/10.5194/bg-17-4025-2020

Huang, M., Piao, S., Janssens, I. A., Zhu, Z., Wang, T., Wu, D., ... Pe~ nue las, J. (2017). Velocity of change in vegetation productivity over northern high latitudes. Nature Ecology & Evolution, 1, 1649–1654. https://doi.org/10.1038/s41559-017-0328-y

Huang, M., Wang, X., Keenan, T.F., Piao, S., 2018. Drought timing influences the legacy of tree growth recovery. Global Change Biology 24, 3546–3559. https://doi.org/10.1111/gcb.14294

Hugelius, G., Strauss, J., Zubrzycki, S., Harden, J. W., Schuur, E. A. G., Ping, C.-L., Schirrmeister, L., Grosse, G., Michaelson, G. J., Koven, C. D., O'Donnell, J. A., Elberling, B., Mishra, U., Camill, P., Yu, Z., Palmtag, J., and Kuhry, P., 2014: Estimated stocks of circumpolar permafrost carbon with quantified uncertainty ranges and identified data gaps. Biogeosciences, 11, 6573–6593, https://doi.org/10.5194/bg-11-6573-2014

Ibáñez, I., Primack, R. B., Miller-Rushing, A. J., Ellwood, E., Higuchi, H., Lee, S. D., ... & Silander, J. A. (2010). Forecasting phenology under global warming. Philosophical Transactions of the Royal Society B: Biological Sciences, 365(1555), 3247-3260.

Ingrisch, J., Bahn, M., 2018. Towards a comparable quantification of resilience. Trends Ecol Evol 33, 251–259.

IPCC 2014 Working Group II. 2014. Climate change 2014: Impacts, adaptation, and vulnerability. Geneva, Switzerland: IPCC

IPCC. (2021). Climate change 2021: The physical science basis. In V. Masson- Delmotte, P. Zhai, A. Pirani, S. L. Connors, C. Pean, S. Berger, N. Caud, Y. Chen, L. Goldfarb, M. I. Gomis, M. Huang, K. Leitzell, E. Lonnoy, J. B. R. Matthews, T. K. Maycock, T. Waterfield, O. Yelekci, R. Yu, & B. Zhou (Eds.), Contribution of Working Group I to the Sixth Assessment Report of the Intergovernmental Panel on Climate Change. Cambridge University Press.

Ivits, E., Horion, S., Fensholt, R., & Cherlet, M. (2014). Drought footprint on European ecosystems between 1999 and 2010 assessed by remo tely sensed vegetation phenology and productivity. Global Change Biology, 20, 581–593. https://doi.org/10.1111/gcb.12393

Joabsson A, Christensen TR, Walle´n B (1999) Vascular plant controls on methane emissions from northern peatforming wetlands. Trends in Ecology and Evolution, 14, 385–388.

Kade, A., Syndonia Bret-Harte, M., Euskirchen, E. S., Edgar, C., Fulweber, R. A., (2012). Upscaling of CO2 fluxes from heterogeneous tundra plant communities in Arctic Alaska. Journal of Geophysical Research: Biogeosciences, 117(G4), 4007. https://doi.org/10.1029/2012JG002065

Kannenberg, S.A., Schwalm, C.R., Anderegg, W.R., 2020. Ghosts of the past: how drought legacy effects shape forest functioning and carbon cycling. Ecol Lett 23, 891–901. https://doi.org/10.1111/ele.13485.

Kim, Y., Ueyama, M., Nakagawa, F., Tsunogai, U., Harazono, Y., & Tanaka, N. (2007). Assessment of winter fluxes of CO2 and CH4 in boreal forest soils of central Alaska estimated by the profile method and the chamber method: A diagnosis of methane emission and implications for the regional carbon budget. Tellus B: Chemical and Physical Meteorology, 59(2), 223. https://doi.org/10.1111/j.1600-0889.2006.00233.x

Klein, T., Zeppel, M. J. B., Anderegg, W. R. L., Bloemen, J., De Kauwe, M. G., Hudson, P., Ruehr, N. K., Powell, T. L., von Arx, G., & Nardini, A. (2018). Xylem embolism refilling and resilience against drought- induced mortality in woody plants: Processes and trade-offs. Ecological Research, 33, 839–855.

Knutzen, F., Averbeck, P., Barrasso, C., Bouwer, L.M., Gardiner, B., Grünzweig, J.M., Hänel, S., Haustein, K., Johannessen, M.R., Kollet, S., Müller, M.M., Pietikäinen, J.-P., Pietras-Couffignal, K., Pinto, J.G., Rechid, D., Rousi, E., Russo, A., Suarez-Gutierrez, L., Veit, S., Wendler, J., Xoplaki, E., Gliksman, D., 2025. Impacts on and damage to European forests from the 2018–2022 heat and drought events. Nat. Hazards Earth Syst. Sci. 25, 77–117. https://doi.org/10.5194/nhess-25-77-2025

Kwok, R., & Cunningham, G. F. (2015). Variability of Arctic sea ice thickness and volume from CryoSat-2. Philosophical Transactions of the Royal Society A: Mathematical, Physical and Engineering Sciences, 373(2045), 20140157.

Leuzinger, S., Zotz, G., Asshoff, R., & K€ orner, C. (2005). Responses of deciduous forest trees to severe drought in Central Europe. Tree physiology, 25, 641–650. https://doi.org/10.1093/treephys/25.6.641

Liu, Q., Fu, Y. H., Zhu, Z., Liu, Y., Liu, Z., Huang, M., ... & Piao, S. (2016). Delayed autumn phenology in the Northern Hemisphere is related to change in both climate and spring phenology. Global change biology, 22(11), 3702-3711.

Lund, M., Falk, J. M., Friborg, T., Mbufong, H. N., Sigsgaard, C., Soegaard, H., & Tamstorf, M. P. (2012). Trends in CO2 exchange in a high Arctic tundra heath, 2000–2010. Journal of Geophysical Research: Biogeosciences, 117(G2), 2011JG001901. https://doi.org/10.1029/2011JG001901

McCarthy, J., 2001. Gap dynamics of forest trees: a review with particular attention to boreal forests. Environ. Rev. 9, 1–59. http://dx.doi.org/10.1139/a00-012.

Min, S.-K., Zhang, X., Zwiers, F.W., Hegerl, G.C., 2011. Human contribution to more-intense precipitation extremes. Nature 470, 378–381. https://doi.org/10.1038/nature09763

Myhre, G., D. Shindell, F.-M. Bréon, W. Collins, J. Fuglestvedt, J. Huang, D. Koch, J.-F. Lamarque, D. Lee, B. Mendoza, T. Nakajima, A. Robock, G. Stephens, T. Takemura, and H. Zhang, 2013: Anthropogenic and natural radiative forcing. In Climate Change 2013: The Physical Science Basis. Contribution of Working Group I to the Fifth Assessment Report of the Intergovernmental Panel on Climate Change. T.F. Stocker, D. Qin, G.-K. Plattner, M. Tignor, S.K. Allen, J. Doschung, A. Nauels, Y. Xia, V. Bex, and P.M. Midgley, Eds., Cambridge University Press, pp. 659-740, doi:10.1017/CBO9781107415324.018.

Nzotungicimpaye, C.-M., Zickfeld, K., 2017. The Contribution from Methane to the Permafrost Carbon Feedback. Curr Clim Change Rep 3, 58–68. https://doi.org/10.1007/s40641-017-0054-1

Oberbauer, S. F., Elmendorf, S. C., Troxler, T. G., Hollister, R. D., Rocha, A. V., Bret-Harte, M. S., ... & Welker, J. M. (2013). Phenological response of tundra plants to background climate variation tested using the International Tundra Experiment. Philosophical Transactions of the Royal Society B: Biological Sciences, 368(1624), 20120481.

Olano, J. M., Linares, J. C., García- Cervigón, A. I., Arzac, A., Delgado, A., & Rozas, V. (2014). Drought- induced increase in water- use effi ciency reduces secondary tree growth and tracheid wall thickness in a Mediterranean conifer. Oecologia, 176, 273–283.

Overland, J., Dunlea, E., Box, J. E., Corell, R., Forsius, M., Kattsov, V., ... & Wang, M. (2019). The urgency of Arctic change. Polar Science, 21, 6-13.

Pellizzari, E., Camarero, J. J., Gazol, A., Sangüesa- Barreda, G., & Carrer, M. (2016). Wood anatomy and carbon- isotope discrimination sup port long- term hydraulic deterioration as a major cause of drought- induced dieback. Global Change Biology, 22, 2125–2137.

Penuelas, J., & Filella, I. (2001). Responses to a warming world.(Perspectives: Phenology). Science, 294(5543), 793-795.

Ponton, S., Dupouey, J.- L., Bréda, N., Feuillat, F., Bodénès, C., & Dreyer, E. (2001). Carbon isotope discrimination and wood anatomy varia tions in mixed stands of Quercus robur and Quercus petraea. Plant, Cell & Environment, 24, 861–868.

Poorter, L., McDonald, I., Alarcón, A., Fichtler, E., Licona, J.- C., Peña- Claros, M., Sterck, F., Villegas, Z., & Sass- Klaassen, U. (2010). The importance of wood traits and hydraulic conductance for the per formance and life history strategies of 42 rainforest tree species. New Phytologist, 185, 481–492.

Richardson, A.D., Keenan, T.F., Migliavacca, M., Ryu, Y., Sonnentag, O., Toomey, M., 2013. Climate change, phenology, and phenological control of vegetation feedbacks to the climate system. Agric. For. Meteorol. 169, 156–173. https://doi.org/10.1016/j.agrformet.2012.09.012

Rita, A., Camarero, J.J., Nolè, A., Borghetti, M., Brunetti, M., Pergola, N., Serio, C., Vicente-Serrano, S.M., Tramutoli, V., Ripullone, F., 2020. The impact of drought spells on forests depends on site conditions: The case of 2017 summer heat wave in southern Europe. Global Chang. Biol 26, 851–863. https://doi.org/10.1111/gcb.14825.

Rubio-Cuadrado, A., Camarero, J.J., del Río, M., Sánchez-González, M., Ruiz-Peinado, R., Bravo-Oviedo, A., Gil, L., Montes, F., 2018. Drought modifies tree competitiveness in an oak-beech temperate forest. For Ecol Manage 429, 7–17.

Russo, S., Dosio, A., Graversen, R.G., Sillmann, J., Carrao, H., Dunbar, M.B., Singleton, A., Montagna, P., Barbola, P., Vogt, J.V., 2014. Magnitude of extreme heat waves in present climate and their projection in a warming world. JGR Atmospheres 119. https://doi.org/10.1002/2014JD022098

Saurer, M., Siegwolf, R. T. W., & Schweingruber, F. H. (2004). Carbon iso tope discrimination indicates improving water- use efficiency of trees in northern Eurasia over the last 100 years. Global Change Biology, 10, 2109–2120.

Schuldt, B., Knutzen, F., Delzon, S., Jansen, S., Müller- Haubold, H., Burlett, R., Clough, Y., & Leuschner, C. (2016). How adaptable is the hydraulic system of European beech in the face of climate change- related precipitation reduction? New Phytologist, 210, 443–458.

Schwalm, C. R., Williams, C. A., Schaefer, K., Baldocchi, D., Black, T. A., Goldstein, A. H., ... Scott, R. L. (2012). Reduction in carbon uptake during turn of the century drought in western North America. Nature Geoscience, 5, 551–556. https://doi.org/10.1038/ngeo1529

Schwalm, C. R., Anderegg, W. R., Michalak, A. M., Fisher, J. B., Biondi, F., Koch, G., ... & Tian, H. (2017). Global patterns of drought recovery. Nature, 548(7666), 202-205.

Schwarz, J., Skiadaresis, G., Kohler, M., Kunz, J., Schnabel, F., Vitali, V., Bauhus, J., 2020. Quantifying growth responses of trees to drought — a critique of commonly used resilience indices and recommendations for future studies. Current Forestry Reports 6, 185–200.

Seibt, U., Rajabi, A., Griffiths, H., & Berry, J. A. (2008). Carbon isotopes and water use efficiency: Sense and sensitivity. Oecologia, 155, 441–454.

Seidl, R., Thom, D., Kautz, M., Martin-Benito, D., Peltoniemi, M., Vacchiano, G., Wild, J., Ascoli, D., Petr, M., Honkaniemi, J., Lexer, M. J., Trotsiuk, V., Mairota, P., Svoboda, M., Fab rika, M., Nagel, T. A., and Reyer, C. P. O.: Forest distur bances under climate change, Nat. Clim. Change, 7, 395–402, https://doi.org/10.1038/nclimate3303, 2017.

Serra-Maluquer, X., Granda, E., Camarero, J.J., Vilà-Cabrera, A., Jump, A., Sánchez-Salguero, R., Sangüesa-Barreda, G., Imbert, B., Gazol, A., 2021. Impacts of recurrent dry and wet years alter long-term tree growth trajectories. J Ecol 109, 1561–1574. https://doi.org/10.1111/1365-2745.13579

Stark, S. C., Breshears, D. D., Garcia, E. S., Law, D. J., Minor, D. M., Saleska, S. R., ... & Redmond, M. D. (2016). Toward accounting for ecoclimate teleconnections: intra-and inter-continental consequences of altered energy balance after vegetation change. Landscape Ecology, 31(1), 181-194.

Ström, L., Ekberg, A., Mastepanov, M., Røjle Christensen, T., 2003. The effect of vascular plants on carbon turnover and methane emissions from a tundra wetland. Global Change Biology 9, 1185–1192. https://doi.org/10.1046/j.1365-2486.2003.00655.x

Szejner, P., Belmecheri, S., Ehleringer, J. R., & Monson, R. K. (2020). Recent increases in drought frequency cause observed multi-year drought legacies in the tree rings of semi-arid forests. Oecologia, 192(1), 241-259.

Toreti, A., Bavera, D., Acosta Navarro, J., Arias-Muñoz, C., Avanzi, F., Marinho Ferreira Barbosa, P., De Jager, A., Di Ciollo, C., Ferraris, L., Fioravanti, G., Gabellani, S., Grimaldi, S., Hrast Essenfelder, A., Isabellon, M., Jonas, T., Maetens, W., Magni, D., Masante, D., Mazzeschi, M., McCormick, N., Meroni, M., Rossi, L., Salamon, P., and

Spinoni, J.: Drought in Europe March 2023, EUR 31448 EN, Publications Office of the European Union, Luxembourg, JRC133025, https://doi.org/10.2760/998985, 2023.

Tripathy, K. P. and Mishra, A. K.: How unusual is the 2022 European compound drought and heatwave event?, Geophys. Res. Lett., 50, e2023GL105453, https://doi.org/10.1029/2023GL105453, 2023.

Trugman, A. T., Detto, M., Bartlett, M. K., Medvigy, D., Anderegg, W. R. L., Schwalm, C., Schaffer, B., & Pacala, S. W. (2018). Tree carbon al location explains forest drought- kill and recovery patterns. Ecology Letters, 21, 1552–1560.

Tyree, M.T., Ewers, F.W., 1991. The hydraulic architecture of trees and other woody plants. New Phytologist 119, 345–360. https://doi.org/10.1111/j.1469-8137.1991.tb00035.x

Walter, J., Jentsch, A., Beierkuhnlein, C., & Kreyling, J. (2013). Ecological stress memory and cross stress tolerance in plants in the face of cli mate extremes. Environmental & Experimental Botany, 94, 3–8. https://doi.org/10.1016/j.envexpbot.2012.02.009

Walther, G.-R., Post, E., Convey, P., Menzel, A., Parmesan, C., Beebee, T.J.C., Fromentin, J.-M., Hoegh-Guldberg, O., Bairlein, F., 2002. Ecological responses to recent climate change. Nature 416, 389–395. https://doi.org/10.1038/416389a

Watson A, Stephen KD, NedwellDB, ArahJRM (1997) Oxidation of methane in peat: kinetics of CH4 and O2 removal and the role of plant roots. Soil Biology and Biochemistry, 29, 1257–1267.

Wheeler, J. K., Sperry, J. S., Hacke, U. G., & Hoang, N. (2005). Inter- vessel pitting and cavitation in woody Rosaceae and other vesselled plants: A basis for a safety versus efficiency trade- off in xylem transport. Plant, Cell & Environment, 28, 800–812.

Xie, B., Qin, Z., Wang, Y., & Chang, Q. (2015). Monitoring vegetation phenology and their response to climate change on Chinese Loess Plateau based on remote sensing. Transactions of the Chinese Society of Agricultural Engineering, 31(15), 153-160.

Yang, Y., Chen, R., Yin, G., Wang, C., Liu, G., Verger, A. et al. (2022) Divergent performances of vegetation indices in extracting photosynthetic phenology for northern deciduous broadleaf forests. IEEE Geoscience and Remote Sensing Letters [Preprint], 19,1–5.

Zhang, Y., Xiao, X., Zhang, Y., Wolf, S., Zhou, S., Joiner, J., ... & De Grandcourt, A. (2018). On the relationship between sub-daily instantaneous and daily total gross primary production: Implications for interpreting satellite-based SIF retrievals. Remote Sensing of Environment, 205, 276-289.

Zhang, X., Li, Q., Yang, Y., Fukuda, K., Morris, H., Jansen, S., Da, L., Song, K., 2024. A higher tissue fraction of parenchyma in secondary xylem supports growth recovery of

angiosperm trees after drought. Functional Ecology 38, 2709–2719. https://doi.org/10.1111/1365-2435.14680

Zhang, G., Bréda, N., Steil, N., Gaertner, P., Levillain, J., Ruelle, J., Massonnet, C., 2025. Analysing resilience of European beech tree to recurrent extreme drought events through ring growth, wood anatomy and stable isotopes. Journal of Ecology 113, 955–973. https://doi.org/10.1111/1365-2745.70014

Zohner, C.M., Mirzagholi, L., Renner, S.S., Mo, L., Rebindaine, D., Bucher, R., Palouš, D., Vitasse, Y., Fu, Y.H., Stocker, B.D., Crowther, T.W., 2023. Effect of climate warming on the timing of autumn leaf senescence reverses after the summer solstice. Science 381, eadf5098. https://doi.org/10.1126/science.adf5098

Remote-sensing evidences of the impacts of combined drought and heatwaves of 2022 on deciduous forests in northern Italy across an elevation gradient

Abstract

The year 2022 in Europe was extreme due to prolonged heatwaves and severe drought. We analyse through high-resolution remote sensing the impacts of the extreme year 2022 on the phenology (onset and end of growing season) and on the occurrence of early crown discoloration of deciduous forests in northern Italy from the lowlands (Monza) to the Prealps (Cernobbio) and the Alps (Valdidentro).

We analysed plant phenology using the normalized difference vegetation index (NDVI) of 2244 images of Sentinel-2 (period 2017-2023) and identified by General Regression Model the drivers of early crown discoloration in the year 2022. We also computed the biomass production at peak season using NDVI provided by Landsat.

The extreme year 2022 produced the largest impact at the lowlands, with early crown discoloration occurring 40 days earlier than mean leaf senescence and decrease of biomass production, but high resilience in 2023. Unexpectedly, the year 2022 produced detectable impacts at the alpine and prealpine sites, with early crown discoloration of 15 days earlier than leaf senescence, mainly driven by vapour pressure deficit at the prealpine site, and with a legacy effect of decreased biomass production in 2023 at the alpine site, suggesting the poor resilience of alpine deciduous forests. The extreme conditions of 2022 did not exert any impact on the greening of the following year at any study site.

Differently from what previously reported, the high elevation deciduous forests are sensitive to extreme heat and drought, indicating the need to assess their future potential resistance and recovery.

Keywords: extreme climatic events; plant phenology; advanced leaf senescence; decreased biomass production; forest ecological requirements

1.Introduction

Phenological shifts are widespread ecosystem responses to climate change (e.g. Walther et al., 2002; Menzel et al., 2006; Min et al., 2011; IPCC 2021; Coumou and Rahmstorf, 2012; Russo et al., 2014). Climate change is increasing the frequency and magnitude of extreme weather events, in particular of heat waves and summer droughts which, both alone as well as combined, could exert relevant impacts on ecosystems, especially on vegetation (e.g. Zscheischler et al., 2014).

Leaf senescence (LS) is an active physiological process of nutrient recovery prior to winter diapause/dormancy in which nutrients and macromolecules are converted into transportable compounds, remobilized from the above-ground biomass and stored for next year's growth (Keskitalo et al., 2005; Lim et al., 2007; Fracheboud et al., 2009). The correct timing of leaf senescence is a trade-off between C acquisition and N storage (Fracheboud et al., 2009; Richardson et al., 2010; Zhao et al., 2012; Estiarte and Peñuelas, 2015). Considered alone, air warming delays leaf senescence, while drought advances leaf senescence (Estiarte and Peñuelas, 2014), with opposite consequences on the efficiency of nutrient resorption (Fracheboud et al., 2009; Zhao et al., 2012; Estiarte and Peñuelas, 2015). The combination of heat waves and droughts exerted divergent impacts on leaf senescence, with uncertainties on the extent and recurrence of early leaf senescence of deciduous forests (Descals et al., 2022) and on their detection through remote sensing (e.g., Brun et al., 2020, Sturm et al., 2022).

In the last decades extreme climatic events, in particular the combination of long-lasting high temperatures and drought, triggered early leaf discoloring, wilting and shedding, with early crown discoloration and defoliation (e.g., Braun et al., 2021; Gazol and Camarero, 2022). Early crow discoloration and defoliation represent the result of accumulated impacts of stressful environmental conditions (e.g. Bussotti et al., 2024) producing hydraulic failure (e.g. Choat et al., 2012; Engelbrecht, 2012), carbon starvation (McDowell and Sevanto, 2010), embolism and consequent failure in water transport (Allen et al., 2015; Schuldt et al., 2016; Knutzen et al.,2025). As observed in Europe during the extreme climatic events occurred in 2003 and 2018, early crown discoloration and defoliation induce the shortening of forest canopy duration, limit photosynthesis and nutrient uptake, reducing forest productivity and the ecosystem capacity of carbon sequestration (Ciais et al., 2005; Richardson et al., 2010; Fridley, 2012; Reichstein et al., 2013; Bastos et al., 2020; Smith et al., 2020; Bigler et al., 2021), with positive feedbacks to climate change (Lindner et al., 2010).

High-resolution satellite data can improve the assessment over vast territories (Torres et al., 2021), the monitoring of remote areas (Gross et al., 2009) and offer the possibility of repeated measurements (White et al., 2016; Wegler and Kuenzer, 2024), tracking the responses of vegetation ecosystems to climate change and, particularly, to the combination of heatwaves and droughts (Hartmann et al., 2022), improving the spatial resolution of the analyses and providing an earlier detection of leaf senescence (Hmimina et al., 2013; Descals et al., 2022; Hartmann et al., 2022) and/or of early crown defoliation and discoloration (e.g., Brun et al., 2020). Moreover, a high spatial resolution may allow to better discriminate the different responses and sensitivity of different vegetation types to these extreme events also for the future assessment of their potential resistance, recovery, and resilience (e.g., Sturm et al., 2022). This information is recommended for a correct landscape management, to achieve ecosystem conservation (e.g., Wei et al., 2022) and promote adaptation to climate change, given that extreme climatic events are now occurring at continental-scale (Sturm et al., 2022) and are expected to further increase in the next future (Rahmstorf and Coumou, 2011). Stressful conditions leading to early crown defoliation and discoloration (e.g., Braun et al., 2022; Bussotti et al., 2024) could be detected over vast territories through remote sensing (e.g., Brun et al., 2020). The normalized difference vegetation index (NDVI) is a structural vegetation index used to characterize vegetation vitality, greening rate and phenology, assess and quantify vegetation responses to climatic and environmental change (e.g., Breshears et al., 2005; Camarero et al., 2015; Gouveia et al., 2017; Senf et al., 2020). As NDVI is a structural index reflecting seasonal changes in leaf biomass (e.g. Descals et al., 2020, 2022), it is used as a proxy of leaf biomass, is suitable to analyse the seasonality of vegetation and its changes. In particular, the decline of NDVI in autumn is a proxy of the timing of leaf senescence, as NDVI decreases when leaves fall (e.g., Yin et al., 2020; Descals et al., 2022), and could be used to dectect stressful conditions in summer inducing a reduction of biomass production. Early leaf discoloring and defoliation, as well as strong reductions in NDVI, were detected in response to summer drought were documented in Italy and Europe for broadleaves tree species (e.g., Pollastrini et al., 2019; Puletti et al., 2019; Rita et al., 2019; Bigler et al., 2021; Bussotti et al., 2021), confirming the potential of remote sensing for early detection and monitoring of forest stress.

The year 2022 in Europe was characterized by extreme climatic conditions due to an unprecedented long-lasting combination of heatwaves and severe drought lasting for several months, from late spring to late summer (Toreti et al., 2023; Knutzen et al., 2025). The most affected regions were France, Italy, and the Iberian Peninsula, where extreme droughts lasted from May to August and temperatures rose by more than 2.5°C above the seasonal means

(Tripathy and Mishra, 2023; Gharun et al., 2024). The impact of the extreme year 2022 was not uniform across Europe, with the highest impacts detected in central Europe and the lowest in the alpine regions, suggesting different sensitivity due to the effect of elevation or the adaptation to historical drought exposure (e.g., Knutzen et al., 2025).

The combination of drought and heatwave of the extreme year 2022 had unprecedented negative impacts on the forest greenness, photosynthetic capacity and vitality of trees, especially in deciduous broadleaf forests in Europe (Choler, 2023; Hermann et al., 2023; Gharun et al., 2024; Knutzen et al., 2025). Several studies demonstrated that the heatwaves and droughts of summer 2022 caused widespread and severe effects on forest phenology and productivity across Europe (Hermann et al., 2023; Choler, 2023; van der Woude et al., 2023; Bucha et al., 2024 a; Bucha et al., 2024 b; Gharun et al., 2024; Knutzen et al., 2023, 2025).

In Italy the ICP Forests monitoring network reported for the year 2022 the occurrence of one of the most relevant defoliation events of deciduous broadleaved trees in the temperate region coinciding with the hottest and driest years (2012, 2017 and 2021-2022) (Bussotti et al., 2024). However, while several studies reported the occurrence of early crown discoloration and defoliation of deciduous broadleaves trees in Italy in response to drought for the first two decades of this century (e.g., Pollastrini et al, 2019; Puletti et al., 2019), only few studies addressed the impacts of the extreme climatic conditions of summer 2022 on vegetation in northern Italy. These studies mainly focused on agricultural systems, such as crops in the Po Valley (e.g., Sofia et al., 2024; Xue at al., 2024) rather than on natural forest ecosystems, and those showing remote sensing evidences were mainly referred to the Mediterranean region (e.g., Baronetti et al., 2023).

Here we analyse through remote sensing the impacts of the extreme climatic events of the year 2022, in particular of the long-lasting and severe drought coupled with warming, on deciduous broadleaves forests at three study sites located across an elevation gradient in northern Italy from the Po plain to the Prealps to the Alps in Lombardy Region. We hypothesize that this extreme climatic event induced: a) early crown discoloration and defoliation of deciduous broadleaves trees in late summer, and b) decrease of biomass production during the peak of the growing season (July and August). We hypothesize that all sites are sensitive to the extreme climatic conditions with the highest impacts occurring at the lowlands and decreasing their intensity with increasing elevation, but with differential sensitivity and resilience at inter- and intra-community level.

2.Material and Methods

2.1. Vegetation and study sites selection

We performed our study across a transect covering an elevation gradient from the Po plain to the Alps, with three main study sites: Monza Park, representative of the lowlands; Cernobbio for the Prealps; Valdidentro in upper Valtellina for the Alps. Deciduous forests are one of the most widespread land cover types characterizing the vegetated natural landscape across our study transect (Pace et al., 2021). At each study site were selected the most representative and widespread forest types according to the "Forest map of the Lombardy Region"

(https://www.geoportale.regione.lombardia.it/en/metadati?p_p_id=detailSheetMetadata_WAR_gptmetadataportlet&p_p_lifecycle=0&p_p_state=normal&p_p_mode=view&_detailSheetMetadata_WAR_gptmetadataportlet_identifier=2r_lombar%3A7ceabf1c-28b2-4c0b-b4ba-4be3d17afa33&_jsfBridgeRedirect=true).

This study represents a case study carried out along an elevational transect in northern Italy. The selected sites correspond to the most widespread deciduous forest types of the Lombardy Region, as documented by the official *Forest Map of Lombardy Region* and confirmed by field surveys, and are representative of the regional forest landscape (Fig. 1 SM). Although our analysis is site-specific, the extent of the surveyed areas provides a suitable level of replication of the data achieved.

At each study site the specific areas have been selected and identified by field survey allowing to confirm the data on landscape classification provided by the Forest Map of Lombardy region and the characterization of each vegetation type as reported in Table 1SM.

As target representing the different natural and semi-natural landscapes across the study gradient, for the lowland we selected the area around Monza and Milan, in particular the Monza Park (160-220m asl) primarily composed by: oak dominated forests of the foothills (dominated by *Quercus robur* L.*, Q. petraea* (Matt.) Liebl.) (QR) and oak-hornbeam forests of the lowlands (dominated by *Quercus, Ulmus minor* Mill.*, Fraxinus, Carpinus betulus* L.*)* (UM) (Table 1SM). For the Prealps we selected the Cernobbio area across an elevation gradient from 200 to 1200 m asl, with the following forest types: oak-hornbeam forests of the hills and sub-montane belt of the *Carpinion betuli* (dominated by *Quercus petraea, Q. robur, Carpinus betulus*) (CB); chesnut forests on calcareous soils dominated by *Castanea sativa* Mill. (CS); ash-oak-hornbeam forests (Typical *Orno-Ostryetum* dominated by *Fraxinus ornus* L. and *Ostrya carpinifolia* Scop.) (OO); ash-maple-hornbeam forest dominated by *Acer* spp., *Fraxinus ornus, Ostrya carpinifolia* (belonging to the *Tilio-Acerion* Alliance) (TA); birch forest dominated by

Betula pendula Roth (BP); typical beech forests of the calcareous soils dominated by *Fagus sylvatica* (FS); green alder forests dominated by *Alnus alnobetula* (Ehrh.) K.Koch (AA) (Table 1SM). For the Alps we selected the area between Bormio and San Carlo (Valdidentro) in upper Valtellina (1400-2600 m asl) with two types of deciduous forests: birch forest dominated by *Betula pendula* (BP) and white alder forests dominated by *Alnus incana* (L.) Moench (AI) (Table 1SM). Each study area extends over 42 km^2.

All these areas were not affected by fire, according to Descals et al. (2022) using the FIRMS active-fire product (Giglio et al., 2016).

2.2. Plant phenology assessment through remote sensing

For the assessment and quantification of plant phenology we selected the Copernicus Sentinel-2 mission, which uses two polar-orbiting satellites launched by the European Space Agency (ESA), on 23 June 2015 and on 07 March 2017, respectively. Sentinel-2 has been used in several studies on forest phenology (Vrieling et al. 2018; Granero-Belinchon et al. 2020, Kowalski et al. 2020, Löw and Koukal 2020, Quesada-Ruiz et al. 2021, Tian et al. 2021; Grabska-Szwagrzyk and Tyminska-Czabanska, 2023), and allows to analyse and monitor the variability in land surface conditions, providing revisit time (5 days with 2 satellites at mid-latitudes) and spatial resolution (10 m for the bands of interest: 2, 3, 4 and 8) (Sentinel 2 user Handbook) suitable for the quantitative assessment and monitoring of plant phenology, in particular for the greening and leaf senescence (Vrieling et al., 2018; Granero-Belinchon et al., 2020; Kowalski et al., 2020; Löw and Koukal 2020; Quesada-Ruiz et al., 2021; Tian et al. 2021; Grabska-Szwagrzyk and Tyminska-Czabanska, 2023). In particular, the high temporal resolution of the Sentinel-2A and-2B satellites allows a precise assessment of the end of season (EoS) (Descals et al., 2022).

For each study area, we selected from one to four scenes per month with the lowest amount of noise (e.g. clouds, shadows) acquired from Sentinel-2. Our study focused on the period May 2017 – December 2023 (17 May 2017 to 7 December 2023 in Monza and Cernobbio; 27 May 2017 to 28 October 2023 at Valdidentro) using the European Space Agency's Scientific Hub, analysing totally 2244 satellite images. Indeed, all satellite images are Level-2, Bottom-Of-Atmosphere (BOA) corrected reflectance products, and were available only from May 2017.

For each image of each selected study site, we processed the normalized difference vegetation index (NDVI) time series, according to the following formula:

$$NDVI = \frac{NIR - RED}{NIR + RED}$$

NDVI was calculated from visible (band 4 Red) and near infrared bands (band 8 NIR) combinations in QGIS software from Sentinel 2.

NDVI allowed to identify the onset of the growing season (DOY, Day Of Year) as a proxy of leaf greening, the end of the season (EoS, DOY) as a proxy of leaf senescence (LS), and the growing season length (days), obtained by computing the difference between the onset and the end of the growing season.

The end of the growing season was estimated as the day when NDVI decreased exceeding the threshold provided by 50% of the annual amplitude plus the annual minimum NDVI value (Descals et al., 2020). This threshold represents low NDVI values that estimate the mid-greendown date. Usually, the threshold for the estimation of the leaf-shedding date is 20% (Descals et al., 2020) but the higher threshold metrics calculated with 50% of the amplitude are less affected by biases due to discontinuities in the time series (Descals et al., 2020). Similarly, the onset of the growing season in spring was identified by the NDVI increase above the same threshold. The identification of leaf senescence provided by NDVI from Sentinel-2 images was ground validated by field surveys of the sites during the autumn 2022 and 2023.

The mean date (DoY, day of year) of leaf senescence obtained by the NDVI time series for the period 2017-2023 allowed to achieve the reference term for the quantification of the inter-annual variability of the date of leaf senescence in autumn (e.g., Brun et al., 2020; Descals et al., 2020, 2022) and for the assessment and quantification of early crown discoloration (instead of leaf senescence) in 2022. The phenological data were analysed at each of the three study sites both at inter-community and at intra-community level.

For the onset of the growing season, leaf senescence (or early crown discoloration in years with extreme climatic conditions) and growing season length were computed with the descriptive statistics (minimum, maximum, median, 25^{th} and 75^{th} percentile) both at inter- and intra-community level for each study site.

2.3. Climate

We collected daily air temperature and precipitation data recorded with a continuous dataset at the three closest ARPA Lombardia automatic weather stations (AWS) to our study areas, during the last two decades in the period 2004-2023, in particular: Osnago AWS for Monza Park, Como viale Geno AWS for Cernobbio area, and Valdisotto Oga S. Colombano AWS for Valdidentro area.

We computed the annual, seasonal (in particular for the summer, JJA = June, July, August) and monthly (from May to September as targets representative of the growing season across the three study sites) means of air temperature (°C) and cumulated precipitation (mm) and analysed through linear regression their trends with time to assess whether 2022 was an extreme year.

We also computed for each study site the extreme temperature index (TX90P) to assess the severity of warming. The extreme temperature index (TX90P) (Zhang et al., 2011; ISTAT, 2020) is the number of days with $T_{max} > 90^{th}$ percentile, calculated on period 2004-2023.

To quantify the effect of warming on drought for each study site we computed the Standardized Precipitation Evapotranspiration Index (SPEI) (Vicente-Serrano et al., 2010), derived from the Standardized Precipitation Index (SPI), and computed using precipitation and potential evapotranspiration (PET) (Begueria et al., 2013; Vicente-Serrano et al., 2010, 2013). SPEI values allow to discriminate dry (extremely dry ≤ -2; severely dry $-2 \leq SPEI < -1.5$; moderately dry $-1.5 < SPEI < -1$) from normal ($-1 < SPEI < 1$) to wet (moderately wet $1 < SPEI < 1.5$; severely wet $1.5 < SPEI \leq 2$; extremely wet $SPEI > 2$) conditions (Wang et al., 2021). In particular, to identify the occurrence of persistent drought conditions from the onset of spring to the end of summer, we computed for each summer month (June, July, August) the SPEI with a window length of 6 months (SPEI_6_months) (e.g., Knutzen et al., 2025). The SPEI computation was performed by Rstudio with SPEI package (RCore T.E.A.M., 2016), using precipitation and Potential Evapotranspiration (PET) data for the period 2017-2023. PET data were calculated through Rstudio using daily maximum and minimum temperature data (Affandy et al., 2023).

High temperatures increase the evaporative water demand of plants (vapour pressure deficit, VPD) inducing stomatal closure and decreasing photosynthesis, and clear relation between increases of tree mortality and increased VPD were detected in Europe in the period 1993-2013 (Gazon and Camarero, 2022). To quantify the impact of the vapour pressure deficit (VPD) on plants, we downloaded the VPD data covering the period 2004–2023 from the TerraClimate dataset (http://www.climatologylab.org/terraclimate.html) (Castellanata et al., 2022).

TerraClimate is a high-resolution (~4 km) monthly dataset that provides climate and climatic water balance information for global land areas. It combines spatial climatology data from the WorldClim and CRU TS4.0 datasets (Castellaneta et al., 2022).

2.4 Drivers of leaf senescence at intra-community level

As leaf senescence was the phenological stage more influenced by the extreme year 2022, we performed General Regression Models (GRM) at intra-community levels to identify the drivers of leaf senescence, with leaf senescence and dependent variable, years as categorical factors and the climatic data (air temperature, precipitation, SPEI) as independent variables. All GRM were computed with the software STATSOFT©.

2.5 Impact of the extreme year 2022 on peak season biomass production

NDVI is a structural index reflecting seasonal changes in leaf biomass (e.g. Descals et al., 2020, 2022), suitable to provide a quantitative assessment of the impact of extreme climatic events on leaf biomass during the summer season, with special reference to decreased biomass production. The dataset provided by Sentinel-2 could not be used to assess the occurrence of decreased biomass production during the study period: indeed, due to the updating processing baseline performed in January 2022, the digital number (DN) data before and after the change was shifted, not allowing the comparison of the reflectance data.

To overcome this problem, we decided to use the dataset provided by the satellite Landsat 8, launched on February 2013 by NASA in collaboration with the U.S. Geological Survey (USGS). It consists of two sensors, the Operational Land Imager (OLI) and the Thermal Infrared Sensor (TIRS), with a spatial resolution of 30 meters (visible, NIR, SWIR) and 100 meters (thermal), and a temporal resolution of 16 days (Landsat 8 Handbook). The Landsat NDVI time series were processed and computed in QGIS software from Landsat 8, using the same equation already used for the Sentinel NDVI time series. To assess whether the extreme year 2022 induced decreased summer biomass production we computed for each year in the period 2014-2023 the descriptive statistics (minimum, maximum, median, 25th and 75th percentile) of NDVI provided by Landsat 8 at peak season (July and August) at intra-community level for each study site.

3. Results

3.1. Climate

Over the last two decades (2004-2023), the year 2022 exhibited the highest mean annual air temperature (MAAT) as well as the highest mean summer air temperature (JJA: June, July, August) at all the three study sites (with the exception of the MAAT of Cernobbio, with 2022 being one of the warmest years) (Fig. 1). In particular the mean temperature of the summer season 2022 largely exceeded the mean of the last two decades (respectively of +2.9°C in Monza; +2.5°C in Cernobbio; +1.9°C in Valdidentro).

The mean monthly air temperatures during the growing season (May to September) further confirmed that the year 2022 was extreme, with temperatures largely exceeding the mean of the last two decades and in particular from May to August (with the only exception of September) and reaching the most extreme values in July (Table 2 SM). It is also notable that c. 50% of the records of mean monthly temperature between May and September was characterized by values higher than the mean of the two decades, well above the mean values and, for the year 2022, exceeding in most cases also the 90th percentile of the last two decades (Table 2 SM).

The number of extreme temperature days (TX90P) occurred during the summer (JJA, June, July, August) confirmed the extreme conditions of the year 2022 in the last two decades, especially in June and July and especially at Monza and Cernobbio (Fig. 1G-I, Table 4SM), with a long record of consecutive extreme temperature days. The year 2015 was characterized by the highest TX90P in July of the last two decades, followed by the year 2022 (Fig. 1G-I, Table 3SM), although the mean summer temperature of the year 2022 was the highest of the last two decades (Fig. 1D-F, Table 3SM).

The lowest amount of total annual precipitation (TAP) in the last two decades was recorded in the year 2022 both at Monza and Cernobbio, with TAP being less than the 25th percentile of the precipitations of the last two decades, accounting a decrease of 51% (at Monza) and 43% (at Cernobbio) respect to the mean value of TAP in the period 2004-2023 (Fig. 2, Table 4SM).

At Valdidentro in 2022 the TAP was 12% lower than the mean of the two decades but not the lowest (Fig. 2, Table 4SM). This trend was confirmed also for the summer precipitation (JJA-P), with 2022 being the year with the lowest summer precipitation at Cernobbio (with a decrease of 67% respect to the summer mean in the period 2004-2023), and one of the three years with lowest summer precipitations at Monza (2013, 2015, 2022) accounting a decrease of of 67% in 2022 (Fig. 2, Table 4SM). At Valdidentro summer precipitations exhibited a fluctuating trend,

with 2022 being one of the years with low precipitation and a decrease of 18% respect to the summer mean of the period 2004-2023 (Fig. 2, Table 4SM).

Over the two decades (period 2004-2023) Monza was characterized by the highest values of VPD (vapour pressure deficit) followed by Cernobbio, with Valdidentro showing the lowest VPD values, as could be expected according to the elevation and, consequent, temperature gradient across the three study sites (Fig. 3).

Monza exhibited the highest VPD of the two decades in the summer 2022, followed by the VPD recorded in summer 2015 (Fig. 3A). Also, Cernobbio exhibited the highest VPD in summer 2022, although very similar conditions were recorded during the summer 2015 (Fig.3B). Conversely, at Valdidentro the highest VPD was recorded in July 2015, with summer 2022 showing relatively high but not the highest VPD conditions (Fig. 3C).

The SPEI computed on the window of the preceding six months indicated in the year 2022 the occurrence of a persistent drought with severely dry (SPEI < 1.5) conditions during the whole summer and also in September both at Monza and Cernobbio, and moderately dry (-1.5<SPEI<1) at Valdidentro (Fig. 4).

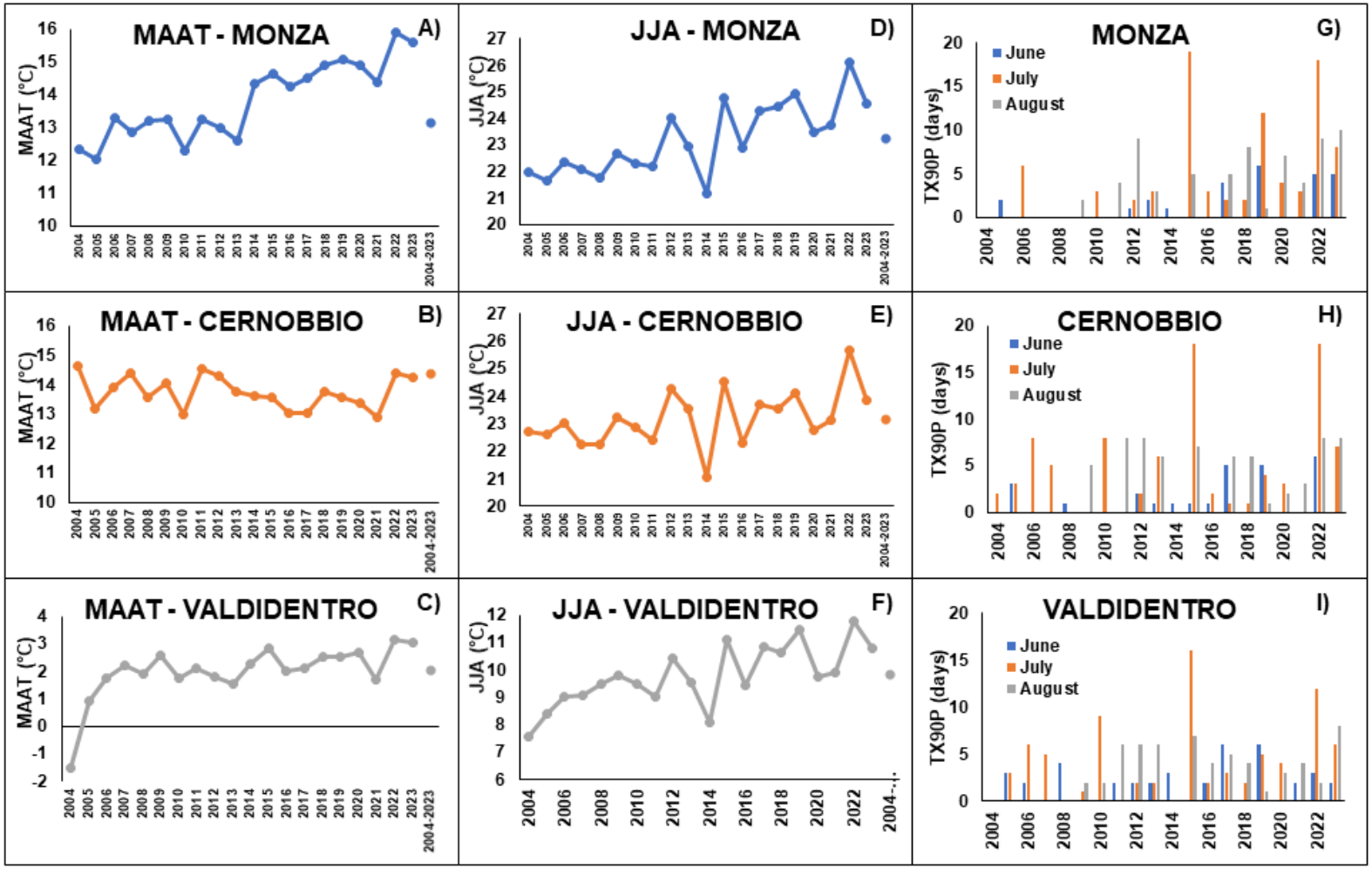

Figure 1. Mean annual air temperature (MAAT, °C) (A, B, C), mean summer air temperature (JJA, June-July-August, °C) (D, E, F) and number of days with extreme temperatures (TX90P, exceeding the 90th percentile of the decade 2004-2023) (G, H, I) for each summer month (June, July, August)of the last two decades (2004-2023) over the three study areas (A, D = Monza, B,E = Cernobbio, C, F = Valdidentro) and the 2004-2023 mean (final dot in each graph A,B,C) as reference.

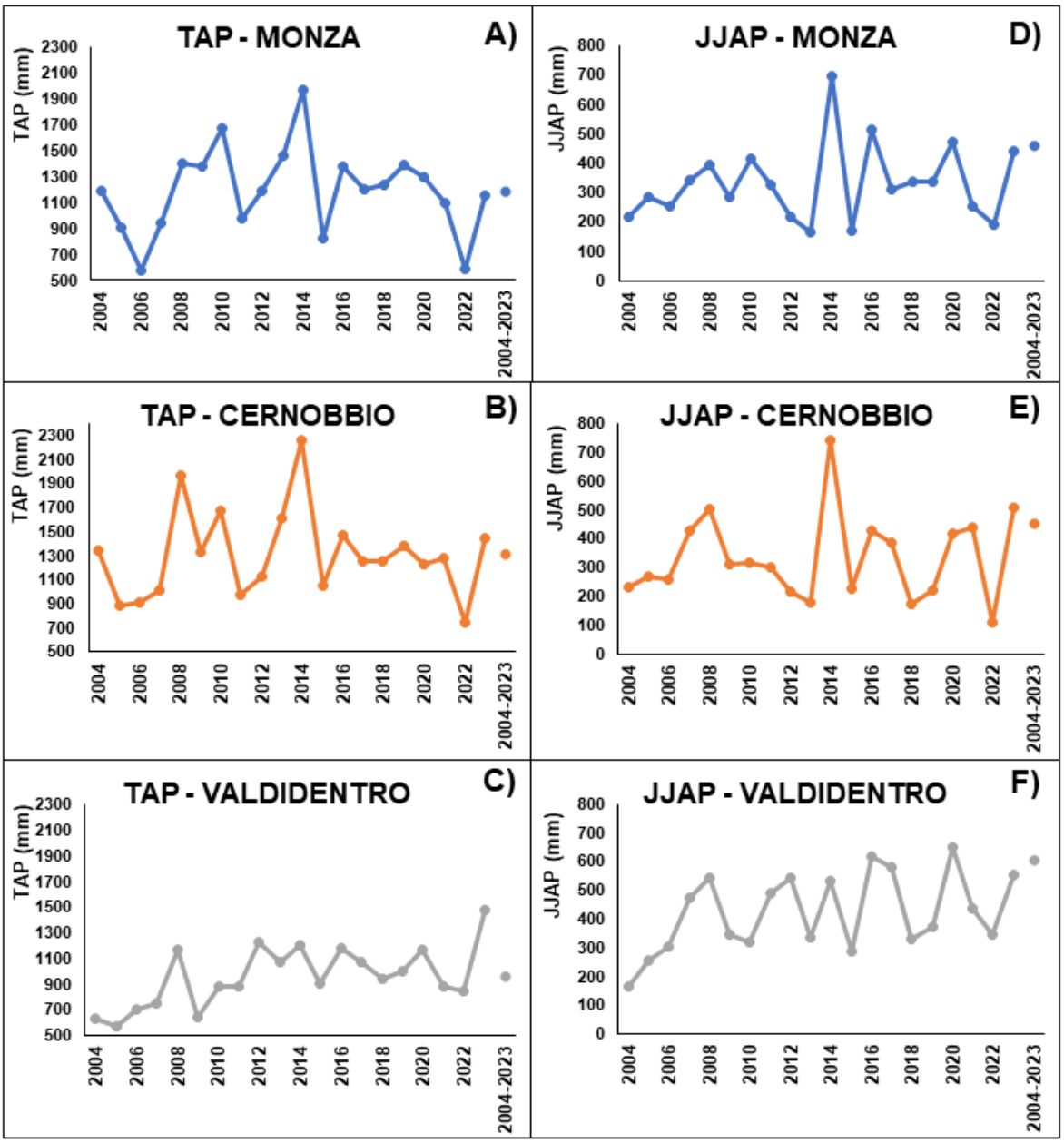

Figure 2. Total annual cumulative precipitation (TAP, mm) and summer cumulative precipitation (June, July, August, mm, JJAP) in the period 2004-2023 over the three study areas (A, D = Monza, B, E = Cernobbio, C, F = Valdidentro), and the 2004-2023 mean (final dot in each graph) as reference.

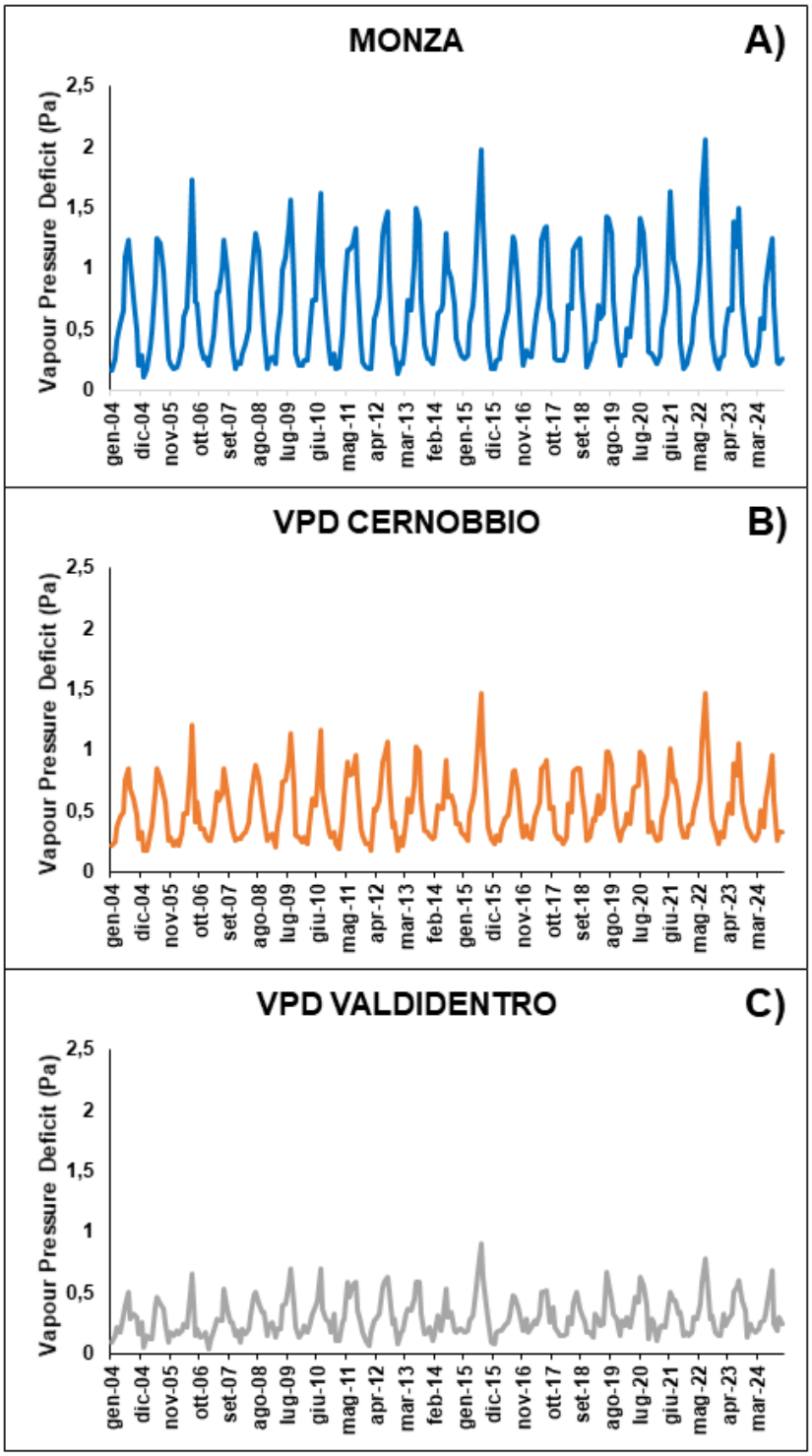

Figure 3. Monthly means of Vapour Pressure Deficit (VPD, Pa) in the period 2004-2023 measured at: A) Monza, B) Cernobbio, C) Valdidentro.

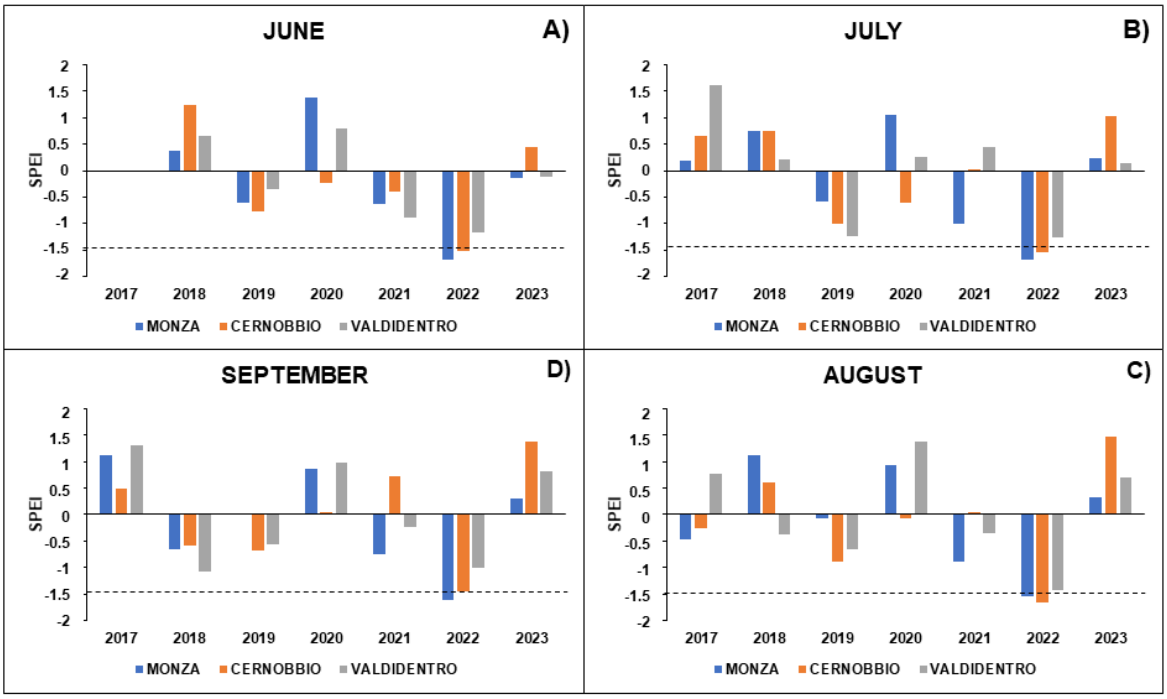

Figure 4. Standardized Precipitation Evapotranspiration Index (SPEI) computed on the window of the six preceding months (SPEI_6_months) in the period 2017-2023 to identify the occurrence of long-lasting drought for each of the three study sites (Monza, Cernobbio, Valdidentro) for the months of A) June; B) July; C) August; D) September. The dotted line indicates the threshold of SPEI = -1.5, indicating severely dry conditions.

3.2. Impacts of the extreme year 2022 on plant phenology at inter-community level

Across the study period and at inter-community level, the onset of the growing season, provided by leaf greening, occurred earlier at the sites located at lower elevations, between the end of March/beginning of April until the end April both at Monza (mean DOY 98, range DOY 91 – 104) and Cernobbio (mean DOY 112, range 88 – 147), while slightly later at Valdidentro, which is located at higher elevation, between the beginning of May and the mid of June (mean DOY 145, range DOY 132 – 164) (Fig. 5A, Table 1).

The end of season, provided by leaf senescence (and for the year 2022 by early crown discoloration), exhibited the opposite trend with elevation, occurring between the beginning of October to mid-November at Valdidentro (mean DOY 298, range DOY 281-322), late November at Cernobbio (mean DOY 310, range DOY 273-351) and mid-December at Monza (mean DOY 315, range DOY 274-350) (Fig. 5B, D, Table 1).

The year 2022 was characterized by a slightly delayed greening (onset of the growing season) respect to the mean of the period 2018-2023 (Table 1), while it exhibited a striking advance of the end of season due to early crown discoloration, with the largest advance (40 days) at Monza,

and comparable advances of 17 and 14 days, respectively, at Cernobbio and Valdidentro (Fig. 5D-F, Table 1). The year 2022 was extreme also for the duration of the growing season, which was the shortest both at Monza (218 days) and Cernobbio (199 days), but not at Valdidentro (149 days). Moreover, Monza exhibited the largest inter-annual variability of growing season duration (86 days) which exceeded by c. the double the variability observed at Cernobbio (48 days) and Valdidentro (34 days) (Fig. 4C, F, Table 1).

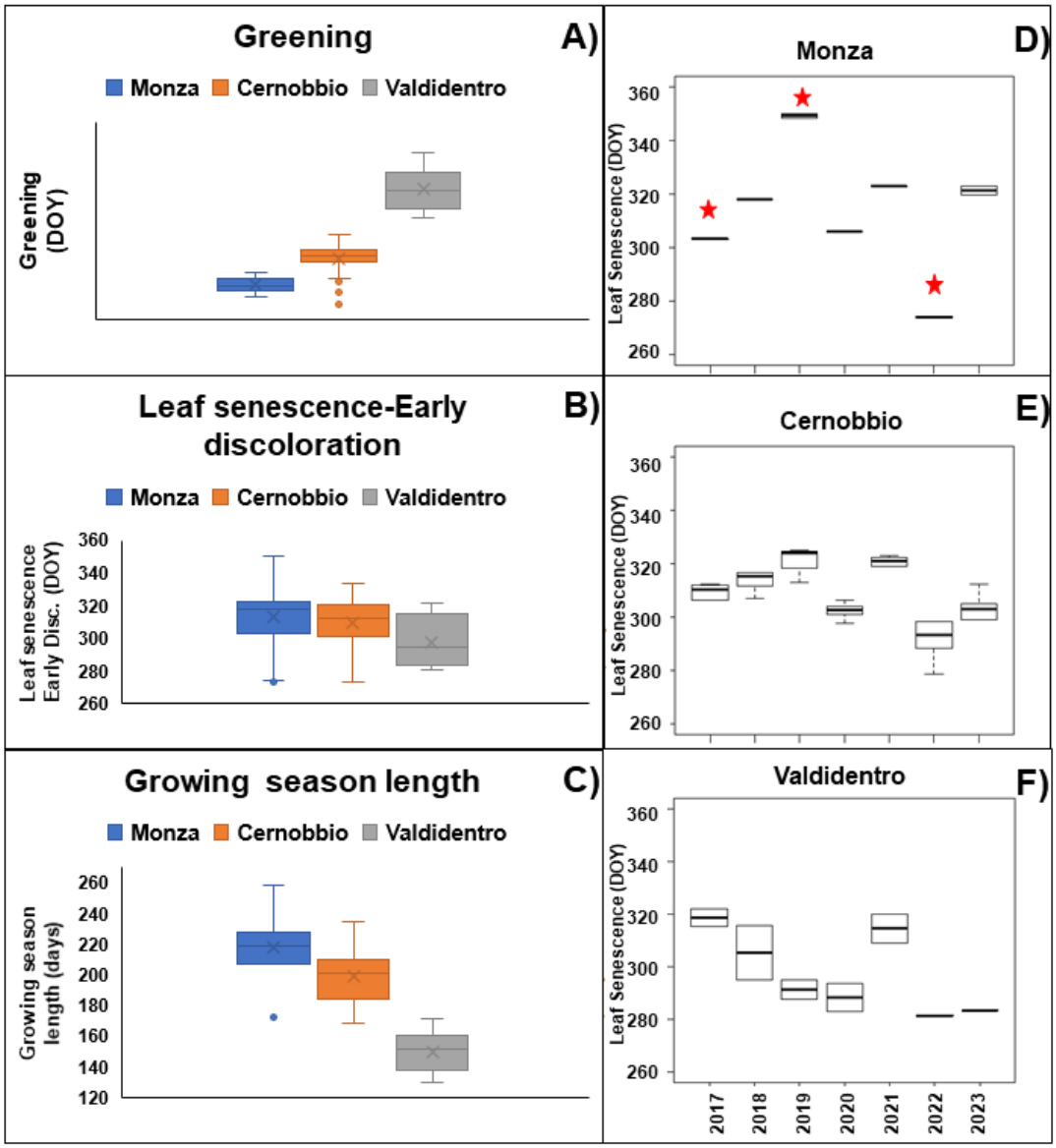

Figure 5. Inter-annual variability at inter-community level in the period 2017 – 2023 at the three study sites of: A) onset of the growing season provided by the leaf greening, B) end of the growing season provided by leaf senescence (and for the year 2022 by crown discoloration), and C) growing season length; D) leaf senescence at Monza; E) leaf senescence at Cernobbio; F) leaf senescence at Valdidentro. Dots indicate the outlier values for graphs A-C. The graphs D-F show median ± percentiles (25-75) ± minimum and maximum of leaf senescence showing its advance at all study areas.

Table 1. Greening, leaf senescence (or early crown discoloration in years with extreme climatic conditions) and growing season length (DOY) for each community type at each of the three study sites in the study period of Sentinel-2.

GREENING (DOY)	**MONZA**			**CERNOBBIO**								**VALDIDENTRO**		
YEAR	**oak (QR)**	**Lowlands oak-hornbeam (UM)**	**All**	**maple (TA)**	**g.alder (AV)**	**birch (BP)**	**chestnut (CS)**	**beech (FS)**	**ash-hornbeam (OO)**	**Hills oak-hornbeam (CB)**	**All**	**w.alder (AI)**	**birch (BP)**	**All**
2018	104	104	104	111	112	114	111	110	110	101	110	155	138	146
2019	91	93	92	112	119	116	112	117	104	100	111	164	157	160
2020	98	99	98	112	115	119	112	114	100	93	109	144	132	138
2021	95	95	95	113	110	115	120	113	99	147	117	155	150	152
2022	101	101	101	115	117	119	115	115	105	101	112	145	141	143
2023	95	96	95	117	114	123	117	115	109	88	112	134	132	133
MIN	91	93	92	111	110	114	111	110	99	88	109	134	132	133
MAX	104	104	104	117	119	119	120	117	109	147	117	164	157	160
MEAN	97	98	98	113	114	118	114	114	104	105	112	149	142	145
LEAF SENESCENCE/EARLY CROWN DISCOLORATION (DOY)	**oak (QR)**	**Lowlands oak-hornbeam (UM)**	**All**	**maple (TA)**	**g.alder (AV)**	**birch (BP)**	**chestnut (CS)**	**beech (FS)**	**ash-hornbeam (OO)**	**Hills oak-hornbeam (CB)**	**All**	**w.alder (AI)**	**birch (BP)**	**All**
2017	303	318	311	306	312	298	312	312	309	273	303	322	315	319
2018	318	318	318	316	307	317	317	312	314	334	317	316	295	306
2019	350	348	349	323	313	324	325	318	325	325	322	295	288	292
2020	306	306	306	304	297	301	304	302	306	323	305	283	294	289
2021	323	323	323	319	323	312	321	322	321	351	324	320	309	315
2022	**274**	**274**	**274**	**298**	290	**288**	**298**	**297**	**279**	314	**295**	**282**	**281**	**282**

2023	323	320	322	305	**286**	301	304	**299**	312	322	304	**283**	**284**	284
MIN	274	274		298	286	288	298	297	279	273	295	282	281	282
MAX	350	348		323	323	324	325	322	325	351	322	322	315	319
MEAN	314	313	315	310	304	306	312	309	309	320	310	300	295	298
GROWING SEASON (DOY)	**oak (QR)**	**Lowlands oak-hornbeam (UM)**	**All**	**maple (TA)**	**g.alder (AV)**	**birch (BP)**	**chestnut (CS)**	**beech (FS)**	**ash-hornbeam (OO)**	**Hills oak-hornbeam (CB)**	**All**	**w.alder (AI)**	**birch (BP)**	**All**
2018	214	214	214	205	195	203	206	202	204	233	207	161	157	159
2019	259	255	257	211	194	208	213	201	221	225	210	131	131	131
2020	208	207	208	192	182	182	192	188	206	230	196	139	162	151
2021	228	228	228	206	213	197	201	209	222	204	207	165	159	162
2022	**173**	**173**	**173**	**183**	**173**	**169**	**183**	**182**	**174**	**213**	**182**	137	140	139
2023	228	224	226	188	172	178	187	184	203	234	192	149	152	151
MIN	173	173	173	183	172	169	183	182	174	213	182	131	131	139
MAX	259	255	257	206	208	208	213	209	222	234	210	165	162	162
MEAN	218	217	218	198	188	190	197	194	205	223	199	147	150	149

3.3 Impacts of the extreme year 2022 on leaf senescence at intra-community level

At Monza and Cernobbio, the onset of the growing season was characterized by a limited inter-annual variability (<10 days) at intra-community level, with the only exception of the oak-hornbeam forest of the hills (CB) at Cernobbio (59 days) (Table 1). Valdidentro exhibited a larger inter-annual variability of the onset of the growing season being of c. one month, as expected at higher elevations at sites where snow cover persistence may change yearly.

At intra-community level the year 2022 was extreme with the occurrence of early crown discoloration, observed many days earlier respect to the range of variability of the leaf senescence for all the selected vegetation communities at each of the three study sites (Fig. 6, Table 1). At Monza and Valdidentro all the analysed vegetation types exhibited the earliest crown discoloration across the whole study period, while at Cernobbio the year 2022 was the most extreme year for all forests, with the exception of the green alder forests (AV) and the oak-hornbeam forest of the hills and sub-montane belt (CB) (Fig. 6, Table 1).

The most sensitive communities were those located at lower elevation (Monza) and dominated by oaks and oaks-hornbeam (QR, UM), showing very similar responses, with early crown discoloring occurring 40 days earlier than mean leaf senescence over the period (Fig. 6, Table 1). At Cernobbio, the vegetation ash-hornbeam (OO) exhibited the earliest crown discoloration (30 days earlier than mean leaf senescence), while all the other forest types exhibited an early crown discoloration occurring between 12 and 18 days earlier than mean leaf senescence, with the only exception of the oak-hornbeam forests of the hills and sub-montane belt (CB), which was characterized by the smallest advance (6 days) (Fig. 5, Table 1). In the alpine area (Valdidentro), the impacts of the 2022 extreme climate were similar to those observed at Cernobbio, with an advance between 14 and 19 days of early crown discoloration respect to mean leaf senescence for the birch and white alder forests, respectively (Fig. 6, Table 1).

The persistence of early crown discoloration was observed also in 2023, particularly for both forest types of Valdidentro (AI, BP) as well as for the beech (FS) and green alder (AV) forests of Cernobbio, showing a LS advance very similar for 2022 and 2023 (Table 1). These data indicate both high sensitivity and lack or poor resilience of these forest types to the effect of extreme climatic events. Conversely, both forest types analyzed at Monza, which exhibited the largest advances observed in 2022, were characterized by high resilience in 2023, with a limited delay (of c. $\geq$ 7 days) of LS respect to the mean values of the study period (Table 1).

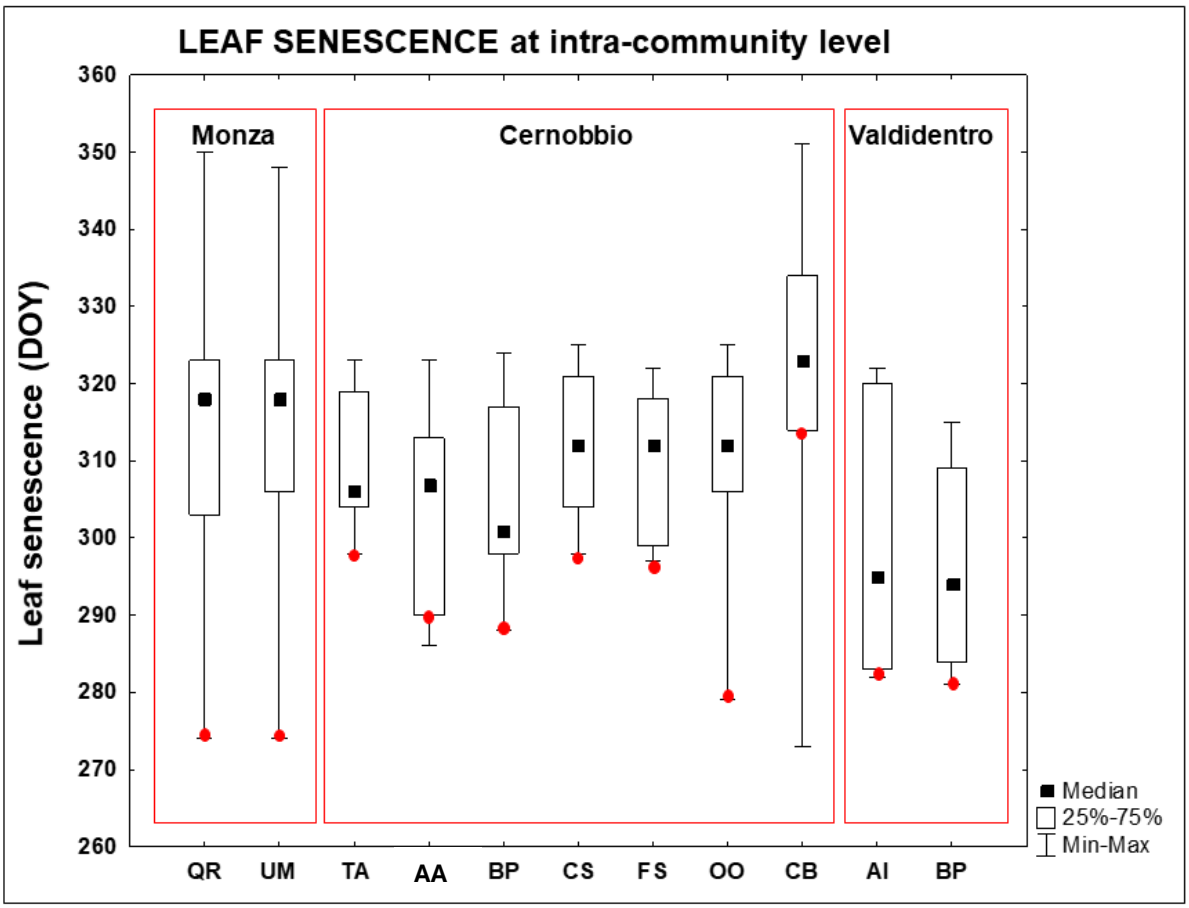

Figure 6. Inter-annual variability at intra-community level of leaf senescence (DOY, day of year) of each selected type of deciduous forests in the period 2017-2023, in the three study areas (Monza, Cernobbio, Valdidentro). The graphs show the descriptive statistics (minimum, maximum, median, 25th and 75th percentile). The red dots represent the year 2022. Legend: **QR** = Oak dominated acidophilous forests of the foothills; **UM** = Oak-Hornbeam forests of the lowlands; **TA** = Ash-Maple-Hornbeam forest dominated by *Acer*., *Fraxinus ornus, Ostrya carpinifolia* (belonging to the *Tilio-Acerion* Alliance); **AA** = green Alder forests dominated by *Alnus alnobetula*; BP = Birch forest dominated by *Betula pendula* (BP); **CS** = Chesnut forests on calcareous soils dominated by *Castanea sativa*; FS = typical Beech forests of the calcareous soils dominated by *Fagus sylvatica*; **OO** = Ash-Oak-Hornbeam forests (Typical *Orno-Ostryetum* dominated by *Fraxinus ornus* and *Ostrya carpinifolia*); **CB** = Oak-Hornbeam forests of the hills and sub-montane belt; **AI** = white Alder forests dominated by *Alnus incana*.

3.4. Drivers of leaf senescence in the extreme year 2022 at intra-community level

As the most important impacts of the extreme climatic year 2022 were observed on early crown discoloration, we analyzed the drivers of early crown discoloration at intra-community level for each study site through GRM (General Regression Models) (Table 2). At all sites and for all the investigated community types the GRM was statistically significant ($p < 0.05$) and explained most of their variance, providing robust support of the influence of some selected climatic factors on early crown discoloration. At Monza, the summer conditions of air temperature and precipitation are the most important drivers of leaf senescence of oak forests

of the foothills (QR) while, for the oak-hornbeam forest of the lowlands (UM) the most important driver is the persistence of drought conditions in the six months preceding the summer (provided by the SPEI July) in combination with air temperature at the peak of the summer (T-July) (Table 2).

At Cernobbio VPD in July was the driving factor triggering early crown defoliation of oak-hornbeam of the hills (CB) and of ash-oak-hornbeam (OO), and VPD in August of ash-maple-hornbeam (TA), green alder (AV) and birch (BP) (Table 2). A different condition was observed for beech (FS), as its early crown discoloration was driven by a combination of factors including summer temperature (JJA-T), vapor pressure deficit in June and July (VPD-Jun, VPD-Jul) and SPEI in August (Table 2).

At Valdidentro, the persistency of drought until the peak of the summer (in particular SPEI Jul) and the precipitations in late spring-early summer (P May, P June) are the key drivers of early crown discoloration of the white alder (AI), while July air temperature and precipitation in August are the most important factors for birch (BP) (Table 2). Concerning the birch forests, it is notable that the drivers affecting their early crown discoloration change from Cernobbio, where VPD-August is the driving factor, and Valdidentro, emphasizing the importance of the combination of summer temperatures and precipitations (Table 2).

Overall, the data indicates that different forest types exhibit varying degrees of sensitivity to climatic variables, with vapor pressure deficit in summer, air temperature and precipitation during the summer months playing critical roles in influencing the early crown discoloration observed in 2022 for these vegetation communities.

Table 2. General regression model shows the climatic drivers affecting crown discoloration in the year 2022 at intra-community level for each of the selected vegetation communities at each study site. Only statistically significant values are reported ($p<0.05$). Legend: JJA-T= Mean temperature of summer season (June, July and August); T-JUL =Mean temperature of July; T-AUG =Mean temperature of August; JJA-P =Total precipitation of summer season; P-MAY = Total precipitation of May; P-JUN = Totale precipitation of June; P-JUL =Total precipitation of July; P-AUG =Total precipitation of August; SPEI JUL = Standardized Precipitation Evapotranspiration Index (SPEI) computed for the 6 months preceding July; SPEI AUG = Standardized Precipitation Evapotranspiration Index (SPEI) computed for the 6 months preceding August; VPD-JUN = vapour pressure deficit June; VPD-JUL = vapour pressure deficit July; VPD-AUG = vapour pressure deficit August. Legend of vegetation types: QR = oak dominated acidophilous forests of the foothills; UM = oak-hornbeam forests of the lowlands; TA = ash-maple-hornbeam forest dominated by *Acer* spp., *Fraxinus ornus, Ostrya carpinifolia* (belonging to the *Tilio-Acerion* Alliance); AA = green alder forests dominated by *Alnus alnobetula* ; BP = birch forest dominated by *Betula pendula* (BP); CS = chesnut forests on calcareous soils dominated by *Castanea sativa*; FS = typical beech forests of the calcareous soils dominated by *Fagus sylvatica*; OO = ash-oak-hornbeam forests (Typical *Orno-Ostryetum* dominated by *Fraxinus ornus* and *Ostrya carpinifolia*); CB = oak-hornbeam forests of the hills and sub-montane belt; AI = white alder forests dominated by *Alnus incana.*

MONZA	**oak (QR)**				**oak-hornbeam (UM)**			
	F	**p**	**R**	**ß**	**F**	**p**	**R**	**ß**
JJA-P	46.6	0.02		1				
JJA-T	64	0.01		2.4				
T-JUL	31.7	0.03		-1.3	115	0.008		-1.3
T-AUG	56.5	0.01		-1.4				
SPEI JUL					116.2	0.008		-1.1
P-JUL					22.5	0.04		0.44
whole model	29	0.033	0.99		79.4	0.01	0.99	
CERNOBBIO	**ash-maple-hornbeam (TA)**				**green alder (AA)**			
	F	**p**	**R**	**ß**	**F**	**p**	**R**	**ß**
VPD JUN								
VPD JUL								

VPD AUG	11.3	0.02		-0.83	21.4	0.005		-0.9
JJA-T								
JJA-P								
SPEI AUG								
T-SEP								
Full model	11.3	0.02	0.83		21.4	0.005	0.9	
CERNOBBIO	**birch (BP)**				**chesnut (CS)**			
	F	**p**	**R**	**ß**	**F**	**p**	**R**	**ß**
VPD JUN								
VPD JUL								
VPD AUG	7.1	0.04		-0.76	15.4	0.01		-0.87
JJA-T								
JJA-P								
SPEI AUG								
T-SEP								
Full model	7.1	0.04	0.76		15.4	0.01	0.87	
CERNOBBIO	**Beech (FS)**				**Oak-hornbeam hills (CB)**			
	F	**p**	**R**	**ß**	**F**	**p**	**R**	**ß**
VPD JUN	63.9	0.01		-0.9				
VPD JUL	96.5	0.01		-0.75	14.3	0.01		-0.86
VPD AUG								

JJA-T	107.2	0.009		0.5				
JJA-P								
SPEI AUG	60.6	0.01		-0.6				
T-SEP								
Full model	363.5	0.002	0.99		14.3	0.01	0.86	
CERNOBBIO	**ash-oak-hornbeam (OO)**							
	F	**p**	**R**	**ß**				
VPD JUN								
VPD JUL	14.3	0,01		-0.86				
VPD AUG								
JJA-T								
JJA-P								
SPEI AUG								
T-SEP								
Full model	14.3	0,001	0.86					
VALDIDENTRO	**white alder (AI)**				**birch (BP)**			
	F	**p**	**R**	**ß**	**F**	**p**	**R**	**ß**
SPEI JUL	28721.9	0.003		1.6				
SPEI AUG	1979.5	0.01		1.1				
JJA-P	634	0.02		0.69				
P-MAY	5536.4	0.008		-2.3				

P-JUN	5066.9	0.008		-2.17	879.7	0.02		0.38
P-JUL								
P-AUG					2420.2	0.01		-0.66
T-JJA					206.5	0.04		-0.27
T-JUL					2463.8	0.01		-0.83
Full model	7761.4	0.008	0.99		2581.8	0.01	0.99	

3.5 Impact of the extreme year 2022 on biomass production at peak season at intra-community level

The negative impact of the extreme year 2022 on biomass production at peak season (July and August) was evident at Monza (Fig. 7A) and Cernobbio (Fig. 7B). The extreme year 2022 induced the largest summer biomass decrease on oak (QR), oak-hornbeam of the lowlands (UM), oak-hornbeam of the hills and submontane belt (CB), and ash-oak-hornbeam (OO) forests, with the lowest NDVI values (obtained by Landsat) recorded across the investigated decade (2014-2023). The largest impact was observed at Cernobbio on the oak-hornbeam of the hills and sub-montane belt (CB), showing the lowest NDVI values, even lower than what observed at Monza (Fig. 7A, B). Interestingly, at Cernobbio the ash-oak-hornbeam forests (OO) exhibited a large NDVI decrease also in 2023, indicating a legacy effect of the extreme climatic conditions of the summer 2022 on the biomass production of the following year (Fig. 7B). The other forest types at Cernobbio and the deciduous forest at Valdidentro apparently did not show any direct impact of the extreme year 2022 on their peak season biomass production, as its values were similar or just slightly lower than the mean of the decade (Fig. 7C, D). The large decrease of NDVI observed at Valdidentro in 2023 (the lowest NDVI of the entire decade) suggested also at this site the occurrence of a legacy effect of the extreme year 2022 with a delayed response of both the birch dominated forests (BP) and of the white alder forests (AI) to the stress induced by the extreme climatic events of the year 2022. On the other hand, both Monza and Cernobbio the most sensitive forests (QR, UM, CB) exhibited a rapid recovery in the year 2023, with NDVI values close to the mean of the decade (Fig. 7A, B). Notably, also the dry and hot summer 2015 induced a decrease in biomass production of the most sensitive forest types, identified by the decrease of NDVI at peak season (July and August) at Monza and Cernobbio, but this decrease was much less than in 2022 (Fig. 7A, B).

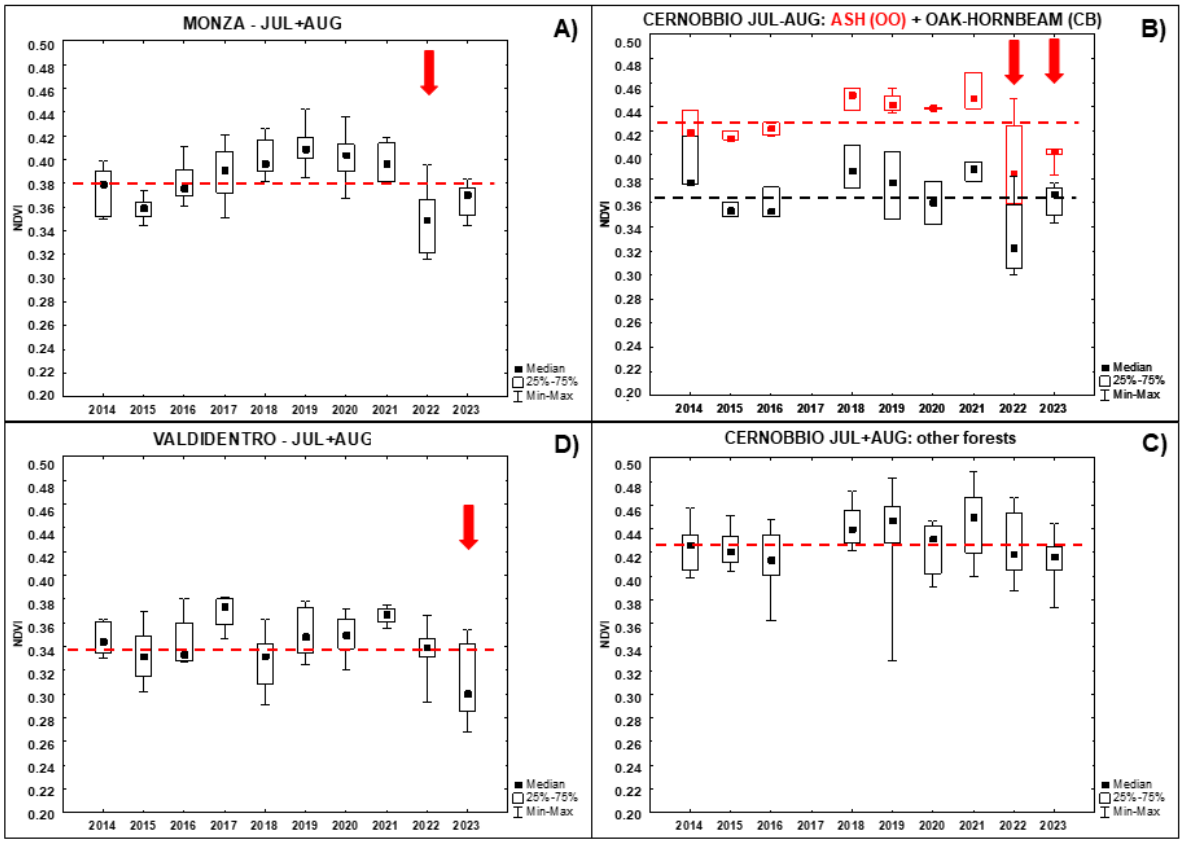

Figure 7. NDVI obtained by Landsat as proxy of biomass production at the peak of the growing season (July and August) in the period 2014-2023 comparing: A) Monza (oak, QR, and oak hornbeam, UM, forests); B) Cernobbio (oak hornbeam of the hills and sub-montane belt, CB (black), and ash-oak-hornbeam, OO (red), forests); C) Cernobbio (all other forest types excluding oak hornbeam); D) Valdidentro (all forest types). The dashed line represents the mean value of NDVI for the period July and August of the decade 2014-2023 for study sites and forest types of the panels A-D. The red arrows indicate the impact of the extreme year 2022 (panels A, B) and its legacy effect on 2023 (panel D).

4. Discussion

4.1 Extreme climatic conditions of the year 2022

Extreme climatic events, with special reference to heatwaves and severe drought, are increasing in the last years, with 2022 being until now the most extreme year, characterized by the warmest and driest summer of the last decades across Europe, and exceeding the conditions recorded in the extreme year 2015 (Hoy et al., 2017; Laaha et al., 2017 da Knutzen). The climatic data of our three study sites confirmed the severity of the conditions recorded in the year 2022, which was recognized as an extreme year across Europe and, in particular in Italy, France and Spain (Tripathy and Mishra, 2023; Gharun et al., 2024; Knutzen et al., 2025). Our data allowed us to assess that the severity of these conditions was not the same across the geographical gradient investigated, as could be expected. In particular, the worst conditions of severe drought and high temperatures (resulting also in the highest vapour pressure deficit) were experienced in

2022 by the lowland site, Monza, in terms of air temperature but above all of precipitation (Figs. 1, 2, 3), followed by Cernobbio, with 2022 being the most extreme year of the last two decades for both sites (Figs. 1, 2). At Valdidentro it is notable that the year 2022 was the most extreme of the last twenty years for air temperature but not for the precipitations (Figs. 1, 2). The data provided by SPEI of the preceding six months (Fig. 4) suggested that the drought conditions were long-lasting across spring and summer. This effect was evident also at Valdidentro, in the alpine zone, where the severity of the extreme year 2022 was more pronounced than could be expected only from the precipitation data, suggesting potentially higher impacts on ecosystems (Fig. 4).

4.2 Impacts of the extreme year 2022 on plant phenology at inter-community level

Forests are particularly vulnerable to the impacts of heat and drought, but their response and degree of sensitivity depend on the forest type, composition and bioclimatic zone (e.g., Pardos et al., 2021). Our analyses, performed at local scale across a geographic gradient from the lowlands to the alpine zone, indicated that the extreme year 2022 produced widespread impacts on the phenology of deciduous woodlands, triggering early crown discoloration at all sites, while it did not affect the onset of the growing season. Indeed, both at inter- and intra-community level, the onset of the growing season exhibited a very small inter-annual variability at the lowland and prealpine sites (Monza and Cernobbio) (Table 1, Fig. 5A), suggesting a strong photoperiodical control of the greening phenophases as the dominant tree species of these forests are late successional long-lived, slowly reproducing plants (Tang et al., 2016). On the other hand, the large inter-annual variability of the growing season onset observed at the alpine site (Valdidentro) is likely influenced by the patterns of snowmelt dates.

The extreme year 2022 triggered the occurrence of early crown discoloration at all sites across the analysed study period both at inter- and intra-community level, with the strongest responses (and sensitivity) at the lowland site (Monza), showing early crown discoloration c. 40 days earlier than the mean date of leaf senescence, and more limited impact at the prealpine (Cernobbio) and alpine (Valdidentro) sites, with advances of c. 15-16 days compared to their mean of the period (Table 1). The highest sensitivity detected at the lowland site is coherent with the occurrence of the worst conditions of long-lasting and severe drought, high temperatures and highest vapour pressure deficit observed at Monza. The smaller impact of the extreme year 2022 observed on the forests located at higher elevation may be due to the thermal gradient, with lower temperatures at higher elevations smoothing the climatic impact on plant phenology (Knutzen et al., 2025). Differently from Knutzen et al. (2025), who reported no o

limited impacts of the extreme year 2022 on forests in the alpine zone, we show that even at higher elevations the deciduous forests were affected by the extreme conditions of the year 2022, with early crown discoloration occurring c. two weeks earlier than the mean date of leaf senescence.

These data confirm the strong negative impact of persistent and severe heat and drought on early crown discoloration produced by a combination of drought and heat stress (e.g. Estiarte and Penuelas, 2015). Combined with drought, a persistent heat exceeding the 30°C growth optimum (Percival, 2023) was observed mainly during July and August 2022. Effects of extreme heat on trees include leaf and twig scorching, sunburn on leaves, branches, and stems, leaf senescence and abscission, inhibition of shoot and root growth and mortality (Teskey et al., 2015; O'Sullivan et al., 2017; Percival and Percival, 2022; Percival, 2023). Furthermore, photosynthesis is affected when leaves exceed their thermal tolerance level (Knight and Ackerly, 2002, Curtis et al., 2014; Percival, 2023): indeed, photosynthesis is recognised as one of the most heat-sensitive processes in plants (Berry and Bjorkman, 1980, Hu et al., 2020, Salvucci and Crafts-Brandner, 2004; Percival, 2023). We can therefore associate early crown discoloration occurred in 2022 to a persistence, extreme warm and dry summer season characterized by high to very high values of vapour pressure deficit which for Monza and Cernobbio where the highest recorded in the last 20 years. These data confirm the findings of previous studies emphasizing the role of high VPD in producing tree defoliation and even mortality (e.g., Pollastrini et al., 2019; Braun et al., 2021; Gazol and Camarero, 2022; Bussotti et al., 2024) Prolonged drought and heat have already caused widespread forest mortality throughout the 1990 s and 2000s across several Mediterranean regions within Europe (Allen et al., 2010; Percival, 2023, Knutzen et al., 2025). During the summer of 2003, air temperatures of almost 40◦C were recorded across northern France and southern Germany coinciding with the depletion of soil water reserves. The combined heat and drought stress caused foliage yellowing and browning, branch die-back, premature leaf loss, and tree death across forest stands. Oak, fir, spruce, beech, and pine were severely affected, raising concern about the consequences for long-term forest health. Comparable heat stress and drought episodes resulted in large-scale tree mortality of Scots pine stands throughout Switzerland and Italy (Bigler et al., 2006, Dobbertin and Rigling, 2006, Vertui and Tagliaferro, 1998; Percival, 2023).

4.3 Impacts and drivers of the extreme year 2022 on plant phenology at intra-community level

The analyses performed at intra-community level indicated different sensitivity and resilience, linked to their ecological requirements, of the investigated forest types to the impact of the extreme year 2022 and highlighted that the drivers triggering the observed early crown discoloration were different (Fig. 5, Table 2).

The termophilous forests of the lowlands (oak (QR) and oak-hornbeam (UM) at Monza) (Fig. 5) exhibited the highest sensitivity toc the impact of heat and drought, as could be expected as these forests grow in riparian and moist environments associated to the Lambro river and its fluvial terraces (Prodrome of the Italian Vegetation https://www.prodromo-vegetazione-italia.org/; Italian interpretation manual of the 92/43/EEC Directive Habitats http://vnr.unipg.it/habitat/).

The conditions of the summer 2022 were so extreme to exert visible impacts also on the forests of the prealpine and alpine sites, typical of cool and moist conditions, such as the beech (FS), green alder (AA), white alder (AI), and birch (BP) forests, or typical of temperate and moist conditions like the ash-oak-hornbeam forest (OO) (Prodrome of the Italian Vegetation https://www.prodromo-vegetazione-italia.org/; Italian interpretation manual of the 92/43/EEC Directive Habitats http://vnr.unipg.it/habitat/). Interestingly, at Cernobbio vapour pressure deficit in summer (July and August) was the driver of early crown discoloration for all the selected forest types. At Cernobbio the early crown discoloration of the beech forest (FS) was influenced also by summer temperature and persistent drought (SPEI-August), suggesting a slightly different sensitivity of beech compared to the other selected forest types.

Extreme climatic events may induce legacy effects, provided by negative impacts observed the year following the extreme event. Extreme drought events occurring during the growth season may influence post-drought tree growth, causing damage to the photosynthetically active leaf area and limiting the photosynthesis (Magnani et al., 2000; Bréda et al., 2006; Galvez et al., 2011; Keith et al., 2012; Huang et al., 2018). Consequently, the ring width of trees is expected to be reduced over the years following a severe drought (Bréda et al., 2006; Keith et al., 2012; Palacio et al., 2014; Huang et al., 2018).

Interestingly, at all sites the early crown discoloration observed in 2022 did not trigger any legacy effect on the greening of the following year, indicating that the onset of the growing season was not influenced by the events of the previous summer, and differently from what observed in other European deciduous forests (e.g., Brun et al., 2020).

In our case, the occurrence of potential legacy effects of the extreme year 2022 on plant phenology was evident only on the patterns of leaf senescence of the following year. We observed a direct relation between sensitivity and resilience to the impact of the extreme year 2022. Indeed, the forests of the lowland site Monza exhibited the highest sensitivity and the highest resilience, as confirmed by the absence of any legacy effect in the following year (2023). The lack of legacy effect at Monza is coherent with the observation that drought-adapted ecosystems are characterized by high sensitivity but also high resilience (Knutzen et al., 2025). On the contrary, despite the direct impact on early crown discoloration in 2022 was less intense than at Monza, both at Cernobbio and Valdidentro we observed a clear legacy effect, with the occurrence of advanced leaf senescence even in 2023, which was not an extreme year (Table 1), indicating a poor resilience of the deciduous forests at these sites. The largest legacy effect was observed for forest types typical of cool and moist conditions, such as the beech (FS), green alder (AA), white alder (AI), and birch (BP), suggesting that the impact of the stress induced by the harsh climatic conditions of the summer 2022 affected on a longer timescale these forests. Our data then confirm that the forests with phenological higher sensitivity are also those with higher resilience (Knutzen et al., 2025).

4.4 Impacts of the extreme year 2022 on biomass production

NDVI is a structural index, and its seasonal changes reflect changes in leaf biomass and could be used as a proxy of biomass production (e.g. Descals et al., 2020, 2022). The decrease of biomass production (desumed by the strong NDVI decrease) at peak season (July and August) in 2022 further emphasized the different sensitivity and resilience of the analysed forest types across the investigated gradient. As could be expected, the forests of the lowlands (UM, QR) and the mesophilous (CB) and thermophilous forests (OO) of the prealpine site exhibited the largest biomass decrease in 2022. The other forest types apparently were not influenced by the extreme conditions of 2022, as we didn't detect any decrease of biomass production at peak season. However, a legacy effect of the extreme conditions of 2022 was evident for the thermophilous ash-oak-hornbeam forest (OO) and, unexpectedly, for the forests of the moist and cool alpine site (AI, BP), with reduced biomass production at peak season in 2023 (Fig. 6). Both the immediate and delayed observed decreases of biomass production can be explained considering that extreme drought events affect photosynthesis and vegetative growth (Ciais et al., 2005; McDowell et al., 2008; Barbeta et al., 2015; Wu et al., 2017) inducing both an immediate reduction in photosynthesis, but also delayed long-lasting effects (McDowell et al., 2008; Anderegg et al., 2015; Wu et al., 2017), such as loss of carbon stocks, increased pathogen attacks, hydraulic failure, and forest mortality (Breshears et al., 2005; Allen et al., 2010, 2015;

Wu et al., 2017). Moreover, it is likely that the large leaf senescence advance occurred in 2022 may have induced a decline of forest primary productivity, as observed during the 2018 drought event in Switzerland (Gharun et al., 2020).

In a scenario of increasing frequency and severity of heat and drought events, the assessment of the impact of these extreme climatic events on forests through remote sensing analysis, can provide important information on forest sensitivity and resilience even in difficult-to-reach areas.

This study highlights the differential sensitivity of deciduous forests across an elevation gradient in Northern Italy to one of the most extreme climate events of the last decades, with severe drought conditions lasting in the year 2022 throughout spring and summer. Our analyses indicate different sensitivity and resilience of the different forest types, linked to their ecological requirements. In particular, the lowland thermophilus forests were the most affected by the impact of heat and drought, with early crown discoloration up to 40 days compared to the mean leaf senescence date, but exhibiting the highest resilience. In the forest types at higher elevations and moist conditions we identified a legacy effect in 2023, indicating prolonged stress from the extreme conditions of 2022 and poor resiliency. We observed also that the early crown discoloration of the previous summer did not influence the onset of the growing season of the following year.

These results show the complexity of forest ecosystem responses to climate change, highlighting the need for site-specific and complex assessments. To better understand the impact of drought on plants, further investigations should be carried out, in particular future research may focus on dendrochronological analyses to obtain long-term information about the impact of climate, in particular of heat waves and drought, on tree growth. Indeed, the identification of climate change impacts on different forest types at different sites is essential for future land management and to promote site-specific and forest-specific conservation and adaptation strategies.

Supplementary materials

Table 1. Forest types selected at each study site according to the Lombardy Region Forest Map. For each forest type is reported the code (of the Lombardy Region Forest Map), the dominant species, and their correspondence to the main vegetation groupds according to the Prodrome of the Italian vegetation, Eunis habitats, Nature 200 habitats and Corine Biotopes habitats. Site legend: M = Monza; C = Cernobbio; V = Valdidentro.

Site	Acronym	Forest map code	Forest map type	Dominant species	Prodrome of the Italian Vegetation	Eunis	Nature 2000	Corine Biotopes
M	UM	3	Oak-hornbeam forests of the lowlands	*Quercus robur, Carpinus betulus, Ulmus minor, Fraxinus angustifolia, F. excelsior*	71.1.10.2 Suball. *Ulmenion minoris*	G1.A1 - *Quercus sp., Fraxinus sp., Carpinus betulus* forests on eutrophic and mesotrophic soils	91F0 Riparian mixed forests of Quercus robur, Ulmus laevis and Ulmus minor, Fraxinus excelsior or Fraxinus angustifolia, along the great rivers (Ulmenion minoris)	44.4 Mixed oak-elm-ash woodland of great rivers
M	QR	10	Oak (*Quercus robur*) dominated acidophilous forests of the foothills	*Quercus robur, Q. petraea*	71.1.6 All. *Carpinion betuli*	G1.88 - *Quercus* dominated acidophilous forests of the foothills	9160 Sub-Atlantic and medio-European oak or oak hornbeam forests of the *Carpinion betuli*	41.59 Insubrian acidophilous oak forests
C	CB	5	Oak-hornbeam forests of the hills and sub-montane belt	*Quercus petraea, Q. robur, Carpinus betulus*	71.1.6 All. *Carpinion betuli*	G1.8 Sub-continental oak-hornbeam forests	9160 Sub-Atlantic and medio-European oak or oak hornbeam forests of the *Carpinion betuli*	41.26 Sub-continental oak-hornbeam forests
C	CS	50	Chesnut forests on calcareous soils	*Castanea sativa*	71.1.6 All. *Carpinion betuli*	G1.7D5 – Woodlands and forests with *Castanea sativa*	9260 *Castanea sativa* woods	41.9 Chestnut woods
C	OO	65	Ash-oak-hornbeam forests (Typical *Orno-Ostryetum*)	*Ostrya carpinifolia, Fraxinus*	71.3.2 All. *Carpinion orientalis*	*G1.74 Italo-Illyrian [Ostrya carpinifolia]*	91H0 Pannonian woods with *Quercus pubescens*	41.7374 Pannonian

				ornus, Quercus pubescens	71.3.2.8 Suball. *Helleboro nigri-Ostryenion carpinifoliae*	*sub-thermophilous [Quercus] woods*		white oak woods
C	TA	72, 73	Ash-maple-hornbeam forest and typical ash-maple forest dominated by *Acer* spp., *Fraxinus ornus, Ostrya carpinifolia*	*Acer spp., Fraxinus ornus, Ostrya carpinifolia*	71.1.4 All. *Tilio platyphylli-Acerion pseudoplatani* 71.1.4.1 Suball. *Ostryo carpinifoliae-Tilienion platyphylli*	G1.A4 Ravine and slope woodland and G1.A1 *Quercus-Fraxinus-Carpinus betulus* woodland	9180 *Tilio-Acerion* forests of slopes, screes and ravines	41.43 Alpine and peri-Alpine slope forests
C, V	BP	84, 86	Birch forest dominated by *Betula pendula*	*Betula pendula*	71.4.1 All. *Corilo avellanae-Populion tremulae*	G1.92 *Populus tremula* woodland	NA	NA
C	FS	97	Typical beech forests of the calcareous soils (Mountain Beech forests)	*Fagus sylvatica*	71.1.1 All. *Galio odorati-Fagion sylvaticae*	G1.63 - European neutrophilous forests dominated by *Fagus sylvatica*	9130 *Asperulo-Fagetum* beech forests	41.133 - Medio-European montane neutrophilous beech forests
V	AI	175	White alder forests	*Alnus incana*	71.1.10 All. *Alnion incanae*	G1.12 Boreo-alpine riparian galleries	91E0 Alluvial forests with *Alnus glutinosa* and *Fraxinus excelsior*	44.2 - Boreo-alpine riparian galleries
C	AA	176	Green alder forests	*Alnus alnobetula*	66.1.1 All. *Alnion viridis*	F2.32 - Subalpine and oroboreal [*Salix*] brush	4080 Sub-Arctic *Salix spp.* scrub	

Table 2SM. Mean monthly air temperatures (°C) at each study site (Monza, Cernobbio, Valdidentro) in the period 2004-2023.

MONZA					
Year	**May**	**June**	**July**	**August**	**September**
2004	15.5	21.3	22.5	22.3	18.6
2005	18.1	21.9	22.8	20.1	18.5
2006	17.2	21.7	25.3	20.1	19.4
2007	17.9	21	23.4	21.3	17
2008	17.2	20.7	22.2	22.2	17.2
2009	19.4	21	22.9	24.1	19.5
2010	16	21.2	24.6	21.1	17.1
2011	19	20.6	22	23.9	20.5
2012	17	22.5	24.3	**25.3**	18.4
2013	15.2	21	24.6	23.1	18.7
2014	16.8	21.3	21.2	20.6	18.3
2015	18	22.4	27.3	23.8	18
2016	16	20.5	23.9	22.5	20.1
2017	17.7	23.1	23.7	24.2	16.5
2018	18.3	22.4	24.3	23.9	19.7
2019	14.5	23.9	24.7	23.7	18.6
2020	18.2	20.5	24	23.6	19.2
2021	15.81	23.3	23.6	22.7	19.7
2022	**19.8**	**24.7**	**27.3**	**25**	18.8
2023	17.4	22.8	24.5	24.3	**20.5**
CERNOBBIO					
Year	**May**	**June**	**July**	**August**	**September**
2004	18.9	21.9	22.9	23.1	20
2005	18.1	22.3	23.9	21.7	19.2
2006	17.4	22.3	25.7	21.1	20.5
2007	18.4	21	24.1	21.7	18.1
2008	16.9	20.7	22.8	23.2	17.6
2009	19.5	21.3	23.5	24.9	20
2010	15.7	21.1	25.4	22.1	18
2011	19.1	20.4	22	24.8	21.8
2012	17.2	22.5	24.4	25.8	19.8
2013	15	21.2	25.2	24.2	20.1
2014	17.2	21.3	21.4	20.9	19.6
2015	17.8	22.6	27.4	24.3	18.9
2016	16.1	20.7	24.4	23.5	21.4
2017	18.1	23.5	24.5	24.8	18
2018	17.8	22.9	25.1	25.2	21.4
2019	15.1	24.3	26	24.5	20.4

2020	18.8	20.9	24.7	24.7	20.7
2021	16.2	23.7	24	23.6	21
2022	**19.9**	**24.5**	**27.7**	**26.1**	20.4
2023	17.5	23.2	25.1	25.3	**21.9**
VALDIDENTRO					
Year	**May**	**June**	**July**	**August**	**September**
2004	2.4	7.4	8.2		5.7
2005	4.8	8.6	9	7.6	6.7
2006	3.9	8.5	12.6	5.9	5.7
2007	4.8	8.3	9.8	9	4.7
2008	4.6	8.7	9.5	10.2	5.2
2009	6.3	7.8	10	11.5	7.7
2010	2.5	8	11.6	8.8	5.3
2011	5.4	7.9	8.1	11.1	9.8
2012	4.5	9.1	10.4	11.8	6.3
2013	1.9	7	11.4	10.2	7
2014	3.3	8	8.8	7.5	6.5
2015	4.9	8.6	13.6	11	4.7
2016	2.8	7.3	10.7	10.3	7.8
2017	5.1	10.3	10.5	11.6	4
2018	5.7	9.1	11.4	11.4	8.5
2019	1.7	11.7	11.7	10.9	7.4
2020	5	7.3	11	10.9	7.4
2021	2.1	10.2	10.3	9.2	7.8
2022	6.8	10.9	12.8	11.5	5.2
2023	4.7	9.6	11.4	11.4	9.9

Table 3SM. Number of days with extreme temperatures (TX90P, exceeding the 90th percentile of the decade 2004-2023) for each summer month (June, July, August) and the total summer value, in the three study areas (Monza, Cernobbio and Valdidentro) in the period 2004-2023.

	MONZA				CERNOBBIO				VALDIDENTRO			
Year	**June**	**July**	**August**	**Total**	**June**	**July**	**August**	**Total**	**June**	**July**	**August**	**Total**
2004	0	0	0	0	0	2	0	2	0	NA	0	0
2005	2	0	0	2	3	3	0	6	3	3	0	6
2006	0	6	0	6	0	8	0	8	2	6	0	8
2007	0	0	0	0	0	5	0	5	0	5	0	5
2008	0	0	0	0	1	0	0	1	4	0	0	4
2009	0	0	2	2	0	0	5	5	0	1	2	3
2010	0	3	0	3	0	8	0	8	0	9	2	11
2011	0	0	4	4	0	0	8	8	2	0	6	8
2012	1	2	9	12	2	2	8	12	2	2	6	10
2013	2	3	3	8	1	6	6	13	2	2	6	10
2014	1	0	0	1	1	0	0	1	3	0	0	3
2015	0	19	5	24	1	18	7	26	0	16	7	23
2016	0	3	0	3	1	2	0	3	2	2	4	8
2017	4	2	5	11	5	1	6	12	6	3	5	14
2018	0	2	8	10	0	1	6	7	0	2	4	6
2019	6	12	1	19	5	4	1	10	6	5	1	12
2020	0	4	7	11	0	3	2	5	0	4	3	7
2021	0	3	4	7	0	0	3	3	2	0	4	6
2022	**5**	**18**	**9**	**32**	**6**	**18**	**8**	**32**	**3**	**12**	**2**	**17**
2023	5	8	10	23	0	7	8	15	2	6	8	16

Table 4SM. Monthly total liquid precipitation (mm) at each study site (Monza, Cernobbio, Valdidentro) in the period 2004-2023.

MONZA					
Year	**May**	**June**	**July**	**August**	**September**
2004	127.7	33.5	90.7	91.1	31
2005	49.7	24.9	140.8	118.6	136.4
2006	62.3	6.6	80.3	167.5	5.7
2007	162.7	190.2	46.7	103.1	178.5
2008	240.2	137.6	181.6	74.6	127.4
2009	10.4	166.5	70.2	49.9	79.8
2010	196.5	109.4	86.5	219.4	154.4
2011	47.8	159.8	103.8	60	144.2
2012	149	156.8	**13.4**	48.4	133.2
2013	290	50.6	47	69.4	47.4
2014	59.6	278.6	237.4	177.6	21.2
2015	88.6	82.2	**6.4**	83.4	128.6
2016	200.6	282	150.4	79	57
2017	189.6	225	61.8	24.8	282.8
2018	120.4	40.8	163.2	134.6	27.8
2019	155.4	88.8	106.2	139.2	79
2020	161	304.2	84.6	84.8	108
2021	143.2	37.8	120.6	92.6	93
2022	**56.6**	**48.2**	**18.8**	125.8	**69.4**
2023	178	176	177.2	85	59
CERNOBBIO					
Year	**May**	**June**	**July**	**August**	**September**
2004	171.8	30.2	57	146.4	47.2
2005	50	47.8	93.4	129.2	150.8
2006	46.6	13.2	118.2	126	190.8
2007	128.6	186.2	22.4	217.8	137
2008	233.4	201.2	191.4	106.8	129.2
2009	39	105.4	161.8	44	124.8
2010	362.6	63.6	71	178.8	156.8
2011	76.2	156.2	124.8	19.4	147.4
2012	108.8	91.4	84.6	37.4	111.4
2013	257.2	71.2	72.6	32	118.2
2014	42.4	140.6	285.8	312.2	26.6
2015	126.6	115	29.2	82.2	176
2016	251.8	148.6	211	70	110.4
2017	157.2	258	63.6	65.2	153
2018	258.2	34.2	76.4	63.6	23
2019	114.8	45.8	43.2	133	60.2
2020	145.8	211.2	42.2	162	104
2021	160.6	20.8	286.4	133	107.4

2022	83.2	**57.8**	**14**	**36.6**	186.4
2023	178	242	175	90.2	160.8
VALDIDENTRO					
Year	**May**	**June**	**July**	**August**	**September**
2004	73.2	41.2	124.6	0	37
2005	71.2	58.4	87.8	111.6	68.6
2006	62.2	55.8	86.6	158.6	74.4
2007	110.8	134.6	148.4	191.2	55.4
2008	136.4	130.2	291.8	118	148.2
2009	29.8	151.6	124.4	67.8	56.6
2010	164.8	73	74	173.6	143.6
2011	108	205.4	178.4	106.2	64
2012	59.8	194.4	156.4	193	222.8
2013	152	89.6	80	165.2	92.2
2014	71.8	129.6	204.6	199.6	58.8
2015	156	109.6	42.6	136.6	267.4
2016	136.8	302.6	161.2	155.4	53.2
2017	95.2	295.2	111	172.2	212
2018	107.6	61.4	134.6	135.8	63
2019	88	105.6	104	160.2	93.8
2020	120.8	211	93.4	343.2	88.4
2021	112	68.2	219.2	149.8	69.4
2022	**78.2**	142	131.4	**72.8**	130.8
2023	130.4	108	178.8	265.4	158.6

References

Affandy, N.A., Anwar, N., Maulana, M.A., Prastyo, D.D., Kurniawan, A., Suryadi, F.X., 2023. Forecasting meteorological drought through SPEI with SARIMA model, in: AIP Conference Proceedings. Presented at the XVII MEXICAN SYMPOSIUM ON MEDICAL PHYSICS, AIP Publishing, Veracruz, México. https://doi.org/10.1063/5.0154230

Allen, C. D., Breshears, D. D., and McDowell, N. G.: On underesti mation of global vulnerability to tree mortality and forest die-off from hotter drought in the Anthropocene, Ecosphere, 6, 1–55, https://doi.org/10.1890/ES15-00203.1, 2015.

Baronetti, A., Menichini, M., Provenzale, A., 2023. Vegetation response to droughts: The case of northern Italy. Int. J. Climatol. 44, 501–520. https://doi.org/10.1002/joc.8340

Bastos, A., et al., 2020. Direct and seasonal legacy effects of the 2018 heat wave and drought on European ecosystem productivity. Sci. Adv. 6 (24).

Beguería, S., Vicente-Serrano, S.M., Reig, F., Latorre, B., 2014. Standardized precipitation evapotranspiration index (SPEI) revisited: parameter fitting, evapotranspiration models, tools, datasets and drought monitoring. Int. J. Climatol. 34, 3001–3023. https://doi.org/10.1002/joc.3887

Bigler, C., Vitasse, Y., 2021. Premature leaf discoloration of European deciduous trees is caused by drought and heat in late spring and cold spells in early fall. Agric. For. Meteorol. 307, 108492. https://doi.org/10.1016/j.agrformet.2021.108492

Braun S, Hopf S-E, Tresch S, Remund J and Schindler C. 2021. 37 Years of Forest Monitoring in Switzerland: Drought Effects on Fagus sylvatica. Front. For. Glob. Change 4:765782. doi: 10.3389/ffgc.2021.765782

Breshears, D.D., Cobb, N.S., Rich, P.M., Price, K.P., Allen, C.D., Balice, R.G., Romme, W.H., Kastens, J.H., Floyd, M.L., Belnap, J., Anderson, J.J., Myers, O.B., Meyer, C.W., 2005. Regional vegetation die-off in response to global-change-type drought. Proc. Natl. Acad. Sci. 102, 15144–15148. https://doi.org/10.1073/pnas.0505734102

Brun, P., Psomas, A., Ginzler, C., Thuiller, W., Zappa, M., & Zimmermann, N. E., 2020. Large-scale early-wilting response of Central European forests to the 2018 extreme drought. Glob. Change Biol., 26(12), 7021-7035. https://doi-org.insubria.idm.oclc.org/10.1111/gcb.15360

Bucha, T., Pavlenda, P., Konôpka, B., Tomaštík, J., Chudá, J., Surový, P., 2024a. Satellite Assessment of Forest Health in Drought Conditions: A Novel Approach Combining Defoliation and Discolouration. Forests 15, 1567. https://doi.org/10.3390/f15091567

Bucha, T., Pavlenda, P., Konôpka, B., Tomaštík, J., Chudá, J., Surový, P., 2024b. Identification of drought-induced forest damage in 2022 and of its key site condition drivers through satellite imagery. Cent. Eur. For. J. 70, 156–175. https://doi.org/10.2478/forj-2024-0013

Bussotti F, Papitto G, Di Martino D, Cocciufa C, Cindolo C, Cenni E, Bettini D, Iacopetti G, Ghelardini L, Moricca S, Panzavolta T, Bracalini M, Pollastrini M. 2024. Extreme climatic events, biotic interactions and species-specific responses drive tree crown defoliation and mortality in Italian forests. iForest 17: 300-308. https://doi.org/10.3832/ifor4531-017

Camarero, J., Franquesa, M., Sangüesa-Barreda, G., 2015. Timing of drought triggers distinct growth responses in Holm Oak: implications to predict warming-induced forest defoliation and growth decline. Forests 6, 1576–1597. https://doi.org/10.3390/f6051576

Castellaneta M., Rita A., Camarero J.J, Colangelo M. Ripullone F.2022. Declines in canopy greenness and tree growth are caused by combined climate extremes during drought-induced dieback. Science of The Total Environment, 813: 152666. https://doi.org/10.1016/j.scitotenv.2021.152666

Choat, B., Jansen, S., Brodribb, T.J., Cochard, H., Delzon, S., Bhaskar, R., Bucci, S.J., Feild, T.S., Gleason, S.M., Hacke, U.G., Jacobsen, A.L., Lens, F., Maherali, H., Martínez-Vilalta, J., Mayr, S., Mencuccini, M., Mitchell, P.J., Nardini, A., Pittermann, J., Pratt, R.B., Sperry, J.S., Westoby, M., Wright, I.J., Zanne, A.E., 2012. Global convergence in the vulnerability of forests to drought. Nature 491, 752–755. https://doi.org/10.1038/nature11688

Choler, P., 2023. Above-treeline ecosystems facing drought: lessons from the 2022 European summer heat wave. Biogeosciences 20, 4259–4272. https://doi.org/10.5194/bg-20-4259-2023

Ciais, P., et al., 2005. Europe-wide reduction in primary productivity caused by the heat and drought in 2003. Nature 437, 529–533.

Coumou, D, and Rahmstorf, S. 2012. A decade of weather extremes. Nat. Clim. Chang. 2.7: 491-496. https://doi-org.insubria.idm.oclc.org/10.1038/nclimate1452

Descals, A., Verger, A., Yin, G., Peñuelas, J., 2020. Improved Estimates of Arctic Land Surface Phenology Using Sentinel-2 Time Series. Remote Sens. 12, 3738. https://doi.org/10.3390/rs12223738

Descals, A., Verger, A., Yin, G., Filella, I., Penuelas, J., 2023. Widespread drought-induced leaf shedding and legacy effects on productivity in European deciduous forests. Remote Sens. Ecol. Conserv. 9.1: 76-89. https://doi-org.insubria.idm.oclc.org/10.1002/rse2.296

Engelbrecht, B.M.J., 2012. Forests on the brink. Nature 491, 675–676. https://doi.org/10.1038/nature11756

Estiarte, M., Peñuelas, J., 2015. Alteration of the phenology of leaf senescence and fall in winter deciduous species by climate change: effects on nutrient proficiency. Glob. Change Biol. 21, 1005–1017. https://doi.org/10.1111/gcb.12804

European Commission. Joint Research Centre., 2023. Drought in Europe: March 2023: GDO analytical report. Publications Office, LU.

Fracheboud, Y., Luquez, V., Björkén, L., Sjödin, A., Tuominen, H., Jansson, S., 2009. The Control of Autumn Senescence in European Aspen. Plant Physiol. 149, 1982–1991. https://doi.org/10.1104/pp.108.133249

Fridley, J.D., 2012. Extended leaf phenology and the autumn niche in deciduous forest invasions. Nature 485, 359–362. https://doi.org/10.1038/nature11056

Gazol A., Camarero J.J., 2022. Compound climate events increase tree drought mortality across European forests. Science of the Total Environment, 816: 151604. https://doi.org/10.1016/j.scitotenv.2021.151604

Gharun, M., Shekhar, A., Xiao, J., Li, X., Buchmann, N., 2024. Effect of the 2022 summer drought across forest types in Europe. Biogeosciences 21, 5481–5494. https://doi.org/10.5194/bg-21-5481-2024

Giglio, L., Schroeder, W., Justice, C.O., 2016. The collection 6 MODIS active fire detection algorithm and fire products. Remote Sens. Environ. 178, 31–41. https://doi.org/10.1016/j.rse.2016.02.054

Gouveia, C.M., Trigo, R.M., Beguería, S., Vicente-Serrano, S.M., 2017. Drought impacts on vegetation activity in the Mediterranean region: An assessment using remote sensing data and multi-scale drought indicators. Glob. Planet. Change 151, 15–27. https://doi.org/10.1016/j.gloplacha.2016.06.011

Grabska-Szwagrzyk, E., Tymińska-Czabańska, L., 2024. Sentinel-2 time series: a promising tool in monitoring temperate species spring phenology. For. Int. J. For. Res. 97, 267–281. https://doi.org/10.1093/forestry/cpad039

Granero-Belinchon, C., Adeline, K., Lemonsu, A., Briottet, X., 2020. Phenological Dynamics Characterization of Alignment Trees with Sentinel-2 Imagery: A Vegetation Indices Time Series Reconstruction Methodology Adapted to Urban Areas. Remote Sens. 12, 639. https://doi.org/10.3390/rs12040639

Gross, J.E., Goetz, S.J., Cihlar, J., 2009. Application of remote sensing to parks and protected area monitoring: Introduction to the special issue. Remote Sens. Environ. 113, 1343–1345. https://doi.org/10.1016/j.rse.2008.12.013

Hartmann, H., Bastos, A., Das, A.J., Esquivel-Muelbert, A., Hammond, W.M., Martínez-Vilalta, J., McDowell, N.G., Powers, J.S., Pugh, T.A.M., Ruthrof, K.X., Allen, C.D., 2022. Climate Change Risks to Global Forest Health: Emergence of Unexpected Events of

Elevated Tree Mortality Worldwide. Annu. Rev. Plant Biol. 73, 673–702. https://doi.org/10.1146/annurev-arplant-102820-012804

Hermann, M., Röthlisberger, M., Gessler, A., Rigling, A., Senf, C., Wohlgemuth, T., Wernli, H., 2023. Meteorological history of low-forest-greenness events in Europe in 2002–2022. Biogeosciences 20, 1155–1180. https://doi.org/10.5194/bg-20-1155-2023

Hmimina, G., Dufrêne, E., Pontailler, J.-Y., Delpierre, N., Aubinet, M., Caquet, B., De Grandcourt, A., Burban, B., Flechard, C., Granier, A., Gross, P., Heinesch, B., Longdoz, B., Moureaux, C., Ourcival, J.-M., Rambal, S., Saint André, L., Soudani, K., 2013. Evaluation of the potential of MODIS satellite data to predict vegetation phenology in different biomes: An investigation using ground-based NDVI measurements. Remote Sens. Environ. 132, 145–158. https://doi.org/10.1016/j.rse.2013.01.010

IPCC. (2021). Climate change 2021: The physical science basis. In V. Masson- Delmotte, P. Zhai, A. Pirani, S. L. Connors, C. Pean, S. Berger, N. Caud, Y. Chen, L. Goldfarb, M. I. Gomis, M. Huang, K. Leitzell, E. Lonnoy, J. B. R. Matthews, T. K. Maycock, T. Waterfield, O. Yelekci, R. Yu, & B. Zhou (Eds.), Contribution of Working Group I to the Sixth Assessment Report of the Intergovernmental Panel on Climate Change. Cambridge University Press.

ISTAT. 2020. Glossario_Dati-meteoclimatici_Anno2020, 2020. https://www.istat.it/wpcontent/uploads/2021/11/Glossario_Dati-meteoclimatici_Anno2020.pdf

Keskitalo, J., Bergquist, G., Gardeström, P., Jansson, S., 2005. A Cellular Timetable of Autumn Senescence. Plant Physiol. 139, 1635–1648. https://doi.org/10.1104/pp.105.066845

Knutzen, F., Averbeck, P., Barrasso, C., Bouwer, L.M., Gardiner, B., Grünzweig, J.M., Hänel, S., Haustein, K., Johannessen, M.R., Kollet, S., Pietikaeinen, J.-P., Pietras-Couffignal, K., Pinto, J.G., Rechid, D., Rousi, E., Russo, A., Suarez-Gutierrez, L., Wendler, J., Xoplaki, E., Gliksman, D., 2023. Impacts and damages of the European multi-year drought and heat event 2018–2022 on forests, a review. https://doi.org/10.5194/egusphere-2023-1463

Knutzen, F., Averbeck, P., Barrasso, C., Bouwer, L.M., Gardiner, B., Grünzweig, J.M., Hänel, S., Haustein, K., Johannessen, M.R., Kollet, S., Müller, M.M., Pietikäinen, J.-P., Pietras-Couffignal, K., Pinto, J.G., Rechid, D., Rousi, E., Russo, A., Suarez-Gutierrez, L., Veit, S., Wendler, J., Xoplaki, E., Gliksman, D., 2025. Impacts on and damage to European forests

from the 2018–2022 heat and drought events. Nat. Hazards Earth Syst. Sci. 25, 77–117. https://doi.org/10.5194/nhess-25-77-2025

Kowalski, K., Senf, C., Hostert, P., Pflugmacher, D., 2020. Characterizing spring phenology of temperate broadleaf forests using Landsat and Sentinel-2 time series. Int. J. Appl. Earth Obs. Geoinformation 92, 102172. https://doi.org/10.1016/j.jag.2020.102172

Landsat 8 (L8) Science Data Users Handbook Version 2; Department of the Interior U.S. Geological Survey: Washington, DC, USA, 2016.

Lim, P. O., Kim, H. J., & Gil Nam, H., 2007. Leaf senescence. Annu. Rev. Plant Biol., 58(1), 115-136. https://doi-org.insubria.idm.oclc.org/10.1146/annurev.arplant.57.032905.105316

Lindner, M., Maroschek, M., Netherer, S., Kremer, A., Barbati, A., Garcia-Gonzalo, J., Seidl, R., Delzon, S., Corona, P., Kolström, M., Lexer, M.J., Marchetti, M., 2010. Climate change impacts, adaptive capacity, and vulnerability of European forest ecosystems. For. Ecol. Manag. 259, 698–709. https://doi.org/10.1016/j.foreco.2009.09.023

Löw, M., Koukal, T., 2020. Phenology Modelling and Forest Disturbance Mapping with Sentinel-2 Time Series in Austria. Remote Sens. 12, 4191. https://doi.org/10.3390/rs12244191

McDowell, N.G., Sevanto, S., 2010. The mechanisms of carbon starvation: how, when, or does it even occur at all? New Phytol.186, 264–266. https://doi.org/10.1111/j.1469-8137.2010.03232.x

Menzel, A., Sparks, T.H., Estrella, N., Koch, E., Aasa, A., Ahas, R., Alm-Kübler, K., Bissolli, P., Braslavská, O., Briede, A., Chmielewski, F.M., Crepinsek, Z., Curnel, Y., Dahl, Å., Defila, C., Donnelly, A., Filella, Y., Jatczak, K., Måge, F., Mestre, A., Nordli, Ø., Peñuelas, J., Pirinen, P., Remišová, V., Scheifinger, H., Striz, M., Susnik, A., Van Vliet, A.J.H., Wielgolaski, F., Zach, S., Zust, A., 2006. European phenological response to climate change matches the warming pattern. Glob. Change Biol. 12, 1969–1976. https://doi.org/10.1111/j.1365-2486.2006.01193.x

Min, S.-K., Zhang, X., Zwiers, F.W., Hegerl, G.C., 2011. Human contribution to more-intense precipitation extremes. Nature 470, 378–381. https://doi.org/10.1038/nature09763

Pace, G., Gutiérrez-Cánovas, C., Henriques, R., Boeing, F., Cássio, F., Pascoal, C., 2021. Remote sensing depicts riparian vegetation responses towater stress in a humid Atlantic

region. Sci. Total Environ. 772 (2021) 145526. https://doi.org/10.1016/j.scitotenv.2021.145526

Pollastrini M, Puletti N, Selvi F, Iacopetti G and Bussotti F. 2019. Widespread crown defoliation after a drought and heat wave in the forests of Tuscany (central Italy) and their recovery—A case study from summer 2017. Front. For. Glob. Change 2:74. doi: 10.3389/ffgc.2019.00074

Puletti N., Mattioli W., Bussotti F., Pollastrini M. 2019. Monitoring the effects of extreme drought events on forest health by Sentinel-2 imagery. Journal of Applied Remote Sensing, 13(2): 020501-1

Quesada-Ruiz, L. C., Caparros-Santiago, J. A., Garcia-Perez, M. A., & Rodriguez-Galiano, V., 2021. "Characterising the spring and autumn land surface phenology of Macaronesian species using Sentinel-2 data: the case of Canary Island." Presented at the Remote Sensing for Agriculture, Ecosystems, and Hydrology XXIII. Vol. 11856. SPIE. https://doi.org/10.1117/12.2600125

R Core Team. 2016. R: A Language and Environment for Statistical Computing. R Foundation for Statistical Computing, Vienna, Austria. https://www.R-project.org/

Rahmstorf, S., Coumou, D., 2011. Increase of extreme events in a warming world. Proc. Natl. Acad. Sci. 108, 17905–17909. https://doi.org/10.1073/pnas.1101766108

Richardson, A.D., Andy Black, T., Ciais, P., Delbart, N., Friedl, M.A., Gobron, N., Hollinger, D.Y., Kutsch, W.L., Longdoz, B., Luyssaert, S., Migliavacca, M., Montagnani, L., William Munger, J., Moors, E., Piao, S., Rebmann, C., Reichstein, M., Saigusa, N., Tomelleri, E., Vargas, R., Varlagin, A., 2010. Influence of spring and autumn phenological transitions on forest ecosystem productivity. Philos. Trans. R. Soc. B Biol. Sci. 365, 3227–3246. https://doi.org/10.1098/rstb.2010.0102

Rita, A., Camarero, J.J., Nolè, A., Borghetti, M., Brunetti, M., Pergola, N., Serio, C., Vicente-Serrano, S.M., Tramutoli, V., Ripullone, F., 2019. The impact of drought spells on forests depends on site conditions: The case of 2017 summer heat wave in southern Europe. Glob. Change Biol. 26, 851–863. https://doi.org/10.1111/gcb.14825

Russo, S., Dosio, A., Graversen, R.G., Sillmann, J., Carrao, H., Dunbar, M.B., Singleton, A., Montagna, P., Barbola, P., Vogt, J.V., 2014. Magnitude of extreme heat waves in present climate and their projection in a warming world. J. Geophys. Res. Atmospheres 119. https://doi.org/10.1002/2014JD022098

Schuldt, B., Knutzen, F., Delzon, S., Jansen, S., Müller-Haubold, H., Burlett, R., Clough, Y., and Leuschner, C.: How adaptable is the hydraulic system of European beech in the face of climate change-related precipitation reduction? New Phytol., 210, 443 458, https://doi.org/10.1111/nph.13798, 2016.

Senf, C., Buras, A., Zang, C.S., Rammig, A., Seidl, R., 2020. Excess forest mortality is consistently linked to drought across Europe. Nat. Commun. 11, 6200. https://doi.org/10.1038/s41467-020-19924-1

Smith, N.E., et al., 2020. Spring enhancement and summer reduction in carbon uptake during the 2018 drought in northwestern Europe. Philos. Trans. R. Soc. B 375 (1810).

Sofia et al. Agricultural *drought* severity in NE Italy: variability, bias, and future scenarios. Int. Soil Water Conserv. Res. (*2024*)

Sturm, J., Santos, M.J., Schmid, B., Damm, A., 2022. Satellite data reveal differential responses of Swiss forests to unprecedented 2018 drought. Glob. Change Biol. 28, 2956–2978. https://doi.org/10.1111/gcb.16136

Tang J., Körner C., Muraoka H., Piao S., Shen M., Thackeray S.J., Yang X., 2016. Emerging opportunities and challenges in phenology: a review. Ecosphere 7(8), e01436. https://doi.org/10.1002/ecs2.1436

Tian, F., Cai, Z., Jin, H., Hufkens, K., Scheifinger, H., Tagesson, T., Smets, B., Van Hoolst, R., Bonte, K., Ivits, E., Tong, X., Ardö, J., Eklundh, L., 2021. Calibrating vegetation phenology from Sentinel-2 using eddy covariance, PhenoCam, and PEP725 networks across Europe. Remote Sens. Environ. 260, 112456. https://doi.org/10.1016/j.rse.2021.112456

Toreti. A., Bavera, D., Acosta Navarro, J., Aria Acosta Navarro J., Arias Muñoz C., Barbosa P., de Jager A., Di Ciollo C., Fioravanti G., Hrast Essenfelder A., Maetens W., Masante D., Magni D., Mazzeschi M., Spinoni J., 2023. European Commission. Joint Research Centre., 2023. Drought in Europe: March 2023: GDO analytical report. Publications Office, LU.

Torres, P., Rodes-Blanco, M., Viana-Soto, A., Nieto, H., García, M., 2021. The Role of Remote Sensing for the Assessment and Monitoring of Forest Health: A Systematic Evidence Synthesis. Forests 12, 1134. https://doi.org/10.3390/f12081134

Tripathy, K.P., Mishra, A.K., 2023. How Unusual Is the 2022 European Compound Drought and Heatwave Event? Geophys. Res. Lett. 50, e2023GL105453. https://doi.org/10.1029/2023GL105453

Van Der Woude, A.M., Peters, W., Joetzjer, E., Lafont, S., Koren, G., Ciais, P., Ramonet, M., Xu, Y., Bastos, A., Botía, S., Sitch, S., De Kok, R., Kneuer, T., Kubistin, D., Jacotot, A., Loubet, B., Herig-Coimbra, P.-H., Loustau, D., Luijkx, I.T., 2023. Temperature extremes of 2022 reduced carbon uptake by forests in Europe. Nat Commun 14, 6218. https://doi.org/10.1038/s41467-023-41851-0

Vrieling, A., Meroni, M., Darvishzadeh, R., Skidmore, A.K., Wang, T., Zurita-Milla, R., Oosterbeek, K., O'Connor, B., Paganini, M., 2018. Vegetation phenology from Sentinel-2 and field cameras for a Dutch barrier island. Remote Sens. Environ. 215, 517–529. https://doi.org/10.1016/j.rse.2018.03.014

Vicente-Serrano, S.M., Beguería, S., López-Moreno, J.I., 2010. A Multiscalar Drought Index Sensitive to Global Warming: The Standardized Precipitation Evapotranspiration Index. J. Clim. 23, 1696–1718. https://doi.org/10.1175/2009jcli2909.1

Vicente-Serrano, S.M., Gouveia, C., Camarero, J.J., Beguería, S., Trigo, R., López-Moreno, J.I., Azorín-Molina, C., Pasho, E., Lorenzo-Lacruz, J., Revuelto, J., Morán-Tejeda, E., Sanchez-Lorenzo, A., 2013. Response of vegetation to drought time-scales across global land biomes. Proc. Natl. Acad. Sci. U.S.A. 110, 52–57. https://doi.org/10.1073/pnas.1207068110

Walther, G.-R., Post, E., Convey, P., Menzel, A., Parmesan, C., Beebee, T.J.C., Fromentin, J.-M., Hoegh-Guldberg, O., Bairlein, F., 2002. Ecological responses to recent climate change. Nature 416, 389–395. https://doi.org/10.1038/416389a

Wang, Q., Zeng, J., Qi, J., Zhang, X., Zeng, Y., Shui, W., Xu, Z., Zhang, R., Wu, X., Cong, J., 2021. A multi-scale daily SPEI dataset for drought characterization at observation stations over mainland China from 1961 to 2018. Earth Syst. Sci. Data 13, 331–341. https://doi.org/10.5194/essd-13-331-2021

Wegler, M., Kuenzer, C., 2024. Potential of Earth Observation to Assess the Impact of Climate Change and Extreme Weather Events in Temperate Forests—A Review. Remote Sens. 16, 2224. https://doi.org/10.3390/rs16122224

Wei, X.; Huang, S.; Huang, Q.; Liu, D.; Leng, G.; Yang, H.; Duan, W.; Li, J.; Bai, Q.; Peng, J., 2022. Analysis of Vegetation Vulnerability Dynamics and Driving Forces to Multiple

Drought Stresses in a Changing Environment. Remote Sens. 14.17: 4231. https://doi.org/10.3390/rs14174231

White, J.C., Coops, N.C., Wulder, M.A., Vastaranta, M., Hilker, T., Tompalski, P., 2016. Remote Sensing Technologies for Enhancing Forest Inventories: A Review. Can. J. Remote Sens. 42, 619–641. https://doi.org/10.1080/07038992.2016.1207484

Xue, C., Ghirardelli, A., Chen, J., Tarolli, P., 2024. Investigating agricultural drought in Northern Italy through explainable Machine Learning: Insights from the 2022 drought. Comput. Electron. Agric. 227, 109572. https://doi.org/10.1016/j.compag.2024.109572

Yin, G., Verger, A., Filella, I., Descals, A., Peñuelas, J., 2020. Divergent Estimates of Forest Photosynthetic Phenology Using Structural and Physiological Vegetation Indices. Geophys. Res. Lett. 47, e2020GL089167. https://doi.org/10.1029/2020GL089167

Zhang, X., Alexander, L., Hegerl, G.C., Jones, P., Tank, A.K., Peterson, T.C., Trewin, B., Zwiers, F.W., 2011. Indices for monitoring changes in extremes based on daily temperature and precipitation data. WIREs Clim. Change 2, 851–870. https://doi.org/10.1002/wcc.147

Zhao, J., Jiang, T., Liu, Z., Zhang, W., Jian, G., Qi, F., 2012. Dominant Gene cplsr 1 Corresponding to Premature Leaf Senescence Resistance in Cotton (Gossypium hirsutum L.) F. J. Integr. Plant Biol. 54, 577–583. https://doi.org/10.1111/j.1744-7909.2012.01127.x

Zscheischler, J., Reichstein, M., Harmeling, S., Rammig, A., Tomelleri, E., and Mahecha, M. D.: Extreme events in gross primary production: a characterization across continents, Biogeosciences, 11, 2909–2924, https://doi.org/10.5194/bg-11-2909-2014, 2014.

Impacts of a heat wave on tree growth, wood anatomy and intrinsic water-use efficiency in temperate forests

Abstract

Climate change is leading to more frequent and severe extreme climate events, such as hot spells. However, we lack information on how heat waves impact wood anatomy, radial growth and intrinsic water-use efficiency (iWUE). This lack of information is notable in temperate forests, where heat waves can reduce productivity and trigger canopy dieback. We assessed the impacts of the 2022 heat wave on two temperate forests located at high (Cernobbio) and low elevation (Monza) sites in northern Italy. Eight winter-deciduous tree species were sampled, forming either diffuse- (*Acer pseudoplatanus*, *Betula pendula*, *Fagus sylvatica*, *Tilia cordata*) or ring-porous wood (*Castanea sativa*, *Fraxinus excelsior*, *Quercus pubescens*, *Quercus robur*). Some species suffered a severe reduction of basal area increment (BAI) during 2022 (*B. pendula*, -58 %; *Q. robur*, -48 %), others experienced a moderate growth drop (*F. excelsior*, -5 to -34 %; *T. cordata*, -29 %; *C. sativa*, -25 %; *Q. pubescens*, -18 %; *A. pseudoplatanus*, -5 %), and others showed a slight increase (e.g., *F. sylvatica*, + 3 %). Moreover, negative growth legacies were detected in *F. excelsior* at the low-elevation site. In terms of growth reduction, *F. excelsior*, *A. pseudoplatanus* and *Q. pubescens* were the most sensitive species to summer maximum temperatures and drought severity. In *A. pseudoplatanus*, the ray parenchyma fraction declined in 2022, indicating lower C storage. Few differences in wood $\delta^{13}C$, a proxy of iWUE, were found between species. *A. pseudoplatanus* (-26.1 ‰) and *F. excelsior* (-25.6 ‰) showed the highest wood $\delta^{13}C$. Responses to heat damage in terms of growth and wood anatomy were uncoupled and depended on leaf phenology, with early-leafing species showing the most severe growth reduction.

Keywords: *Acer pseudoplatanus*, *Fraxinus excelsior*, summer heat wave, temperate forests.

1. Introduction

A major component of climate warming is the increase in year-to-year climate variability leading to more frequent and severe climate extremes (IPCC, 2023). These extremes include heat waves and dry spells, that trigger forest die-off and raise tree mortality rates worldwide (Allen et al. 2015). In many cases, trees recover after such negative climate impacts, but their recovery capacity depends on multiple factors including: the severity and frequency of climate extremes (e.g., maximum temperatures reached during a heat wave), post-event weather conditions, site variables (topography, soil depth and texture), stand structure and composition or functional traits enhancing resilience (Anderegg et al., 2015; Rita et al., 2020). For instance, either too frequent drought or heat waves and carryover effects (legacies) constrain recovery trajectories, affecting growth resilience (Ingrisch and Bahn, 2018; Kannenberg et al., 2020; Schwarz et al., 2020; Serra-Maluquer et al., 2021). A high shoot-to-root ratio in trees due to previous favorable weather conditions, the so-called structural overshoot (Jump et al., 2017), may exacerbate die-off damage because overbuilt stands may be susceptible to subsequent dry and stressful conditions (Italiano et al., 2024). In contrast, favorable conditions after an extreme event such as a wet period after a severe drought can offset growth losses (Jiang et al., 2019). Such varied responses indicate that the drivers of the pace of recovery must be understood when assessing the return of tree functionality after extreme climate events (Ruehr et al., 2019).

Long-term field observations or reconstructions following extreme climate events may improve our understanding of tree recovery given the opportunistic nature of many die-off cases. In this regard, tree rings provide retrospective proxies of tree functioning which may be analyzed to disentangle the influences of antecedent, current and subsequent conditions on post-stress tree recovery (Camarero et al., 2018). Multi-proxy approaches combining several sources of information on tree functioning including tree-ring width or basal area increment data, wood anatomy and C isotope ratios ($\delta^{13}C$) provide relevant information on post-stress resilience (e.g., Colangelo et al., 2017, 2025; Italiano et al., 2023). $\delta^{13}C$ of tree-ring wood is a proxy of intrinsic water-use efficiency (iWUE), i.e. the ratio between photosynthesis and stomatal conductance rates (Francey and Farquhar, 1982; McCarroll and Loader, 2004). In this study, we followed this multi-proxy framework to assess the impacts of a heat wave on different aspects of tree functioning (growth, gas-water exchange, theoretical hydraulic conductivity, carbon storage in xylem). We investigated temperate forests in northern Italy because the impacts of hot spells on these mesic forests remain understudied.

Temperate forests are very vulnerable to heat and drought stress, that cause growth decline and die-off (Bréda et al., 2006; Nardini et al., 2013; Martín-Benito and Pederson, 2015; Rubio-Cuadrado et al., 2018). For instance, a record drought caused die-off in temperate mesic forests of Eastern North America, and the main mechanism involved was hydraulic failure, i.e. plant desiccation due to cavitation-induced loss of water transport exceeding a lethal species-specific threshold (Hoffmann et al., 2011). The timing of the extreme climate event with respect to major tree phenological phases (bud burst, leaf flushing, tree-ring formation) is a critical factor determining damage. For example, in North American temperate forests, drought-induced growth decline was more intense due to early-season droughts coinciding with peaks in radial growth, particularly for early-growing trees located in the warmest regions (D'Orangeville et al., 2018). Moreover, legacy effects were very important for tree species that form diffuse-porous wood, in sites with deep water tables, and in response to late-season droughts (Kannenberg et al., 2019). Overall, these findings indicate that the timing of heat waves or droughts, site conditions and species traits, including leaf and wood phenology, contribute to explaining the recovery after extreme climate events such as hot spells.

An exceptional heat wave affected many European countries from May to September 2022, particularly impacting regions of the Po River basin in northern Italy, where crop losses, wildfires and excess mortality rates reached very high numbers (Ballester et al., 2023). Forests in the region were also affected, showing extensive canopy dieback. We selected two sites that presented this type of damage after the 2022 hot spell and sampled stands of eight winter-deciduous tree species along a 1080-m elevation gradient. Tree species forming both diffuse-porous (*Acer pseudoplatanus*, *Betula pendula*, *Fagus sylvatica*, *Tilia cordata*) and ring-porous (*Castanea sativa*, *Fraxinus excelsior*, *Quercus pubescens*, *Quercus robur*) wood types were selected to encompass a wide range of wood anatomical traits.

Our specific objectives were: (i) to reconstruct radial-growth patterns and relate them to climate variables, paying particular attention to impacts of summer heat waves on wood production, (ii) to quantify the resilience after the hot spell in terms of growth, wood anatomy and $\delta^{13}C$ records, and (iii) to highlight the main responses to the studied extreme climate event. Using such a retrospective approach allows to pinpoint the impacts of a heat wave on tree functioning within a wide temporal framework. We expect that the species showing the earliest leaf unfolding in spring will be the most exposed and negatively impacted by the summer hot spell in terms of radial growth reduction.

2. Materials and methods

2.1. Study sites

We selected two study sites (Cernobbio, Monza) located in Insubria, Lombardia region, northern Italy (Fig. 1). Selected sites showed extensive canopy dieback and damage, characterized by leaf browning and abundant shedding, which were observed after the 2022 heat wave. Each site showed different forest composition and climate conditions. In the mid-elevation Cernobbio site (9º 04' 14" – 9º 04' 55" E, 45º 51' 15" – 45º 52' 27" N, 539 – 1249 m a.s.l.), six species were sampled (from lowest to highest elevation: *C. sativa*, *Q. pubescens*, *F. excelsior*, *A. pseudoplatanus*, *B. petula*, and *F. sylvatica*; Table 1). In the piedmont, low-elevation Monza site (9º 16' 10'' – 9º 17' 08" E, 45º 35' 41" – 45º 36' 11" N, 170 – 195 m a.s.l.), three species were sampled (*F. excelsior*, *Q. robur*, and *T. cordata*).

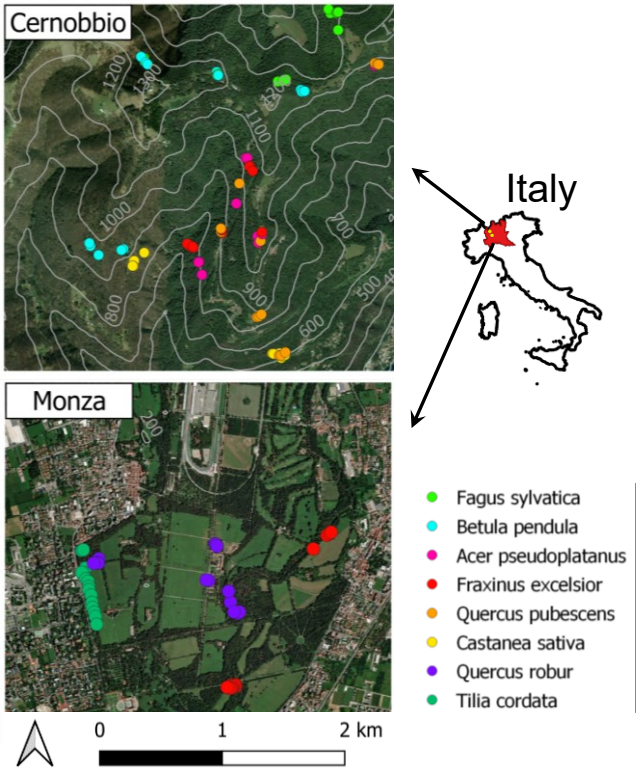

Figure 1. Maps showing the location of the two study sites (Cernobbio, Monza) in northern Italy and the sampled trees of the eight species. Elevation curves were not plotted in the Monza map because of the short elevation range (25 m). See also Table 1.

The study forests are dominated by broadleaf, winter-deciduous temperate tree species (e.g., *Q. robur*), but are subjected to sub-Mediterranean influence (Pignatti, 1998). The mean annual temperature ranges 12.0–13.0 ºC and the total annual precipitation increases upwards and ranges 1162–1250 mm. The warmest month is July (maximum temperature between 26.2 and 28.1 ºC), and the driest periods are the winter and July, with precipitation peaking in November.

In ring-porous species, stem radial growth may occur at least one month before buds were swollen, whereas in diffuse-porous species these two phenological events are more synchronous (Suzuki et al., 1996). According to 2022 phenological data taken at the nearby Sagno Swiss station (9º 02' E, 45º 52' N, 670 m a.s.l.), half of the crown leaves were formed by *F. sylvatica*, *B. pendula*, *T. cordata* and *C. sativa* on 16 April, 22 April, 25 April and 5 May, respectively (data available at https://app.phaenonet.ch/stations/2022_SGO).

Soils are acidic and poor in nutrients, particularly in the Cernobbio site. The study sites correspond to secondary, young forests not being managed since the 1960s (Table 1). In Monza, the sampled *T. cordata* trees were located in a semi-urban area (Fig. 1).

Table 1. Location and elevation of stands sampled in northern Italy. The last two columns show data on tree diameter at breast height (dbh) and age (estimated at 1.3 m). Values are means ± SD.

Site	Tree species	Latitude N	Longitude E	Elevation (m a.s.l.)	Dbh (cm)	Height (m)	Age (years)
Cernobbio	*Castanea sativa*	45° 51' 15"	9° 04' 47"	591–876	40.8 ± 12.5	14.0 ± 3.4	43 ± 16
	Quercus pubescens	45° 51' 44"	9° 04' 40"	539–1088	38.5 ± 9.6	17.6 ± 4.8	55 ± 9
	Fraxinus excelsior	45° 51' 43"	9° 04' 14"	730–1050	48.9 ± 10.2	20.5 ± 3.0	52 ± 9
	Acer pseudoplatanus	45° 51' 46"	9° 04' 39"	791–1088	48.9 ± 11.1	23.7 ± 4.3	41 ± 8
	Betula pendula	45° 52' 24"	9° 04' 55"	928–1261	45.5 ± 13.4	17.7 ± 1.5	44 ± 14
	Fagus sylvatica	45° 52' 27"	9° 04' 49"	1061–1249	40.1 ± 11.8	18.4 ± 4.1	64 ± 15
Monza	*Fraxinus excelsior*	45° 35' 41"	9° 17' 08"	170–177	36.0 ± 12.8	27.8 ± 6.2	41 ± 14
	Quercus robur	45° 36' 11"	9° 16' 59"	173–195	57.0 ± 11.2	27.6 ± 5.7	88 ± 30
	Tilia cordata	45° 36' 11"	9° 16' 10"	187–191	46.3 ± 9.0	32.5 ± 8.4	53 ± 17

2.2. Climate data

Due to the lack of long-term, homogeneous climate datasets in the two study locations, we used 0.1º-gridded monthly climate data (mean maximum and minimum temperatures, total precipitation; period 1960–2024) corresponding to the E-OBS climate dataset version 28.0e (Cornes et al., 2018). Using these data, we calculated monthly values of the Standardized Precipitation Evapotranspiration Index (SPEI), a multi-scalar drought index, at scales from 1 to 24 months of cumulative water balance. The water balance calculation depends on temperature and precipitation and determines if climate conditions are wet or dry (Vicente-Serrano et al., 2010). The SPEI was calculated using the R package (Beguería and Vicente-Serrano, 2023). To assess changes in soil moisture availability, we also obtained 0.1º-gridded monthly soil moisture data at 0–10 cm depth for the period 1982–2018 based on land surface model simulations with precipitation-based forcing (Rodell et al., 2004). To illustrate the conditions impacting on radial growth during the 2022 heat wave, we calculated the mean maximum temperatures during the growing season (from May to October). Mean maximum temperatures from May to August were +0.5 ºC higher in 2003, a widely study hot spell affecting Europe, than in 2022, and this period would not encompass the period of latewood formation (Michelot et al., 2012).

2.3. Field sampling and tree-ring width data

In each site, we selected 15 mature trees per species with visible canopy dieback after the 2022 hot spell. We measured the diameter at breast height (dbh), measured at 1.3 m, using tapes, and the total tree height using a laser rangefinder (Nikon Forestry Pro). We sampled and extracted three cores from each tree at 1.3 m. Two cores were used to obtain tree-ring width and wood-anatomy data, whereas the third core was used to measure $\delta^{13}C$. The cores were extracted using Pressler increment borers with a 5-mm diameter. The cores for ring-width and wood anatomy data were glued onto wood supports. Then, they were air dried and sanded with sandpapers of increasing finer grain until tree-ring boundaries were conspicuous. Cores were visually cross-dated under the binocular scope using dendrochronological methods (Fritts, 1976). Then, they were scanned at 1,200 dpi (Epson Expression 10000XL). The tree-ring widths (RW) were measured with a 0.001 mm resolution along two cores per tree using the CDendro-CooRecorder software (Larsson and Larsson, 2018). The visual cross-dating was checked using the COFECHA software, which calculates moving correlations between individual series and the mean species series (Holmes, 1983). The tree age at 1.3 m was estimated by counting the number of rings along the oldest core of each tree whenever it reached the pith or presented curved, innermost rings.

2.4. Processing tree-ring width data

Tree-ring widths were converted into basal area increment (BAI) to analyze growth trends or into ring-width indices (RWI) to calculate climate-growth relationships. The BAI was calculated using the following formula:

$$\mathrm{BAI} = \pi\,(R_t^2 - R_{t\text{-}1}^2) \qquad (1),$$

where R_t and $R_{t\text{-}1}$ are the radii measured in years t and t-1, respectively, corresponding to the cumulative sums of annual ring widths ($\sum_l^t RW$ and $\sum_l^{t-1} RW$, respectively).

Using the individual RWI series, we calculated several growth resilience indices for each species and site to quantify the impact of the 2022 heat wave and the subsequent recovery. We used simple indices to overcome some of the problems associated with widely used resilience indices (Schwarz et al., 2020). Specifically, we calculated the following ratios for RWIs of several years (subscripts): RWI_{2022} / RWI_{2021}, RWI_{2023} / RWI_{2022}, RWI_{2024} / RWI_{2023}, and $RWI_{2024\text{-}2023}$ / RWI_{2022}. The $RWI_{2024\text{-}2023}$ is the mean RWI for the years 2023 and 2024.

To calculate climate-growth relationships, the individual ring-width series were converted into standardized ring-width indices through detrending (Fritts, 1976). These procedures allowed the removal of most size-related trends in ring-width data and emphasized high-frequency variability. We fitted negative linear or exponential functions to individual ring-width series and obtained ring-width indices by dividing observed values by fitted values. Then, autoregressive models were fitted to remove the first-order autocorrelation of the series of dimensionless indices. The resulting pre-whitened individual series were averaged using a bi-weight robust mean to obtain mean ring-width series for each species. The BAI and RWI series were obtained using the dplR package (Bunn, 2008, 2010; Bunn et al., 2025) in the R statistical software (R Core Team, 2024).

2.5. Wood anatomy

To analyze wood anatomy, we selected five trees per species showing a high correlation between their indexed ring-width series and the species' mean series of each site, except in *A. pseudoplatanus*, with four trees being analyzed. We focused on the period 2020–2024, encompassing two years before and after the 2022 heat wave. Wood cross-sections (thickness of 10–20 µm) of the core part, including the rings formed in 2020–2024 were obtained using a sledge microtome (Gärtner et al., 2015). Sections were stained with safranin (1 %) and Astra blue (2 %) and fixed with Eukitt®. The high-resolution images of the sections were then captured using an Olympus BH2 microscope equipped with an Olympus DP73 camera. The images were stitched with the PT-Gui software (New House Internet Services BV, Rotterdam, NL) to create one composite image for each annual ring. Finally, the images were analyzed

along a 4-mm tangential window using the image analysis software ImageJ version 1.54i (Schneider et al., 2012).

Wood-anatomical variables were selected and measured following Scholz et al. (2013) and Ziemińska et al. (2023). In total, 40218 vessels were measured. For the diffuse porous species, the cut-off measurement value for vessel diameter was set at 35 μm, while 80 μm was used for the ring-porous species (cf. Granda et al., 2018).

In each annual ring of each tree, we measured: the xylem vessel fraction (VF, $\mu m^2\ \mu m^{-2}$) corresponding to the portion of the transversal area occupied by vessels; the mean radial vessel diameter (MVD, μm); the vessel density (VD, number of vessels per mm^2); and the fraction of the transversal area occupied by ray parenchyma (RP, %). Based on the measurements of transversal area of all vessels in each ring, we calculated the theoretical (*Kh*) and total (*TKh*) specific xylem hydraulic conductivity (both in Kg m^{-1} MPa^{-1} s^{-1}).

2.6. Carbon isotope discrimination

To analyze $\delta^{13}C$, we selected the same five trees per species used for wood anatomy analyses. In this case, we focused on the period 2022–2024. The individual rings were separated under the binocular using scalpels. Then, they were milled and homogenised using a ball mixer mill (Retsch MM301, Haan, Germany). We used whole wood instead of cellulose because previous studies on hardwood species showed that they lead to similar trends and results considering $\delta^{13}C$ (D'Alessandro et al., 2004). In total, 135 samples were analyzed. Lastly, wood aliquots (0.8–1.2 mg) were weighed on a microbalance (AX205 Mettler Toledo, OH, USA) into tin foil capsules.

Isotope analyses were carried out at the Stable Isotope Laboratory of the University of Almería (Almería, Spain). Encapsulated wood samples were combusted to CO_2 with a combustion module (CM) coupled to a cavity ring-down spectroscopy (CRDS) System (G2201-I Analyzer, Picarro), achieving a flash combustion at temperatures of 1700–1800 ºC. The released CO_2 was transferred to a Picarro Liaison A0301 interface and entered into CRDS for analysis. The $\delta^{13}C$ values were referenced to the Vienna PeeDee Belemnite (V-PDB) scale. Sugarcane, acetanilide, and urea were used as working reference standards for consecutive $\delta^{13}C$ analyses of the wood samples, covering a wide calibration range from − 11.9 ‰ to − 44.3 ‰. These working reference standards were initially calibrated against the USGS (USGS-40 l-Glutamic acid) and the IAEA standards (IAEA-603 and NBS-18 calcites). Based on analyses of these international standards, the precision ranged between 0.01 and 0.34 ‰ (n = 9) and, in terms of accuracy, the $\delta^{13}C$ error ranged from − 0.03 ‰ to 0.88 ‰.

2.7. Statistical analyses

First, the normality of variables was checked using Shapiro-Wilk tests. Second, several variables, such as BAI, vessel density and hydraulic diameter, were log-transformed to fulfill normality. To compare resilience indices, $\delta^{13}C$ values (2022, 2023, and 2024) or wood-anatomical variables of each species between years (2020, 2021, 2022, 2023, and 2024), we used ANOVAs and Bayesian *t* tests (Rouder et al., 2009). Bayes factor values larger than 3 or 10 indicate substantial or strong evidence, respectively, for unequal means. ANOVAs were then followed by Tukey's *Q* tests to compare means between species. To quantify the temperature and BAI trends, we used Mann-Kendall *S* tests.

To obtain climate-growth relationships, Pearson correlations were calculated between species' series of ring-width indices and monthly climate variables (mean maximum and minimum temperatures, precipitation, SPEI). The climate window of these analyses spanned from the prior (year *t*-1) to the current (year *t*-1) September. Correlations with the SPEI were calculated for 1- to 24-month long scales. Correlations were calculated for the common, best-replicated period 1962–2024 using the treeclim R Package (Zang and Biondi, 2015). We also compared RWIs of the study species between hot, normal and cold summer (June to August) conditions. Hot, cold and normal summers were defined as those showing maximum summer temperatures above and below the highest and lowest 10th percentiles, respectively, and the rest of the years. Data analyses were carried out using the PAST version 5.2.2. software (Hammer et al., 2001) and the R statistical software (R Core Team, 2024).

3. Results

3.1. Maximum temperature, growth trends and wood anatomy

Maximum temperatures in the growing season showed significant ($p < 0.001$) positive trends in Cernobbio ($S = 1082$) and Monza ($S = 1156$; Fig. 2). Temperatures rose since 1960 at a mean rate of 0.045º yr^{-1}. In 2022, the maximum temperatures were +1.45 ºC and +1.61 ºC higher than the expected values, according to this trend, in Cernobbio and Monza, respectively. In addition, the 2022 hot spell occurred after two relatively cold years.

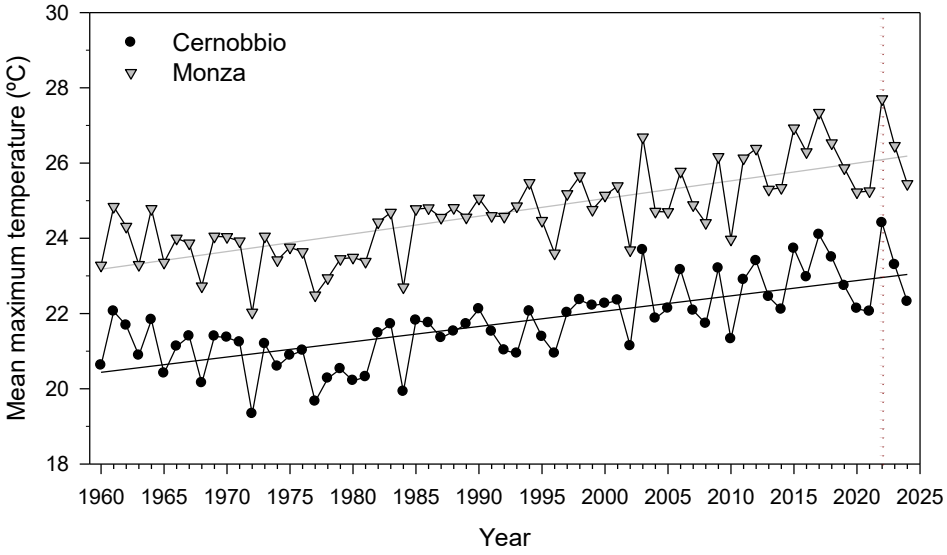

Figure 2. Values and linear trends of mean maximum temperatures of the growing season (May to October) in the Cernobbio and Monza study sites. The dotted vertical line indicates the 2022 heat wave.

The rbar values indicated we built robust and well-replicated tree-ring chronologies, but differences in growth rate, AR1 and MS suggested diverse growth responses to climate variability (Table S1). *A. pseudoplatanus*, *F. excelsior*, and *B. pendula* showed the highest growth rates (2.94–4.02 mm), whereas *B. pendula* and *Q. robur* showed the highest (0.45) and lowest (0.25) MS values, respectively.

According to Mann-Kendall tests, all species showed significant BAI trends, except *B. pendula* in Cernobbio and *Q. robur* in Monza (Table 2, Fig. 3). Positive BAI trends were common and particularly strong in some species (*T. cordata*, *F. sylvatica*, and *Q. pubescens*), except for *C. sativa*, which showed a negative BAI trend.

In 2022, BAI in Cernobbio was on average 85 % (-15 % loss) of the BAI measured in 2021, whereas in Monza it was 63 % (-37 % loss) (Figs. **3** and **S1**). However, there were great differences between species. In Cernobbio, the strongest and weakest BAI reductions corresponded to *B. pendula* (-58 %) and *A. pseudoplatanus* and *F. excelsior* (-5 %), respectively. Other species showed moderate BAI decreases (*C. sativa*, -25 %; *Q. pubescens*, -18 %). Unexpectedly, *F. sylvatica* showed a relative increase of BAI in 2022 (+ 3 %). In Monza, *Q. robur* showed the strongest BAI reduction (-48 %), whereas the other two species showed moderate and similar losses in BAI (*F. excelsior*, -34 %; *T. cordata*, -29 %). Interestingly, the BAI reduction during 2022 of *F. excelsior* was significantly stronger at the low-elevation Monza site than at the high-elevation Cernobbio site ($F = 194$, $p < 0.001$; Bayes factor = 3.1). Moreover, BAI of *F. excelsior* in Monza showed another BAI reduction in 2023 (-17 %) when it reached a minimum value since 1995.

(a)

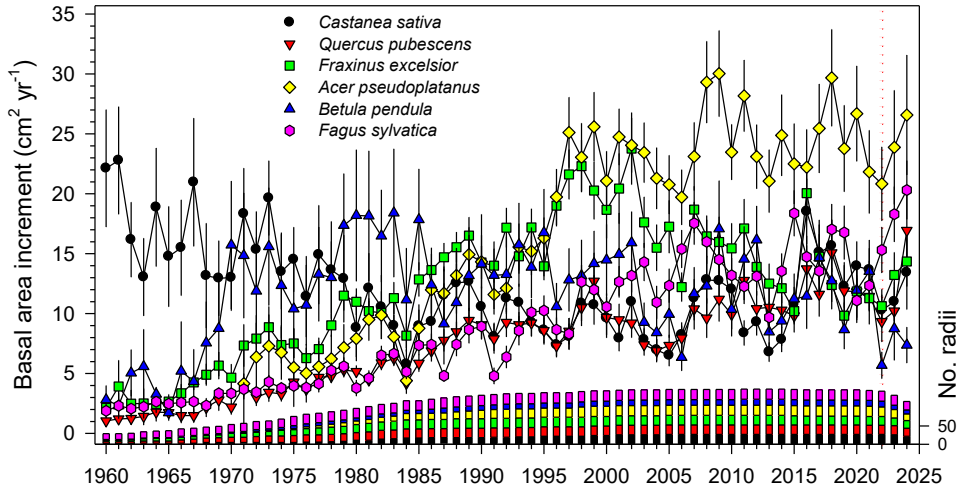

(b)

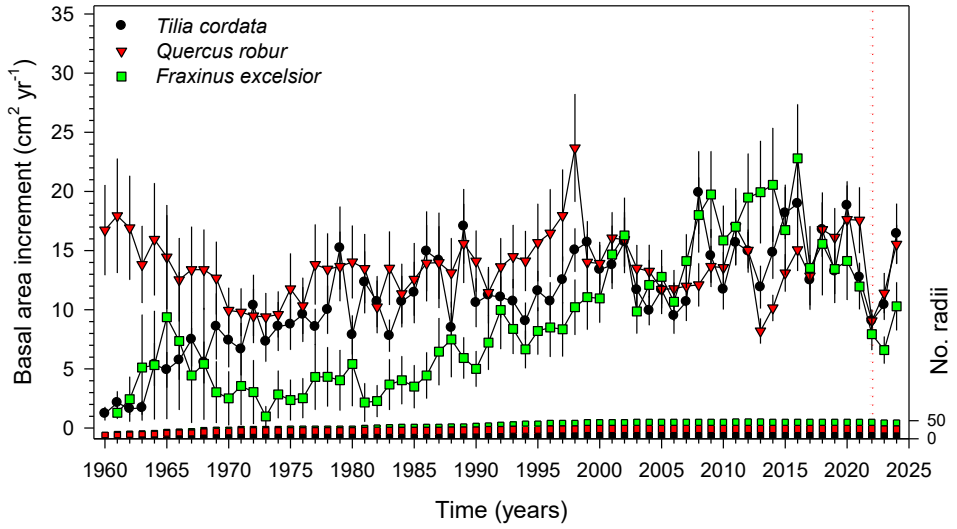

Figure 3. Basal area increment measured in the tree species sampled in (a) Cernobbio and (b) Monza sites. The vertical dotted lines indicate the 2022 summer heat wave. Values are means ± SE. The annual number of measured radii is shown on the right y-axes (bars).

In the period 2020–2024. *F. sylvatica* showed the highest BAI value (21.1 cm^2) and vessel density (83 vessels mm^{-2}) (Table 2). The highest ray parenchyma fraction (21.1 %) corresponded to *Q. pubescens*, whilst *Q. robur* presented the highest vessel area fraction (32 %), hydraulic diameter (216 μm), *Kh* (1300 Kg m^{-1} MPa^{-1} s^{-1}) and T*Kh* (1.18 Kg m^{-1} MPa^{-1} s^{-1}).

Table 2. Mean values (± SD) of the growth and wood anatomical variables measured in the period 2020-2024. Abbreviations: BAI, basal area increment; Kh, theoretical specific xylem hydraulic conductivity; TKh, total ring area hydraulic conductivity. The BAI trend was assessed using Mann-Kendall S tests. Underlined S values were not significant ($p > 0.05$). Different letters indicate significant ($p < 0.05$) differences between species within each site according to Tukey's Q tests.

Site	Tree species	Ring width (mm)	BAI (cm^2)	BAI trend, *S*	No. measured vessels	Vessel density (No. mm^{-2})	Vessel area fraction (%)	Fraction of ray parenchyma (%)	Hydraulic diameter (□m)	*Kh* (Kg m^{-1} MPa^{-1} s^{-1})	T*Kh* (Kg m^{-1} MPa^{-1} s^{-1})
Cernobbio	*C. sativa*	1.17 ± 0.37	6.6 ± 2.1a	-640	3702	34 ± 5ab	22.7 ± 3.2ab	9.5 ± 1.3a	169.3 ± 9.0c	310.9 ± 76.4c	0.19 ± 0.07b
	Q. pubescens	1.20 ± 0.32	7.9 ± 2.3a	1646	1939	38 ± 7ab	17.1 ± 4.2ab	21.1 ± 2.3b	207.2 ± 15.2c	305.4 ± 81.9c	0.19 ± 0.04b
	F. excelsior	1.40 ± 0.30	11.2 ± 2.5a	1002	1824	14 ± 2a	20.5 ± 3.5ab	11.8 ± 1.1a	198.7 ± 9.4c	243.3 ± 52.8c	0.21 ± 0.03b
	A. pseudoplatanus	1.75 ± 0.48	16.5 ± 5.0ab	981	2893	23 ± 4a	9.7 ± 1.8[a]	13.8 ± 2.2ab	74.5 ± 5.0a	17.7 ± 4.8a	0.02 ± 0.01a
	B. pendula	1.06 ± 0.49	8.6 ± 3.9a	168	2800	32 ± 4ab	15.1 ± 2.9ab	15.4 ± 3.9ab	86.4 ± 4.4b	36.9 ± 12.0b	0.03 ± 0.01a
	F. sylvatica	2.28 ± 0.71	21.1 ± 6.8b	1716	15417	83 ± 9b	23.3 ± 2.8ab	13.3 ± 2.1a	62.7 ± 6.0a	32.7 ± 5.9b	0.06 ± 0.03a
Monza	*F. excelsior*	1.07 ± 0.34	10.5 ± 3.2a	1230	1747	19 ± 5a	21.2 ± 3.8ab	13.9 ± 1.7ab	192.4 ± 14.2c	242.3 ± 53.1c	0.27 ± 0.06b
	Q. robur	1.29 ± 0.49	13.1 ± 4.6ab	2	3646	41 ± 13ab	32.0 ± 1.5b	17.4 ± 1.6ab	216.3 ± 36.5c	1300.0 ± 1702.3d	1.18 ± 1.36c
	T. cordata	1.19 ± 0.74	11.6 ± 6.7a	2318	6250	66 ± 16ab	19.4 ± 3.7ab	14.5 ± 2.3ab	64.2 ± 5.0a	27.5 ± 6.5ab	0.03 ± 0.02a

When comparing between years of the period 2020–2024, growth and wood-anatomy variables for the selected trees, the ray parenchyma fractions of *A. pseudoplatanus* in Cernobbio showed a significant reduction in 2022, whereas the hydraulic diameter increased (Table 3, Fig. S2). At this site, *F. excelsior* showed a reduction in vessel density during 2024.

Table 3. Comparisons of growth and wood-anatomy data between years 2020, 2021, 2022 (heat wave), 2023, and 2024 based on ANOVAs. Data correspond to five trees per species, except in *A. pseudoplatanus* (n = 4 trees). The statistics show *F* values, and bold values indicate significant ($p < 0.05$) differences between years. Bold and underlined values indicate significant ($p < 0.05$) *F* values with strong evidence for unequal means (Bayes factor > 10). Upward and downward arrows indicate increases or decreases of the corresponding variable, respectively.

Site	Tree species	Ring width	BAI	Vessel density	Vessel fraction	Fraction of ray parenchyma	Hydraulic diameter	*Kh*
Cernobbio	*C. sativa*	1.479	0.904	0.657	1.122	1.537	0.167	0.426
	Q. pubescens	0.367	0.331	0.215	0.346	0.314	0.192	0.460
	F. excelsior	0.582	0.504	↓ **3.492**	1.025	0.285	0.377	0.305
	A. pseudoplatanus	0.143	0.155	0.146	0.257	↓ **<u>6.502</u>**	↑ **3.144**	0.618
	B. pendula	0.977	1.007	0.019	0.633	0.393	0.110	0.647
	F. sylvatica	1.750	2.123	1.165	0.180	0.403	0.342	0.178
Monza	*F. excelsior*	0.550	0.179	0.804	0.567	0.106	0.397	0.131
	Q. robur	0.849	1.156	1.398	0.369	0.277	0.962	0.762
	T. cordata	2.131	1.662	1.059	0.991	0.279	0.091	0.219

3.2. Year-to-year growth variability

Regarding the series of ring-width indices, they again highlighted again the severe growth reductions during 2022 of *B. pendula* and *Q. robur* in Cernobbio and Monza, respectively, and the negative legacy effects of *F. excelsior* in Monza (Fig. S3). In Cernobbio, the RWI series of all species showed significant ($p < 0.05$) and positive correlations (period 1962–2024), except for *F. sylvatica*. In Monza, the RWI series of the three species also showed significant and positive correlations, except for *T. cordata* and *F. excelsior*.

The resilience indices illustrated how *B. pendula* showed a stronger RWI reduction in Cernobbio during 2022 than the rest of species, but also a stronger relative recovery in 2023 and 2024 (Fig. S4). *F. excelsior* and *Q. pubescens* also showed remarkable RWI increases in 2023 and 2024, respectively. In Monza, we found the lowest recovery of growth indices in the case of *F. excelsior* (Fig. S5).

3.3. Comparing wood $\delta^{13}C$ values between years and species

During the period 2022–2024, we found no significant differences in wood $\delta^{13}C$ values between species neither in Cernobbio nor in Monza, exceptbetween *F. excelsior* and *Q. robur* from Monza in 2023 and 2024 (Figs. S6 and S7). Taking into account the data for the three years analyzed, *F. excelsior* showed higher $\delta^{13}C$ values (mean SD = -25.6 ± 1.0 ‰) than *Q. robur* (-27.0 ± 0.9 ‰) in Monza (Q = 6.18, p = 0.0004). In Cernobbio, *A. pseudoplatanus* showed significantly higher ^{13}C values (-26.1 ± 1.2 ‰) than *Q. pubescens* (-27.6 ± 1.0 ‰; Q = 5.52, p = 0.003) and *F. sylvatica* (-27.7 ± 1.6 ‰; Q = 5.67, p = 0.002).

3.4. Growth responses to climate variables and a drought index

Warm and dry June conditions constrained growth in Cernobbio (Fig. 4). The negative impact of maximum temperatures on growth indices extended until July in *F. excelsior*, *A. pseudoplatanus*, and *B. pendula*. High minimum temperatures in spring enhanced the growth of *Q. pubescens* and *F. sylvatica*, but elevated minimum temperatures in the previous autumn reduced the growth of *A. pseudoplatanus*. Wet spring conditions improved the growth of *Q. pubescens* and *A. pseudoplatanus*, but similar conditions in the previous November reduced the growth of *Q. pubescens*. This species and *C. sativa* were very sensitive to dry soil conditions from June to September, whereas *B. pendula* responded positively to wet soil conditions in the previous autumn.

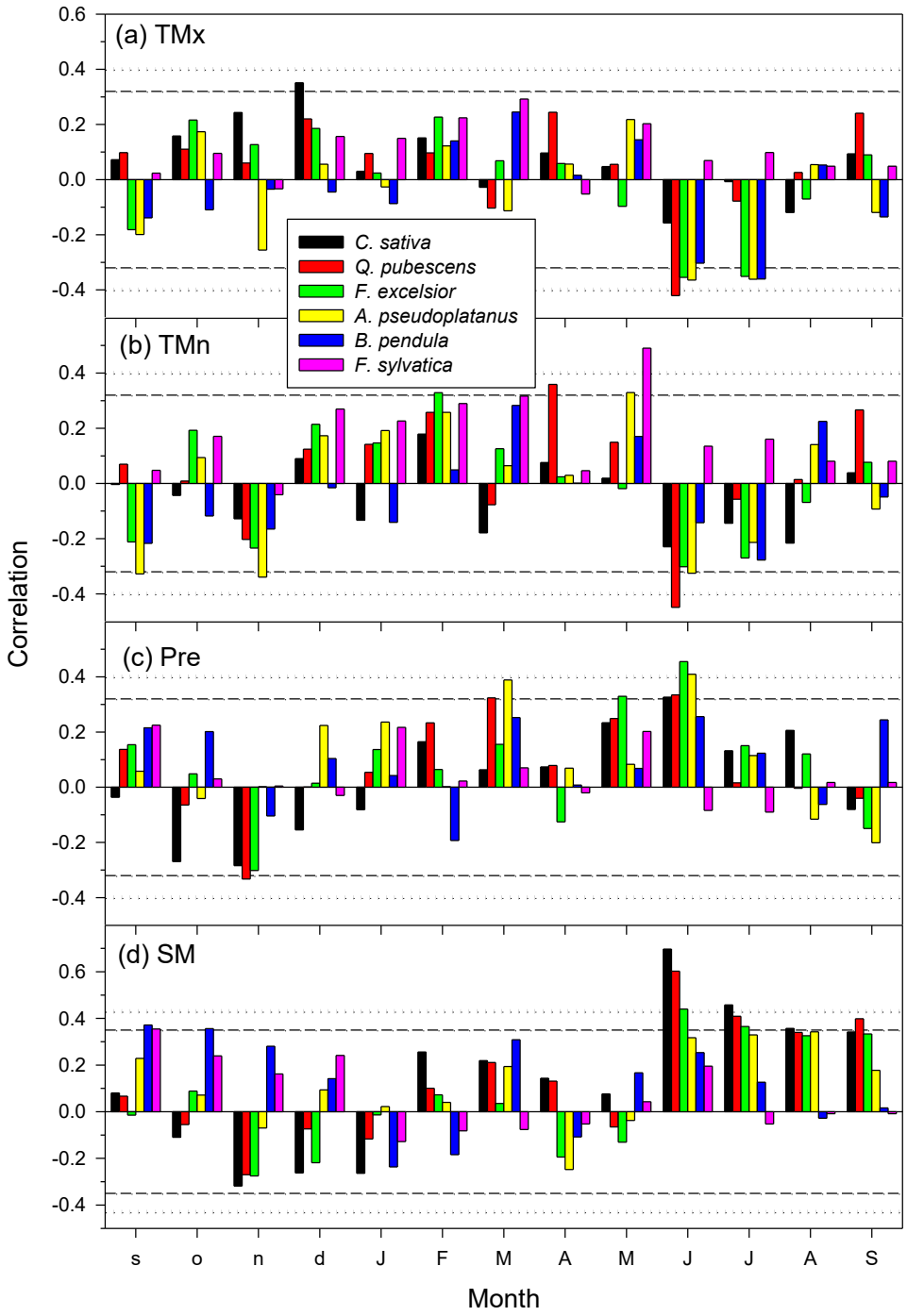

Figure 4. Climate-growth relationships calculated for tree species sampled in Cernobbio. Climate variables include: mean maximum (TMx) and minimum (TMn) temperatures, precipitation (Pre), and soil moisture (SM). Bars are Pearson correlations and dashed and dotted horizontal lines show the 0.05 and 0.01 significance levels, respectively. The window of correlations goes from the previous (months abbreviated by lowercase letters) to current (months abbreviated by uppercase letters) years.

In Monza, high maximum and minimum temperatures in June reduced the growth of *F. excelsior*, whereas moist soil conditions in April and July improved growth (Fig. 5). In contrast, elevated minimum temperatures in the previous November-December reduced it. The growth of *T. cordata* decreased as the minimum temperatures of the previous autumn rose but increased as soil moisture levels in August did. High minimum temperatures and precipitation in the prior winter enhanced the growth of *Q. robur*.

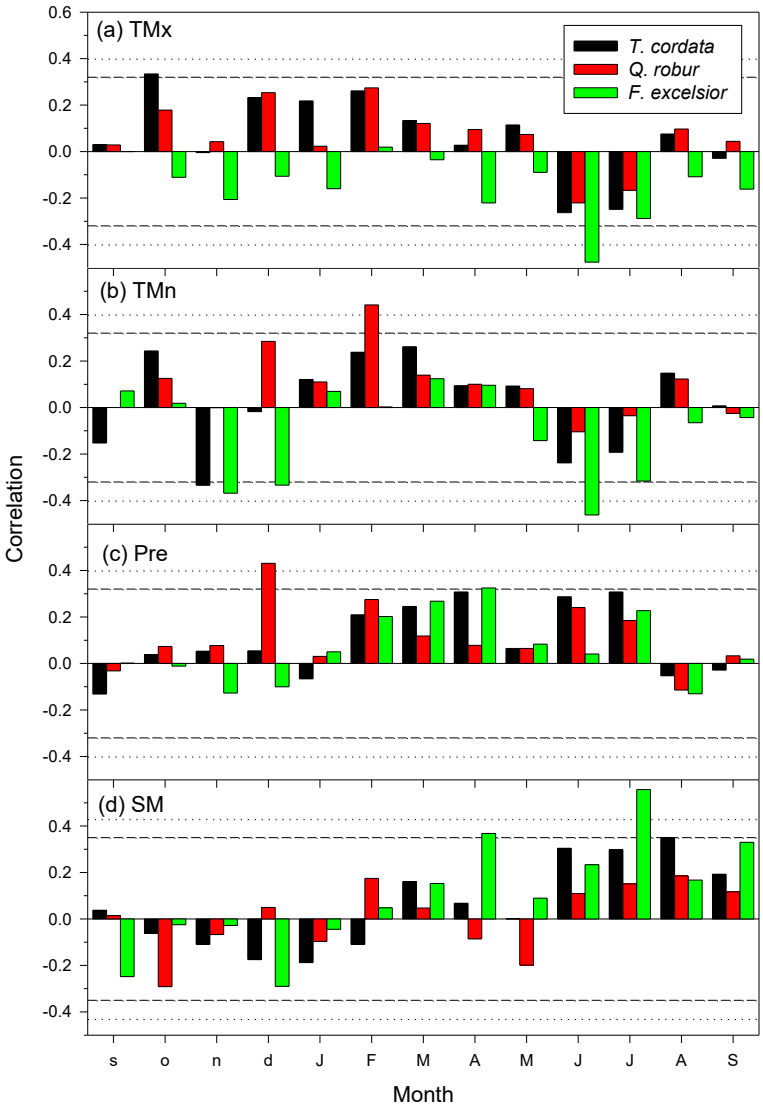

Figure 5. Climate-growth relationships calculated for tree species sampled in Monza. Climate variables include: mean maximum (TMx) and minimum (TMn) temperatures, precipitation (Pre), and soil moisture (SM). Bars are Pearson correlations and dashed and dotted horizontal lines show the 0.05 and 0.01 significance levels, respectively. The window of correlations goes from the previous (months abbreviated by lowercase letters) to current (months abbreviated by uppercase letters) years.

The highest RWI–SPEI correlations in Cernobbio corresponded to *F. excelsior* ($r = 0.64$, $p < 0.001$; July, 3-month long SPEI), *A. pseudoplatanus* ($r = 0.49$, $p < 0.01$; July, 9-month long SPEI), and *Q. pubescens* ($r = 0.47$, $p < 0.01$; June, 5-month long SPEI, Fig. S8). In Monza, the species most responsive to drought was again *F. excelsior* ($r = 0.45$, $p < 0.01$; October, 9-month long SPEI), followed by *T. cordata* ($r = 0.44$, $p < 0.01$; July, 6-month long SPEI) and *Q. robur* ($r = 0.42$, $p < 0.05$; October, 12-month long SPEI; Fig. S9).

3.5. Growth responses to maximum temperatures

We only found a significant correlation between the mean maximum temperatures from May to October and the ring-width indices in the case of *F. excelsior* from Monza (r = -0.439, p = 0.004; Fig. 6).

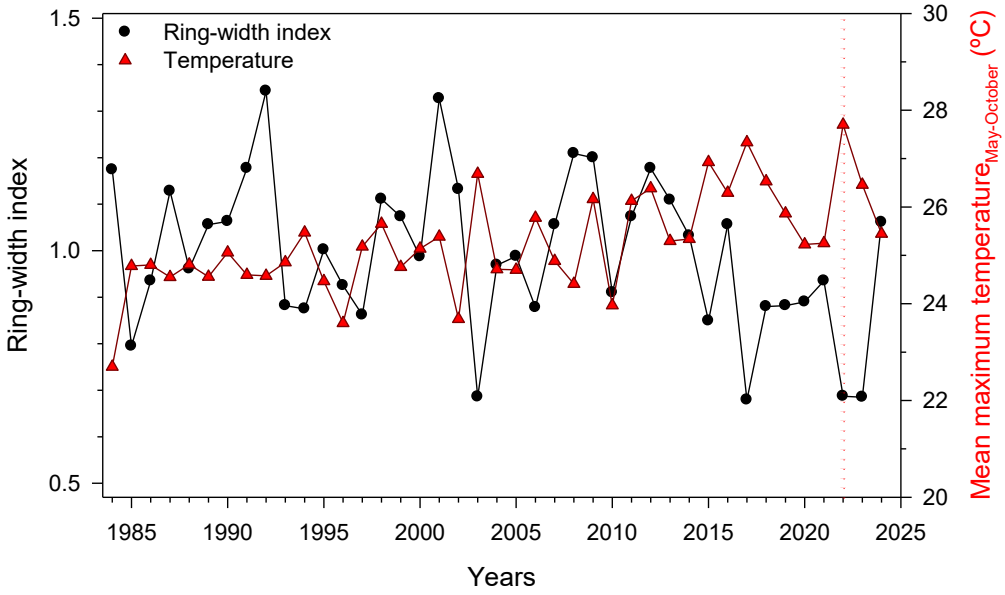

Figure 6. Negative relationship found between the series of *F. excelsior* ring-width indices and the mean maximum temperatures from May to October (right y-axis) in Monza. The vertical dotted line indicates the 2022 heat wave.

When comparing RWIs of *F. excelsior* from Monza for years with hot, normal and cold summer conditions, we found significantly lower values during hot summers (F = 12.85, p = 0.005, Bayes factor = 4.3; Fig. S10). In Cernobbio, differences in RWIs between summers of different thermal conditions were almost significant for *Q. pubescens* (F = 4.75, p = 0.055, Bayes factor = 1.1).

4. Discussion

We hypothesized that early-flushing tree species would be the most negatively impacted by the heat wave of 2022 in terms of growth loss. Phenological data from Switzerland ranked *B. pendula*, *F. sylvatica*-*A. pseduplatanus* and *T. cordata*-*C. sativa* as early, intermediate and late leaf unfolding species, respectively (Bigler and Bugmann, 2018). Bud break may start about two weeks earlier in *Q. robur* as compared to *F. sylvatica* (Sass-Klaassen et al., 2011; Michelot et al., 2012), whereas leaf unfolding occurs about 10 days later in *F. excelsior* than *F. sylvatica* (Vitasse et al., 2009). According to these phenological data, early-leafing species such as *B. pendula* and *Q. robur* would show the strongest growth reduction and this was the case, whereas late-leafing species (*T. cordata*, *C. sativa*, *F. excelsior*, *Q. pubescens*) showed moderate growth

losses. Remarkably, *B. pendula* also presented a high recovery capacity. The growth of the intermediate leaf-unfolding *F. sylvatica* was not negatively impacted by the hot spell, which is contradictory to its early flushing observed in 2022. Furthermore, warm and dry spring-summer conditions cause premature leaf discoloration, particularly in drought-sensitive species such as *F. sylvatica*, which should lead to growth reduction (Bigler and Vitasse, 2021). Beech showed a notable growth drop in 2020, when growing-season conditions were cool, and recovered afterwards, which could explain its elevated BAI in 2022. Besides, it was growing at the highest-elevation site, near *B. pendula*, which could have buffered the impacts of the heat wave. The intermediate-leafing *A. pseudoplatanus* showed a low growth reduction during 2022, despite its responsiveness to heat and drought stress. This is explained because it presented a prior BAI drop in 2021 (-18 %), which could also be related to cool conditions, as in *F. sylvatica*. This idea is supported by the strong correlations found between the growth indices of *F. sylvatica* and *A. pseudoplatanus* and May minimum temperatures in May.

Three species (*F. excelsior*, *A. pseudoplatanus* and *Q. pubescens*) were the most sensitive to summer maximum temperatures, low soil moisture levels and drought severity, and also showed high $\delta^{13}C$ values, indicative of improved iWUE. In addition, the low-elevation *F. excelsior* stand was the only one showing legacy effects (reduced growth in 2023, reduction in vessel density in 2024) and presented low resilience and a negative correlation between growth and maximum temperatures, whereas the vessel density increased during 2024 in the high-elevation *F. excelsior* stand. These findings do not agree with studies on drought impacts on temperate central European forests, who found marked growth reductions in diffuse-porous species such as *F. sylvatica* (Bader et al., 2022). They ascribed the higher tolerance to drought of ring-porous species to a tighter regulation of sap flow. However, wood production does not only depend on sap flow because elevated temperatures may damage foliage and reduce meristem turgor pressure that constrains cambial meristem activity (Peters et al., 2021). Under such C source and sink limitations, heat and drought stress may trigger the cessation of growth well before photosynthetic rates cease (Muller et al., 2011).

Other European ash species, such as *Fraxinus angustifolia*, were also very sensitive to summer drought under temperate conditions (Pericolo et al., 2023). *Fraxinus* tree species can be considered semi-obligate phreatophytes (cf. Hultine et al., 2020) because their roots maintain continuous contact with the water table, but they may also extract water from the vadose zone. However, under severe heat stress, they can behave as obligate phreatophytes whose water requirements are derived exclusively from the water table to cool their leaves (Posch et al., 2024). Ash species form shallow and deep (bimodal) root systems, show isohydric behavior and are prone to xylem cavitation by drought. These traits could explain the vulnerability of *F.*

excelsior to heat waves and soil drying, which would impair leaf cooling, leading to damage to the photosynthetic apparatus. In the case of *A. pseudoplatanus*, its fast-growing, pioneer strategy would explain its sensitivity to drought. This species shows rapid stomatal closure in response to a high vapor pressure deficit (VPD) during the early growing season, exposing it to heat stress (Battipaglia et al., 2008). Lastly, oaks show a more anisohydric behavior, and the stronger growth reduction of *Q. robur* as compared to *Q. pubescens* could be due to the higher drought-tolerance of the second species (Rubio-Cuadrado et al., 2018; Bose et al., 2024; Colangelo et al., 2025).

Under drier conditions, plants form smaller xylem conduits, increased ray parenchyma, and higher vessel density to enhance resistance to drought-induced xylem embolism (Gleason et al., 2016; Hacke et al., 2022). However, we did not find any significant impact of the heat wave on the hydraulic diameter or theoretical hydraulic conductivity, except in *A. pseudoplatanus*. In this species, the hydraulic diameter increased in 2022, and the ray parenchyma decreased, two responses attributable to the hot spell and which could indicate a decline in stored non-structural carbohydrates and a response to increase hydraulic conductivity. Radial parenchyma mainly contributes to storage functions and radial conduction (Carlquist, 2013), and it increases with higher precipitation and lower temperature (Martínez-Cabrera et al., 2009; Plavcová and Jansen, 2015). A limitation of our study was that we could not measure the axial parenchyma, which is a relevant proxy of carbon storage in the xylem for species with wide vessels (Morris et al., 2018).

The carbon sink in European temperate forests declined by 12% from the 2000s to the 2010s (Pan et al., 2024), but it is unclear how heat waves contributed to such decline. Predicting tree growth responses to heat stress is challenging because (i) species have developed several strategies to withstand thermal damage, and (ii) heat, VPD, and drought stress are strongly coupled (Evans et al., 2025). On one side, compound droughts characterized by low soil moisture levels and elevated VPD lead to sharp declines in ecosystem productivity, vegetation browning and trigger elevated defoliation and mortality rates (Gazol and Camarero, 2022; Gu et al., 2025). In this sense, the 2022 heat wave was associated with flash droughts, characterized by a rapid increase in evapotranspiration, accelerating the drying of soil moisture over humid regions (Yuan et al., 2023). On the other side, high VPD and low soil moisture often occur during hot spells, but they can decouple during extreme heat waves leading to vegetation browning (Liu et al., 2023). For instance, *Populus fremontii* shows an efficient leaf cooling via transpiration in riparian forests of warm deserts, but small reductions in soil water availability during heat waves inhibit the cooling capacity, causing leaf necrosis and die-off (Moran et al., 2023; Posch et al., 2024). Lastly, our findings indicate that after disturbances such as heat

waves, there may be few coordination between post-event growth rates and anatomical traits because wood production does not reflect the diverse aspects of tree growth, such as the formation of branches or roots (Hilty et al., 2021; Ziemińska et al., 2023).

5. Conclusions

In two temperate forests, early-leafing species such as *B. pendula* and *Q. robur* showed the strongest growth reductions linked to the 2022 heat wave. Shade-intolerant pioneer species such as *F. excelsior* and *A. pseudoplatanus* were particularly vulnerable to the heat wave in terms of reduction in radial growth. Moreover, *F. excelsior* showed legacy effects after the heat wave, which affected growth and vessel density. Only *A. pseudoplatanus* presented a strong response in wood anatomy showing a lower ray parenchyma fraction which indicates a decline in xylem C storage. When assessing the impacts of heat waves on tree growth, the aboveground phenology should be considered. Growth reduction, recovery and legacy effects differ among coexisting species. Thus, winner (heat-tolerant) and loser (heat-intolerant) species will emerge after heat waves leading to shifts in forest composition and productivity.

Supplementary materials

Table S1. Tree-ring statistics calculated for the study species. Abbreviations: AR1, first-order autocorrelation; MS, mean sensitivity; rbar, mean correlation. Values are means ± SD. Different letters indicate significant ($p < 0.05$) differences between species within each site according to Tukey's *Q* tests.

Site	Tree species	Timespan	Tree-ring width (mm)	AR1	MS	rbar
Cernobbio	*C. sativa*	1941–2024	2.74 ± 0.80ab	0.69 ± 0.19	0.32 ± 0.07ab	0.39 ± 0.29
	Q. pubescens	1954–2024	2.20 ± 0.80a	0.73 ± 0.14	0.27 ± 0.05a	0.44 ± 0.21
	F. excelsior	1953–2024	2.94 ± 0.77ab	0.78 ± 0.14	0.27 ± 0.04a	0.60 ± 0.20
	A. pseudoplatanus	1962–2024	4.02 ± 1.24b	0.69 ± 0.16	0.27 ± 0.07a	0.46 ± 0.33
	B. pendula	1958–2024	2.99 ± 1.12ab	0.60 ± 0.19	0.45 ± 0.09b	0.48 ± 0.21
	F. sylvatica	1925–2024	2.09 ± 0.64a	0.57 ± 0.15	0.34 ± 0.06ab	0.39 ± 0.15
Monza	*F. excelsior*	1961–2024	3.17 ± 1.32ab	0.64 ± 0.16	0.30 ± 0.04a	0.47 ± 0.28
	Q. robur	1897–2024	2.05 ± 0.50a	0.70 ± 0.19	0.25 ± 0.04a	0.38 ± 0.29
	T. cordata	1944–2024	2.75 ± 0.80	0.59 ± 0.17	0.36 ± 0.07b	0.37 ± 0.27

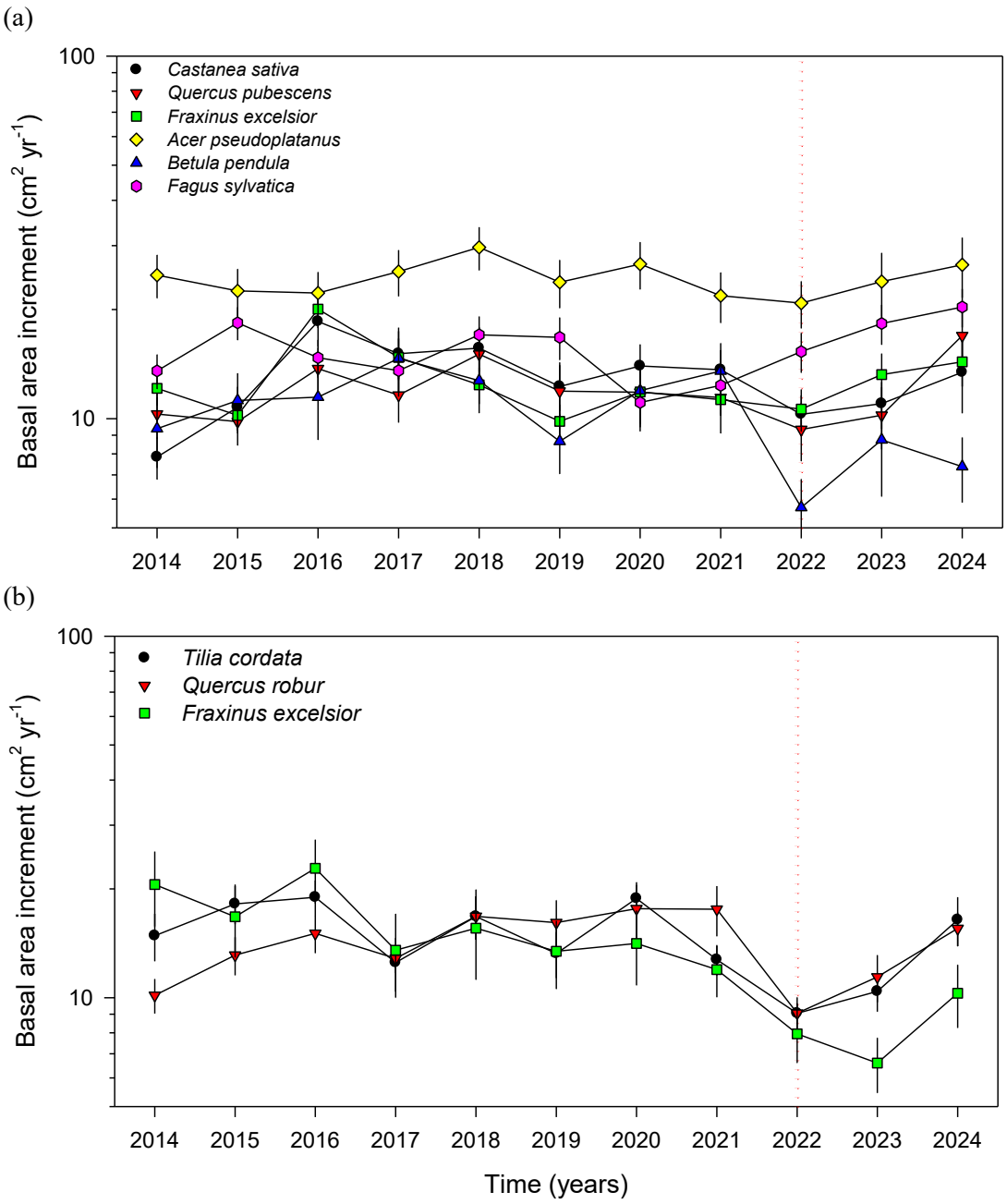

Figure S1. Basal area increment (log scale) measured in the tree species sampled in (a) Cernobbio and (b) Monza sites. The vertical dotted line indicates the 2022 summer heat wave. Values shown are means ± SE for the period 2014–2024.

(a)

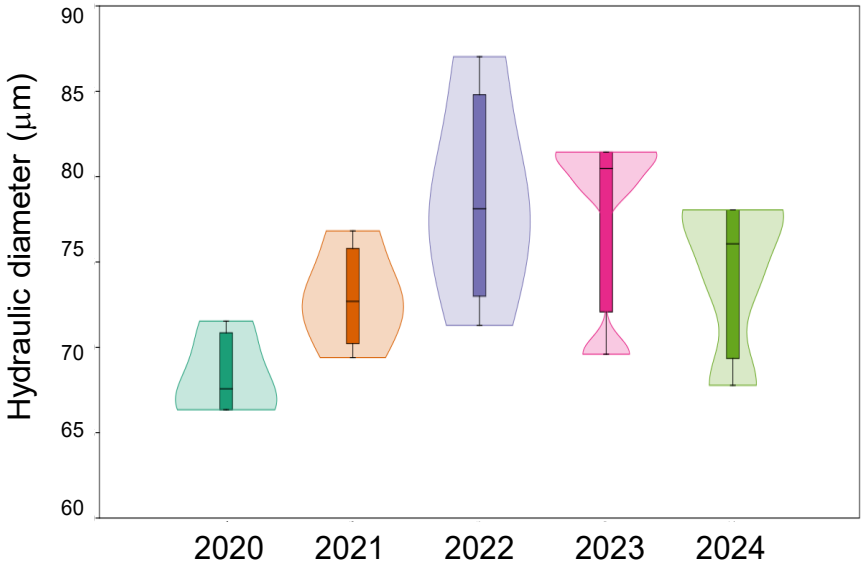

(b)

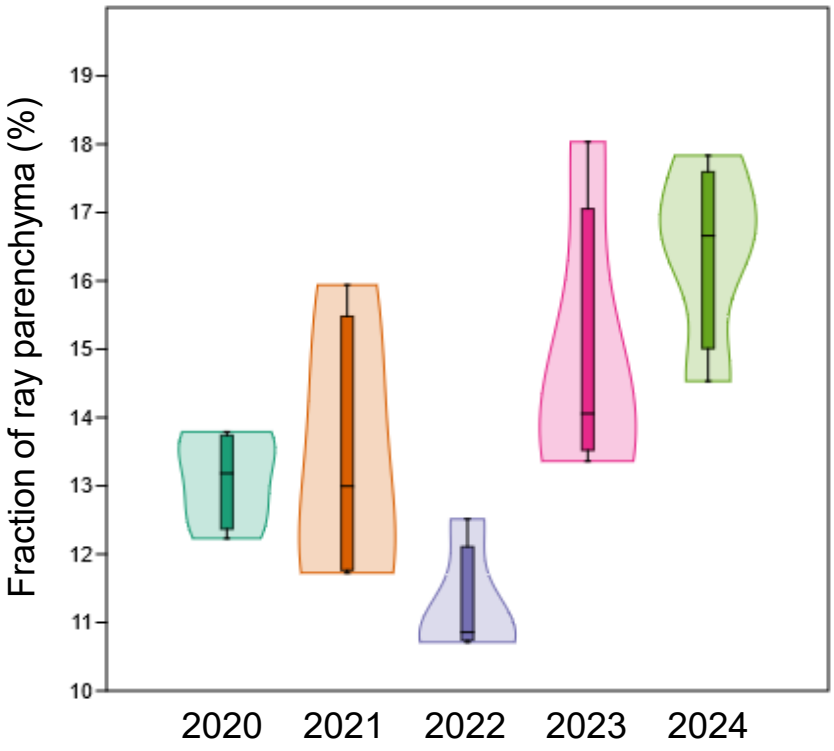

Figure S2. (a) Hydraulic diameter and (b) ray parenchyma fractions measured in *A. pseudoplatanus* tree rings during the period 2020–2024 in Cernobbio.

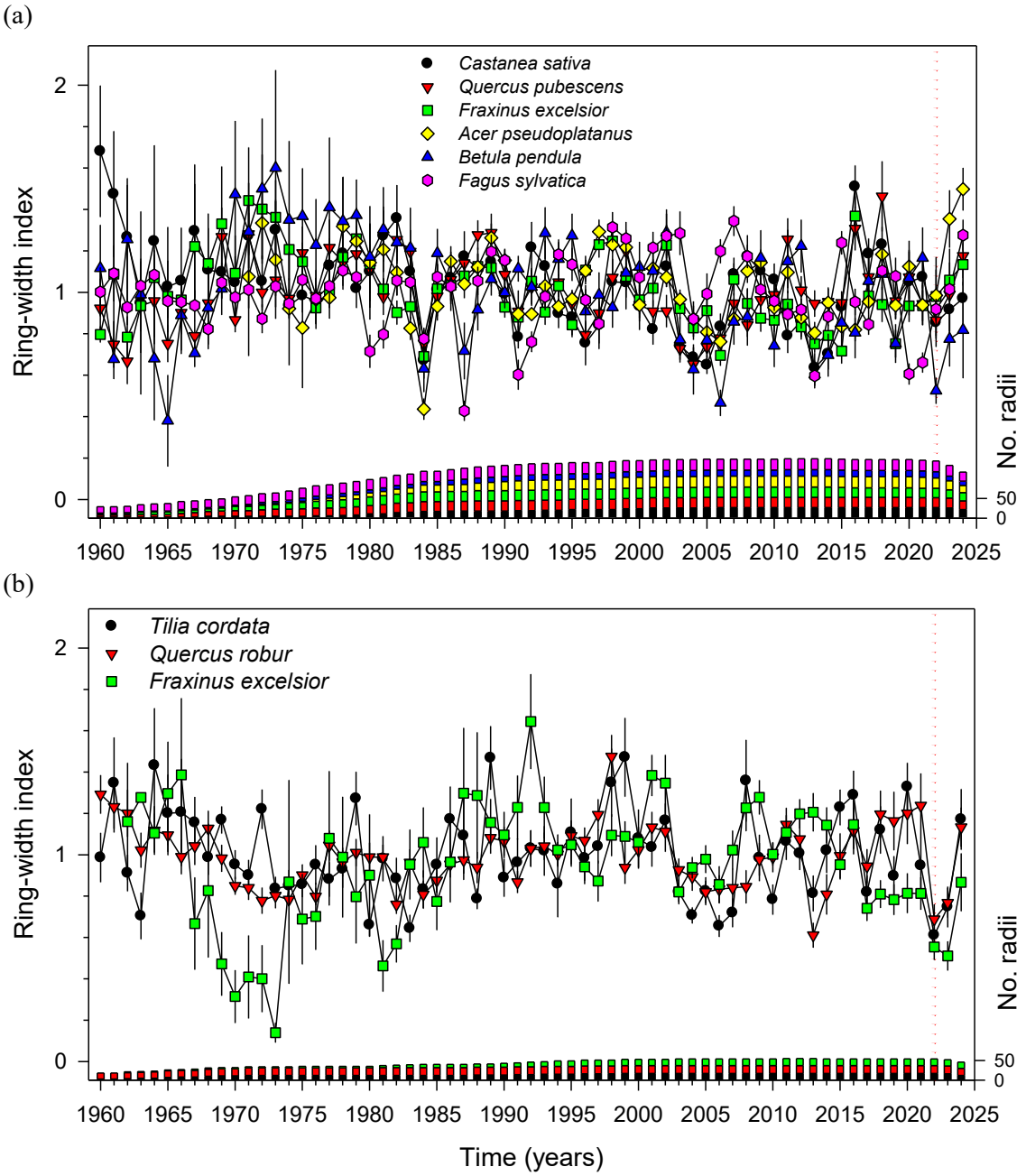

Figure S3. Series of ring-width indices calculated for the tree species sampled in (a) Cernobbio and (b) Monza sites. The vertical dotted line indicates the 2022 summer heat wave. Values are means ± SE. The annual number of measured radii is shown in the right y axes (bars).

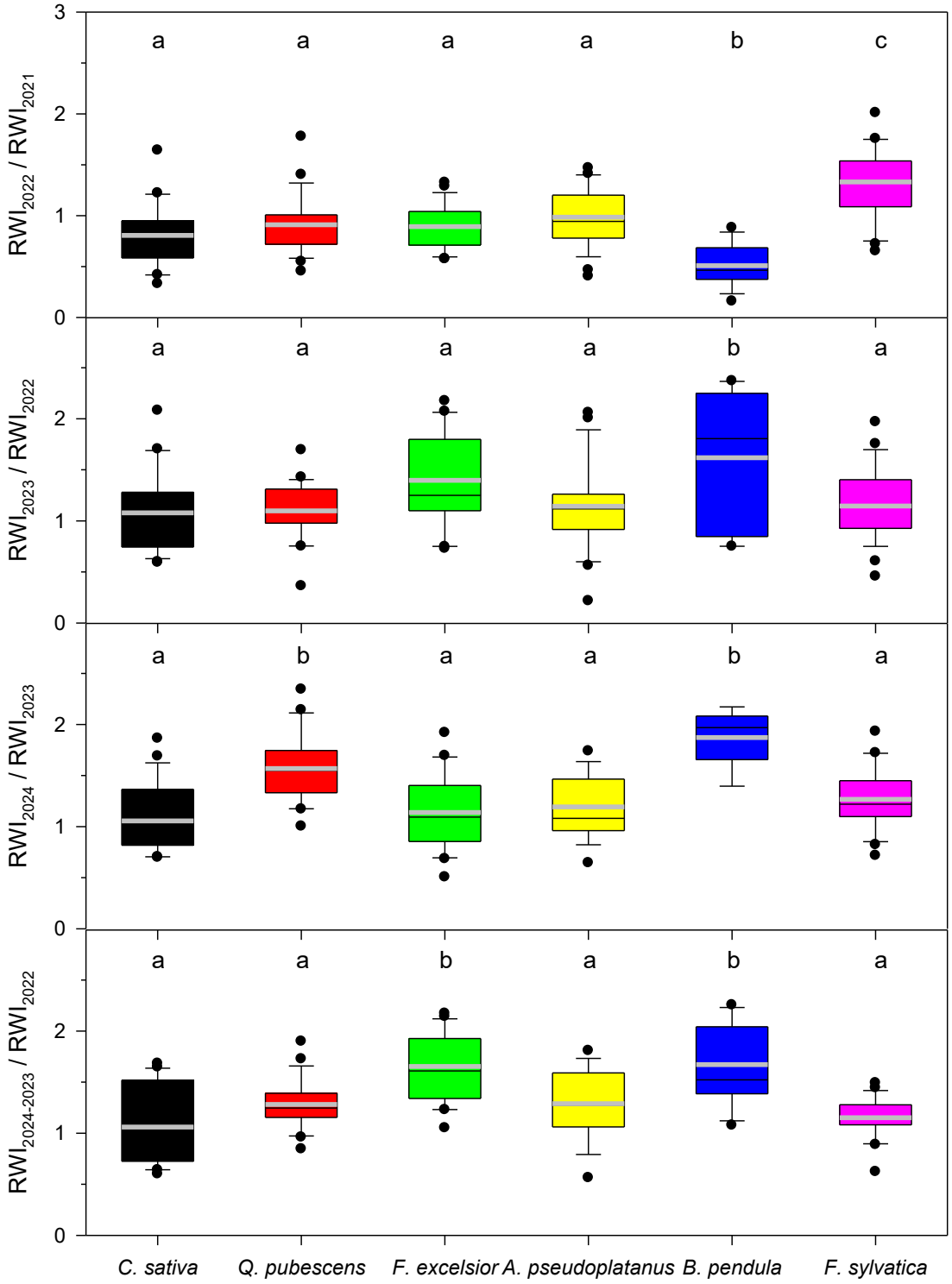

Figure S4. Resilience indices based on ring-width indices and calculated for species sampled in Cernobbio. Different letters indicate significant ($p < 0.05$) differences between species according to Tukey's Q tests.

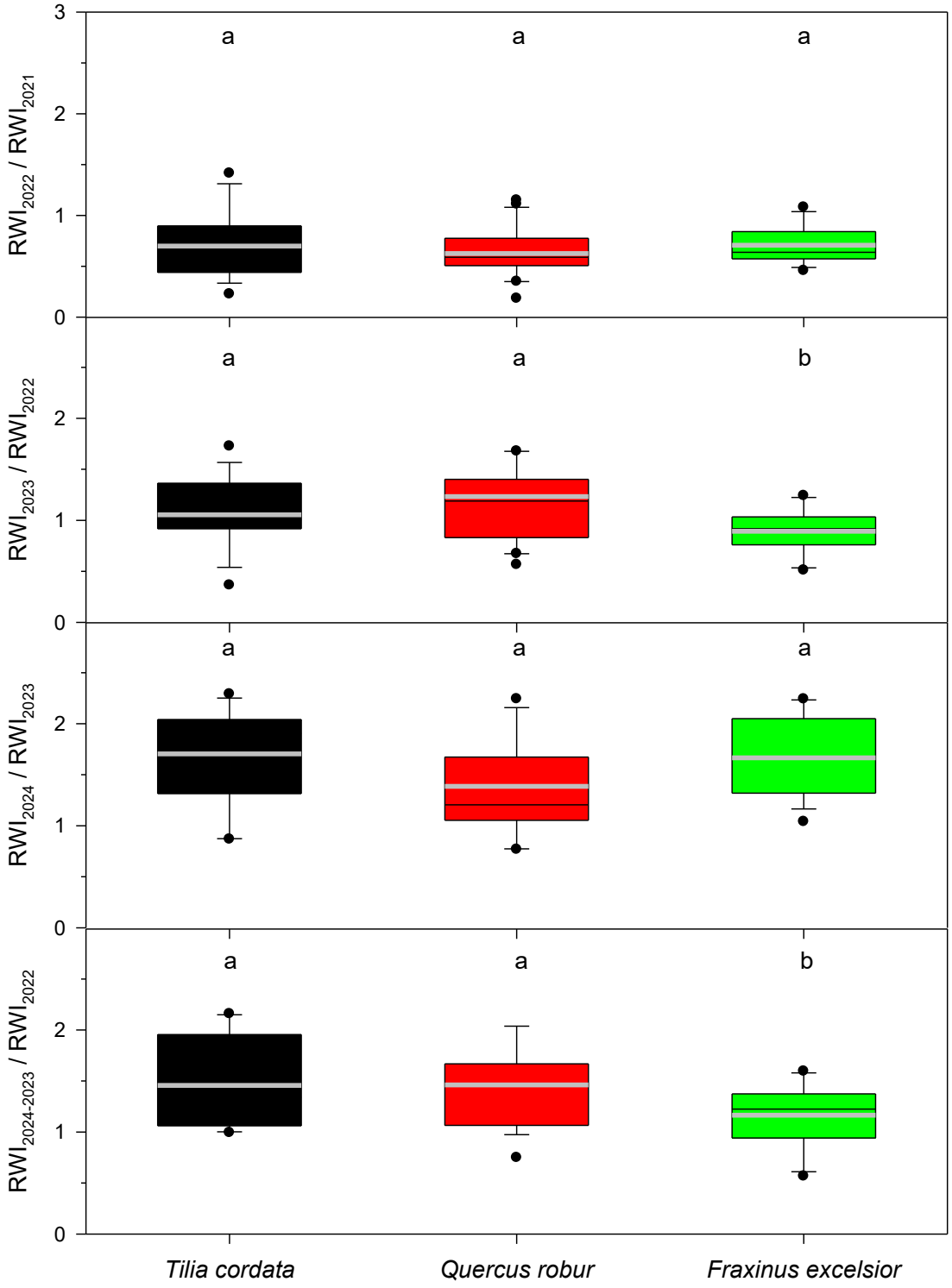

Figure S5. Resilience indices based on ring-width indices and calculated for species sampled in Monza. Different letters indicate significant ($p < 0.05$) differences between species according to Tukey's *Q* tests.

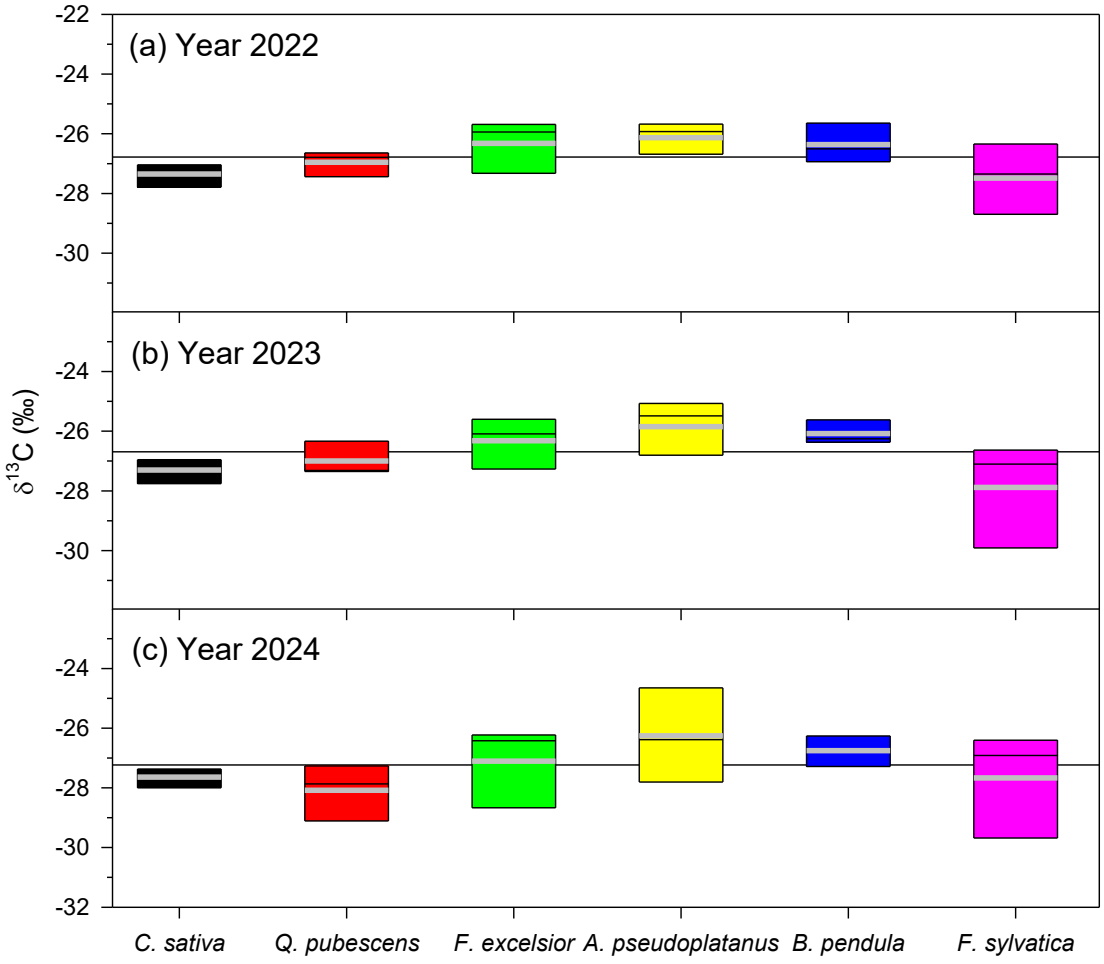

Figure S6. Wood $\delta^{13}C$ values measured in tree species sampled in Cernobbio. The horizontal lines are the mean $\delta^{13}C$ values for each study year.

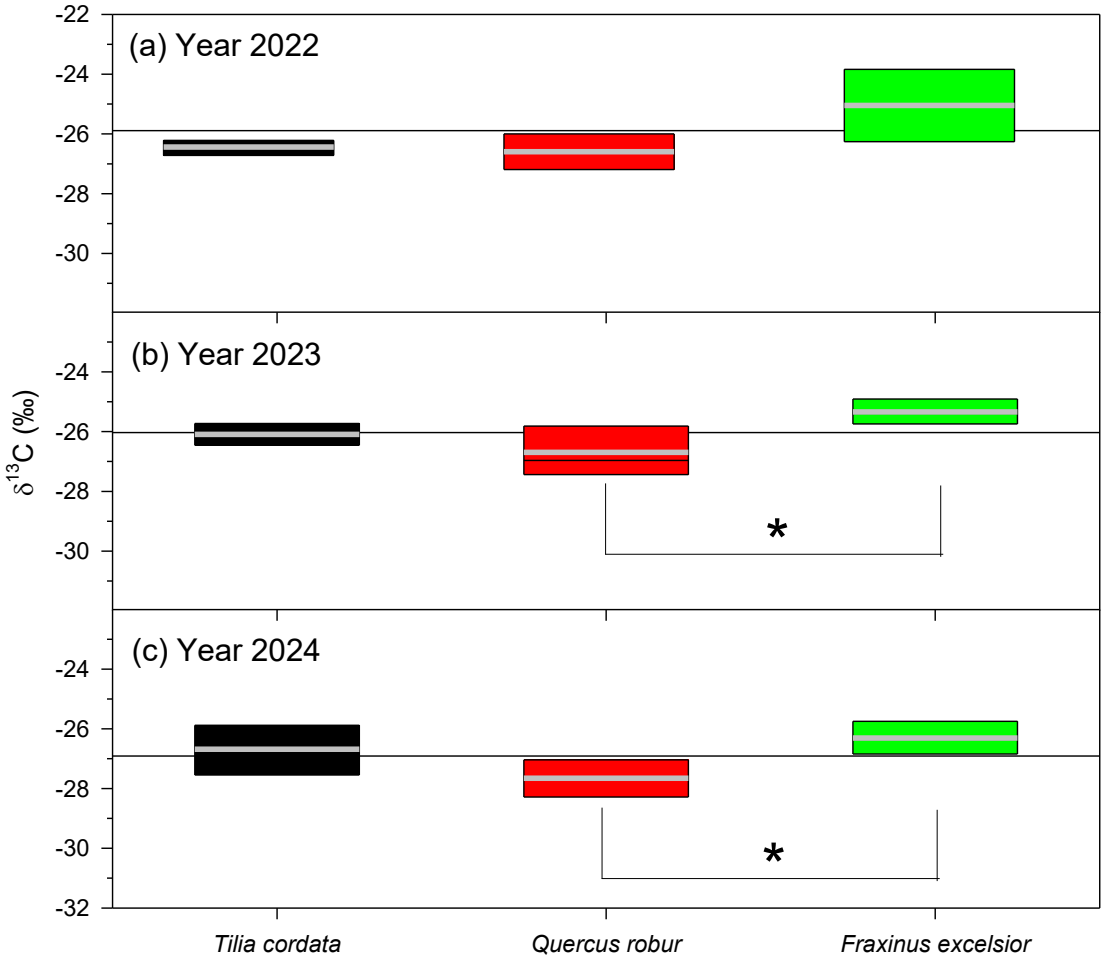

Figure S7. Wood $\delta^{13}C$ values measured in tree species sampled in Monza. The asterisks indicate significant ($p < 0.05$) differences between species in years 2023 ($p = 0.019$) and 2024 ($p = 0.024$) according to Tukey`s Q tests. The horizontal lines are the mean $\delta^{13}C$ values for each study year.

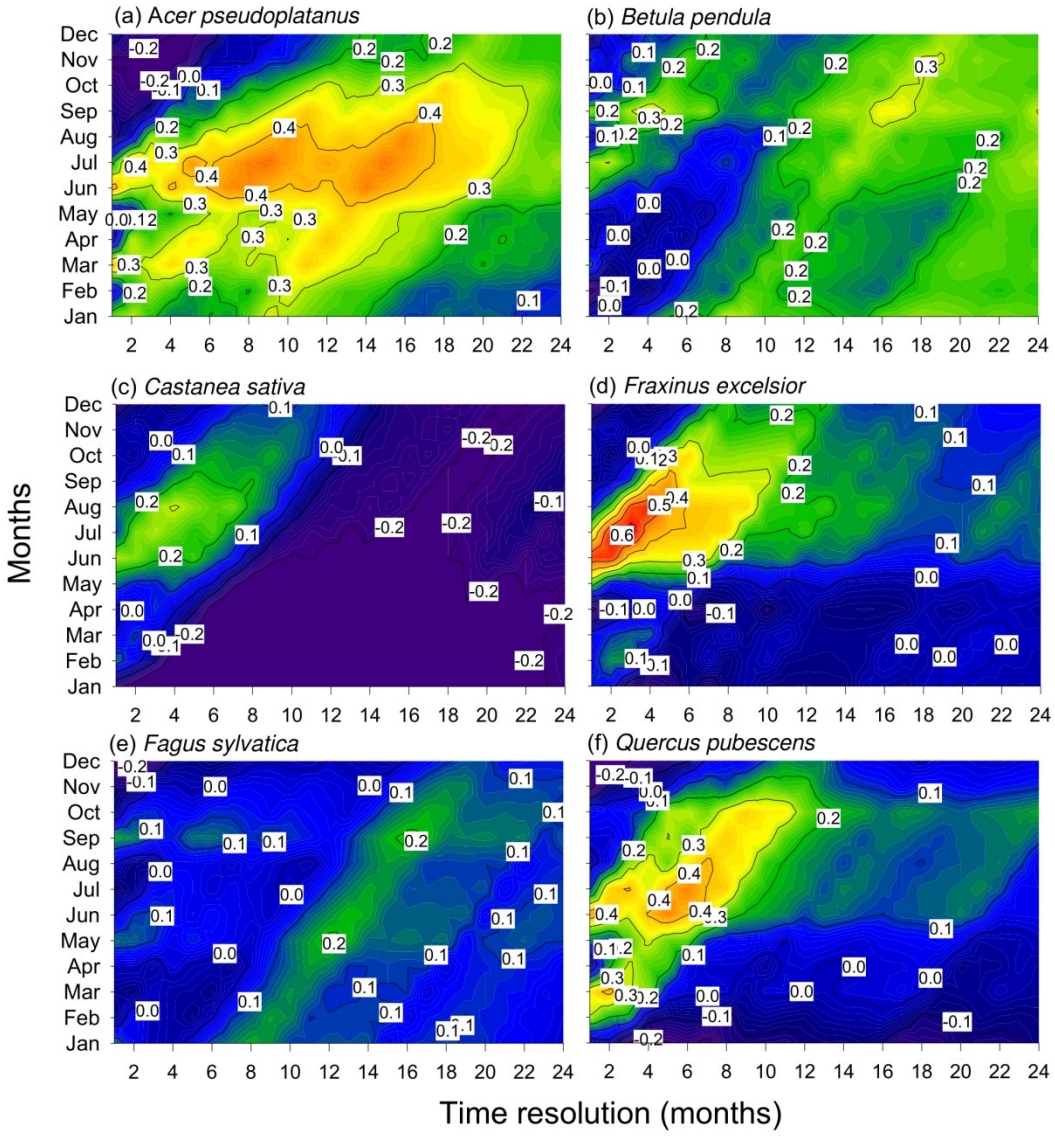

Figure S8. Drought-growth relationships in Cernobbio. For each tree species, the graphs show Pearson correlations (color scale) calculated for 1- to 24-month long resolutions of the SPEI (*x* axes) and from January to December (*y* axes).

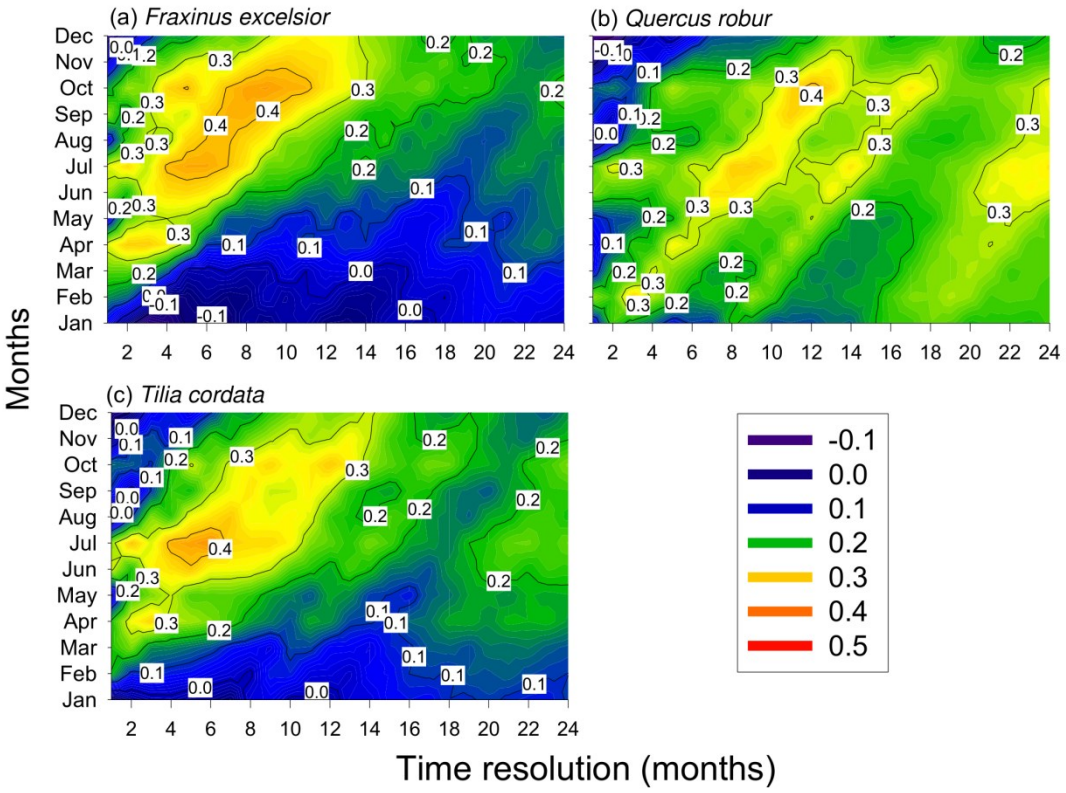

Figure S9. Drought-growth relationships in Monza. For each tree species, the graphs show Pearson correlations (color scale) calculated for 1- to 24-month long resolutions of the SPEI (*x* axes) and from January to December (*y* axes).

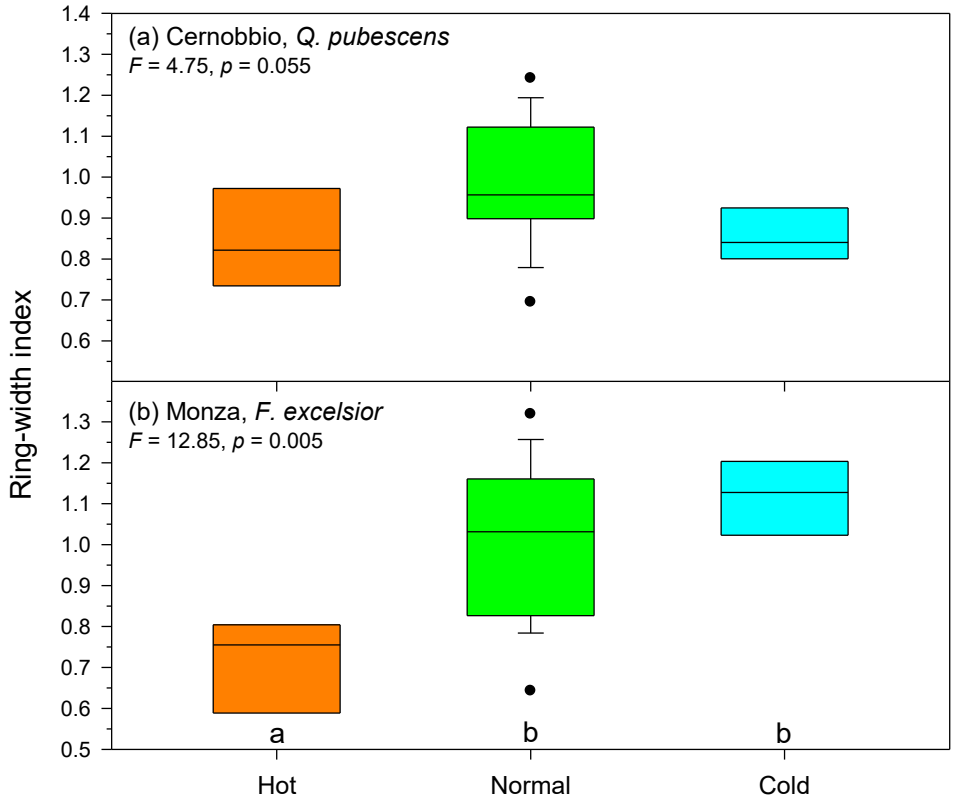

Figure S10. Values or ring-width indices during years with hot, normal and cold summers calculated for (a) *Q. pubescens* in Cernobbio, and (b) *F. excelsior* in Monza. Different letters indicate significant ($p < 0.05$) differ

References

Allen, C.D., Breshears, D.D., McDowell, N.G., 2015. On underestimation of global vulnerability to tree mortality and forest die-off from hotter drought in the Anthropocene. Ecosphere 6, 1–55.

Anderegg, W.R.L., Schwalm, C., Biondi, F., et al., 2015. Pervasive drought legacies in forest ecosystems and their implications for carbon cycle models. Science 349, 528–532.

Bader, M. K.-F., Scherrer, D., Zweifel, R., Körner, C., 2022. Less pronounced drought responses in ring-porous than in diffuse-porous temperate tree species. Agric For Meteorol 327, 109184. https://doi.org/10.1016/j.agrformet.2022.109184.

Ballester, J., Quijal-Zamorano, M., Méndez Turrubiates, R.F. et al. 2023. Heat-related mortality in Europe during the summer of 2022. Nat Med 29, 1857–1866. https://doi.org/10.1038/s41591-023-02419-z

Battipaglia, G., Jäggi, M., Saurer, M., Siegwolf, R.T.W., Cotrufo, M.F., 2008. Climatic sensitivity of $\delta^{18}O$ in the wood and cellulose of tree rings: Results from a mixed stand of *Acer pseudoplatanus* L. and *Fagus sylvatica* L. Palaeogeogr Palaeoclimatol Palaeoecol 261, 193–202

Beguería, S., Vicente-Serrano, S.M., 2023. SPEI: Calculation of the Standardized Precipitation-Evapotranspiration Index. https://github.com/sbegueria/SPEI

Bigler, C., Bugmann, H., 2018. Climate-induced shifts in leaf unfolding and frost risk of European trees and shrubs. Sci Rep 8, 9865. https://doi.org/10.1038/s41598-018-27893-1

Bigler, C., Vitasse, Y., 2021. Premature leaf discoloration of European deciduous trees is caused by drought and heat in late spring and cold spells in early fall. Agric For Meteorol 307, 108492. https://doi.org/10.1016/j.agrformet.2021.108492

Bose, A.K., Doležal, J., Scherrer, D., Altman, J., Ziche, D., et al., 2024. Revealing legacy effects of extreme droughts on tree growth of oaks across the Northern Hemisphere. Sci Total Environ 926, 172049.

Bréda, N., Huc, R., Granier, A., Dreyer, E., 2006. Temperate forest trees and stands under severe drought: a review of ecophysiological responses, adaptation processes and long-term consequences. Ann For Sci 63, 625–644. https://doi.org/10.1051/forest:2006042.

Bunn, A.G., 2008. A dendrochronology program library in R (dplR). Dendrochronologia 26, 115–124. doi: 10.1016/j.dendro.2008.01.002.

Bunn, A.G., 2010. Statistical and visual crossdating in R using the dplR library. Dendrochronologia 28, 251–258. doi: 10.1016/j.dendro.2009.12.001.

Bunn, A.G., Korpela, M., Biondi, F., Campelo, F., Mérian, P., Qeadan, F., Zang, C., 2025. dplR: Dendrochronology Program Library in R. R package version 1.7.8, https://CRAN.R-project.org/package=dplR.

Camarero, J.J., Gazol, A., Sangüesa-Barreda, G., Cantero, A., Sánchez-Salguero, R., Sánchez-Miranda, A., Granda, E., Serra-Maluquer, X., Ibáñez, R., 2018. Forest growth responses to drought at short- and long-term scales in Spain: squeezing the stress memory from tree rings. Front. Ecol. Evol. 6, 9. https://doi.org/10.3389/fevo.2018.00009.

Carlquist, S., 2013. Comparative wood anatomy: systematic, ecological, and evolutionary aspects of Dicotyledon wood. Springer, Berlin.

Colangelo, M., Camarero, J.J., Battipaglia, G., Borghetti, M., De Micco, V., Gentilesca, T., Ripullone, F., 2017. A multi-proxy assessment of dieback causes in a Mediterranean oak species. Tree Physiol 37, 617–631.

Colangelo, M., Gazol, A., Camarero, J.J., Borghetti, M., Sánchez-Salguero, R., Matias, L., Castellaneta, M., Nola, P., Ripullone, F., 2025. Earlywood vessel characteristics are early indicators of drought-induced decline in ring-porous oak species within the Mediterranean Basin. Sci Tot Environ 980, 179565. 10.1016/j.scitotenv.2025.179565

Cornes, R., van der Schrier, G., van den Besselaar, E.J.M., Jones, P.D., 2018. An ensemble version of the E-OBS temperature and precipitation datasets. J Geophys Res Atmos 123, 9391–9409. https://doi.org/10.1029/2017JD028200.

D'Alessandro, C.M., Guerrieri, M.R., Saracino, A., 2004. Comparing carbon isotope composition of bulk wood and holocellulose from *Quercus cerris*, *Fraxinus ornus* and *Pinus radiata* tree rings. Forest@ 1, 51–57.

D'Orangeville, L., Maxwell, J., Kneeshaw, D., Pederson, N., Duchesne, L., et al., 2018. Drought timing and local climate determine the sensitivity of eastern temperate forests to drought. Glob Chang Biol 24, 2339–2351. doi: 10.1111/gcb.14096.

Evans, M.E.K., Hu, J., Michaletz, S.T., 2025. Scaling plant responses to heat: From molecules to the biosphere. Science 388, 1167–1173. 0.1126/science.adv7597

Francey, R.J., Farquhar, G.D., 1982. An explanation of $^{13}C/^{12}C$ variations in tree rings. Nature 297, 28–31.

Fritts, H., 1976. Tree Rings and Climate. Academic Press, London.

Gärtner, H., Lucchinetti, S., Schweingruber, F.H., 2015. A new sledge microtome to combine wood anatomy and tree-ring ecology. IAWA J 36, 452–459. https://doi.org/10.1163/22941932-20150114.

Gazol, A., Camarero, J.J., 2022. Compound climate events increase tree drought mortality across European forests. Sci Tot Environ 816, 151604.

Gleason, S.M., Westoby, M., Jansen, S., et al., 2016. Weak tradeoff between xylem safety and xylem-specific hydraulic efficiency across the world's woody plant species. New Phytol 209, 123–136.

Granda, E., Alla, A. Q., Laskurain, N. A., Loidi, J., Sánchez-Lorenzo, A., Camarero, J.J., 2018. Coexisting oak species, including rear-edge populations, buffer climate stress through xylem adjustments. Tree Physiol 38, 159–172. doi: 10.1093/treephys/tpx157

Gu, L., Schumacher, D.L., Fischer, E.M., Slater, L.J., Yin, J., Sippel, S., Chen, J., Liu, P., Knutti, R., 2025. Flash drought impacts on global ecosystems amplified by extreme heat. Nat Geosci https://doi.org/10.1038/s41561-025-01719-y

Hacke, U.G., Jacobsen, A.L., Pratt, R.B., 2022. Vessel diameter and vulnerability to drought-induced embolism: within-tissue and across-species patterns and the issue of survivorship bias. IAWA J 44, 304–319.

Hammer, Ø., Harper, D.A.T., Ryan, P.D., 2001. PAST: Paleontological Statistics Software Package for Education and Data Analysis. Palaeontologia Electr 4, 9.

Hilty, J., Muller, B., Pantin, F., Leuzinger, S., 2021. Plant growth: The what, the how, and the why. New Phytol 232, 25–41.

Hoffmann, W.A., Marchin, R.M., Abit, P., Lau, O.L., 2011. Hydraulic failure and tree dieback are associated with high wood density in a temperate forest under extreme drought. Global Change Biol 17, 2731–2742.

Holmes, R.L., 1983. Computer-assisted quality control in tree-ring dating and measurement. Tree-Ring Bull 43, 69–78.

Hultine, K.R., Froend, R., Blasini, D., Bush, S.E., Karlinski, M., Koepke, D.F., 2020. Hydraulic traits that buffer deep-rooted plants from changes in hydrology and climate. Hydrol Process 34, 209−222. https://doi.org/10.1002/hyp.13587

Ingrisch, J., Bahn, M., 2018. Towards a comparable quantification of resilience. Trends Ecol Evol 33, 251–259.

IPCC, 2023. Climate Change 2023: Synthesis Report. Contribution of Working Groups I, II and III to the Sixth Assessment Report of the Intergovernmental Panel on Climate Change [Core Writing Team, H. Lee and J. Romero (eds.)]. IPCC, Geneva, Switzerland, pp. 35−115. doi: 10.59327/IPCC/AR6-9789291691647.

Italiano, S.S.P., Camarero, J.J., Borghetti, M., Colangelo, M., Pizarro, M., Ripullone, F., 2023. Radial growth, wood anatomical traits and remote sensing indexes reflect different impacts of drought on Mediterranean forests. For Ecol Manage 548, 121406.

Italiano, S.S.P., Camarero, J.J., Borghetti, M., Colangelo, M., Rita, A., Ripullone, F., 2024. Drought legacies in mixed Mediterranean forests: analysing the effects of structural overshoot, functional traits and site factors. Sci Tot Environ 927, 172166.

Jiang, P., Liu, H., Piao, S., Ciais, P., Wu, X., Yin, Y., Wang, H., 2019. Enhanced growth after extreme wetness compensates for post-drought carbon loss in dry forests. Nat Comm 10, 195. https://doi.org/10.1038/s41467-018-08229-z.

Jump, A.S., Ruiz-Benito, P., Greenwood, S., Allen, C.D., Kitzberger, T., Fensham, R., Martínez-Vilalta, J., Lloret, F., 2017. Structural overshoot of tree growth with climate variability and the global spectrum of drought-induced forest dieback. Global Change Biol 23, 3742–3757. https://doi.org/10.1111/gcb.13636.

Kannenberg, S.A., Maxwell, J.T., Pederson, N., D'Orangeville, L., Ficklin, D.L., Phillips, R.P., 2019. Drought legacies are dependent on water table depth, wood anatomy and drought timing across the eastern US. Ecol Lett 22, 119–127. doi: 10.1111/ele.13173.

Kannenberg, S.A., Schwalm, C.R., Anderegg, W.R., 2020. Ghosts of the past: how drought legacy effects shape forest functioning and carbon cycling. Ecol Lett 23, 891–901. https://doi.org/10.1111/ele.13485.

Larsson, L.A., Larsson, P.O., 2018. CDendro and CooRecorder (v. 9.3.1); Cybis Elektronik and Data AB. Saltsjöbaden, Sweden.

Liu, X., Sun, G., Fu, Z., Ciais, P., Feng, X. et al., 2023. Compound droughts slow down the greening of the Earth. Global Change Biol 29, 3072–3084. 10.1111/gcb.16657

Martín-Benito, D., Pederson, N., 2015. Convergence in drought stress, but a divergence of climatic drivers across a latitudinal gradient in a temperate broadleaf forest. J Biogeogr 42, 925–937. https://doi.org/10.1111/jbi.12462

Martínez-Cabrera, H.I., Jones, C.S., Espino, S., Schenk, H.J., 2009. Wood anatomy and wood density in shrubs: Responses to varying aridity along transcontinental ransects. American J Botany 96, 1388–1398.

McCarroll, D., Loader, N.J., 2004. Stable isotopes in tree rings. Quat Sci Rev 23, 771–801. https://doi.org/10.1016/j.quascirev.2003.06.017.

Michelot, A., Simard, S., Rathgeber, C., Dufrêne, E., Damesin, C., 2012. Comparing the intra-annual wood formation of three European species (*Fagus sylvatica, Quercus petraea* and *Pinus sylvestris*) as related to leaf phenology and non-structural carbohydrate dynamics. Tree Physiol 32, 1033–1045. doi: 10.1093/treephys/tps052.

Moran, M.E., Aparecido, L.M.T., Koepke, D.F., Cooper, H.F., Doughty, C.E., et al., 2023. Limits of thermal and hydrological tolerance in a foundation tree species (*Populus*

fremontii) in the desert southwestern United States. New Phytol 240, 2298–2311. https://doi.org/10.1111/nph.19247.

Morris, H., Gillingham, M. A. F., Plavcová, L., Gleason, S. M., Olson, M.E., et al., 2018. Vessel diameter is related to amount and spatial arrangement of axial parenchyma in woody angiosperms. Plant, Cell Environ 41, 245–260.

Muller, B., Pantin, F., Génard, M., Turc, O., Freixes, S., Piques, M., Gibon, Y., 2011. Water deficits uncouple growth from photosynthesis, increase C content, and modify the relationships between C and growth in sink organs. J Exp Bot 62, 1715–1729.

Nardini, A., Battistuzzo, M., Savi, T., 2013. Shoot desiccation and hydraulic failure in temperate woody angiosperms during an extreme summer drought. New Phytol 200, 322−329. doi: 10.1111/nph.12288.

Pan, Y., Birdsey, R.A., Phillips, O.L., Houghton, R.A., Fang, J. et al., 2024. The enduring world forest carbon sink. Nature 631, 563–569. https://doi.org/10.1038/s41586-024-07602-x

Pericolo, O., Camarero, J.J., Colangelo, M., Valeriano, C., Sánchez-Salguero, R., et al., 2023. Species-specific vulnerability to increased drought in temperate and Mediterranean floodplain forests. Agric For Meteorol 328, 109238. https://doi.org/10.1016/j.agrformet.2022.109238.

Peters, R.L., Steppe, K., Cuny, H.E., De Pauw, D.J.W., Frank, D.C., Schaub, M., Rathgeber, C.B.K., Cabon, A., Fonti, P., 2021. Turgor – a limiting factor for radial growth in mature conifers along an elevational gradient. New Phytol 229, 213–229.

Pignatti, S., (ed.). 1998. I boschi d'Italia. UTET, Torino, 677 pp

Plavcová, L., Jansen, S., 2015. The role of xylem parenchyma in the storage and utilization of nonstructural carbohydrates. In U. Hacke (Ed.), Functional and ecological xylem anatomy. Springer, Cham, pp. 209–234.

Posch, B.C., Bush, S.E., Koepke, D.F., Schuessler, A., Anderegg, L.L.D., et al., 2024. Intensive leaf cooling promotes tree survival during a record heatwave. PNAS USA 121, e2408583121. https://doi.org/10.1073/pnas.2408583121

R Development Core Team. 2024. R: A Language and Environment for Statistical Computing. Vienna, Austria.

Rita, A., Camarero, J.J., Nolè, A., Borghetti, M., Brunetti, M., Pergola, N., Serio, C., Vicente-Serrano, S.M., Tramutoli, V., Ripullone, F., 2020. The impact of drought spells on forests depends on site conditions: The case of 2017 summer heat wave in southern Europe. Global Chang. Biol 26, 851–863. https://doi.org/10.1111/gcb.14825.

Rodell, M., Houser, P.R., Jambor, U., Gottschalck, J., Mitchell, K., Meng, C.J., et al., 2004. The global land data assimilation system. Bull Am Meteorol Soc 85, 381–394. https://doi.org/10.1175/BAMS-85-3-381.

Rouder, J.N., Speckman, P.L., Sun, D., Morey, R.D., Iverson, G., 2009. Bayesian *t* tests for accepting and rejecting the null hypothesis. Psychonomic Bull & Rev 16, 225–237.

Rubio-Cuadrado, A., Camarero, J.J., del Río, M., Sánchez-González, M., Ruiz-Peinado, R., Bravo-Oviedo, A., Gil, L., Montes, F., 2018. Drought modifies tree competitiveness in an oak-beech temperate forest. For Ecol Manage 429, 7–17.

Ruehr, N.K., Grote, R., Mayr, S., Arneth, A., 2019. Beyond the extreme: recovery of carbon and water relations in woody plants following heat and drought stress. Tree Physiol 39, 1285–1299. https://doi.org/10.1093/treephys/tpz032

Sass-Klaassen, U., Sabajo, C.R., den Ouden, J., 2011. Vessel formation in relation to leaf phenology in pedunculate oak and European ash. Dendrochronologia 29, 171–175.

Schneider, C., Rasband, W., Eliceiri, K., 2012. NIH image to ImageJ: 25 years of image analysis. Nat. Methods 9, 671–675. https://doi.org/10.1038/nmeth.2089.

Scholz, A., Klepsch, M., Karimi, Z., Jansen, S., 2013. How to quantify conduits in wood? Frontiers in Plant Sci 4, 56.

Schwarz, J., Skiadaresis, G., Kohler, M., Kunz, J., Schnabel, F., Vitali, V., Bauhus, J., 2020. Quantifying growth responses of trees to drought — a critique of commonly used resilience indices and recommendations for future studies. Current Forestry Reports 6, 185–200.

Serra-Maluquer, X., Granda, E., Camarero, J.J., Vilà-Cabrera, A., Jump, A., Sánchez-Salguero, R., Sangüesa-Barreda, G., Imbert, B., Gazol, A., 2021. Impacts of recurrent dry and wet years alter long-term tree growth trajectories. J Ecol 109, 1561–1574. https://doi.org/10.1111/1365-2745.13579

Suzuki, M., Yoda, K., Suzuki, H., 1996. Phenological comparison on the onset of vessel formation between ring-porous and diffuse-porous deciduous trees in a Japanese temperate forest. IAWA J 17, 431–444.

Vitasse, Y., Delzon, S., Dufrêne, E., Pontailler, J.-Y., Louvet, J.-M., Kremer, A., Michalet, R., 2009. Leaf phenology sensitivity to temperature in European trees: Do within-species populations exhibit similar responses? Agric For Meteorol 149, 735–744.

Yuan, X., Wang, Y., Ji, P., Wu, P., Sheffield, J., Otkin, J.A., 2023. A global transition to flash droughts under climate change. Science 380, 187–191. doi: 10.1126/science.abn6301

Zang, C., Biondi, F., 2015. Treeclim: An R package for the numerical calibration of proxy-climate relationships. Ecography 38, 431–436.

Ziemińska, K., Bibbo, S., Farrar, S., Thompson, J., Uriarte, M., Ziaco, E., Zimmerman, J.K., Muscarella, R., 2023. Shifts in wood anatomical traits after a major hurricane. Funct. Ecol 37, 3000–3014. https://doi.org/10.1111/1365-2435.14451

Divergent seasonal processes drive CH_4 fluxes across tundra in Alaska

Abstract

Arctic tundra largely contributes to global CH_4 emissions which are influenced by several factors, including climate, soil properties, vegetation, permafrost thaw and seasonality.

We analysed the CH_4 fluxes from peak growing season to autumn 2023 of three vegetation types (dry, wet and tussock tundra) at Toolik (Alaska). We aim to analyse the spatial and temporal variability of CH_4 fluxes, identify its biotic and abiotic drivers, emphasize the occurrence of divergent seasonal processes.

The general regression models indicated vegetation type and air temperature as drivers of CH_4 fluxes. The tussock tundra, unexpectedly, produced the highest CH_4 emissions followed by the wet tundra. In summer the high CH_4 production was favoured by soil water saturation, unfrozen thickness and warm temperatures. The higher emissions in the tussock tundra are due to the CH_4 transport through the tussocks' aerenchyma, avoiding its re-oxidation to CO_2, bypassing the soil oxic layers. The highest CH_4 emissions occurred in November both in tussock and wet tundra, when the two-sided front of the soil freezing decreased the soil unfrozen thickness, inducing CH_4 compression, pushing it up to the surface through the plants' tissues. The dry tundra performed CH_4 uptake during summer, while it was inactive in autumn, differently from other studies recording CH_4 emissions in winter. Our findings suggest more investigations to encompass the effect of vegetation on the variability of CH_4 fluxes and disentangle the potential for high emissions during the cold seasons and their contribution to the annual budget.

Keywords: Methane; Arctic tundra; vegetation; plant mediated transport; cold season emissions; divergent seasonal dynamics.

1. Introduction

Northern permafrost regions are estimated to store 1,100-1,500 Pg of Carbon within permafrost (Hugelius et al., 2014), corresponding to 1.6 Gt of soil organic carbon (SOC) (Schuur et al., 2015), which could be released to the atmosphere as CH_4 and CO_2 emissions triggering relevant positive feedbacks to recent climatic change.

Despite low temperatures, the Arctic tundra contributed to c. 45% of all Arctic CH_4 sources and provides a large contribution to global CH_4 emissions, estimated to range between 7% (McGuire et al., 2012; Kirschke et al., 2013) and 20 to 25% of global natural CH_4 emissions (15 to 50 Tg CH_4 $year^{-1}$) Kirschke et al., 2013; Wang et al., 2024). CH_4 emissions are particularly important as their global warming potential is 28–34 times greater than CO_2 (Myhre et al., 2013), making CH_4 a greenhouse gas 80 times more effective than CO_2. It is responsible for approximately 20% of the direct radiative forcing since 1750 and contributes to a radiative forcing of 0.43–0.65 Wm^{-2} (Forster et al., 2021; Mar et al., 2022). Out of a total observed warming of 1.07 °C during the period 2010 to 2019, the Working Group I (WGI) 2021 Intergovernmental Panel on Climate Change (IPCC) Sixth Assessment Report (AR6) attributed 0.5 °C to CH_4 emissions (Shindell et al., 2024).

The Arctic tundra is a significant carbon reservoir, containing approximately 14% of the global soil organic carbon (Billings, 1987; Zona et al., 2009). CH_4 production in the carbon-rich soils of this region is primarily driven by microbial metabolic processes (LAI, 2009; Kirschke et al., 2013). The conversion of organic carbon into CH_4 involves a complex series of biochemical reactions (Whalen, 2005; Howard et al., 2020). In this pathway, methanogenic archaea play a crucial role in the final stages, converting acetate and CO_2 into CH_4. However, the final CH_4 outcome depends on the overall composition of the microbial communities, since there are methanotrophic bacteria involved in CH_4 oxidation (Oh et al., 2020). Methanogenic archaea are obligate anaerobic microorganisms, so CH_4 production occurs only in absence of oxygen. Consequently, methanogenesis predominantly occurs in the anoxic layers of soils, such as those below the water table or in water-saturated environments (Dunfield et al., 1993; Conrad, 2009; Le Mer and Roger, 2001; Nazaries et al., 2013). CH_4 is then released into the atmosphere through three primary pathways: diffusion, ebullition, or plant-mediated transport via vascular plants (Preuss et al., 2013; Xu et al., 2016).

Empirical observations of CH_4 flux indicate that both meteorological conditions and soil properties influence CH_4 dynamics. Data from the Carbon in Permafrost Experimental Heating Research (CiPEHR) project demonstrated significant increases in methane emissions under elevated soil temperatures even in the upland tundra ecosystems, where ecosystem warming, permafrost thaw, and soil moisture change increased CH_4 emissions (Natali et al., 2015). The

rate of methanogenesis is temperature-dependent, with an increased rate of change per unit of warming, as indicated by activation energies of 123-127 kJ mol-1 at 25 °C, and Q10 values ranging from 5.3 to 16 (Dunfield et al., 1993), and observed positive correlations between surface soil temperature and CH_4 fluxes (Zona et al., 2016). The depth of the water table is another critical factor regulating CH_4 emissions from peatlands. Numerous studies have reported an inverse relationship between average water table depth and seasonal CH_4 emissions (Zona et al., 2009), while in some cases water table depth was found positively correlated with CH_4 emission (Hiyama et al., 2021). Soil pH also may play a significant role in CH_4 production, with more neutral soils producing higher CH_4 emissions compared to more acidic soils (Wagner et al., 2017). Also changes of snow cover may affect CH_4 emissions, as the Arctic tundra transitioned from being a minor CH_4 source to a sustained CH_4 sink under conditions of reduced winter snow, and the opposite with increases in winter snow depth (Blanc-Betes et al., 2016).

CH_4 emissions from permafrost soil in Arctic have been well documented (Tom and Chapin, 1993; Ueyama et al., 2006; Kim et al., 2007; Kim, 2015) and recognised as a significant biogenic source of high-latitude atmospheric methane concentrations (Zhuang et al., 2004; McGuire et al., 2009). There have been several studies documenting scale and dynamics of CH_4 emissions using chamber flux measurements within Arctic in growing and winter season (Mastepanov et al., 2013; Howard et al., 2020; Kade et al., 2024), specific vegetation communities (Kim et al., 2007; Davidson et al., 2016), using above ground climatic variables (Sturtevant et al., 2012; Howard et al., 2020) or below ground abiotic parameters (Christensen et al., 2003; Davidson et al., 2016). Some studies focused on autumn freeze shoulder season and summer season for CH_4 fluxes due to challenging conditions also pointed out by Howard et al., (2020) and Kim et al., (2007), with recent observations suggesting that CH_4 emissions during the cold season could largely contribute to the annual CH_4 emissions (Ward et al., 2024). The role of vegetation was emphasized as an integrator of processes controlling CH_4 emissions (Davidson et al., 2016), with wetlands being one of the most important sources of CH_4 emissions among the heterogeneous vegetation communities occurring in the Arctic tundra (e.g. McGuire et al., 2009; McEwing et al., 2015; Davidson et al., 2016; Euskirchen et al., 2017). In particular, a simplified vegetation classification using just three classes (wet sedge, wet tussock and other) has been indicated as effective in explaining a large amount of the variation in CH_4 fluxes measured at different locations in Alaska (Davidson et al., 2016).

This study focuses on assessment of the role of different key biotic, abiotic variables of soil to understand their role to CH_4 fluxes from mid-summer to autumn freeze winter season.

Here, we analyse a dataset obtained by daily CH_4 flux measurements measured twice a week from peak growing season (July, 2023) to autumn freeze shoulder season (November, 2023) on

three different vegetation types (dry tundra, wet tundra, tussock tundra, with three replicates for each) representative of the most widespread vegetation communities occurring at Toolik Field Station, in northern Arctic Alaska (US) and congruent with the three vegetation classes indicated by Davidson et al. (2016) as suitable for the analysis of most of the variation in CH_4 fluxes.

We aim to: a) identify the spatial and temporal trends of CH_4 fluxes at inter- and intra-community level; b) assess which are the main biotic and abiotic drivers of CH_4 fluxes at inter- and intra-community level; c) highlight the role of autumn as shoulder/transition season when the highest CH_4 emissions were observed.

2. Materials and Methods

2.1. Study area

The study area lies in a continuous permafrost zone near to the North slope of Brooks Range, in northern Arctic Alaska at Toolik Field Station (68°38' N 149°34' W, 760 m elevation) (Fig.1). The active layer thickness (ALT) measured not far from our sites has been monitored since 1995 and ranges from 67.5 (2002) to 100 (2001) cm (Shiklomanov, 2023). The region faces cold winters (air temperatures down to -30°C) and for relatively warm summers (up to 13°C), with annual rainfall range of ca. 300 mm (Huryn and Hobbie, 2012; Greaves et al., 2019). The snowpack melting starts in mid-May, while the soil freezing occurs between late September to early October.

Vegetation is a mosaic of different tundra types, with the most widespread communities being the dry heath tundra (hereafter named “dry tundra”), the moist acidic tussock tundra (hereafter named “tussock tundra”), and the wet sedge tundra (hereafter named “wet tundra”) (Euskirchen et al., 2012; Greaves et al., 2019; Kade et al., 2012; Walker & Maier, 2008). The dry tundra is dominated by dwarf evergreen and deciduous shrubs, *Arctostaphylos alpina, Dryas octopetala* and *Vaccinium vitis-idaea,* deciduous dwarf shrubs such as *Salix chamissonis,* the graminoid *Carex bigelowii,* mosses such as *Tomenthypnum nitens, Distichium capillaceum* and lichens. The tussock tundra community, also known as moist acidic tussock-tundra, is dominated by *Eriophorum vaginatum, Sphagnum* spp., with deciduous shrubs such as *Betula nana* and *Salix* spp., evergreen dwarf shrubs such as *Rhododendron tomentosum, Rubus chamaemorus, Cassiope tetragona, Empetrum nigrum, Vaccinium vitis-idaea* and thick moss layers consisting of *Aulacomnium turgidum, Hylocomium splendens*, *Sphagnum* spp. and lichens. The wet meadow tundra, also known as wet sedge tundra, is dominated by *Carex aquatilis*, *Eriophorum angustifolium*, dwarf deciduous shrubs such as *Rubus chamaemorus, Betula nana, Salix* spp.,

Rhododendron tomentosum, Andromeda polifolia, the forb *Pedicularis capitata,* and the mosses *Aulacomnium turgidum, Sphagnum* spp..

2.2. CH_4 Flux-measurement

The sites for the flux measurements were chosen in a very small area with very similar topographical characteristics (Table 1) in correspondence of the three most widespread and characteristic vegetation communities of the Arctic tundra: dry tundra, tussock tundra, wet tundra (Walker & Maier, 2008; Euskirchen et al., 2012; Kade et al., 2012; Greaves et al., 2019).

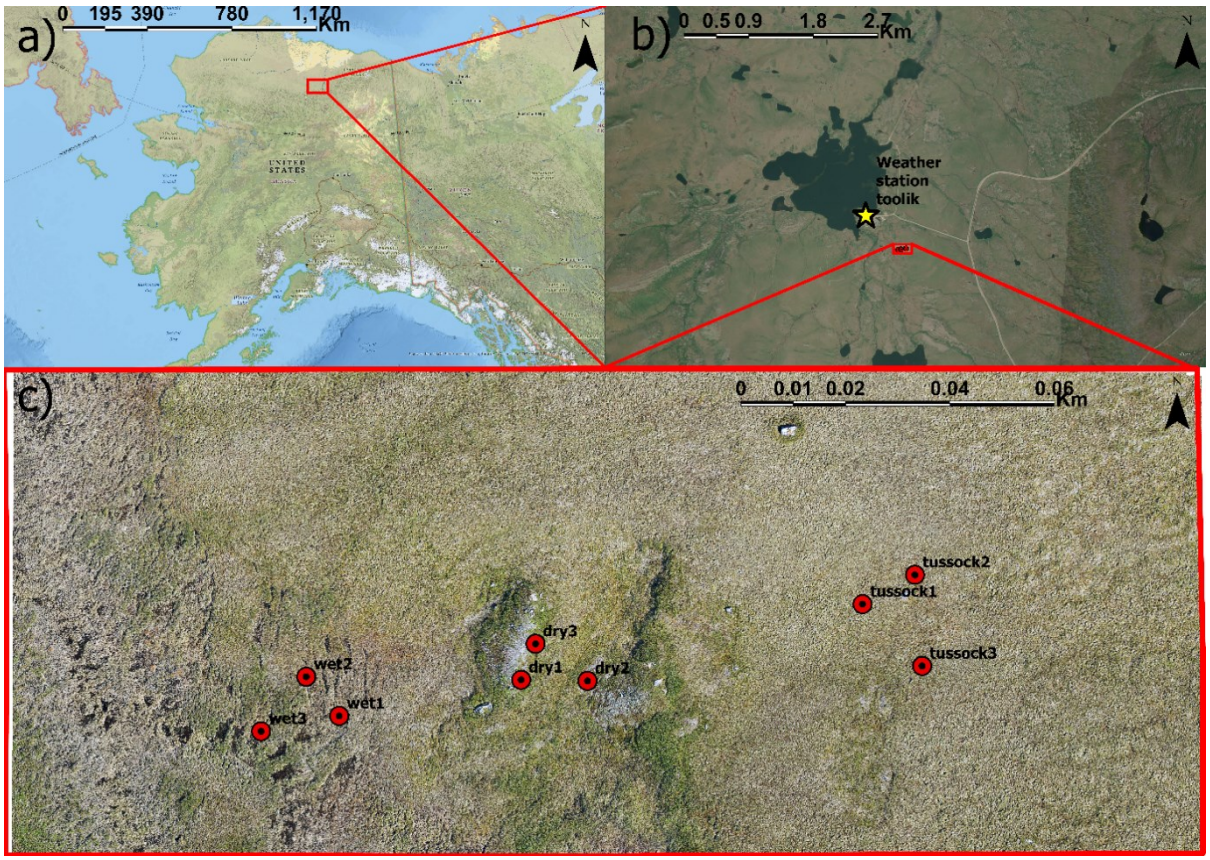

Figure 1. a) location of the study area in the North Slope Alaska, Toolik field station, b) ortophoto of the Toolik field station area and location of its automatic weather stations (AWSs) used in this study (yellow triangle), c) high resolution RGB drone image of the study area where the red circular points represent ground location of CH_4 flux chambers in the different vegetation types along a west-east transect (from West to East: Wet Tundra; Dry Tundra; Tussock Tundra .

Manually operated closed soil chambers have been widely employed for the measurement of CH_4 fluxes due to their applicability across diverse ecosystems and varying site conditions (Flessa et al., 2002; Jiang et al., 2010). These chamber-based methods, in contrast to the eddy covariance technique, offer the sensitivity needed to detect low flux magnitudes, which are typical of CH_4 emissions between climatic events (Baldocchi et al., 2012). Furthermore, chambers facilitate the detection of spatial variability in greenhouse gas fluxes (Merbold et al., 2011), particularly important for CH_4, whose sources and sinks are often spatially heterogeneous (Sun et al., 2013; Reuss-Schmidt et al., 2019).

Table 1. Study site location coordinates and main site characteristics: elevation (m a.s.l.); slope (°); aspect; total vegetation cover (%) and bryophytes cover (%); mean of the Ground Surface Temperature (GST, °C) measured at 2 cm of depth for the entire analysed period and its standard deviation.

Plot	Coordinates	Elevation (m a.s.l)	Slope (°)	Aspect	Vegetation cover (%)	bryophytes cover (%)	GST (°C)
Wet1	68°37'25.72"N 149°35'3.93"W	724	1	N	90	55	5.71± 6.30
Wet2	68°37'25.95"N 149°35'4.52"W	724	5	W	70	10	4.55± 5.51
Wet3	68°37'25.62"N 149°35'5.24"W	724	3	W	100	55	5.21± 6.43
Dry1	68°37'25.98"N 149°35'0.86"W	728	3	S	85	10	4.57± 7.76
Dry2	68°37'25.87"N 149°34'59.94"W	730	7	W	100	50	4.57± 7.76
Dry3	68°37'26.20"N 149°35'0.51"W	729	7	SE	65	30	5.00± 7.34
Tussock1	68°37'26.54"N 149°34'55.15"W	734	4	SW	100	50	3.84± 5.68
Tussock2	68°37'26.74"N 149°34'54.27"W	735	2	W	100	90	3.68± 5.76
Tussock3	68°37'26.18"N 149°34'54.08"W	735	1	SW	100	60	3.27± 5.94

Chamber flux measurements of CH_4 were carried out using a static closed polycarbonate chamber of cubic shape (size 50 x 50 x 50 cm, with 125 L volume) at each of the three vegetation communities (dry, tussock, wet tundra) with three replicates sites for each community (e.g., dry 1, dry2, dry3, etc) from July to November 2023 (shoulder or transition season) (Table 1). At each site, measurement chambers were placed 20 minutes prior to measuring reaching a standard depth of 2cm and were removed after the complete cycle every day. Methane concentrations were measured using LiCor Analyzer (LI-7810 $CH_4/CO_2/H_2O$ Trace Gas Analyzer) which uses OF-CEAS (Optical Feedback - Cavity Enhanced Absorption Spectroscopy) measurement technique with precision (1σ): 0.60 ppb at 2 ppm with 1 second (±2.4 * 10^4 nmol/m^2*s under 0°C) averaging (2024 LI-COR, 2024). CH_4 exchange rate was measured in ppb (parts per billion) then converted to nmol/m^2*s (Levy et al., 2011; Maier et al.,

2022). For each plot of each community fluxes were measured under ambient light conditions and between measurements the chamber was opened, and the canopy was ventilated. The manual chambers were equipped with two holes for fixed nozzles at the top of the chamber (1.4*1.4 cm) allowing air inflow and outflow and connected through a tube (2 m long) to LICOR 7810 Trace Gas Analyzer using a male and female connector (2 cm long) for air collection and for balancing air pressure inside and outside chamber. A third hole was used to connect an 8 V fan for air mixing inside the chamber and the Arduino Mega microcontroller sensors measuring: air temperature/humidity (I2C sensor, ±0.5°C/±5% accuracy), soil moisture (2 sensors inside and 1 sensor outside chamber (±10% accuracy), soil temperature (±0.3°C accuracy).

Measurements were run for 15 minutes three times a day (morning, midday, afternoon) twice a week at each site from July 2023 to November 2023. Individual chamber fluxes were calculated from the gradients of the relationship between gas concentration and sampling period using the central 11 minutes of the measure performing a linear regression and selecting data with R^2 ≥0.9 (Kim et al., 2007; Kim, 2015).

2.3 Climate

Supporting climate data were provided by the Toolik Field Station Environmental Data Center from the weather station located at the field station (68° 38'N, 149° 36'W) (Fig. 1b). Air temperature (°C) (accuracy, ±0.2 °C) and relative humidity (%, accuracy 1.0) measured at 3 m, wind speed at 5 m (accuracy, ±0.3 m/s), Photosynthetically Active Radiation (PAR) at 1.8 m (accuracy, ±5%), barometric pressure (accuracy, ±1.5 hPa). The climate data were recorded hourly and successively averaged to daily mean from first week July to first week of November 2023.

2.4 Microclimatic and edaphic parameters

At each of the nine selected study sites (Table 1), microclimatic variables inside the chamber, including air humidity (%) and air temperature (°C) at 44 cm above the ground inside the chamber, as well as 2 soil temperatures (°C) and 2 moisture (%) at 2 cm below the surface, were recorded every second and subsequently averaged to yield daily values using an Arduino microcontroller. Snow cover thickness (cm) was measured manually during all the season in a ray of 5 m of each plot. At each site a shallow borehole (maximum depth 100 cm) was drilled where ground temperature (°C) was monitored at different depths between 20 and 100 cm depending on the plots and logged using Hobo data loggers (HoBO Pro v2 Logger U23-003 by Onset). Additionally, soil temperature (°C) at 2 cm was recorded using a 12-bit temperature smart sensor (S-TMB-M002, by Onset). Soil water saturation (%) was measured at 2, 20, 30,

and 60 cm in the boreholes using a Soil Moisture Smart Sensor (S-SMC-M005 by Onset). The soil surface temperature and soil water saturation sensors did not work in the dry tundra plots in November. Maximum thaw depths in summer and unfrozen thickness (cm) in the freezing season, were obtained by linear extrapolation of the maximum daily ground temperatures at different depths closer to the depth of the daily 0 °C isotherm in each borehole (Adlam et al., 2010; Guglielmin, 2006)

2.5 Soil chemical and physical properties

To analyse the physico-chemical characteristics of the soil, in correspondence of each of the nine sites a soil core maximum 1 m long and 75 mm in diameter was extracted using a Snow-Ice Permafrost Research Establishment (SIPRE) auger with an engine-powered head (Niendorf, 2023) in 2 different periods (early beginning of July and beginning of September 2023). The soils were described according to the World Reference Base for Soil Resources 2014: International Soil Classification System for Naming Soils and Creating Legends for Soil Maps (FAO, 2014) and stored at -80°C until analysis. Each horizon of the core was analysed separately.

Soil grain size was analysed by dry sieving, separating the coarser fraction (skeleton, >2 mm) from the sand (2-0.075 mm) and the finest fraction, composed of silt and clay (<0.075 mm) (ASTM, 2007). The analysis. The analysis of water content, pH, electrical conductivity, total organic carbons (TOC), carbonates and total carbons (TC) analysis were performed on the <2 mm soil fraction. To quantify soil water content, the samples were dried at 105 °C in the oven for 24 hours by measuring the sample weight before and after drying (Gardner, 1986; Cannone et al., 2016, 2019). TOC, TC and carbonates were evaluated by loss of ignition (Blume et al., 1990; Nelson and Sommers, 1996), measuring the loss of weight after incubation for 6 hours at 600 °C for TOC and after incubation for 2 hours at 900 °C for carbonates. TC was calculated using the following equation: TC = TOC + Carbonates. Soil pH and electrical conductivity (µS/cm) was determined by mixing 5 g of sample (< 2 mm) in a 1:5 ratio with deionized water and after homogenization and after calibration of the instruments (Kalra, 1995; Cannone et al., 2019). The physical and chemical characteristics of the soils reported in table 2 are weighted based on the different horizons thickness.

2.6 Data elaboration

Multivariate analysis was performed to characterize the selected vegetation sites, in particular Principal Component Analysis (PCA) was performed using the software CANOCO for Windows (ter Braak and Šmilauer, 1998). For the PCA the data were square-root transformed,

the scaling was made through the inter-species correlation, the standardization by species was centered, and without sample standardization.

To identify the main drivers of the CH_4 fluxes, we performed a Pearson correlation matrix of the climatic and micro-edaphic data allowed to select the variables for further statistical analyses, thus avoiding multicollinearity and redundancy. General regression models (GRMs) allowed to identify the drivers of CH_4 fluxes (as dependent variable) from July to October, encompassing the peak and the end of the growing season both at: a) inter-community level (i.e., analysing the fluxes from all vegetation types and all sites, with month (as proxy of seasonality during the measurement period), plot and vegetation type as categorical factors), and b) intra-community level (i.e., performing separate analyses for the dry, wet and tussock tundra, with month as categorical factor). Moreover, to better understand the drivers of the large and unexpected CH_4 emissions recorded in November, we performed two further GRMs at inter-community level, one focusing on July-August to be compared with the GRM focusing on the period October-November. All analyses were performed using the software Statsoft©.

3. Results

3.1 Climate, microclimate and soils

The monthly means of the main climatic parameters measured during the period of the flux chambers measurements (July-November 2023) provided an unexpected pattern for air temperature, which ranged between -11.8 and +16.9°C, showing a progressive decrease during the season, but the lowest values in October instead than in November (Fig. 2A). Air humidity and PAR exhibited an opposite temporal trend, with the former showing a continuous increase from July to November, while the latter had an exponential decrease from July to November (Fig. 2B, C). Wind speed did not show large variations, and the minimum was recorded in November (Fig. 2D).

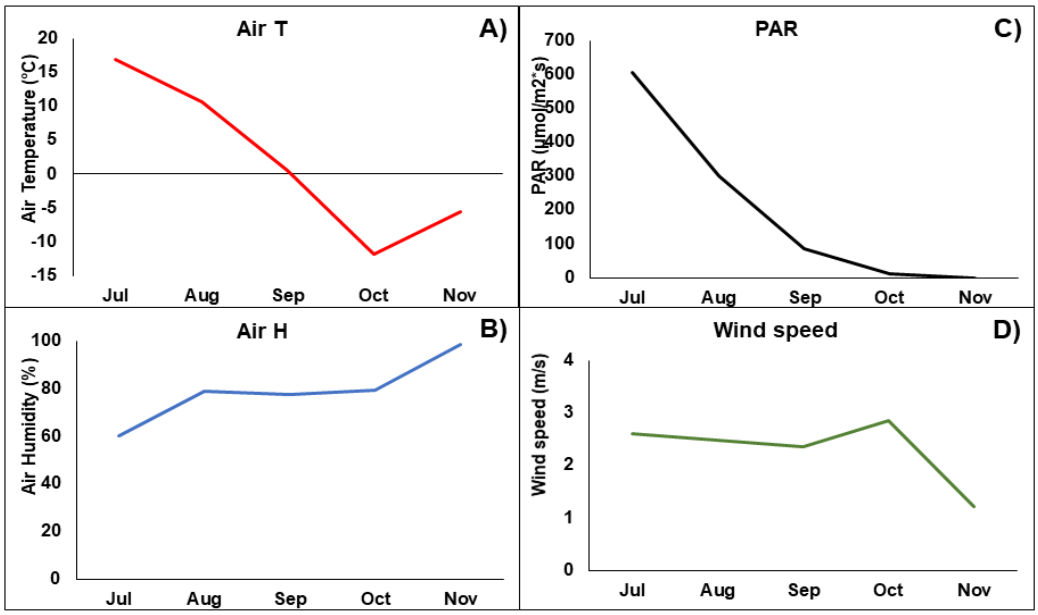

Figure 2. Mean monthly values of the main climatic parameters recorded by the Toolik AWS: A) air temperature (°C); B) relative air humidity (%); C) PAR (µmol/m^2*s); D) wind speed (m/s).

The three selected vegetation communities were characterized by different microclimatic and edaphic conditions concerning the maximum thawing depth/unfrozen thickness, ground surface temperature, and surface soil water saturation, although their temporal trends were similar (Fig. 3).

The maximum thawing depth was recorded between August and September, with the highest values observed in the dry tundra, reaching the maximum value of 149 cm in September (and a very rapid freezing in October), followed by the wet tundra (103 cm in August) and the tussock tundra (89 cm in September) (Fig. 3A). Notably, both in the wet and tussock tundra the unfrozen thickness accounted for up to almost 20 cm even in November (Fig. 3A), when the double side freezing left a certain thickness of unfrozen soil between the two freezing fronts. In all the selected vegetation communities the ground surface temperature exhibited a clear decreasing trend from July to November, with the dry tundra being characterized by the highest temperatures in summer (with the wet tundra) and the lowest temperatures in fall (Fig. 3B). The surface soil water saturation (measured at 2 cm) was highest in the wet tundra (where the soil was completely saturated by water between July and September), as expected, and was slightly higher in the tussock than in the dry tundra (Fig. 3C). The temporal trends of GST and soil water saturation were similar in all vegetation types, while the maximum thawing was anticipated in August in the wet tundra (Fig. 3).

The plots were also characterized by different physico-chemical soil conditions, as confirmed by the multivariate analysis (PCA, Principal Component Analysis), with the dry tundra plots showing different characteristics compared to the tussock and wet tundra (Fig. 4, Table 2). The

plots are characterized by a gradient of increasing water content, electric conductivity, TOC, and TC from the dry to tussock to the wet tundra, with the former showing values much lower than the latter, and with the dry tundra having a much coarser texture (Fig. 4, Table 2). Relatively homogeneous values characterize pH, showing acidic values across all sites and vegetation communities (Table. 2). The PCA emphasized the differences of soil characteristics among the three vegetation types (dry, tussock and wet tundra) and allowed to highlight also some intra-community differences, in particular for the tussock tundra (with tussock 1 being different from tussock 2 and 3) and partially for the wet tundra (wet 3 showing some differences respect to wet 1 and 2), while the dry tundra was characterized by very high similarity of the soil characteristics of the three analysed plots (Fig. 4).

Table 2. Weighted mean of physico-chemical characteristics of soils: WC (water content, %); pH; Electrical Conductivity (µS/cm); Skeleton (%), Sand (%), Silt+Clay (%); TOC, Carbonates and TC are expressed as %.

Site	WC	pH	Electrical Conductivity	Skeleton	Sand	Silt + Clay	TOC	Carbonates	TC
DRY1	24.7	4.88	83.6	39.4	42.5	18.1	10.6	2.45	13
DRY2	16.9	4.95	63.6	40.9	46.7	12.4	5	1.71	6.8
DRY3	14.8	5.30	60.6	40.2	53.5	6.2	7.1	1.71	8.8
WET1	73.9	4.99	193	2.1	86	11.9	68.3	7.23	75.5
WET2	82.2	4.81	200.2	1	85.8	13.1	75.9	8.25	84.2
WET3	71.6	6.13	186.5	3.6	60.4	36	48.3	6.27	54.6
TUSSOCK1	34.9	5.43	62.4	3.4	74.7	21.9	13.5	3.33	16.8
TUSSOCK2	59.3	5.45	116.3	3	69.7	27.2	39.5	5.32	44.8
TUSSOCK3	73.1	4.81	131.2	5.6	74.8	19.6	59.1	9.07	68.2

3.2 CH_4 fluxes at inter-community level

The amount and seasonality of the CH_4 fluxes exhibited large differences comparing the three selected vegetation types (Fig. 5), with the tussock tundra showing the largest CH_4 emissions, followed by the wet tundra, while the dry tundra exhibited slight negative emissions (i.e. CH_4 uptake). At intra-community level along the whole season, the plot wet 2 exhibited the largest emissions within the wet tundra, and the plot tussock 1 for the tussock tundra (Fig. 5).

Analysing the temporal trends at intra-community level, the wet tundra exhibited an unimodal trend, with an increase from July to August, when the largest emissions were observed, and then a progressive decrease towards the end of the season (Fig. 6B), while the tussock tundra was characterized by the opposite pattern, with increasing emissions from July to November, and the largest amount recorded in November (Fig. 6C), which were the largest measured across all sites and vegetation types during the whole period of measurement. The uptake of the dry tundra was characterized by a unimodal pattern, with the largest uptake in August (Fig. 6A).

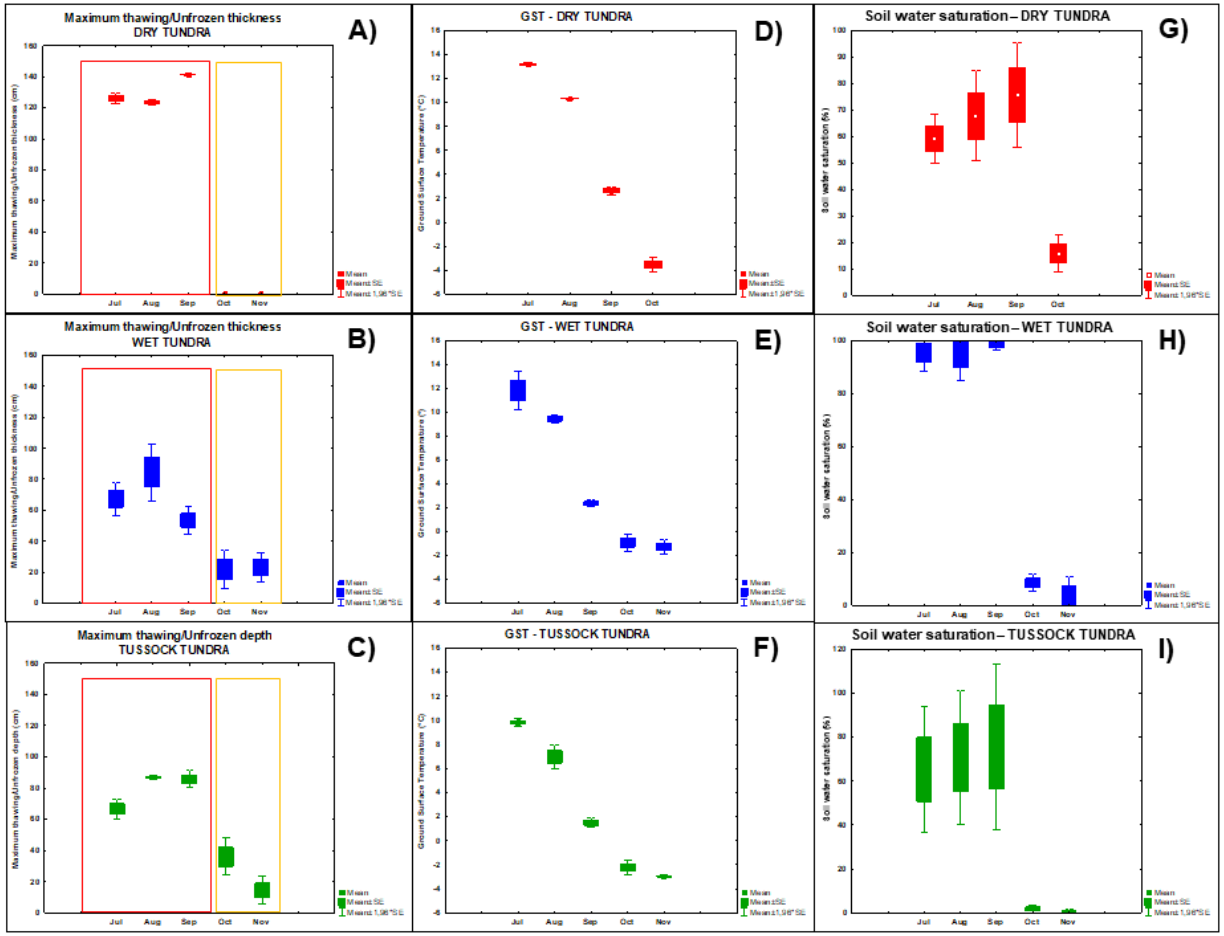

Figure 3. Microclimatic and edaphic characteristics of the three selected vegetation communities (period July – November 2023) concerning: A, B, C) maximum thawing (July- September, identified by the red rectangle) and unfrozen thickness (October- November, identified by the orange rectangle) (cm); D, E, F) ground surface temperature at 2 cm depth (mean monthly values, °C); G, H, I) surface soil water saturation (%).

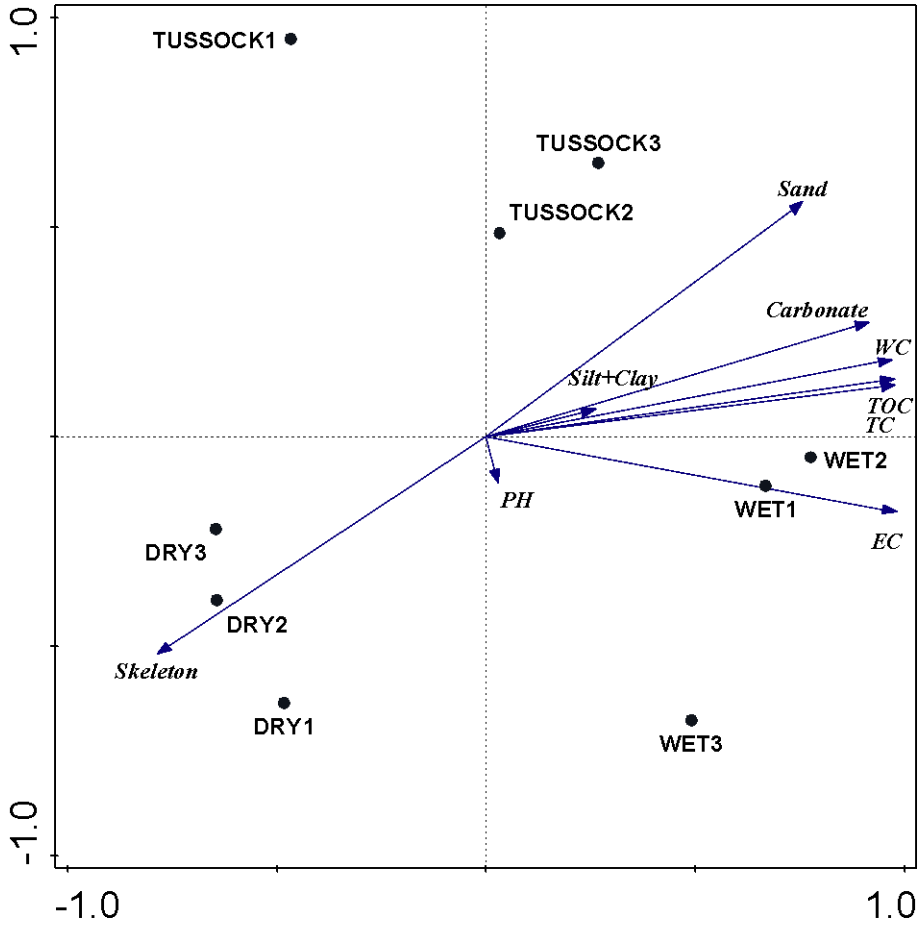

Figure 4. Principal Component Analysis of the analysed vegetation plots (dry tundra, dry 1, 2, 3; tussock tundra, tussock 1, 2, 3; wet tundra, wet 1, 2, 3) explaining 96.8% of the environmental variance (cumulative explained variance: Axis 1 = 91.6 %; Axis 2 = 96.8%). Legend: EC = electric conductivity; WC = water content; TC = total Carbon; TOC = total organic Carbon.

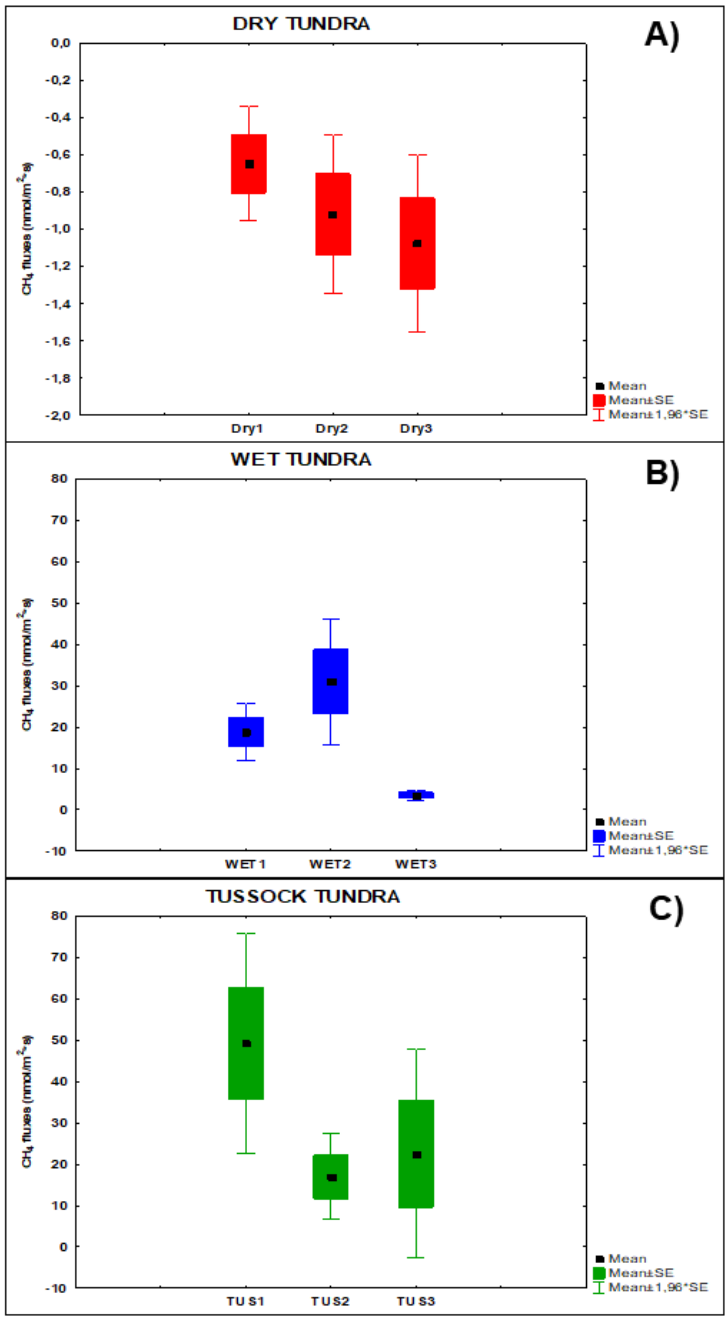

Figure 5. Descriptive statistics of the seasonal CH_4 fluxes (mean + standard error + 1.96*standard error) of each of the nine plots of the three vegetation types (dry: A; wet: B; tussock: C).

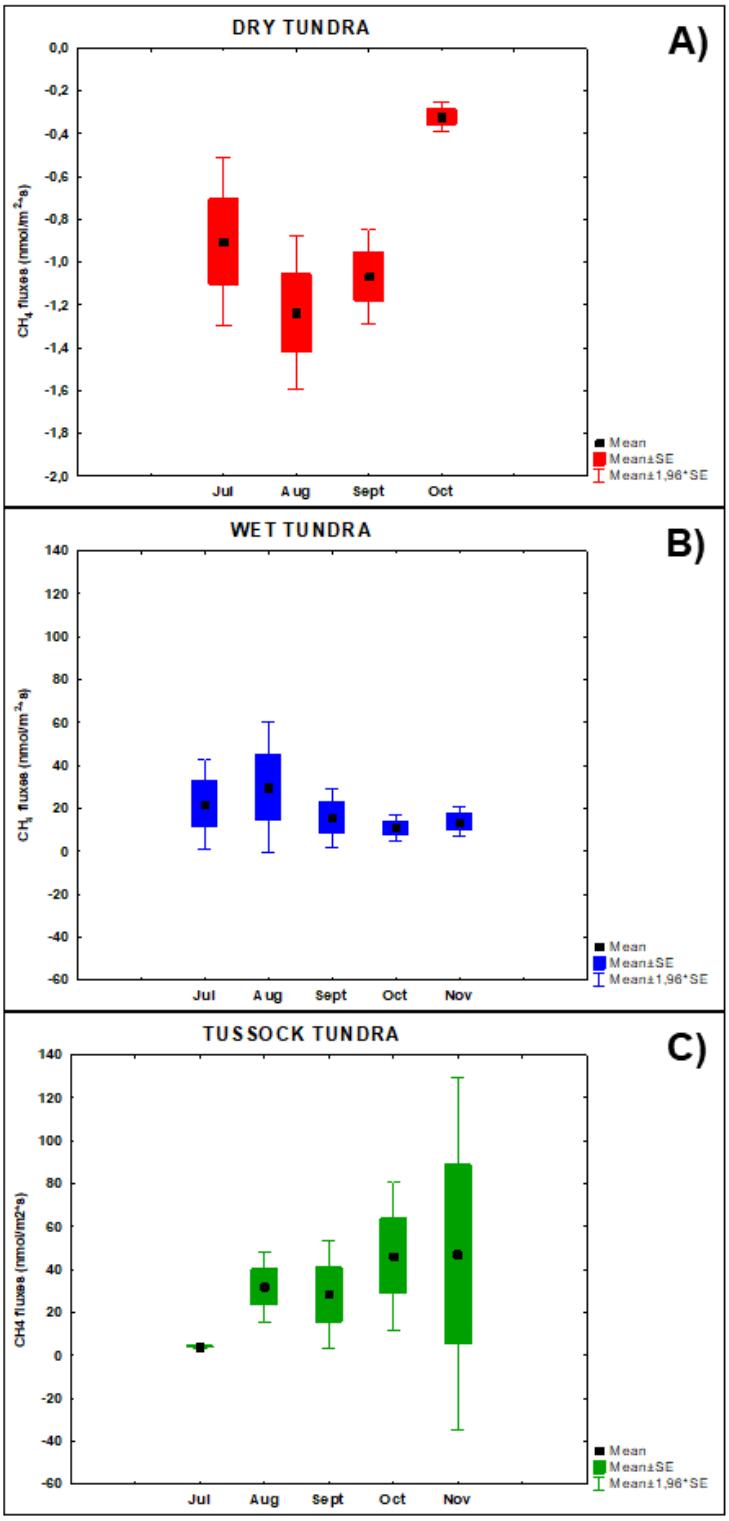

Figure 6. Seasonal patterns of CH_4 emissions (mean + standard error + 1.96*standard error) from July to November 2023 at inter-community level: A) dry tundra; B) wet tundra; C) tussock tundra. Note that panel A has a negative Y scale.

3.3. Drivers of the CH_4 fluxes at inter- and intra-community level

The GRM performed at inter-community level over the period July-October (from the peak to the end of the growing season) identified vegetation type, air temperature, maximum thawing-unfrozen thickness and period (provided by the month as categorical factor) as drivers exerting a statistically significant impact on the CH_4 fluxes (Table 3). However, our analyses emphasize that the drivers of the CH_4 fluxes at inter-community level changed from the peak of the growing season (July-August) to the cold season characterized by winter dormancy (October-November) (Table 3). The most important drivers affecting in a statistically significant way the CH_4 fluxes during the peak of the growing season (July-August) were vegetation type and plot, followed by some climatic parameters (atmospheric pressure, air temperature, air humidity and wind speed) and ground surface temperature (Table 3). During the cold season, in October and November, snow cover, air humidity, air temperature and vegetation type were the drivers of CH_4 fluxes (Table 3), with large emissions observed especially in the tussock tundra (Fig. 5).

The analysis at intra-community level allowed to emphasize the sensitivity to different climatic and environmental drivers of the CH_4 fluxes associated to the selected vegetation types. The most important drivers for the CH_4 fluxes in the wet tundra were associated to soil water saturation, period (provided by the month as proxy of seasonality during the measurement period) and maximum thawing/unfrozen thickness, while snow depth and ground surface temperature were the most important drivers influencing the CH_4 fluxes of the dry tundra (Table 4). The drivers of the tussock tundra were air humidity, maximum thawing/unfrozen thickness, air temperature and wind speed (Table 4).

Table 3. General Regression Model to identify the main drivers of CH_4 fluxes (dependent variable) at inter-community level (all plots of all vegetation types) across the whole growing season (July-October 2023) and then comparing the peak of the growing season (July-August) with the cold season of winter dormancy (October-November). Only statistically significant variables have been reported and the statistics of the whole model.

CH_4 flux inter-community Jul-Oct	**F**	**p**	**R^2**
Unfrozen thickness (cm)	14.9	<0.001	
Air Temperature (°C)	22.5	<0.001	
Vegetation type	24.7	<0.001	
Month	9.3	<0.001	
whole model	8.9	<0.001	0.69
CH_4 flux inter-community Jul-Aug	**F**	**p**	**R^2**
Ground Surface Temperature (°C)	22.3	0.009	
Atmospheric pressure (atm)	45.4	0.002	
Wind speed (m/s)	35.2	0.004	
Air humidity (%)	29.7	0.005	
Air temperature	30.3	0.005	
Plot*Vegetation type	122.7	<0.001	
whole model	111.1	<0.001	0.99
CH_4 flux inter-community Oct-Nov	**F**	**P**	**R^2**
Snow cover (cm)	275.2	<0.001	
Air humidity (%)	181.5	<0.001	
Air temperature (°C)	178.2	<0.001	
Vegetation type	221.6	<0.001	
whole model	160	<0.001	0.99

Table 4. Drivers affecting the temporal patterns of the CH_4 fluxes at intra-community level (dry tundra, wet tundra, tussock tundra). Only statistically significant variables have been reported and the statistics of the whole model.

CH_4 Wet tundra Jul-Oct	**F**	**P**	**R^2**
Unfrozen thickness (cm)	7	0.038	
Soil water saturation (%)	27.1	0.002	
Month	11.8	0.006	
whole model	12.7	0.003	0.91
CH_4 Dry tundra Jul-Oct	**F**	**P**	**R^2**
Snow cover (cm)	28.5	<0.001	
Ground Surface Temperature (°C)	21.7	0.001	
whole model	19.6	<0.001	0.88
CH_4 Tussock tundra Jul-Oct	**F**	**p**	**R^2**
Unfrozen thickness (cm)	24.9	0.001	
Wind speed (m/s)	22.3	0.002	
Air humidity (%)	30.6	<0.001	
Air temperature (°C)	23.9	0.002	
whole model	11.4	0.003	0.87

4. Discussion

4.1 Spatial and temporal patterns of CH_4 fluxes

Our data identified the patterns of spatial and temporal variability of CH_4 fluxes, highlighting differences across the three selected tundra types (wet, tussock and dry tundra) both at inter- and intra-community level, as well linked to seasonality, from the peak of the growing season (July 2023) to the winter dormancy (November 2023).

Vegetation type was a key factor in explaining the observed differences in CH_4 fluxes, in agreement with previous studies (e.g. McGuire et al., 2009; McEwing et al., 2015; Natali et al., 2015; Davidson et al., 2016; Zona et al., 2016; Euskirchen et al., 2017), as indicated by the results of the GRMs performed at inter-community level both across the whole growing season as well comparing the peak of the growing season (July-August) with the cold season characterized by winter dormancy (October-November) (Table 3).

Despite most studies reported that the wetland and/or wet sedge tundra performed the highest CH_4 emissions at most Arctic sites (e.g. McEwing et al., 2015; Davidson et al., 2016,

Euskirchen et al. 2017; Parmentier et al., 2024), unexpectedly in our study the largest CH_4 emissions were observed in the tussock tundra (dominated by *E. vaginatum* and mosses) and not in the wetland tundra (dominated by *C. aquatilis* and mosses). The tussock tundra here is characterized by higher total vegetation cover (%) compared to the wet tundra (respectively, 100% at all plots versus 70-100%) and, above all, by a high cover of the tussock *E. vaginatum* (>50%). The occurrence of tussocks and in particular of *E. vaginatum* has been recognized to promote larger CH_4 emissions because its tissues are characterized by the aerenchyma and large lacunae, enabling the transport of CH_4 from the soil to the atmosphere inside the plant tissue and, thus, bypassing the soil oxic layers where CH_4 would be re-oxized (McEwing et al., 2015). Also *C. aquatilis* has aerenchyma too, but recent laboratory experiments suggested that in this species the production of root exudates (stimulating microbial methanogenesis) is much more important and efficient than the CH_4 transport through the roots' aerenchyma (Waldo et al., 2019). Moreover, our wet tundra plots are characterized by high bryophytes' cover, not providing a root system and hence unsuitable for CH_4 transport within the soil to bypass the oxic layers. Therefore, the high bryophytes' cover could contribute to the lower CH_4 emissions recorded at the wet tundra compared to the tussock tundra plots. The occurrence and cover of tussocks could be more important in promoting CH_4 emissions than the amount of TOC (which was much higher at the wet than at the tussock tundra soils, Table 1), thus indirectly confirming that CH_4 emissions in these community types are not limited by C input (Zona et al., 2009; Sturtevant and Oechel, 2013; Davidson et al., 2016).

The dry tundra at our study sites always acted as a CH_4 sink, with a slight uptake observed from July to October at all plots, confirming previous observations both from the Arctic Alaska as well as from the European Arctic (e.g., Natali et al., 2015; D'Imperio et al., 2017; Virkkala et al., 2024). The CH_4 uptake observed was due to the occurrence of oxic conditions in the soil, thus enhancing methane oxidation (Voigt et al., 2023). Indeed, our dry tundra plots were characterized by a coarser soil texture (>90% of skeleton + sand, Table 2) promoting soil drainage and the aerobic respiration (e.g., Lipson et al., 2012; Ma et al., 2023).

The seasonal patterns of CH_4 emissions allowed to further discriminate the tussock from both the wet and dry tundra (Fig. 5), as the former was characterized by an increasing trend of CH_4 emissions from July to November, with the highest values recorded in autumn and in particular in November, while both the latter exhibited the largest emissions between July and August (Fig. 5), as expected according to most studies carried out in the Arctic (e.g., Euskirchen et al., 2017). The largest emissions recorded at the tussock tundra in autumn confirmed the importance of the transition seasons and of winter, as high CH_4 emissions have been recorded during the

cold season even with very low air temperature and occurrence of snow cover (e.g. Zona et al., 2016; Arndt et al., 2019; Bao et al., 2021), suggesting that autumn CH_4 emissions could contribute up to 34%–50% of yearly emissions (Ward et al., 2024). The wet tundra exhibited the highest emissions during the peak of the growing season, when soil water saturation and the soil unfrozen thickness were highest (Fig. 3), as observed in other previous studies (e.g., Davidson et al., 2016; Euskirchen et al., 2017).

Our data show that the dry tundra did not exhibit any activity (CH_4 uptake or CH_4 emission) later than October, differently from the findings at some other Arctic sites, where the upland dry tundra ecosystems produced CH_4 emissions during the cold season and even a shift from summer CH_4 uptake to winter CH_4 emission (Zona et al., 2016). In our case, the lack of CH_4 emissions in autumn from the dry tundra could be due the lack of any unfrozen depth within the soil, as the soil was completely frozen (Fig. 3), not allowing CH_4 production and/or transport within the soil. Considering that the upland dry tundra is extended over a very large amount of the Arctic (Virkkala et al., 2024), this finding indicates that not all upland tundra may provide a valuable contribution to the winter CH_4 emissions, differently from what hypothesized by Zona et al. (2016). These findings suggest that the winter modelling needs further investigations and to be carefully addressed to avoid overestimations.

4.2 Biotic and abiotic drivers of CH_4 fluxes at inter-community level

Climate, soil physico-chemical characteristics and vegetation of our site are coherent with the findings of previous studies performed both at the same location and in similar Arctic environments (Walker et al., 1989; Morrissey & Livingston, 1992; Christensen, 1993; Tom and Chapin, 1993; Kim, 2007, 2015; Walker and Maier, 2008; Davidson et al., 2016; Howard et al., 2020).

Air temperature allowed to assess that the climatic conditions during the period of measurement in the year 2023 were consistent with the mean monthly and seasonal values of the last decades (Christensen, 1993; Howard et al., 2020). Concerning soils, pH across the nine plots exhibited minimal variation (Table 2), suggesting that soil acidity or alkalinity did not significantly influence methane fluxes in these ecosystems (Ohtsuka et al., 2006; Davidson et al., 2016). TOC and TC were highest in wet followed by tussock and dry tundra (Table. 2, Fig. 4) in agreement with previous observations (Jobbagy et al., 2000; Wu et al., 2012). Although soil temperature is a known driver of microbial activity involved in methanogenesis (Chen et al., 2020; Yvon-Durocher et al., 2014), the range of soil temperatures across sites was rather limited (Fig. 3B).

The GRM allowed to identify the drivers of CH_4 fluxes highlighting differences linked to the tundra type and seasonality (Table 3). At inter-community level, all the GRMs (across the whole growing season - July to October and comparing the peak of the growing season - July-August - versus the cold season - October-November, Table 3) indicated vegetation type and air temperature among the most important drivers of CH_4 fluxes. The influence of vegetation on CH_4 fluxes mainly rely on the role of plants in enabling the transport of CH_4 within soil, avoiding the soil oxic layers, and on the contribution of plants in providing organic matter for the microbial decomposition in particular through root exudates (e.g. McGuire et al., 2009; McEwing et al., 2015; Natali et al., 2015; Davidson et al., 2016; Zona et al., 2016; Euskirchen et al., 2017). These effects allow to identify opposite conditions in favouring CH_4 transport and/or methanogenesis in the wet and tussock tundra opposed to the dry tundra, as confirmed by the large CH_4 emissions observed in the former two and the slight CH_4 uptake of the latter. According to Davidson et al. (2016), the analysis of the CH_4 fluxes associated to the three selected tundra types (dry, tussock and wet tundra) may explain most of the observed variation of the CH_4 fluxes within heterogeneous tundra landscapes encompassing multiple vegetation communities.

Air temperature is another important driver of the CH_4 fluxes across the whole season, as higher temperatures may increase the potential of anaerobic respiration (Yvon-Durocher et al., 2014; Jeong et al., 2018; Ma et al., 2023). Interestingly, our analyses emphasize the importance of air temperature especially in the cold season, as the effect of this driver is larger in October-November compared to July-August (Table 3). This finding could be explained with the fact that during the peak of the growing season air temperature is an important but not limiting factor, differently from what may happen during the cold season. During the peak of the growing season at inter-community level, atmospheric pressure and wind speed are other important drivers (Table 3): decreasing atmospheric pressure and increasing wind speed may facilitate CH_4 emission by increasing the steepness of the gradient of CH_4 concentration between the soils and the atmosphere (e.g. Sachs et al., 2008; McEwing et al., 2015). Our analyses confirm the importance of the soil unfrozen thickness, as it increases the thickness of soils rich in organic matter available for respiration and, further, the unfrozen soil could be inundated and/or waterlogged, promoting anaerobic respiration, highlighting the importance of the hydrological implications of active layer thaw (Lawrence et al., 2015; Rodenhizer et al., 2020).

During the cold season (October-November, Table 3) snow cover is the most important driver at inter-community level. In particular, in November the tussock and the dry tundra showed a thinner snow cover (respectively, 30 and 32 cm) than the wet tundra (45 cm), but the tussock

tundra produced the largest CH_4 emissions, while the dry tundra was inactive. These data suggest that the influence of snow cover on CH_4 fluxes may change depending on the tundra type and seasonality and that this issue needs further investigations also considering that uplands (including the dry tundra) cover a large part of the Arctic (Vikkala et al., 2024).

4.3 Biotic and abiotic drivers of CH_4 fluxes at intra-community level

The intra-community analyses, referred only to the whole growing season (July-October 2023), allowed to highlight the differences of behaviour and abiotic drivers of the three selected tundra types (Table 4). In the wet tundra soil water saturation was the primary driver of the CH_4 emissions, followed by month (as proxy of seasonality) and unfrozen thickness. These results confirm the role of soil water saturation as an important driver of elevated CH_4 emissions from the ground (Zona et al. 2009; Sturtevant and Oechel 2013; Kim, 2015; McEwing et al., 2015), and are congruent with the observation that the CH_4 emissions in the wet tundra are highest when soil water saturation and unfrozen thickness are highest (July and especially August) (Fig. 3 Table 4). From July to August the soil water saturation reaches its highest value, as also confirmed by the occurrence of a water table on the surface of the wet tundra, providing the best conditions for anaerobic respiration (e.g., Bridgham et al., 2013).

In the dry tundra snow depth and ground surface temperature were the most important drivers (Table 4), with the CH_4 uptake decreasing at the end of the season when a thin snow cover occurs. Dry tundra sites acted as net sinks for CH_4 throughout the season, likely due to enhanced methane oxidation associated with higher soil temperatures (Kutzbach et al., 2004; Olefeldt et al., 2013; Davidson et al., 2016). At our sites dry tundra exhibited slightly above average soil temperatures than the tussock and wet sites, and low organic compound during the data collection period (Table 1, Fig. 3) supporting dry tundra act as net sinks (Juncher Jørgensen et al., 2014; D'Imperio et al., 2017).

Air humidity and air temperature with wind speed and unfrozen thickness were the most important drivers of the tussock tundra during the growing season (Table 4). These findings highlight the importance of the steepness of the gradient of CH_4 concentration between the tussock tundra soils and the atmosphere in promoting higher CH_4 emissions and confirm indirectly also the role of tussocks (and in particular of *E. vaginatum*) in promoting the CH_4 transport bypassing the oxic layers within soils (e.g., McEwing et al., 2015). The role of unfrozen thickness could be better appreciated until the period of maximum thawing (September 2023) when the tussock tundra exhibits the combination of maximum unfrozen thickness providing the maximum availability of unfrozen organic matter to anaerobic

respiration (e.g., Zona et al. 2009; Bridgham et al., 2013; Sturtevant and Oechel 2013; Kim, 2015; McEwing et al., 2015).

4.4. Peculiarity of autumn CH_4 fluxes

The rates of methane emissions are linked to three main different processes: production, oxidation, transport (e.g., McEwing et al., 2015). Our data allow to emphasize the shift in the prevailing importance of these processes by comparing the growing season (and in particular the peak of the growing season) with the cold season. The high rates of CH_4 emissions in August observed in the tussock and wet tundra confirm the findings of previous studies showing that CH_4 production is high when there is the combination of high soil water saturation, unfrozen thickness and air temperatures (e.g., Verville et al. 1998; Zona et al. 2009; Sturtevant and Oechel 2013; McEwing et al., 2015; Davidson et al., 2016).

However, the largest CH_4 emissions were recorded in the tussock and wet tundra during the cold season (October and, above all, November), highlighting the occurrence of a different process mainly linked to CH_4 transport. During the autumn the CH_4 emissions from these two tundra types accounted c. 77% of the total emissions recorded during the whole study period (July-November 2023) in a period when the unfrozen thickness of the soils was rapidly decreasing, and the soil water saturation was minimal due to the freezing (Fig. 3). These emissions exceed those observed in the mid-summer season and are consistent with the ranges reported by Howard et al., (2020) and Zona et al., (2016).

These findings confirm the importance of CH_4 emissions during the transition seasons, characterized by cold air temperatures and refreezing of soils and support the hypothesis that cold season emissions could provide a valuable contribution to the annual budget of CH_4 fluxes (e.g., Zona et al., 2016; Bao et al., 2020; Ward et al., 2024).

These very high emissions during the cold season could be explained with the occurrence of a two-sided front of the soil freezing front, occurring both from the surface downward driven by cold air temperatures, as well as from below upward due to the presence of permafrost. As the two-sided front freezing decreases the soil unfrozen thickness, the CH_4 here accumulated suffers increasing pressure and compression until it is pushed out towards the surface, being transported by the plant's aerenchyma and/or ground cracking and/or frost-induced ground fissures, and released into the snowpack and the atmosphere (Kim et al., 2007; Mastepanov et al., 2013; Arndt et al., 2020; Bao et al., 2021).

In conclusion, we analysed the CH_4 fluxes of three widespread vegetation communities (tussock tundra, wet tundra and dry tundra) in the high Arctic region in Alaska. Our data allowed us to

assess the importance of the interaction of different biotic and abiotic factors in understanding the dynamics of the patterns of CH_4 fluxes. We emphasized that the drivers of CH_4 fluxes change both at inter-community and intra-community level and also with seasonality. Unexpectedly we recorded highest emissions in the tussock and not in the wet tundra both in summer and in autumn. During summer the high CH_4 production in tussock and wet tundra was favoured by soil water saturation, unfrozen thickness and warm temperatures and the higher emissions in the tussock tundra can be due to the CH_4 transport through the tussocks' aerenchyma, avoiding its re-oxidation to CO_2, bypassing the soil oxic layers. In autumn the highest CH_4 emissions can be explained by the effect of a different process. In particular, the two-sided front of the soil freezing decreases the soil unfrozen thickness, inducing CH_4 compression, and pushing it up to the surface through the plants' tissues. We emphasized that the dry tundra acted as a CH_4 sink with CH_4 uptake during summer and was inactive in winter, differently from what observed in other sites where the dry tundra shifted to be a CH_4 source in winter. Our data improved our understanding of the key factors affecting the CH_4 fluxes in the sensitive Arctic ecosystems and our findings suggest the need for more investigations to encompass the effect of vegetation on the variability of CH_4 fluxes and disentangle the potential for high emissions during the cold seasons and their contribution to the annual budget.

References

2024 LI-COR, I. (2024). LI-7810 | Specifications. https://www.licor.com/env/support/LI-7810/topics/specifications.html#top

ASTM, 2007. Standard Test Method for Particle Size Analysis of soil. ASTM D422-63.

Adlam L. S., Balks, M. R., Seybold, C. A., Campbell, D. I., 2010. Temporal and spatial variation in active layer depth in the McMurdo Sound Region, Antarctica. Antarctic Science, 22 45–52. https://doi.org/10.1017/s0954102009990460

Arndt, K. A., Lipson, D. A., Hashemi, J., Oechel, W. C., Zona, D., 2020. Snow melt stimulates ecosystem respiration in Arctic ecosystems. Global Change Biology, 26(9), 5042–5051. https://doi.org/10.1111/GCB.15193

Arndt, K. A., Oechel, W. C., Goodrich, J. P., Bailey, B. A., Kalhori, A., Hashemi, J., Sweeney, C., Zona, D., 2019. Sensitivity of Methane Emissions to Later Soil Freezing in Arctic Tundra Ecosystems. Journal of Geophysical Research: Biogeosciences, 124(8), 2595–2609. https://doi.org/10.1029/2019JG005242

Baldocchi, D., Detto, M., Sonnentag, O., Verfaillie, J., Teh, Y. A., Silver, W., Kelly, N. M., 2012. The challenges of measuring methane fluxes and concentrations over a peatland

pasture. Agricultural and Forest Meteorology, 153, 177–187. https://doi.org/10.1016/J.AGRFORMET.2011.04.013

Bao, T., Xu, X., Jia, G., Billesbach, D. P., Sullivan, R. C., 2021. Much stronger tundra methane emissions during autumn freeze than spring thaw. Global Change Biology, 27(2), 376–387. https://doi.org/10.1111/GCB.15421

Billings, W. D., 1987. Carbon balance of Alaskan tundra and taiga ecosystems: past, present and future. Quaternary Science Reviews, 6(2), 165–177. https://doi.org/10.1016/0277-3791(87)90032-1

Blanc-Betes, E., Welker, J. M., Sturchio, N. C., Chanton, J. P., Gonzalez-Meler, M. A, 2016. Winter precipitation and snow accumulation drive the methane sink or source strength of Arctic tussock tundra. Global Change Biology, 22(8), 2818–2833. https://doi.org/10.1111/GCB.13242

Blume, L.J., B.A. Schumacher, P.W., 1990. Handbook of Methods for Acid Deposition Studies Laboratory Analyses for Soil Chemistry. EPA/600/4-90/023. U.S. Environmental Protection Agency, Las Vegas, NV.

Bridgham, S. D., Cadillo-Quiroz, H., Keller, J. K., Zhuang, Q., 2013. Methane emissions from wetlands: Biogeochemical, microbial, and modeling perspectives from local to global scales. Global Change Biology, 19(5), 1325–1346. https://doi.org/10.1111/gcb.12131

Cannone, N., Augusti, A., Malfasi, M., Pallozzi, E., Calfapietra, C., Brugnoli, E., 2016. The interaction of biotic and abiotic factors at multiple spatial scales affects the variability of CO_2 fluxes in polar environments. Polar Biol. 39 (9), 1581–1596. https://doi.org/10.1007/s00300-015-1883-9.

Cannone, N., Ponti, S., Christiansen, H. H., Christensen, T. R., Pirk, N., Guglielmin, M., 2019. Effects of active layer seasonal dynamics and plant phenology on CO_2 land-atmosphere fluxes at polygonal tundra in the High Arctic, Svalbard. CATENA, 174, 142–153. https://doi.org/10.1016/J.CATENA.2018.11.013

Chen, H., Zhu, T., Li, B., Fang, C., Nie, M., 2020. The thermal response of soil microbial methanogenesis decreases in magnitude with changing temperature. Nature Communications 11:1, 11(1), 1–7. https://doi.org/10.1038/s41467-020-19549-4

Christensen, T. R., 1993. Methane emission from Arctic tundra. Biogeochemistry, 21(2), 117–139. https://doi.org/10.1007/BF00000874/METRICS

Christensen, T. R., Panikov, N., Mastepanov, M., Joabsson, A., Stewart, A., Öquist, M., Sommerkorn, M., Reynaud, S., Svensson, B. O., 2003. Biotic controls on CO_2 and CH_4 exchange in wetlands-a closed environment study. Biogeochemistry, 64, 337–354. https://doi.org/10.1023/A:1024913730848

Computer Corporation, O., 2018. Soil Moisture Smart Sensor (S-SMx-M005) Manual Specifications (continued). www.onsetcomp.com

Computer Corporation, O., 2020. HOBO Pro v2 (U23-00x) Manual Specifications (continued). www.onsetcomp.com

Computer Corporation, O., 2022. 2-Bit Temperature Smart Sensor (S-TMB-M0xx) Manual. www.onsetcomp.com/support/contact

Conrad, R., 2009. The global methane cycle: recent advances in understanding the microbial processes involved. Environmental Microbiology Reports, 1(5), 285–292. https://doi.org/10.1111/J.1758-2229.2009.00038.X

Davidson, S. J., Sloan, V. L., Phoenix, G. K., Wagner, R., Fisher, J. P., Oechel, W. C., Zona, D., 2016. Vegetation Type Dominates the Spatial Variability in CH4 Emissions Across Multiple Arctic Tundra Landscapes. Ecosystems, 19(6), 1116–1132. https://doi.org/10.1007/S10021-016-9991-0/FIGURES/8

D'Imperio, L., Nielsen, C. S., Westergaard-Nielsen, A., Michelsen, A., Elberling, B., 2017. Methane oxidation in contrasting soil types: responses to experimental warming with implication for landscape-integrated CH4 budget. Global Change Biology, 23(2), 966–976. https://doi.org/10.1111/GCB.13400

Dunfield, P., knowles, R., Dumont, R., Moore, T. R., 1993. Methane production and consumption in temperate and subarctic peat soils: Response to temperature and pH. Soil Biology and Biochemistry, 25(3), 321–326. https://doi.org/10.1016/0038-0717(93)90130-4

Environmental Data Center Team, M. monitoring program at T. Alaska. T. F. S. I. of A. B. U. of A.F.F.A.99775., 2023. Weather Environmental Data Center. https://www.uaf.edu/toolik/edc/monitoring/abiotic/met-data-query.php

Euskirchen, E. S., Bret-Harte, M. S., Scott, G. J., Edgar, C., Shaver, G. R., 2012. Seasonal patterns of carbon dioxide and water fluxes in three representative tundra ecosystems in northern Alaska. Ecosphere, 3(1), 1–19. https://doi.org/10.1890/ES11-00202.1

Euskirchen, E. S., Edgar, C. W., Bret-Harte, M. S., Kade, A., Zimov, N., & Zimov, S., 2017. Interannual and seasonal patterns of carbon dioxide, water, and energy fluxes from ecotonal and thermokarst-impacted ecosystems on carbon-rich permafrost soils in northeastern Siberia. Journal of Geophysical Research: Biogeosciences, 122, 2651–2668. https://doi.org/10.1002/2017JG004070

FAO, 2014. World reference base for soil resources 2014: International soil classification system for naming soils and creating legends for soil maps.

Flessa, H., Ruser, R., Schilling, R., Loftfield, N., Munch, J. C., Kaiser, E. A., Beese, F., 2002. N2O and CH4 fluxes in potato fields: automated measurement, management effects and temporal variation. Geoderma, 105(3–4), 307–325. https://doi.org/10.1016/S0016-7061(01)00110-0

Forster, P., Alterskjaer, K., Smith, C., Colman, R., Damon Matthews, H., Ramaswamy, V., Storelvmo, T., Armour, K., Collins, W., Dufresne, J., Frame, D., Lunt, D., Mauritsen, T., Watanabe, M., Wild, M., Zhang, H., Pirani, A., Connors, S., Péan, C., … Zhou, B., 2021. The Earth's Energy Budget, Climate Feedbacks and Climate Sensitivity 923–1054. https://doi.org/10.1017/9781009157896.009

Gardner W.A., 1986. Water Content. Methods of soil analysis, Part 1: Physical and Mineralogical Methods, American Society of Agronomy, Soil Society of America, 493-544.

Greaves, H. E., Eitel, J. U. H., Vierling, L. A., Boelman, N. T., Griffin, K. L., Magney, T. S., Prager, C. M., 2019. 20 cm resolution mapping of tundra vegetation communities provides an ecological baseline for important research areas in a changing Arctic environment. Environmental Research Communications, 1(10), 105004. https://doi.org/10.1088/2515-7620/AB4A85

Guglielmin, M., 2006. Ground surface temperature (GST), active layer and permafrost monitoring in continental Antarctica. Permafrost and Periglacial Processes, 17(2), 133–143. https://doi.org/10.1002/ppp.553

Hiyama, T., Ueyama, M., Kotani, A., Iwata, H., Nakai, T., Okamura, M., Ohta, T., Harazono, Y., Petrov, R. E., Maximov, T. C., 2021. Lessons learned from more than a decade of greenhouse gas flux measurements at boreal forests in eastern Siberia and interior Alaska. Polar Science, 27, 100607. https://doi.org/10.1016/J.POLAR.2020.100607

Howard, D., Agnan, Y., Helmig, D., Yang, Y., Obrist, D.,2020. Environmental controls on ecosystem-scale cold-season methane and carbon dioxide fluxes in an Arctic tundra ecosystem. Biogeosciences, 17, 4025–4042. https://doi.org/10.5194/bg-17-4025-2020

Hugelius, G., Strauss, J., Zubrzycki, S., Harden, J. W., Schuur, E. A. G., Ping, C.-L., Schirrmeister, L., Grosse, G., Michaelson, G. J., Koven, C. D., O'Donnell, J. A., Elberling, B., Mishra, U., Camill, P., Yu, Z., Palmtag, J., and Kuhry, P., 2014: Estimated stocks of circumpolar permafrost carbon with quantified uncertainty ranges and identified data gaps. Biogeosciences, 11, 6573–6593, https://doi.org/10.5194/bg-11-6573-2014

Huryn A., Hobbie J., 2012. Land of Extremes: A Natural History of the Arctic North Slope of Alaska. University of Alaska Press.

Jiang, C., Yu, G., Fang, H., Cao, G., Li, Y., 2010. Short-term effect of increasing nitrogen deposition on CO2, CH4 and N2O fluxes in an alpine meadow on the Qinghai-Tibetan Plateau, China. Atmospheric Environment, 44(24), 2920–2926. https://doi.org/10.1016/J.ATMOSENV.2010.03.030

Jeong, S. J., Bloom, A. A., Schimel, D., Sweeney, C., Parazoo, N. C., Medvigy, D., et al., 2018. Accelerating rates of arctic carbon cycling revealed by long-term atmospheric CO2 measurements. Science Advances, 4(7), 1–7. https://doi.org/10.1126/sciadv.aao1167

Jobbagy, E. G., Jobbagy, J., Jackson, R. B., 2000. The vertical distribution of soil organic carbon and its relation to climate and vegetation. Ecological Applications, 10(2), 423–436. https://doi.org/10.1890/1051-0761(2000)010

Juncher Jørgensen, C., Lund Johansen, K. M., Westergaard-Nielsen, A., Elberling, B., 2014. Net regional methane sink in High Arctic soils of northeast Greenland. Nature Geoscience 2014 8:1, 8(1), 20–23. https://doi.org/10.1038/ngeo2305

Kade, A., Syndonia Bret-Harte, M., Euskirchen, E. S., Edgar, C., Fulweber, R. A., 2012. Upscaling of CO2 fluxes from heterogeneous tundra plant communities in Arctic Alaska. Journal of Geophysical Research: Biogeosciences, 117(G4), 4007. https://doi.org/10.1029/2012JG002065

Kade, A., Walker, D. A., Raynolds, M. K., Breen, A. L., Hobgood, O. M., 2024. Landscape patterns of carbon fluxes in natural and disturbed ice-wedge-polygon tundra. Arctic, Antarctic, and Alpine Research, 56(1). https://doi.org/10.1080/15230430.2024.2391244

Kalra Y.P., 1995. Determination of pH of Soils by Different Methods: Collaborative Study, Journal of AOAC INTERNATIONAL, Volume 78, Issue 2, Pages 310–324, https://doi.org/10.1093/jaoac/78.2.310

Kim, Y., 2015. Effect of thaw depth on fluxes of CO2 and CH4 in manipulated Arctic coastal tundra of Barrow, Alaska. Science of the Total Environment, 505, 385–389. https://doi.org/10.1016/j.scitotenv.2014.09.046

Kim, Y., Ueyama, M., Nakagawa, F., Tsunogai, U., Harazono, Y., Tanaka, N., 2007. Assessment of winter fluxes of CO2 and CH4 in boreal forest soils of central Alaska estimated by the profile method and the chamber method: A diagnosis of methane emission and implications for the regional carbon budget. Tellus, Series B: Chemical and Physical Meteorology, 59(2), 223–233. https://doi.org/10.1111/j.1600-0889.2006.00233.x

Kirschke, S., Bousquet, P., Ciais, P., Saunois, M., Canadell, J. G., Dlugokencky, E. J., Bergamaschi, P., Bergmann, D., Blake, D. R., Bruhwiler, L., Cameron-Smith, P., Castaldi, S., Chevallier, F., Feng, L., Fraser, A., Heimann, M., Hodson, E. L., Houweling, S., Josse,

B., … Zeng, G., 2013. Three decades of global methane sources and sinks. Nature Geoscience 2013 6:10, 6(10), 813–823. https://doi.org/10.1038/ngeo1955

Kutzbach, L., Wagner, D., Pfeiffer, E. M., 2004. Effect of microrelief and vegetation on methane emission from wet polygonal tundra, Lena Delta, Northern Siberia. Biogeochemistry, 69(3), 341–362. https://doi.org/10.1023/B:BIOG.0000031053.81520.DB/METRICS

LAI, D. Y. F., 2009. Methane Dynamics in Northern Peatlands: A Review. Pedosphere, 19(4), 409–421. https://doi.org/10.1016/S1002-0160(09)00003-4

Lawrence, D. M., Koven, C. D., Swenson, S. C., Riley, W. J., Slater, A. G., 2015. Permafrost thaw and resulting soil moisture changes regulate projected high-latitude CO2 and CH4 emissions. Environmental Research Letters, 10(9), 094011. https://doi.org/10.1088/1748-9326/10/9/094011

Le Mer, J., Roger, P., 2001. Production, oxidation, emission and consumption of methane by soils: A review. European Journal of Soil Biology, 37(1), 25–50. https://doi.org/10.1016/S1164-5563(01)01067-6

Levy, P.E., Gray, A., Leeson, S.R., Gaiawyn, J., Kelly, M.P.C., Cooper, M.D.A., Dinsmore, K.J., Jones, S.K., Sheppard, L.J., 2011. Quantification of uncertainty in trace gas fluxes measured by the static chamber method. European Journal of Soil Science 62, 811–821. https://doi.org/10.1111/j.1365-2389.2011.01403.x

Lipson, D. A., Zona, D., Raab, T. K., Bozzolo, F., Mauritz, M., Oechel, W. C., 2012. Water table height and microtopography control Biogeochemical cycling in an Arctic coastal tundra Ecosystem. Biogeosciences, 9(1), 577–591. https://doi.org/10.5194/bg-9-577-2012

Ma, S., Bloom, A.A, Watts, J.D., Quetin, G.R., Zona., D., Euskirchen, E., Norton, A.J., Yin, Y., Levine, P.A., Braghiere, R.K., Parazoo, N.C., Worden, J.R., Schimel, D.S., Miller, C.E., 2023. Resolving the Carbon-Climate Feedback Potential of Wetland CO2 and CH4 Fluxes in Alaska. Global Biogeochemical Cycles, 37, e2022GB007524. https://doi.org/10.1029/2022GB007524

Maier, M., Weber, T.K.D., Fiedler, J., Fuß, R., Glatzel, S., Huth, V., Jordan, S., Jurasinski, G., Kutzbach, L., Schäfer, K., Weymann, D., Hagemann, U., 2022. Introduction of a guideline for measurements of greenhouse gas fluxes from soils using non-steady-state chambers. J. Plant Nutr. Soil Sci. 185, 447–461. https://doi.org/10.1002/jpln.202200199

Mar, K. A., Unger, C., Walderdorff, L., Butler, T., 2022. Beyond CO_2 equivalence: The impacts of methane on climate, ecosystems, and health. Environmental Science Policy, 134, 127–136. https://doi.org/10.1016/J.ENVSCI.2022.03.027

Mastepanov, M., Sigsgaard, C., Tagesson, T., Ström, L., Tamstorf, M. P., Lund, M., Christensen, T. R., 2013. Revisiting factors controlling methane emissions from high-Arctic tundra. Biogeosciences, 10, 5139–5158. https://doi.org/10.5194/bg-10-5139-2013

McEwing, K.R., Fisher, J.P. & Zona, D. Environmental and vegetation controls on the spatial variability of CH4 emission from wet-sedge and tussock tundra ecosystems in the Arctic. Plant Soil 388, 37–52 (2015). https://doi.org/10.1007/s11104-014-2377-1

McGuire, A. D., Anderson, L. G., Christensen, T. R., Scott, D., Laodong, G., Hayes, D. J., Martin, H., Lorenson, T. D., Macdonald, R. W., Nigel, R., 2009. Sensitivity of the carbon cycle in the Arctic to climate change. Ecological Monographs, 79(4), 523–555. https://doi.org/10.1890/08-2025.1

McGuire, A. D., Christensen, T. R., Hayes, D., Heroult, A., Euskirchen, E., Kimball, J. S., Koven, C., Lafleur, P., Miller, P. A., Oechel, W., Peylin, P., Williams, M., Yi, Y., 2012. An assessment of the carbon balance of Arctic tundra: Comparisons among observations, process models, and atmospheric inversions. Biogeosciences, 9(8), 3185–3204. https://doi.org/10.5194/bg-9-3185-2012

Merbold, L., Ziegler, W., Mukelabai, M. M., Kutsch, W. L., 2011. Spatial and temporal variation of CO2 efflux along a disturbance gradient in a miombo woodland in Western Zambia. Biogeosciences, 8(1), 147–164. https://doi.org/10.5194/BG-8-147-2011

Morrissey, L. A., Livingston, G. P., 1992. Methane emissions from Alaska Arctic tundra: An assessment of local spatial variability. Journal of Geophysical Research: Atmospheres, 97(D15), 16661–16670. https://doi.org/10.1029/92JD00063

Myhre, G., D. Shindell, F.-M. Bréon, W. Collins, J. Fuglestvedt, J. Huang, D. Koch, J.-F. Lamarque, D. Lee, B. Mendoza, T. Nakajima, A. Robock, G. Stephens, T. Takemura, and H. Zhang, 2013: Anthropogenic and natural radiative forcing. In Climate Change 2013: The Physical Science Basis. Contribution of Working Group I to the Fifth Assessment Report of the Intergovernmental Panel on Climate Change. T.F. Stocker, D. Qin, G.-K. Plattner, M. Tignor, S.K. Allen, J. Doschung, A. Nauels, Y. Xia, V. Bex, and P.M. Midgley, Eds., Cambridge University Press, pp. 659-740, doi:10.1017/CBO9781107415324.018.

Natali, S. M., Schuur, E. A. G., Mauritz, M., Schade, J. D., Celis, G., Crummer, K. G., Johnston, C., Krapek, J., Pegoraro, E., Salmon, V. G., Webb, E. E., 2015. Permafrost thaw and soil moisture driving CO2 and CH4 release from upland tundra. Journal of Geophysical Research: Biogeosciences, 120(3), 525–537. https://doi.org/10.1002/2014JG002872

Nazaries, L., Murrell, J. C., Millard, P., Baggs, L., Singh, B. K., 2013. Methane, microbes and models: Fundamental understanding of the soil methane cycle for future predictions.

Environmental Microbiology, 15(9), 2395–2417. https://doi.org/10.1111/1462-2920.12149

Nelson, D.W., Sommers L.E., 1996. Total carbon, organic carbon, and organic matter. Methods of Soil Analysis, Part 2, 2nd ed., A.L. Page et al., Ed. Agronomy. 9:961-1010. Am. Soc. of Agron., Inc. Madison, WI.

Niendorf, C. R., 2023. SIPRE Hand Augers-Operations and Maintenance Manual Document #8507-0011 SIPRE HAND AUGER Operations and Maintenance Manual.

Ohtsuka, T., Adachi, M., Uchida, M., Nakatsubo, T., 2006. Relationships between vegetation types and soil properties along a topographical gradient on the northern coast of the Brgger Peninsula, Svalbard. Polar Bioscience, 19, 63–72. https://doi.org/10.15094/00006240

Oh, Y., Zhuang, Q., Liu, L. et al., 2020. Reduced net methane emissions due to microbial methane oxidation in a warmer Arctic. Nature Climate Change 10, 317–321. https://doi.org/10.1038/s41558-020-0734-z

Olefeldt, D., Turetsky, M. R., Crill, P. M., Mcguire, A. D., 2013. Environmental and physical controls on northern terrestrial methane emissions across permafrost zones. Global Change Biology, 19(2), 589–603. https://doi.org/10.1111/GCB.12071

Parmentier, F-J. W., Thornton, B.F., Silyakova, A., Christensen, T.R., 2024. Vulnerability of Arctic-Boreal methane emissions to climate change. Front. Environ. Sci. 12:1460155. doi:10.3389/fenvs.2024.1460155

Preuss, I., Knoblauch, C., Gebert, J., Pfeiffer, E. M., 2013. Improved quantification of microbial CH4 oxidation efficiency in arctic wetland soils using carbon isotope fractionation. Biogeosciences, 10(4), 2539–2552. https://doi.org/10.5194/BG-10-2539-2013

Reuss-Schmidt, K., Levy, P., Oechel, W., Tweedie, C., Wilson, C., Zona, D., 2019. Understanding spatial variability of methane fluxes in Arctic wetlands through footprint modelling. Environmental Research Letters, 14(12), 125010. https://doi.org/10.1088/1748-9326/AB4D32

Rodenhizer, H., Ledman, J., Mauritz, M., Natali, S. M., Pegoraro, E., Plaza, C., et al., 2020. Carbon thaw rate doubles when accounting for subsidence in a permafrost warming experiment. Journal of Geophysical Research: Biogeosciences, 125(6), 1–16. https://doi.org/10.1029/2019JG005528

Sachs, T., C. Wille, J. Boike, and Kutzbach L., 2008. Environmental controls on ecosystem-scale CH4 emission from polygonal tundra in the Lena River Delta, Siberia, J. Geophys. Res., 113, G00A03, https://doi.org/10.1029/2007jg000505

Schuur, E., McGuire, A., Schädel, C. et al., 2015. Climate change and the permafrost carbon feedback. Nature 520, 171–179. https://doi.org/10.1038/nature14338

Shiklomanov, N., 2023. Seasonal soil active layer measurements from a Circumpolar Active Layer Monitoring (CALM) grid, U12A Toolik 1 kilometer grid, Alaska, 1995-2020. https://doi.org/10.18739/A2S756M7J

Shindell, D., Sadavarte, P., Aben, I., De Oliveira Bredariol, T. S., Dreyfus, G., Höglund-Isaksson, L., Poulter, B., Saunois, M., Schmidt, G. A., Szopa, S., Rentz, K., Parsons, L., Qu, Z., Faluvegi, G., Maasakkers, J. D., Nisbet, E., O'connor, F., Reisinger, A., 2024. The methane imperative. Frontiers in Science, 2, 1349770. https://doi.org/10.3389/FSCI.2024.1349770

Sturtevant, C. S., Oechel, W. C., Zona, D., Kim, Y., Emerson, C. E., 2012. Soil moisture control over autumn season methane flux, Arctic Coastal Plain of Alaska. Biogeosciences, 9, 1423–1440. https://doi.org/10.5194/bg-9-1423-2012

Sun, L., Song, C., Miao, Y., Qiao, T., Gong, C., 2013. Temporal and spatial variability of methane emissions in a northern temperate marsh. Atmospheric Environment, 81, 356–363. https://doi.org/10.1016/J.ATMOSENV.2013.09.033

ter Braak, C.J.F., Šmilauer, P., 1998. CANOCO. Reference manual and user's guide to CANOCO for windows. Software for Canonical Community Ordination (version 4). Centre for Biometry, Wageningen

Tom, M. S., Chapin, F. S., 1993. Environmental and biotic controls over methane flux from Arctic tundra. Chemosphere (Vol. 26, Issue 4).

Ueyama, M., Harazono, Y., Okada, R., Nojiri, A., Ohtaki, E., Miyata, A., 2006. Micrometeorological measurements of methane flux at a boreal forest in central Alaska. Memoirs of National Institute of Polar Research. Special Issue, 59, 156–167. https://nipr.repo.nii.ac.jp/records/2516

Verville, J., Hobbie, S., Chapin Iii, F., Hooper, D.,1998. Response of tundra CH4 and CO2 flux to manipulation of temperature and vegetation. In Biogeochemistry (Vol. 41).

Virkkala, A.M., Niittynen, P., Kemppinen, J., Marushchak, M. E., Voigt, C., Hensgens, G., Kerttula, J., Happonen, K., Tyystjärvi, V., Biasi, C., Hultman, J., Rinne, J., Luoto, M. 2024. High-resolution spatial patterns and drivers of terrestrial ecosystem carbon dioxide, methane, and nitrous oxide fluxes in the tundra. Biogeosciences, 21, 335–355. https://doi.org/10.5194/bg-21-335-2024

Voigt, C., Virkkala, A., Gosselin, G. H., Bennett, K. A., Black, T. A., Detto, M., Chevrier-Dion, C., Guggenberger, G., Hashmi, W., Kohl, L., Kou, D., Marquis, C., Marsh, P., Marushchak, M. E., Nesic, Z., Nykänen, H., Saarela, T., Sauheitl, L., Walker, B., . . . Sonnentag, O., 2023. Arctic soil methane sink increases with drier conditions and higher ecosystem

respiration. Nature Climate Change, 13(10), 1095–1104. https://doi.org/10.1038/s41558-023-01785-3

Wagner, R., Zona, D., Oechel, W., Lipson, D., 2017. Microbial community structure and soil pH correspond to methane production in Arctic Alaska soils. Environmental Microbiology, 19(8), 3398–3410. https://doi.org/10.1111/1462-2920.13854

Waldo, S., Russell, E. S., Kostyanovsky, K., Pressley, S. N., O'Keeffe, P. T., Huggins, D. R., et al., 2019. N2O emissions from two agroecosystems: High spatial variability and long pulses observed using static chambers and the flux-gradient technique. Journal of Geophysical Research: Biogeosciences, 124, 1887–1904. https://doi.org/10.1029/2019JG005032

Walker, D. A., Binnian, E., Evans, B. M., Lederer, N. D., Nordstrand, E., Webber, P. J., 1989. Terrain, vegetation and landscape evolution of the R4D research site, Brooks Range Foothills, Alaska. Ecography, 12(3), 238–261. https://doi.org/10.1111/J.1600-0587.1989.TB00844.X

Walker, D. A., Maier, A., 2008. Vegetation in the vicinity of the Toolik Field Station, Alaska. 28. http://www.ArcticAtlas.

Wang, Y., He, L., Liu, J., Arndt, K. A., Mazza Rodrigues, J. L., Zona, D., Lipson, D. A., Oechel, W. C., Ricciuto, D. M., Wullschleger, S. D., Xu, X., 2024. Intensified Positive Arctic–Methane Feedback under IPCC Climate Scenarios in the 21st Century. Ecosystem Health and Sustainability, 10. https://doi.org/10.34133/ehs.0185

Ward, R. H., Sweeney, C., Miller, J. B., Goeckede, M., Laurila, T., Hatakka, J., Ivakov, V., Sasakawa, M., Machida, T., Morimoto, S., Goto, D., Ganesan, A. L., 2024. Increasing methane emissions and widespread cold-season release from high-Arctic regions detected through atmospheric measurements. Journal of Geophysical Research: Atmospheres, 129(11), e2024JD040766. https://doi.org/10.1029/2024JD040766

Whalen, S. C., 2005. Biogeochemistry of Methane Exchange between Natural Wetlands and the Atmosphere. Https://Home.Liebertpub.Com/Ees, 22(1), 73–94. https://doi.org/10.1089/EES.2005.22.73

Wu, X., Zhao, L., Chen, M., Fang, H., Yue, G., Chen, J., Pang, Q., Wang, Z., Ding, Y., 2012. Soil Organic Carbon and Its Relationship to Vegetation Communities and Soil Properties in Permafrost Areas of the Central Western Qinghai-Tibet Plateau, China. Permafrost and Periglacial Processes, 23(2), 162–169. https://doi.org/10.1002/PPP.1740

Xu, X., Yuan, F., Hanson, P. J., Wullschleger, S. D., Thornton, P. E., Riley, W. J., Song, X., Graham, D. E., Song, C., Tian, H., 2016. Reviews and syntheses: Four decades of modeling

methane cycling in terrestrial ecosystems. Biogeosciences, 13(12), 3735–3755. https://doi.org/10.5194/BG-13-3735-2016

Yvon-Durocher, G., Allen, A. P., Bastviken, D., Conrad, R., Gudasz, C., St-Pierre, A., Thanh-Duc, N., Del Giorgio, P. A., 2014. Methane fluxes show consistent temperature dependence across microbial to ecosystem scales. Nature, 507:7493, 507(7493), 488–491. https://doi.org/10.1038/nature13164

Zhuang, Q., Melillo, J. M., Kicklighter, D. W., Prinn, R. G., McGuire, A. D., Steudler, P. A., Felzer, B. S., Hu, S., 2004. Methane fluxes between terrestrial ecosystems and the atmosphere at northern high latitudes during the past century: A retrospective analysis with a process-based biogeochemistry model. Global Biogeochemical Cycles, 18(3). https://doi.org/10.1029/2004GB002239

Zona, D., Gioli, B., Commane, R., Lindaas, J., Wofsy, S. C., Miller, C. E., Dinardo, S. J., Dengel, S., Sweeney, C., Karion, A., Chang, R. Y. W., Henderson, J. M., Murphy, P. C., Goodrich, J. P., Moreaux, V., Liljedahl, A., Watts, J. D., Kimball, J. S., Lipson, D. A., Oechel, W. C., 2016. Cold season emissions dominate the Arctic tundra methane budget. Proceedings of the National Academy of Sciences of the United States of America, 113(1), 40–45. https://doi.org/10.1073/pnas.1516017113

Zona, D., Oechel, W. C., Kochendorfer, J., Paw U, K. T., Salyuk, A. N., Olivas, P. C., Oberbauer, S. F., Lipson, D. A., 2009. Methane fluxes during the initiation of a large-scale water table manipulation experiment in the Alaskan Arctic tundra. Global Biogeochemical Cycles, 23(2). https://doi.org/10.1029/2009GB003487

High-resolution vegetation mapping at Toolik Lake (Alaska) integrating UAS imagery and field surveys

Abstract

The Arctic is one of the most sensitive regions to climate change, with shrub encroachment being among its most widespread impacts. Vegetation serves as an excellent bio-indicator of climatic change, and its monitoring is essential. This requires the combination of high spatial resolution mapping with a detailed characterization of vegetation composition and dynamics

In this study, we propose a mapping to realize high-resolution vegetation maps (both phytosociological and physiognomic map) using the drone-based ortho-imagery as a basemap for field mapping integrated with vegetation surveys applying the phytosociological method. We tested this protocol by mapping the vegetation in an area close to Toolik (Alaska) during the summer 2024 and we analyzed the phytosociological data using multivariate analyses

We mapped an area of > 13 ha providing very detailed information on vegetation spatial distribution, floristic composition, community types and physiognomy. Five communities accounted for more than 65% of the mapped area, with moist sedge tundra with low shrubs (*Carex bigelowii, Betula nana*, and *Ericaceae*; 17.3%), tussock tundra (15%), low to tall shrubs of *Betula nana* (17.6%), and *Carex aquatilis* wetlands (16.6%) representing the most extensive formations.

The use of the drone ortho-imagery as a basemap for field mapping resulted particularly effective in relatively flat areas and/or very homogeneous geomorphological conditions, but with heterogeneous vegetation, features common to many Arctic landscapes.

These maps provide an essential baseline for monitoring future vegetation dynamics and detecting fine-scale changes in response to climate warming in Arctic tundra ecosystems.

.

Keywords: drone ortho-imagery; phytosociological relevés; field mapping; physiognomic maps; Toolik field station; Arctic vegetation monitoring

1. Introduction

The Arctic is one of the most climate-sensitive regions (IPCC, 2018), partly due to the Arctic amplification (Serreze and Barry, 2011), with Alaska experiencing the strongest warming in the period 1950-2000 (Walsh et al., 2019). Climate warming has been driving several impacts on the ecosystems, among which the northward expansion of species ranges (Sturm et al., 2001; Tape et al., 2006; Forbes et al. 2010; Myers-Smith et al., 2011), the advancement of phenological stages (Høye et al., 2007; Ovaskainen et al., 2013) and the increased reproductive investment for many species (Barrett et al., 2015). Moreover shrubs encroachment (Sturm et al. 2001; Tape et al., 2006; Elmendorf et al., 2012; Kapfer and Grytnes, 2016), in particular of *Salix* species of *Betula nana* (Jones et al., 1997; Shaver et al., 2001; Hill & Henry, 2011; Kapfer and Grytnes, 2016), but also of graminoids and forbs (Myers-Smith et al., 2011; Walker et al., 2012; Kapfer and Grytnes, 2016) have been observed.Differently, mosses and lichens are decreasing in abundance (Jägerbrand et al., 2006; Kapfer and Grytnes, 2016).

Change in species composition, in particular the increase of shrub abundance, could alter above-ground carbon storage, changing the quantity and decomposability of litter (Callaghan et al., 2004; Sturm and Douglas, 2005; Petrenko et al., 2016; Bjorman et al., 2020), increase winter soil temperatures and change the snow cover depth ((Myers Smith and Hik 2013; Bjorman et al., 2020), decrease winter albedo and increase solar radiation absorption (Sturm et al., 2001, 2005; Chapin et al., 2005, Sturm and Douglas 2005; Tape et al., 2006, 2012; Lawrence and Swenson 2011; Loranty et al., 2011; Myers-Smith et al., 2011; Elmendorf et al., 2012; DeMarco et al., 2014; Dial et al., 2016; Myers-Smith and Hik, 2018; Bjorman et al., 2020),with feedback to the global climate (Chapin et al. 2005; Pearson et al. 2013; Bjorman et al., 2020).

Vegetation plays a key role in shaping the structure, biodiversity, processes and dynamics of the terrestrial ecosystems. Due to its lack of vagility, it is also one of the most reliable bio-indicators of environmental and climatic change. Vegetation mapping has therefore been recognized as a key component for the development of terrestrial ecosystem models (Euschirken et al., 2009). Vegetation surveys and monitoring can be conducted at various spatial and temporal scales, from plot-scale measurements to track changes of vegetation with high spatial heterogeneity, to satellite remote sensing, which enables the assessment of changes across broad geographic areas (Fraser et al., 2016).

Detailed field surveys at the plot scale provide different data depending on the methodology used. These include information on floristic composition, vegetation communities and successional dynamics (e.g., phytosociological method as in in Walker et al., 1994, Boggs et al., 2018, as well as data on plant cover, dominance, functional types and traits (e.g. point-frame methods as in Hudson and Henry, 2008 and in Elmendorf et al., 2012). Conversely, satellite-

based remote sensing allows to assess the general distribution of main vegetation physiognomic types, biomass and phenology over large areas, but in most cases lack spatial resolution necessary to detect fine-scale changes at species and/or community level (Cruzan et al., 2016; Moffatt et al., 2016). A particularly expensive remote sensing method is high-resolution airborne LiDAR, which allows for detailed vegetation mapping (with spatial resolution of 20 cm) using the Random Forest model trained on ground reference plots (Greaves et al., 2019).

More recently, micro–unmanned aerial vehicles (UAVs) have been increasingly used for vegetation mapping, as their high spatial resolution and image details are adequate for estimating the spatial distribution and abundance of vegetation over relatively large areas with relatively low efforts and costs (Anderson and Gaston, 2013; Cruzan et al., 2016; Oldeland et al., 2021). In most cases, drones-based photogrammetry has been used to classify and map vegetation (Fraser et al., 2016; Oldeland et al., 2021). Drone ortho-imagery has been used also as a base map to support field mapping of individual plant species at very high spatial resolution (Oldeland et al., 2021), suggesting its potential as a flexible, effective and low-cost tool for detailed vegetation mapping.

High-resolution vegetation mapping is essential for capturing the heterogeneity of the Arctic tundra ecosystems and for monitoring their spatial and temporal dynamics in response to climate change (Greaves et al., 2019). This task is even more important at sites with previous vegetation surveys and/or vegetation maps, such as the Toolik Lake area (Northern Brooks Range, Alaska), where vegetation was first described and mapped using the permanent plot method in 1989 (Walker and Barry 1991) and the phytosociological method in 1991 (Walker and Maier, 2008) and where a high-resolution physiognomic map of vegetation was produced in 2013 (Greaves et al., 2019).

In the frame of the project INSUBRE-Polar, a detailed vegetation survey and field mapping was carried out in the summer 2024. The survey covered an area of 13.39 ha close to Toolik Field Station and employed the phytosociological method and the drone ortho-imagery as a base map to support field mapping and to produce new high resolution phytosociological and physiognomic maps. The aims of this study are: (a) to characterized the most recent species composition, structure and spatial distribution of the plant communities; (b) to provide a detailed reference data for the monitoring and the assessment of any impact of future environmental changes; and (c) to offer a support for any multi-disciplinary and high-resolution experimental or modelling studies which involve vegetation features in the study area.

2. Materials and Methods

2.1 Study area

The study area is located in the Brooks Range on Alaska's North Slope (Fig. 1SM), close to the Toolik Field Station (68°38' N 149°34' W, 760 m elevation). This site is characterized by cold winters, with air temperature as low as to -40°C, and relatively short but warm summers, with air temperatures reaching up 13°C. The mean annual air temperature is approximately -16°C, with mean annual precipitation sum of ca. 300 mm. Snow cover is continuous between late September/early October until late May/beginning of June (Huryn and Hobbie, 2012; Greaves et al., 2019). Permafrost is continuous in the area, with active layer ranging between 67.5 cm to 100 cm in depth (Shiklomanov 2023).

The study site is located in the bioclimatic subzone E, in the floristic province of North Alaska-Yukon territory and in the erect dwarf-shrub tundra (low shrub moss tundra) (Walker et al., 2005). The vegetation is a mosaic of different vegetation types including: erect shrub; dwarf-shrub, tussock-sedge, moss tundra; and wetlands (Walker, 2000; Walker et al., 2005, 2016).

2.2 Field survey and data

The phytosociological map of the vegetation of the study area was obtained through field surveys carried out in summer 2024. The Toolik Field Station GIS and Remote Sensing Dept. created an orthophoto mosaic (hereafter, OPM) of the study area using a DJI Matrice M210 unmanned aerial system (UAS) on 16th of June 2024. The OPM was printed at a scale of 1:250 and used as basemap to support the vegetation field surveys. Indeed, drone-derived ortho-imagery has been suggested as suitable tools to support field surveys and to allow more accurate mapping with just-in-time aerial imagery (Oldeman et al., 2021), compared to the simple use of topographic maps. For the vegetation mapping, each patch of homogeneous vegetation identificable on the OPM was delineated by the expert (N.C.), resulting in polygons of distinct vegetation communities. Each mapped polygon on the OPM was then verified in the field and for each polygon a phytosociological relevés was carried, using a standard plot of 1x1 m. GPS location (accuracy ± 2m), elevation, aspect, detailed location within the mapped polygons and one or more photos taken from different point of views of each plot enabled reliable future resurvey of the study area. For each plot were recorded the total vegetation cover and the cover of each species of vascular plants, bryophytes, lichens, visually estimated as a percentage (%) with a range from 0% to 100% to provide detailed information also on species with low cover values (Cannone et al., 2007, 2010; Cannone and Pignatti, 2014; Malfasi and Cannone, 2021). Vascular plants, bryophytes and lichens were identified to the species level according to Hulten (1968) and Thomson and Brehmer (1984). Species identifications were visually validated

though comparison with herbarium specimens at Toolik Field Station. Species nomenclature was standardized according to the Global Biodiversity Information Facility (www.gbif.org).
For each relevés were recorded also the mean and maximum height of the main species of the erect-shrubs layer [29], to better characterize the vegetation physiognomy and structure.
For the accurate identification of the vegetation syntaxa, in particular of the vegetation communities obtained by the phytosociological survey and of the physiognomic classes, our data were compared with the available literature for Alaska and also for the Arctic region (Walker and Barry, 1991; Walker et al., 1994; Walker and Walker, 1996; CAVM Team 2003; Raynolds et al., 2005; Jorgenson et al., 2009; Viereck et al., 2012; Boggs et al., 2018; Wells et al., 2022).

2.3 Multivariate analyses and phytosociological map

The data of the 349 phytosociological relevés were analyzed by means of multivariate analysis, performing the Principal Component Analysis (PCA-349 relevés). PCA was carried out using a log transformation of the data of the 50 most abundant species through the software CANOCO for Windows (ter Braak and Smilauer, 1998). According to the main species and relevés clusters identified by the PCA, the main vegetation communities occurring in the study site were identified and, for each community type, the mean floristic composition and cover (%) of each species were computed.
To confirm the attribution of the 19 vegetation communities obtained by the 349 relevés to the syntaxa already identified by the available literature, a second PCA (PCA-communities) was carried out using the mean floristic composition and cover of the 19 communities identified at our study site and the 28 more similar vegetation communities described by Boggs et al (2018) for Alaska for comparison. The results of the PCA-communities analysis allowed us to confirm the congruence between the 19 vegetation communities identified in our study and those previously described in the literature referred to the study area (Walker et al., 1994; Greaves et al., 2019; Wells et al., 2022), as well as to Alaska and other Arctic and Subarctic vegetation (Jorgenson et al., 2009; Viereck et al., 2012; Boggs et al., 2018), and to finalize the phytosociological map.
The field map was scanned, geo-referenced (n. 433 ground control points; RMS error <1 m), and manually digitalized to produce a single vector layer (ESRI shapefile format) composed of 314 polygons. All the GIS analyses were conducted using the open-source program QGIS (3.28.4), in the projected coordinate system NAD83/UTM6N (EPSG: 26906).

2.4 Physiognomic map

The physiognomic map was derived from the phytosociological map by comparing the physiognomic classes of the 19 vegetation communities observed in this study with those described by Walker et al (1994), Boggs et al (2018), and Greaves et al (2019) (Table 1SM)). To further support the attribution of our communities to the main physiognomic classes, for each of our 19 plant communities the descriptive statistics (minimum, maximum, median, 25th and 75th percentiles) of the height of the shrubs species *Betula nana, Salix pulchra, Vaccinium uliginosum* and *Rhododendron tomentosum* as well as of the mean shrub height recorded in each relevé were calculated (Fig. 2SM). These data allowed to confirm the attribution of each of the 19 vegetation communities identified by our analyses to the main vegetation classes and to the main physiognomic classes (according to Walker et al., 1994; Boggs et al., 2018; Greaves et al., 2019). For each of the identified physiognomic classes we also compared photo of reference plots with our own field images, that corroborated the consistency of the attribution. These data were used to assign a unique physiognomic class to each vegetation communities and digitalized polygons of the field map and allowed to produce the physiognomic map of the study site at scale 1:250.

3. Results

3.1 Identification of vegetation communities and phytosociological map

A total of 349 phytosociological relevés were carried out in the study area. Our assessments included 177 taxa: 102 vascular plants (6 not determined at the species leve), 38 bryophytes and 37 lichens and the general category Cyanobacteria crust. A multivariate analysis (PCA) of the 349 relevés (Fig. 1a, 1b; Table 1) and of the 53 most abundant species enabled the identification of nine main species clusters (Fig. 1a) labelled from A1 to I, each characterized by specific target species. Based on the same dataset, the PCA also distinguished nine main community clusters and 19 distinct vegetation communities (Fig. 1b, Table 1). These included dwarf shrub tundra (A1, A2), dry heath tundra (B1, B2, B3, C), moist sedge tundra (D1, D2), low to tall shrub tundra (E1, E2, E3), tussock tundra (F1), shrubby tussock tundra (F2), wet tussock sedge tundra (G1, G2), wetland (H1, H2, H3) and pond (I). The average vascular plants, bryophytes and lichens species richness are 28, 12 and 12, respectively.

Dwarf shrub tundra cluster refers to hemi-prostrate and prostrate dwarf shrubs and fruticose lichens (i.e. *Pertusaria dactylina, Thamnolia subuliformis*) and it comprises two vegetation communities. The first is a dwarf shrub tundra of moist sites (A1), co-dominated by the dwarf shrubs *Dryas integrifolia* (11.0%)*, Salix reticulata* (11.8%) and *Cassiope tetragona* (11.7%)

and by a significant mosses cover, mainly composed by *Rhytidium rugosum* (26.7%). Differently, the second is a dwarf shrub tundra of dry exposed sites (A2), dominated by *Dryas octopetala* (40.7%) with *Vaccinium vitis-idaea* (6.3%) and *Salix phleboohylla* (4.2%), and with a higher lichens cover. In A1 the species richness is relatively low (v=21; b=10; l=14), while it increases in A2 (v=30; b=8; l=25), especially for lichens.

Dry heath tundra (B, C) cluster is dominated by prostrate dwarf shrubs, with many fruticose lichens (i.e. *Stereocaulon alpinum*, *Cetraria cucullata*, *Cladina rangiferina*), and it comprises four different communities characterised by the dominance of different vascular species. The first (B1) is a dry heath tundra of *Kalmia procumbens* (34.6%), with different species of lichens, mainly composed by *Cetraria cucullata* (13.2%) and *Stereocaulon alpinum* (10.3%), with high constancy also of other lichens species such as *Masonhalea richardsonii*, *Sphaerophorus globosus* and *Peltigera malacea.* The community has a relatively low species richness (v=30; b=11; l=17). The second vegetation community (B2) is co-dominated by dwarf shrubs *Arctostaphylos alpinus* (27.5%), *Vaccinium vitis-idaea* (22%) and *Empetrum nigrum* (18.7%) and is characterised by the presence of *Dryas octopetala* (5.1%), despite with lower frequency and abundance than in A2. The cover of mosses (i.e. *Dicranum spadiceum* (4.9%)) and lichens (i.e. *Cetraria cucullata* (6.1%)) are low, while the species richness reaches in this community the highest values of the whole study area (tot=98; v=54; b=18; l=26). The third community (B3) is characterized by the *Ericaceae* dwarf shrubs *Vaccinium uliginosum* (12.8%) and *Vaccinium vitis-idaea* (9.3%) with a significant understorey mainly dominated by lichens (i.e. *Cladina rangiferina* (29.5%)) and secondly by mosses (i.e. *Racomitrium lanuginosum* (14.1%)). The species richness of lichens and mosses are relatively high and low, respectively (v=23; b=9; l=20). The forth community (C) of this cluster still includes shrubs *Vaccinium uliginosum* (26.8%) and *Vaccinium vitis idaea* (10.5%), but with the co-dominance of *Betula nana* (38.9%), a significant increase of mosses cover (mean = 76%) than the previous communities of the cluster, mainly composed by *Rhytidium rugosum* (26.8%), *Aulacomium turgidum* (17.3%) and *Hylocomium splendens* (15.2%), and a decrease in lichens. The species richness is relatively high (v=41; b=16; l=16).

Moist sedge tundra (D) cluster is dominated by the sedge *Carex bigelowii* and includes two vegetation communities those differ according to the dwarf shrubs and mosses covers. The first is a moist sedge tundra (D1) of *Carex bigelowii* (48.1%) and *Salix reticulata* (23.3%), and a low mosses cover, mainly composed by *Dicranum* species (*Dicranum spadiceum* (10.5%); *Dicranum elongatum* (6.3%)). The second (D2) is a shrubby moist sedge tundra co-dominated by *Carex bigelowii* (34.7%), *Betula nana* (23.5%) and *Rhododenron tomentosum* (19.7%) and with a significant mosses cover, mainly composed by *Hylocomium splendens* (40.1%) and

Aulacomnium turgidum (17.8%). The species richness is lower in D1 (v=32; b=12; l=9) than in D2 (v=32; b=18; l=18).

Low to tall shrub tundra (E) cluster is characterized by the dominance or co-dominance of different shrubs species (*Betula nana, Salix pulchra*) with a moss-rich understorey and it comprises three vegetation communities.

The first community (E1) is dominated by the shrubs *Betula nana* (53.6%) with a frequent occurrence of *Vaccinium vitis-idaea* (7.7%) and a significant mosses cover, mainly composed by *Hylocomium splendens* (52.6%) and *Aulacomnium turgidum* (12.7%). The second (E2) is co-dominated by the shrubs *Betula nana* (47.8%) and *Salix pulchra* (23.4%), with dense mosses cover mainly composed by *Hylocomium splendens* only (60.1%). The third is a tall shrub community (E3) dominated by *Salix pulchra* (75.5%), with frequent and relatively abundant *Carex bigelowii* 15.2%) in the herbaceous strata and with a significant mosses cover, composed by *Hylocomium splendens* (47.4%). The species richness reaches one of the highest values in E1 (tot=75; v=40; b=18; l=17), with a decreasing trend in E2 (tot=48; v=23; b=15; l=10) and E3 (tot=40; v=23; b=10; l=7).

Tussock and shrubby tussock tundra (F) cluster includes two plant communities characterized by tussock species (*Eriophorum vaginatum*), with other graminoids (*Carex bigelowii*) and shrub species (*Betula nana,Vaccinium uliginosum, Salix pulchra, Rhododendon tomentosum*), and by a moss-rich understory, that is shared also with cluster E.

The tussock tundra (F1) is dominated by *Eriophorum vaginatum* (66.8%), with a relatively low abundance of *Betula nana* (17.1%) and *Salix pulchra* (7.7%) and a discontinuous mosses cover mainly composed by *Hylocomium splendes* (36.7%) and *Aulacomnium turgidum* (16.4%). In the shrubby tussock tundra (F2) the abundances of shrubs species such as *Betula nana* (22.6%), *Salix pulchra* (13.7%), *Vaccinium uliginosum* (9.9%) increase, while *Eriophorum vaginatum* decreases in cover (21.1%), compared to F1. The moss-rich understory is still composed by *Hylocomium splendes* (45.2%) and *Aulacomnium turgidum* (17.6%). The species richness is relatively high for both F1 (v=25; b=15; l=13) and F2 (v=31; b=16; l=13).

Wet tussock sedge tundra (G) cluster is characterized by the dominance of mosses of *Sphagnum* species and by the occurrence of non-dominant vascular species such *Rubus chamaemorus* and *Andromeda polifolia*. This cluster comprises two vegetation communities, which differ according to the relative abundances of the target species *Carex bigelowii* and *Betula nana*. The two plant communities G1 and G2 share a thick moss layer dominated by *Sphagnum warnstorfii* (32.2% and 32.0%, respectively) and *Sphagnum angustifolium* (28.6% and 20.0%, respectively) but differ in vascular species composition and shrubs cover. Indeed, if *Andromeda polifolia* (4.4%) is more common in G1, while *Rubus chamaemorus* (6.0%), *Carex bigelowii* (35.4%)

and *Betula nana* (23.8%) increase in G2, allowing to differentiate the two vegetation communities. The species' richness is relatively high for G1 (v=35; b=13; l=6) and high for G2 (v=41; b=18; l=16).

Wetland cluster (H) refers to sites with shallow standing of flowing water, and it includes three communities which differ by the dominance or co-dominance of the target vascular species and by the abundance and composition of the mosses understory. The first vegetation community (H1) is dominated by *Carex aquatilis* (33.6%) with a rich moss understory mainly composed by *Sphagnum warnstorfii* (43.6%). Other diagnostic species, although not abundant, are the low shrubs *Salix chamissonis* (5.0%), *Andromeda polifolia* (3.1%) and *Vaccinium oxycoccos* (0.9%) and the forb *Pedicularis labradorica* (0.3%). The second vegetation community (H2) is dominated by *Carex aquatilis* (60.3%) with a lower moss coverage than H1, mainly composed by *Tomentypnum nitens* (19.8%). In the third vegetation community (H3), the diagnostic and dominant species is the sedge *Eriophorum angustifolium* (59.1%), which replaces *Carex aquatilis* (3.6%), with locally abundant species such as *Carex membranacea* (14.4%) and *Drepanocladus brevifolius* (28.6%). Frequent species are also *Polygonum viviparum* and *Pedicularis sudetica*. The species richness is low in all these three communities, with a decreasing trend from H1 (v=23; b=11; l=4), H2 (v=20; b=8; l=0) and H3 (v=15; b=8; l=2).

Ponds (I) are characterized only by mosses cover of *Leptodictyum riparium* (100%), occurring in temporary water bodies within wetland during the peak of summer season.

To assess the ecological relevance of these communities, a second PCA (PCA-communities) was performed, comparing the 19 vegetation communities identified in our study site (A1 to I) with 28 communities selected from those described by Boggs et al (2018) for Alaska (Fig. 2). This analysis revealed the same clusters of target species (Fig. 1c, d) as those found in the previous PCA of the 349 relevés (PCA-relevés, Fig. 1a, b, Table 1). The consistency between the two PCA results (Fig. 1a-d, Table 1), confirmed the classification of the 19 vegetation communities and supported their attribution to the main syntaxa previously described for Alaska. Moreover, the comparison with synoptic tables other than Boggs et al (2018) allowed to better locate some of the vegetation communities within the syntaxonomical framework of Alaska and Arctic regions available in literature.

The dwarf shrub tundra communities A1 correspond to *Cassiope tetragona–Dryas integrifolia* and *Dryas integrifolia–Salix reticulata* communities described by Komarkova and Webber (1978, 1980), Walker et al. (1994), and Boggs et al. (2018), which are characterized by hemi-prostrate dwarf shrubs and fruticose lichens in subxeric to mesic, non-acidic conditions (Walker and Maier, 2008). The dwarf shrub tundra A2 fits with *Selaginello sibiricae–Dryadetum*

octopetalae, Dryas octopetala–Hierochloe alpina and *Dryas octopetala- Salix phlebophylla* described by Walker et al. (1994), Jorgenson et al. (2009) and Boggs et al. (2018), respectively, representative of prostrate dwarf-shrub tundra on xeric to acidic sites (Walker and Maier, 2008). *Dry heath tundra* communities (B1–B2) correspond to *Loiseleuria procumbens–Cladonia* (B1) and *Arctostaphylos alpina–Vaccinium vitis-idaea* (B2), described by Hanson et al. (1953). The *dry heath tundra* B3 and C show a strong affinity with *Vaccinium uliginosum–Vaccinium vitis-idaea* and *Betula nana exilis–Vaccinium uliginosum* communities, respectively, described by Hettinger and Janz (1974), representative of hemi-prostrate dwarf-shrub, fruticose lichen tundra, of subxeric to mesic and acidic sites (Walker and Maier, 2008).

The *moist sedge tundra* (D1) had similarity with the *Carex lugens–Salix reticulata* community described by Boggs et al. (2018), whereas the *moist sedge with low shrub* tundra (D2) corresponds to *Carex bigelowii–Betula nana–Salix planifolia–Ledum decumbens–Vaccinium spp.* described by Viereck et al. (1992) and *Betula nana–Carex bigelowii* reported by Boggs et al. (2018).

The low to tall shrub community (E1) corresponds to *Betula nana-Rhododendron tomentosum* (Birch ericaceous low shrub) and *Hierochloë alpina-Betula nana*, described by Boggs et al. (2018) and Walker et al., (1994), respectively. E2 community had similarity with *Betula nana-Salix planifolia-Vaccinium uliginosum* (Craighead et al. 1988) and *Betula nana-Rhododendron tomentosum* (Boggs et al., 2018). The third community of low to tall shrub (E3) fits with *Betula nana–Salix planifolia ssp. pulchra– Eriophorum,* described by Jorgenson et al., 2009, and *Salix pulchra-Hylocomium* (Boggs et al., 2018).

The tussock tundra (F1) and shrubby tussock tundra (F2) correspond to *Betula nana–Eriophorum vaginatum* and *Salix pulchra–Hylocomium* types, respectively (Boggs et al., 2018).

The wet tussock sedge tundra (G1) is consistent with *Sphagno–Eriophoretum vaginati* (Walker et al., 1994) and partially with *Salix pulchra-Eriophorum vaginatum* (Boggs et al., 2018). G2 has affinity with *Carex aquatilis-Eriophorum spp./Sphagnum spp*., described by Boggs et al. (2018).

Finally,the wetland community H1 is best aligned with the *Carex aquatilis–Salix planifolia ssp. pulchra* association reported by Jorgenson et al. (2009), while H2 and H3 correspond to *Carex aquatilis–Sphagnum* and *Eriophorum angustifolium–Carex spp.* (Boggs et al., 2018).

This validation enabled the completion of the phytosociological map (Fig. 2a).

The phytosociological map confirmed that the vegetation of the study area represents a heterogeneous tundra landascape, and that the spatial distribution is primarily driven by topographic and moisture gradient (Fig. 2a). The eastern side of the map consists of nearly flat

terrain dominated by moist tussock and sedge communities. In contrast, dry dwarf tundra and dry heath tundra communities are mostly found on small hilltops and elevated sites, while wetland communities are primarily located in the low-lying, depressed areas in the western side of the map (Fig. 2a). Low to tall shrubs occur both in flat terrain as well as on gentle slopes, with *Betula nana*-dominated shrublands being more common in the flat areas and *Salix pulchra*-dominated shrublands more frequent on sloped terrain (Fig. 2a).

Five vegetation communities accounted for more than 65% of the total surface area of the study site. These are the moist sedge tundra with shrubs, dominated by *Carex bigelowii*, and as co-dominants by *Betula nana* and *Ericaceae* (D2), which covered 17% of the area; the tussock and shrubby tussock tundra dominated by *Eriophorum vaginatum* (F1, F2), covering 15% and 13% respectively; the low to tall shrub tundra dominated by *Betula nana* (E1) covering 13%; and the wetland dominated by *Carex aquatilis* (H2), which occupied 10%. All other communities each covered less than 5% of the study area (Table 2).

3.2 Physiognomic map

The mean shrub height of the 19 vegetation communities (Fig. 2SM, 3SM) supported their classification into to eight physiognomic classes, encompassing a total of eleven sub-classes (Table 2), and contributed to the finalization of the physiognomic map (Fig. 2B).

Moist sedge with low shrubs and low to tall shrub communities, were the most abundant physiognomic classes, with an extent of 17.3% and 17.6% of the study area, respectively. These two classes were also characterized by the tallest shrub species, with average shrub heights between 12.0 to 22.4 cm. The highest values were recorded in low to tall shrub communities, particularly in E3 (22.4 cm) and E2 (18.7 cm). Wetlands covered 16.6% of the area and showed shrub heights between 11.3 and 15.4 cm, while tussock tundra (15%) and shrubby tussock tundra (13.4%) had intermediate shrub heights of 11.2 and 12.3 cm, respectively. Dry heath tundra (10.2%) had smaller shrubs, averaging between 5.3 and 13.7 cm, and wet tussock sedge tundra (7.8%) showed similar values (10.7–13.8 cm). The remaining communities, including moist sedge tundra (0.8 cm), dwarf shrub tundra (0.1–1.1 cm), and ponds (0.1 cm), contributed marginally to the total area (0.1–1%) and were characterized by very low or absent shrub cover. Among the species measured, *Salix pulchra* and *Betula nana* were identified as the tallest shrubs, however, their height varied considerably across different community types (Fig. 4SM). Tall shrubs reached heights of up to 80 cm, with *Betula nana* ranging from 2 to 75cm and *Salix pulchra* from 3-80 cm. In contrast, low shrubs were significantly shorter, with *Rhododendron tomentosum* ranging from 2 to 20 cm and *Vaccinium uliginosum* from 2 to 25 cm.

Table 1. Floristic composition, mean species cover (%) and mean height of the eleven vegetation communities (A1 to I) identified by the two PCAs (Figs. 1, 2). Bright yellow background = target species characteristics of each community. Light yellow background = target species preferential for multiple groups. Black = vascular plants (v); blue = mosses (m); red = lichens (l).

	Species	Acronym	PCA group	A1	A2	B1	B2	B3	C	D1	D2	E1	E2	E3	F1	F2	G1	G2	H1	H2	H3	I
v	*Cassiope tetragona*	Cass.tet	A	11.7	.	4.8	1.2	0.9	0.2	6.9	.	0.3	.	0.2	1.6	0.6	3.6	1.2	.	.	.	.
v	*Dryas integrifolia*	Dry.inte	A	11.0	.	.	.	.	.	1.3	.	.	.	.	.	.	0.7	.	.	.	.	.
v	*Salix reticulata*	Sal.ret	A;D	11.8	.	0.8	0.03	0.4	0.2	23.3	0.3	0.04	0.1	3.7	0.3	2.0	0.6	0.2	.	.	.	.
v	*Dryas octopetala*	Dry.oct	A	2.0	40.7	1.0	5.1	.	0.7	0.1	.	.	0.1	.	.	.	.	0.1	.	.	.	.
v	*Salix phlebophylla*	Sal.phleb	A	0.7	4.2	.	0.2	0.1	.	.	.	0.0	.	.	.	.	.	.	.	.	.	.
l	*Pertusaria dactylina*	Pertus.dact	A	6.0	9.2	7.2	2.2	0.5	0.2	.	0.0	0.0	.	.	.	.	.	.	.	.	.	.
l	*Thamnolia subuliformis*	Thamn.subul	A	3.0	1.3	1.7	0.5	0.9	0.6	0.1	0.4	0.1	.	.	0.3	0.2	0.2	0.2	.	.	.	.
l	*Flavocetraria nivalis*	Flavoc.niv	A:B	.	2.2	1.2	0.5	.	.	0.3	0.1	0.04	.	0.1	0.01	.	0.4	0.1	.	.	.	.
v	*Kalmia procumbens*	Kalm.proc	B	.	.	34.6	2.8	.	.	0.3	.	.	.	.	.	.	.	.	.	.	.	.
l	*Stereocaulon alpinum*	Stereo.alp	B	.	0.2	10.3	1.2	2.5	0.8	0.3	.	0.4	.	.	0.00	.	.	.	.	.	.	.
l	*Masonhalea richardsonii*	Masol.rich	B	0.3	0.1	4.6	0.6	4.5	1.9	0.3	0.8	0.9	0.2	0.1	0.2	0.5	.	0.2	.	.	.	.
l	*Sphaerophorus globosus*	Sphaerob.glob	B	0.3	0.2	3.3	0.6	1.0	.	0.4	.	0.1	.	.	.	.	.	.	.	.	.	.
l	*Peltigera malacea*	Peltig.mal	B	0.3	1.0	1.1	0.5	0.8	0.0	.	0.1	0.5	.	.	0.1	0.2	.	0.3	.	.	.	.
l	*Cetraria cucullata*	Cetr.cuc	B	3.3	3.8	13.2	6.1	10.1	3.1	2.1	4.4	3.0	1.2	0.2	2.7	2.9	1.8	0.7	0.1	.	.	.
v	*Arctostaphylos alpina*	Arct.alp	B	.	5.0	4.4	27.5	.	2.9	.	0.7	1.8	.	.	0.0	0.1	.	0.5	.	.	.	.
v	*Empetrum nigrum*	Emp.nig	B	.	0.8	11.2	18.7	10.7	5.8	.	6.3	6.2	4.3	17.0	7.5	3.4	2.3	4.6	.	.	.	.
l	*Cladina rangiferina*	Cladi.rang	B	0.3	.	2.8	2.2	29.5	10.5	3.0	8.3	4.8	0.6	0.5	3.0	4.6	0.4	1.2	0.1	.	0.1	.
l	*Cladonia gracilis*	Clad.graci	B	.	.	.	0.1	3.0	0.2	.	0.3	0.3	0.2	.	0.5	1.2	.	0.8	.	.	.	.
m	*Racomitrium lanuginosum*	Racom.lag	B	.	.	.	1.9	14.1	1.2	.	1.8	0.1	0.1	.	.	0.7	.	.	0.1	.	.	.
m	*Polytrichum strictum*	Poly.strict	B	0.7	0.4	0.1	2.1	5.8	0.3	0.1	0.6	1.2	1.4	8.0	1.2	0.2	1.2	0.6	.	.	.	.
m	*Dicranum spadiceum*	Dicra.spad	B	8.3	.	10.3	4.9	9.4	8.3	10.5	1.8	1.2	1.1	2.5	1.3	3.7	7.7	0.4	2.1	5.0	.	.
m	*Dicranum elongatum*	Dicra.elon	B	.	0.7	.	4.3	11.4	5.7	6.3	5.6	1.4	.	.	10.1	2.7	.	1.0	.	.	8.6	.
v	*Vaccinium vitis-idaea*	Vac.vitid	B;C	.	6.3	1.0	22.0	9.3	10.5	1.0	14.0	7.7	6.0	3.2	10.6	8.3	0.6	2.2	.	.	.	.
v	*Vaccinium uliginosum*	Vac.uli	B;C	1.8	0.8	14.4	7.4	12.8	20.6	1.5	4.8	8.1	10.3	14.0	6.7	9.9	10.3	8.7	0.3	1.0	0.2	.
m	*Rhytidium rugosum*	Rhyt.rug	C	26.7	12.3	3.2	3.1	.	26.8	.	4.4	7.8	2.7	0.2	1.9	4.4	1.5	1.5	.	.	.	.

v	*Bistorta officinalis*	Bis.off	C	1.7	0.1	1.4	0.1	1.3	1.3	1.6	2.0	1.6	0.6	4.6	0.8	1.4	0.1	0.4	.	0.1	.	.
l	*Dactylina arctica*	Dactyl.arct	C	0.1	0.4	0.01	0.1	0.9	0.5	0.4	0.4	0.7	0.2	0.04	0.5	1.1	.	0.2	.	.	.	.
v	*Carex bigelowii*	Car.big	D	4.7	0.6	7.3	2.4	9.2	4.7	48.1	34.7	4.4	12.3	15.2	5.6	9.0	5.5	35.4	10.0	0.1	.	.
v	*Rhododendon tomentosum*	Rhod.tom	D	.	.	0.9	4.0	7.8	7.1	1.8	19.7	6.9	8.2	2.8	9.9	6.4	0.4	2.2	0.4	.	0.04	.
l	*Cetraria islandica*	Cetr.isl	D	1.0	.	0.1	0.1	0.2	.	0.6	0.1	0.2	0.1	0.3	0.3	0.4	0.5	0.1	0.3	.	.	.
v	*Betula nana*	Bet.nan	E	.	0.6	1.3	3.1	2.8	38.9	1.6	23.5	53.6	47.8	12.8	17.1	22.6	10.0	23.8	16.8	1.4	6.0	.
v	*Salix pulchra*	Sal.pulcr	E	.	.	.	0.1	0.5	4.9	0.4	6.7	4.0	23.4	75.5	7.7	13.7	4.7	8.6	0.8	1.3	0.7	.
m	*Aulacomnium turgidum*	Aulac.tur	E	.	.	.	0.7	10.5	17.3	.	17.8	12.7	8.7	1.3	16.4	17.6	2.2	9.7	2.1	.	0.3	.
m	*Hylocomium splendens*	Hylo.splen	E	.	.	1.3	0.5	2.8	15.2	5.6	40.1	52.6	60.1	47.4	36.7	45.2	9.2	10.9	9.3	2.1	0.7	.
v	*Eriophorum vaginatum*	Eri.vag	F	.	0.1	0.1	0.2	1.6	1.3	.	3.4	2.5	2.7	0.2	66.8	21.1	7.9	5.3	1.4	1.3	2.3	.
v	*Pedicularis lapponica*	Pedic.lap	F	.	.	.	0.0	0.1	0.0	.	0.1	0.1	0.1	0.0	0.4	0.2	0.1	0.2	0.2	.	.	.
v	*Rubus chamaemorus*	Rub.cham	G	.	.	.	0.0	.	0.2	1.0	0.4	0.9	0.8	0.5	1.2	3.1	1.5	6.0	0.4	0.0	.	.
v	*Andromeda polifolia*	Andr.poly	G	0.7	.	0.3	0.2	.	0.0	0.6	0.4	0.4	2.4	0.1	2.8	1.8	4.4	3.9	3.1	2.5	4.2	.
m	*Sphagnum warnstorfii*	Spha.warn	G	8.3	.	.	.	.	.	0.5	2.2	0.7	4.7	8.1	6.0	4.9	32.2	32.0	43.6	1.5	3.0	.
m	*Sphagnum angustifolium*	Spha.angu	G	.	.	.	.	.	.	.	1.7	0.9	5.2	10.6	5.8	1.4	28.6	20.0	11.4	0.8	.	.
v	*Salix chamissonis*	Sal.cham	H	.	.	.	.	.	0.4	1.3	0.1	0.0	0.1	.	0.0	0.1	0.2	0.4	5.0	2.3	0.3	.
v	*Vaccinium oxycoccos*	Vac.oxyc	H	.	.	.	.	.	.	.	0.00	0.1	.	.	0.5	0.3	0.5	0.9	0.9	.	.	.
v	*Carex aquatilis*	Car.aquat	H	.	.	.	.	.	0.1	.	0.2	0.4	1.5	.	.	.	2.9	0.7	33.6	60.3	3.6	.
m	*Tomentypnum nitens*	Toment.nit	H	5.0	.	.	0.6	.	0.2	3.1	0.4	1.9	0.3	.	.	0.1	1.2	2.5	.	19.8	0.7	.
v	*Eriophorum angustifolium*	Eri.angus	H	.	.	.	.	0.4	.	.	.	0.5	.	.	.	0.4	5.5	0.8	2.9	4.8	59.1	.
v	*Carex membranacea*	Car.membr	H	.	.	.	0.1	.	.	.	.	.	.	.	.	.	0.5	.	0.7	1.2	14.4	.
v	*Pedicularis labradorica*	Pedic.labr	H	.	.	.	.	0.02	0.1	.	0.1	0.01	.	0.1	0.1	0.01	0.04	0.1	0.3	.	.	.
v	*Carex rariflora var. rariflora*	Car.rarif	H	.	0.02	.	0.01	0.4	0.8	0.1	.	.	.	.	.	.	3.5	1.1	2.1	4.3	2.1	.
m	*Leptodictyum riparium*	Leptod.rip	I	.	.	.	.	.	.	.	0.1	.	.	.	0.3	0.1	.	.	1.4	.	.	100.0
v	*Polygonum viviparum*	Poly.viv	other	0.3	.	0.2	0.03	.	0.3	0.3	0.0	0.02	.	.	.	.	0.00	0.1	.	0.2	0.2	.
v	*Poa arctica*	Poa.arct	other	.	0.2	.	0.1	.	0.3	.	0.1	0.6	.	7.7	0.00	.	0.4	.	.	0.0	.	.
v	*Salix glauca*	Sal.glau	other	.	.	.	.	.	1.7	.	1.0	0.4	.	.	.	.	.	.	.	0.2	.	.
v	*Calamagrostis inexpansa*	Calam.inex	other	0.7	.	.	0.1	.	.	.	.	0.01	.	.	.	3.6	.	.	.	.	.	.
Mean shrub height (cm)				4.3	2.8	5.3	6.9	6.3	13.7	8.2	12.0	17.6	18.7	22.4	11.2	12.3	10.7	13.8	15.4	11.3	13.1	0

Table 2. Overall extent in the year 2024 (expressed in ha and in % on the total study area) of each main vegetation community and corresponding physiognomic class (PCAs Figs. 1,2, Tables 1, 1SM).

PCA group	Physiognomic classes of PCA	Area (ha)	Area (%)	Physiognomic classes	Area (ha)	Area (%)
A1	Dwarf shrub tundra - Moist snowbed	0.02	0.1	Dwarf shrub tundra - Moist snowbed	0.02	0.1
A2	Dwarf shrub tundra - Dry exposed tundra	0.15	1.1	Dwarf shrub tundra - Dry exposed tundra	0.15	1.1
B1	Dry heath tundra	0.11	0.8	Dry heath tundra	1.37	10.2
B2	Dry heath tundra	0.31	2.3			
B3	Dry heath tundra	0.23	1.7			
C	Dry heath tundra	0.72	5.4			
D1	Moist sedge tundra	0.11	0.8	Moist sedge tundra	0.11	0.8
D2	Moist sedge with low shrub	2.32	17.3	Moist sedge with low shrub	2.32	17.3
E1	Low to tall shrub	1.75	13.1	Low to tall shrub	2.46	17.6
E2	Low to tall shrub	0.55	4.1			
E3	Low to tall shrub	0.05	0.4			
F1	Tussock tundra	2.01	15	Tussock tundra	2.01	15
F2	Shrubby tussock	1.79	13.4	Shrubby tussock tundra	1.78	13.4
G1	Wet tussock sedge tundra	0.28	2.1	Wet tussock sedge tundra	0.94	7.8
G2	Wet tussock sedge tundra	0.76	5.7			
H1	Wetland	0.27	2	Wetland	2.22	16.6
H2	Wetland	1.4	10.5			
H3	Wetland	0.55	4.1			
I	Pond	0.01	0.1	Pond	0.01	0.1
total	total	13.39	100		13.39	100

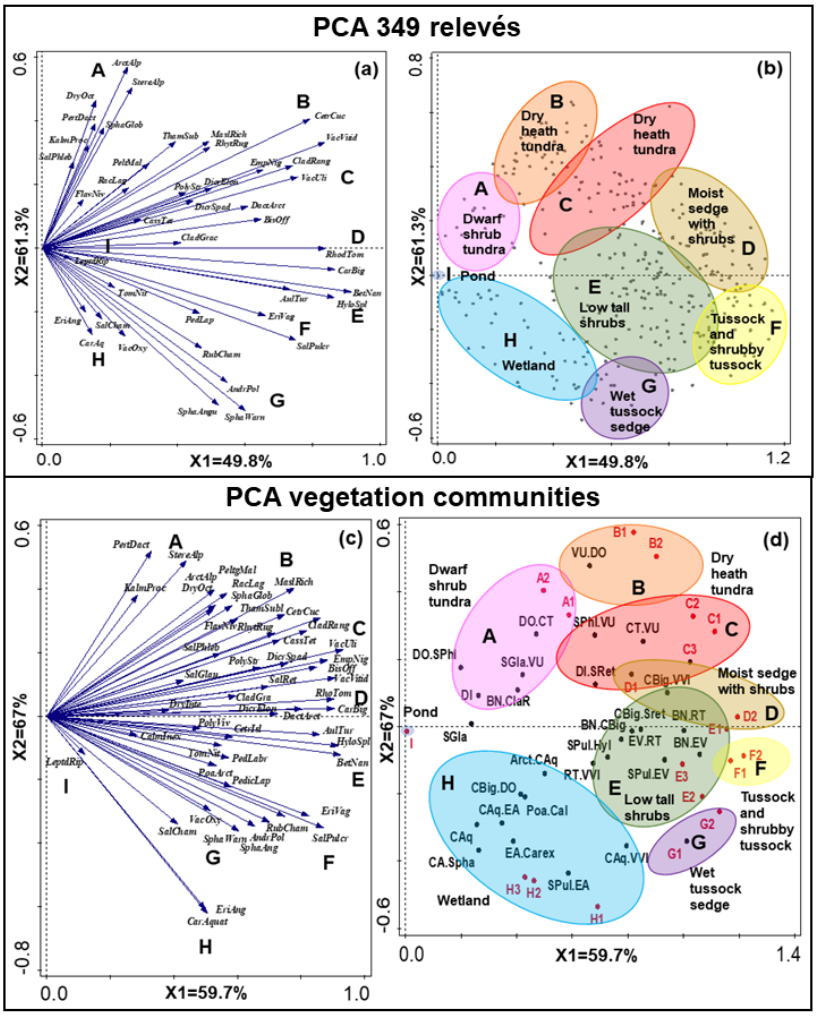

Figure 1. Multivariate analyses with: a, b) the first PCA (Principal Component Analysis) performed on the 349 phytosociological relevés of the study area explaining 61.3% of the cumulative variance: (with a) species diagram with species' clusters (A-I) and b) relevés diagram with relevés' clusters (A-I) and main physiognomic classes associated); c,d) the second PCA performed using the 19 vegetation communities (A1 to I) obtained by the first PCA (a,b) and for comparison, a selection of the main vegetation communities of Alaska as in Boggs et al., (2018) (black dots and community names) (with c) species diagram with species' clusters (A-I); d) vegetation communities' diagram with clusters of main communities (A-I) and main physiognomic classes. Legend: arrows: species; circles: relevés (b) or vegetation communities (d). Physiognomic classes associated to the main species-relevés' clusters: A = Dwarf shrub tundra; B = Dry heath tundra; C = Dry heath tundra; D = Moist sedge with shrub; E = Low to tall shrub; F = Tussock and shrubby tussock; G = Wet tussock sedge; H = Wetland; I = Pond. Species' name abbreviations: the full names of the species are given in Table 1. Legend of the communities selected from Boggs et al (2018): Do.SPhl = *Dryas octopetala-Salix phlebophylla*; BN.ClaR = *Betula nana-Cladina rangiferina*; DI = *Dryas integrifolia*; SGla.VU = *Salix glauca-Vaccinium uliginosum*; DO.CT = *Dryas octopetala-Cassiope tetragona*; VU.DO = *Vaccinium uliginosum-Dryas octopetala*; SPhl.VU = *Salix phlebophylla-Vaccinium uliginosum*; CT.VU = *Cassiope tetragona-Vaccinium uliginosum*; DI.SRet = *Dryas integrifolia-Salix reticulata*; CBig.VVI = *Carex bigelowii- Vaccinium vitis idaea*; CBig.SRet = *Carex bigelowii-Salix reticulata*; BN.CBig = *Betula nana-Carex bigelowii*; BN.RT = *Betula nana-Rhododendron tomentosum*; BN.EV = *Betula nana-Eriophorum vaginatum*; EV.RT = *Eriophorum vaginatum-Rhododendron tomentosum*; SPul.Hyl =*Salix pulchra-Hylocomium splendens*; SPul.EV = *Salix pulchra-Eriophorum vaginatum*; RT.VVI = *Rhododendron tomentosum -Vaccinium vitis-idaea*; CAq.VVI = *Carex aquatilis - Vaccinium vitis idaea*; SPul.EA = *Salix pulchra-Eriophorum angustifolium*; EA.Carex = *Eriophorum angustifolium-Carex* spp. ; CA.Spha = *Carex aquatilis-Sphagnum* spp.; CAq = *Carex aquatilis*; CAq.EA = *Carex aquatilis-Eriophorum angustifolium*; Poa.Cal = *Poa arctica-Calamagrostis stricta ssp. inexpansa*; CBig.DO = *Carex bigelowii-Dryas octopetala*; Arct.CAq = *Arctosptaphylos alpinus-Carex aquatilis*; SGla = *Salix glauca*.

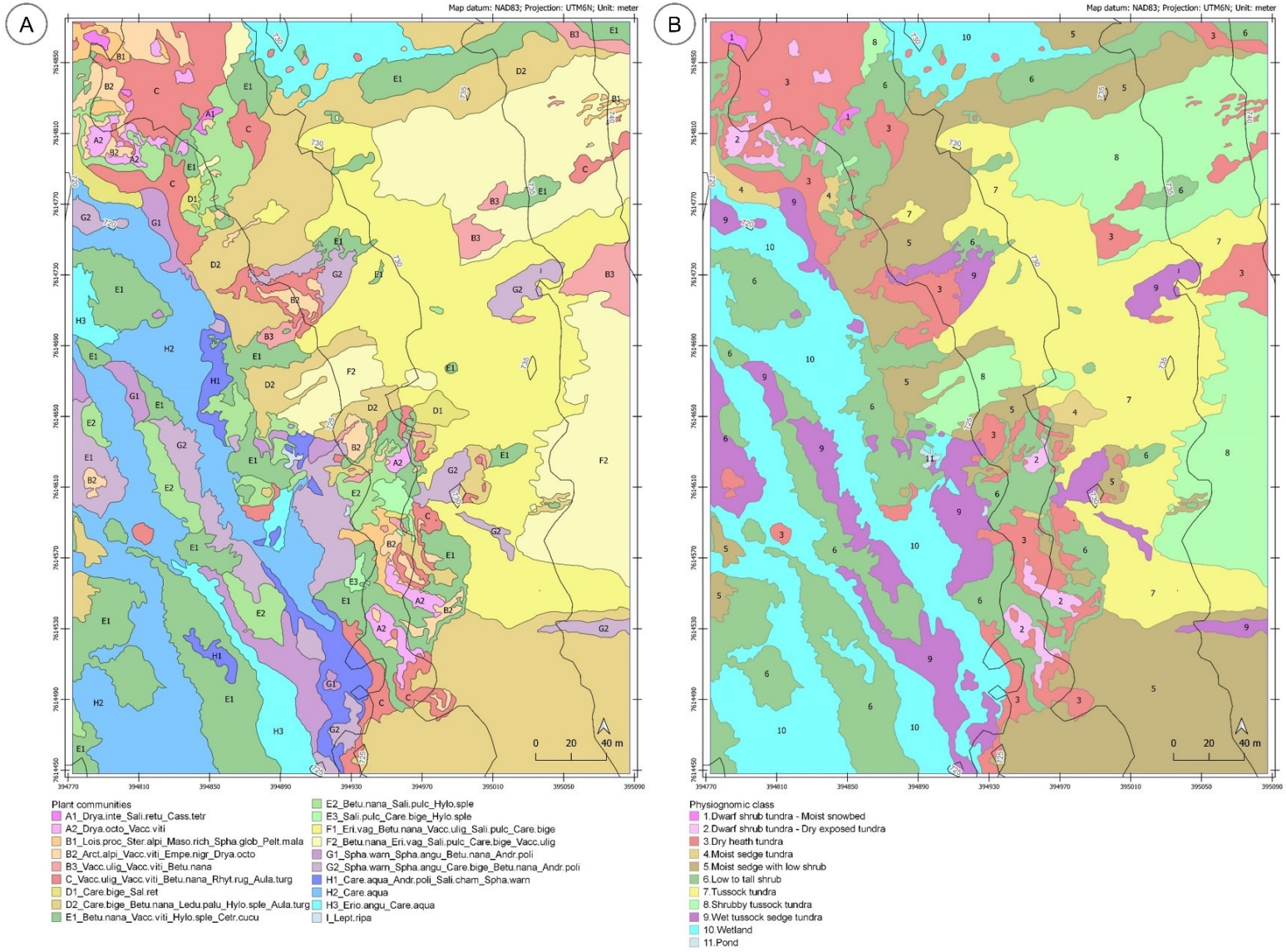

Figure 2. A) Phytosociological map of the study area provided by the multivariate analyses (PCAs Figs. 1, 2); B) Physiognomic map of the study area obtained according to the results of the PCAs (Figs. 1)

4. Discussion

High-resolution vegetation mapping provides all the information mandatory for the assessment and monitoring of the natural variability and responses of the heterogeneous Arctic tundra to climatic and environmental changes (Greaves et al., 2019). The possibility to detect and quantify small-scale changes in vegetation distribution and composition is particularly relevant in the context of rapid climate warming, which is already affecting species distribution, phenological patterns and community structure (Linderholm, 2006; Bertin et al., 2008; Richardson et al., 2013; Liu et al., 2018; Antão et al., 2022).

Our data show that the drone ortho-imagery used as a base for the field mapping combined with the detailed vegetation characterization through the phytosociological survey is a reliable and well applicable method to achieve a high-resolution vegetation mapping providing three kind of products: a) high resolution phytosociological map, b) derived high resolution physiognomic map, c) detailed data on vegetation floristic composition, cover, species richness, growth form, traits, community type of each mapped polygon.

The approach proposed here is highly suitable for many Arctic sites characterized by almost flat topography and/or very homogeneous geomorphological conditions without well recognizable features, but with vegetation mosaics following micro scale topographic and edaphic gradients.

Together, these products provide a robust ecological baseline for monitoring future vegetation changes in tundra ecosystems.

In this study area, we identified 19 distinct vegetation communities, which reflect the environmental gradients of moisture, topography, and soil conditions, with dry heath tundra on elevated and exposed sites, tussock and moist sedge tundra in nearly flat areas, and wetlands in depressions. The five main communities covering the area are characterized by *Carex bigelowii*, *Eriophorum vaginatum, Carex aquatilis* and dwarf shrubs as *Betula nana* and *Ericecae*,

Studies that describe the characteristics of plant communities and that contribute to monitoring the mid- to long-term changes of the ecosystems are needed to better understand the dynamics of tundra vegetation (Harris et al., 2022) and address knowledge gaps on the mechanisms driving recent and future vegetation trends (Martin et al., 2017).

The use of drone ortho-imagery as base for the field mapping allows to select the most proper scale for the efficient mapping by regulating the height and resolution of the drone flight and also to perform the flight in the best meteorological conditions avoiding some inconveniences related to the occurrence of clouds which could occur when using satellite derived images (Gamon et al., 2013).

These high-resolution datasets are important for assessing ecosystem responses to climate change, supporting ecological modelling, and guiding future experimental and multidisciplinary studies in tundra ecosystems (Berner et al., 2024; Virkkala et al., 2024; Orndhal et al., 2025).

5. Conclusion

This study shows that combining drone-based ortho-imagery with phytosociological surveys is an effective method for producing high-resolution vegetation maps in Arctic tundra ecosystems. The resulting datasets provides a robust baseline for monitoring future vegetation dynamics and detecting fine-scale changes in response to climate warming. The 19 vegetation communities identified reflect strong environmental gradients of moisture, topography, and soil conditions, mainly represented by moist sedge with low shrub, tussock tundra and wetland.

These patterns highlights the importance of micro-environmental gradients in determining community distribution and provides essential data to detect responses of Arctic ecosystems to climatic changes. High-resolution maps can be used for ecosystem process assessments, carbon dynamics modelling, and experimental projects that require detailed vegetation information. A shifts in vegetation composition, such as shrub expansion and the decline of mosses and lichens, can generate significant feedbacks to the climate, the availability of detailed phytosociological and physiognomic maps represents a fundamental tool for monitor, understand, and predict the ecological consequences of climate change in Arctic tundra ecosystems.

Supplementary materials

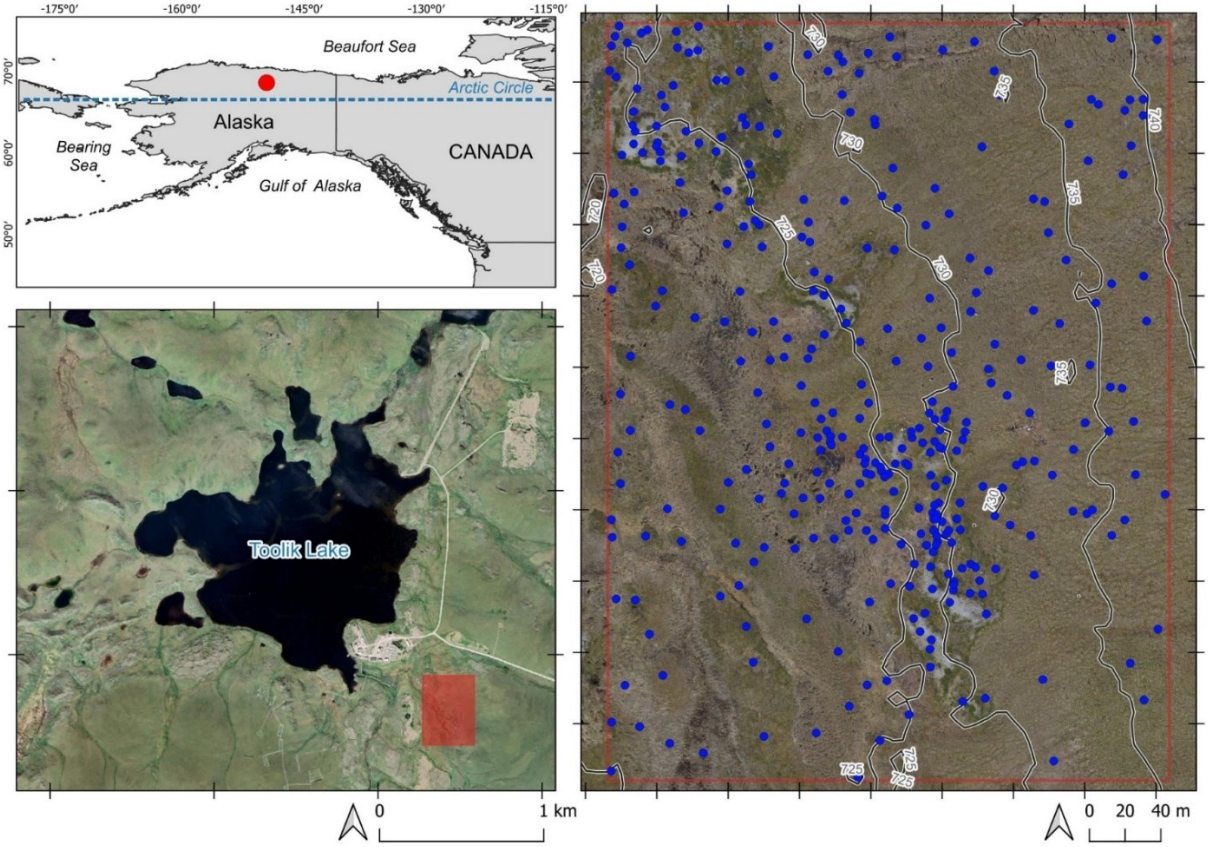

Figure 1SM. Study area reference to (a) the site location within Alaska and (b) the study area within Toolik Lake and (c) the specific location of all the vegetation relevés.

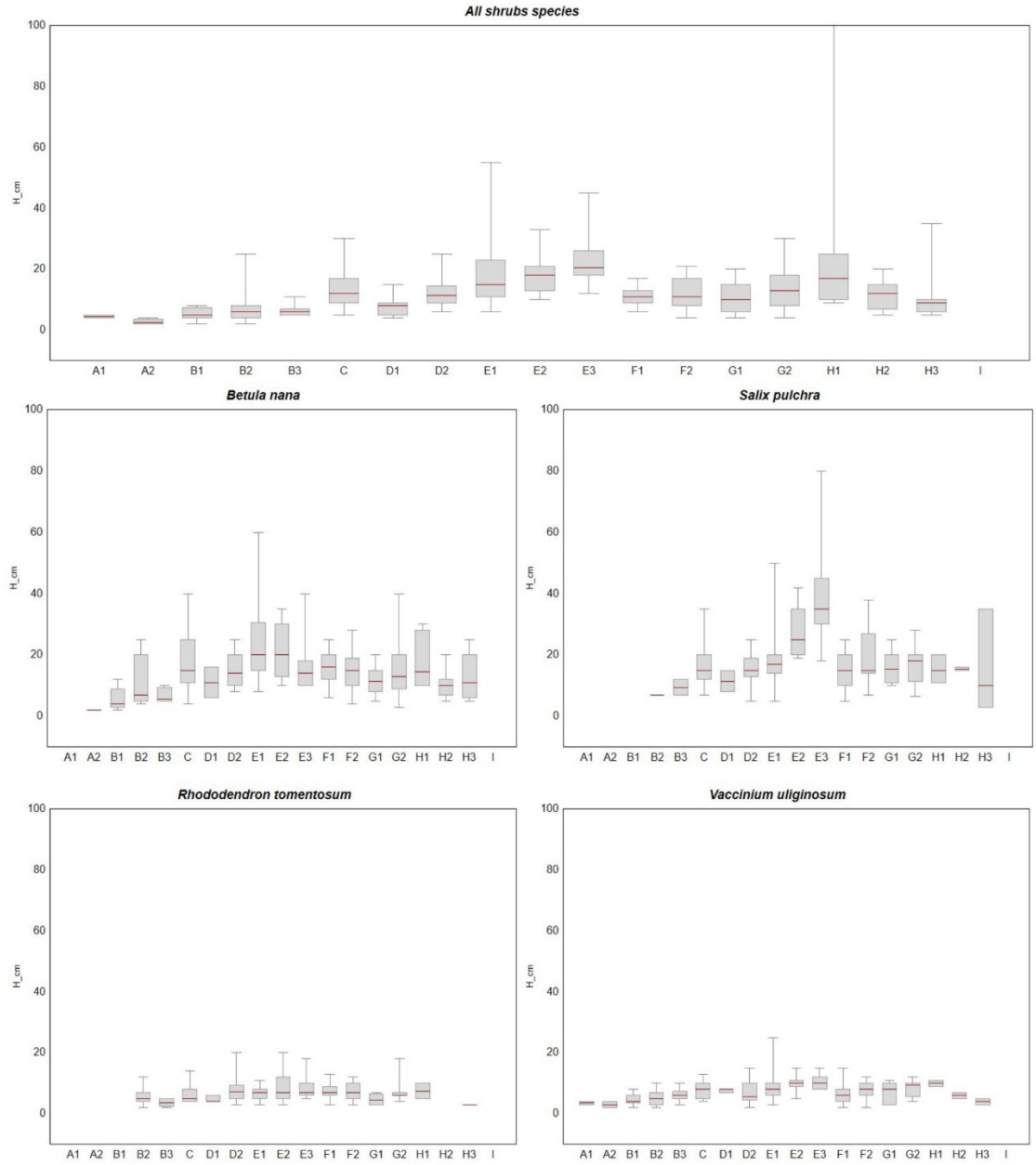

Figure 2SM. Descriptive statistics (minimum, maximum, median, 25th and 75th percentile) of the shrub height (cm), in particular: total shrub species: *Betula nana*; *Salix pulchra*; *Rhododendron tomentosum; Vaccinium uliginosum*.

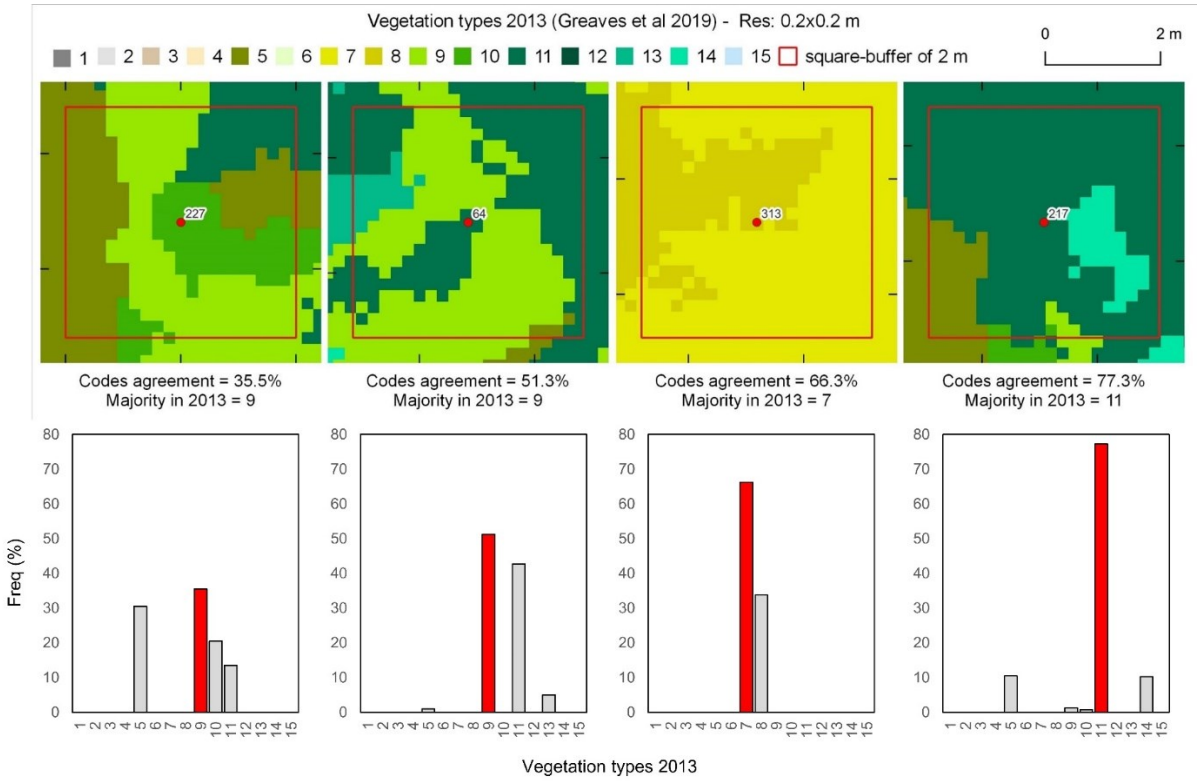

Figure 3SM. Visual example of the application of the majority method to backward assign a physiognomic class in 2013 (Greaves et al., 2019) to each of the relevé carried out in 2024, with the indication of the spatial distribution (top panels) and of the frequencies (bottom panels) of the classes. Red dot = phytosociological relevés in 2024; red frame = square-buffer of 2 m (correspondent to the GPS accuracy) applied on each of the phytosociological relevé and where the frequencies of vegetation types were accounted.

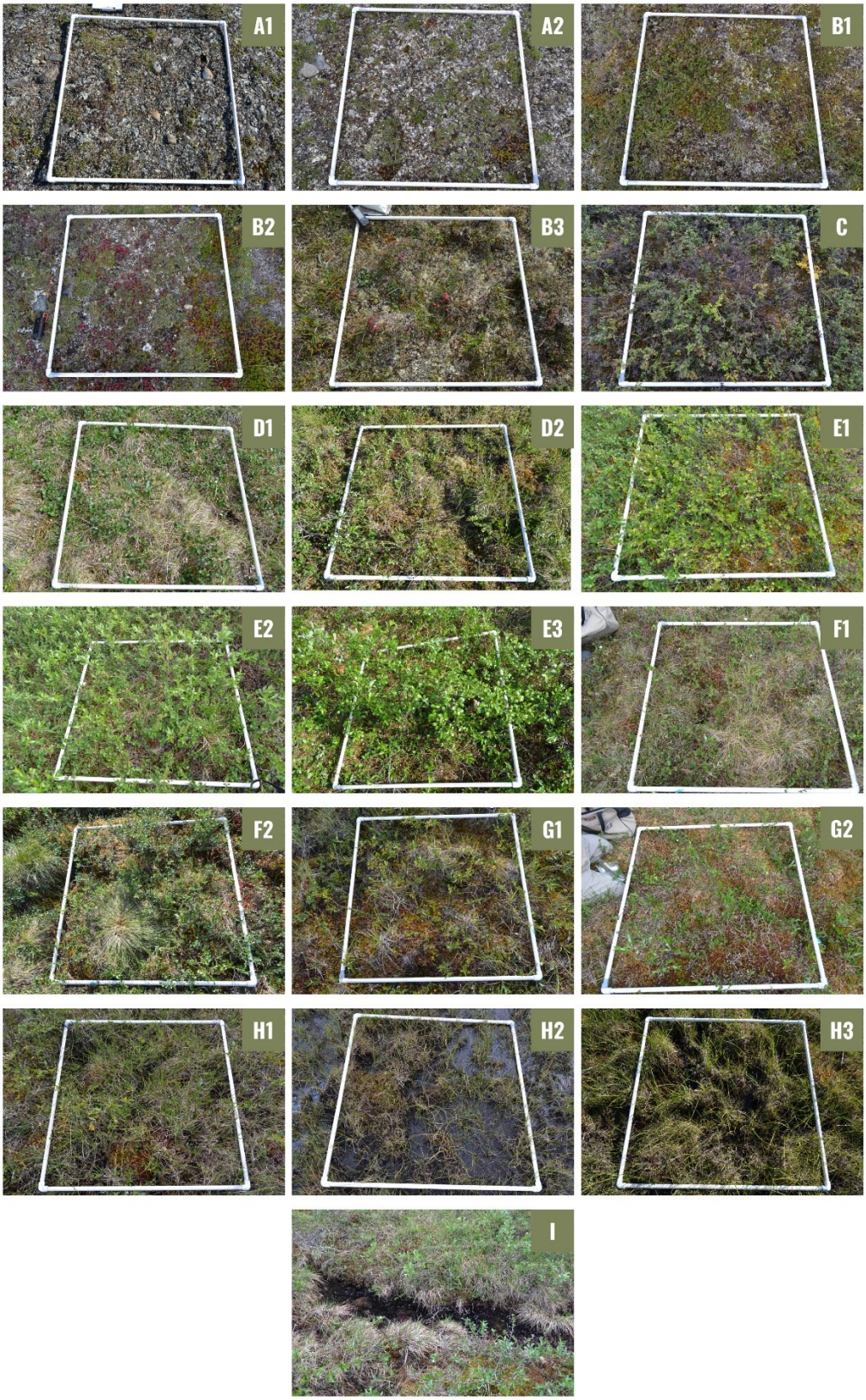

Figure 4SM. A picture of the representative plots of each community type identified by the PCA analysis (see Figs. 1, 2).

Table 1SM. Summary table of all the vegetation communities (from A1 to I, according to the PCAs' results) and physiognomic classes obtained by the PCA and associated to the available information on vegetation communities/phytosociological associations and physiognomic classes as reported by the available literature.

PCA community CODE	***Target species***	**PCA class**	**Greaves et al., 2019 Class description**	**Greaves et at., 2019 Class CODE**	***Walker & Maier, 2008 TLG Codes refered to Greaves et al., 2019***	***Walker & Maier TLG Class description***	***Walker & Maier, 2008 Class TLG CODE***	***Walker & Maier, 2008 TLG Codes refered to main species***	***Walker & Maier TLA Class description***	***Walker & Maier TLA CODE***	***Plant association/communities title from exsisting literature***	***Citation***
A1	*Dryas integrifolia, Salix reticulata, Cassiope tetragona*	Dwarf shrub tundra	Moist snowbed	6	113, 204, 205, 206, 207	Hemi-prostrate dwarf-shrub, fruticose lichen tundra. Subxeric to mesic and non acidic	17	113, 204, 205	Hemi-prostrate and prostrate dwarf shrub, forb, moss, fruticose lichen tundra	11	Cassiope tetragona-Dryas integrifolia (Komarkova and Webber 1978, 1980)	Viereck et al.,1992
											Dryas integrifolia-Cassiope tetragona	Walker et al., 1994
											Dryas integrifolia-Salix reticulata (Dwarf shrub dryas)	Boggs et al., 2018
A2	*Dryas octopetala, Vaccinium vitis-idaea*	Dwarf shrub tundra	Dry exposed tundra	3	101, 102, 103, 105	Prostrate dwarf-shrub, forbs, fruticose lichen tundra. Xerix to acidic	13	101	Prostrate dwarf shrub, fruticose lichen tundra	9	Selaginello sibiricae-Dryadetum octopetalae	Walker et al., 1994
											Dryas octopetala–Hierochloe alpina	Jorgenson et al., 2009

											Dryas octopetala-Vaccinium spp. (Jorgenson 1984, Racine and Young 1978, Talbot and others 1984)	Viereck et al.,1992
											Dryas octopetala- Salix phlebophylla	Boggs et al., 2018
B1	*Kalmia procumbens, Masonhalea richardsonii, Stereocaulon alpinum, Spaherophorus globusus, Peltigera malacea*	Dry heath tundra	Dry exposed tundra	3	101, 102	n/a	n/a	n/a	n/a	n/a	Loiseleuria procumbens-Cladonia	Hanson et al. 1953
B2	*Arctostaphylos alpinus, Vaccinium vitis-idaea, Empetrum nigrum, Dryas Octopetala*	Dry heath tundra	Dry exposed tundra	3	103, 105	Prostrate dwarf-shrub, fruticose lichen tundra	12	103	Prostrate dwarf shrub, fruticose lichen tundra	9	Salici phlebophyllae-Arctoetum alpinae	Walker et al., 1994
											Arctostaphylos alpina-Vaccinium vitis-idaea	Hanson et al. 1953
B3	*Vaccinium uliginosum, Vaccinium*	Dry heath tundra	Low dense shrub	5	110	Hemi-prostrate dwarf-shrub, fruticose lichen tundra.	18	110	Hemi-prostrate dwarf shrub,	12	Vaccinium uliginosum-Vaccinium vitis-idaea (Hettinger and Janz 1974)	Viereck et al.,1992

	vitis-idaea, Betula nana					Subxeric to mesic and acidic			fruticose lichen tundra			
C	*Vaccinium uliginosum, Vaccinium vitis-idaea, Betua nana, Aulacomnium turgidum, Hylocomium splendens, Rhytidium rugosum, Cladinia rangiferina*	Dry heath tundra	Low dense shrub	5	110	Hemi-prostrate dwarf-shrub, fruticose lichen tundra. Subxeric to mesic and acidic	18	110	Hemi-prostrate dwarf shrub, fruticose lichen tundra	12	Hierochloë alpina-Betula nana	Walker et al., 1994
											Betula nana-Rhoodendron tomentosum (Birch Ericaceous Low Shrub)	Boggs et al., 2018
											Betula nana exilis - Vaccinium uliginosum (Hettinger and Janz 1974)	Viereck et al.,1992
D1	*Carex bigelowii,Salix reticulata*	Moist sedge tundra	Moist non-tussock tundra	9	401, 403	Nontussock sedge, dwarf-shrub, moss tundra (moist nonacidic tundra)	5	401, 403	Non tussock sedge, dwarf shrub, moss tundra	5	Carex lugens/Salix reticulata	Boggs et al., 2018
D2	*Carex bigelowii, Betula nana, Ledum palustre, Hylocomium splendens, Aulacomnium turgidum*	Moist sedge with low shrub	Shrubby moist non-tussock tundra	10	110, 201, 302. 303	Hemi-prostrate dwarf shrub, fruticose lichen tundra. Subxeric to mesic and acidic	18	302.303	Hemi-prostrate dwarf shrub, fruticose lichen tundra	12	Carex bigelowii-Betula nana-Salix planifol-Ledum decumbens-Vaccinium spp. (Craighead and others 1988, Racine and Anderson 1979, Racine and Young 1978)	Viereck et al.,1992

											Carex bigelowii-Vaccinium spp./Sphagnum spp.	Brock and Burke 1980
											Betula nana- Carex bigelowii (Tussock shrub tundra)	Boggs et al., 2018
E1	*Betula nana, Vaccinium vitis-idaea, Hylocomium splendens, Aulacomnium turgidum*	Low to tall shrub	Low to tall moist shrub	11	304, 306, 307	Dwarf-shrub, moss tundra dominated by dwarf birch (*Betula nana*)	21	306, 307	Dwarf-shrub or low shrub, sedge, moss tundra	13	Hierochloë alpina-Betula nana	Walker et al., 1994
											Betula nana-Rhododendron tomentosum (Birch ericaceous low shrub)	Boggs et al., 2018
E2	*Betula nana, Salix pulchra, Hylocomium splendens*	Low to tall shrub	Low to tall moist shrub	11	304, 306, 307	n/a	n/a	n/a	Dwarf-shrub or low shrub, sedge, moss tundra	13	Betula nana-Salix planifolia-Vaccinium uliginosum (Craighead and others 1988).	Viereck et al.,1992
											Betula nana-Rhododendron tomentosum (Birch ericaceous low shrub)	Boggs et al., 2018
E3	*Salix pulchra, Carex bigelowii,*	Low to tall shrub	Low to tall moist shrub	11	314, 315, 316, 318	Low shrubland	23	314, 315, 316, 318	Dwarf-shrub or low shrub, sedge, moss tundra	13	Betula nana–Salix planifolia ssp. pulchra–Eriophorum angustifolium	Jorgenson et al., 2009

	Hylocomium splendens										Salix pulchra-Hylocomium (Low tall willow	Boggs et al., 2018
F1	*Eriphorum vaginatum, Betula nana, Vaccinium uliginosum, Salix pulchra, Carex bigelowii, Hylocomium splendens, Aulacomnium turgidum*	Tussock tundra	Tussock tundra	7	406, 407	Tussock sedge, dwarf shrub, moss tundra (tussock tundra, moist acidic tundra)	4	406, 407	Tussock sedge , dwarf-shrub, moss tundra	4	Betula nana-Eriophorum vaginatum (Tussock shrub tundra)	Boggs et al., 2018
F2	*Eriophorum vaginatum, Betula nana, Salix pulchra, Carex bigelowii, Vaccinium uliginosum, Hylocomium splendens, Aulacomnium turgidum*	Shrubby tussock tundra	Shrubby tussock tundra	8	308	Dwarf shrub, sedge, moss tundra (shrubby tussock tundra dominated by dwarf birch, *Betula*)	19	308	Dwarf-shrub or low shrub, sedge, moss tundra	13	Salix pulchra-Hylocomium (Low tall willow	Boggs et al., 2018
G1	*Sphagnum spp., Betula*	Wet tussock	Raised areas in	13	409, 506		8	409	Sedge, moss tundra	6	Sphagno-Eriophoretum vaginati (typicum)	Walker et al., 1994

	nana, Andromeda polifolia	sedge tundra	wet tundra			Sedge, prostrate dwarf-shrub, moss tundra					Partially Salix pulchra-Eriophorum vaginatum (Tussock shrub tundra)	Boggs et al., 2018
G2	*Sphagnum spp., Carex bigelowii, Betula nana, Salix pulchra, Rubus chamaemorus*	Wet tussock sedge tundra	Raised areas in wet tundra	13	409, 506	Sedge, prostrate dwarf-shrub, moss tundra	8	409	Sedge, moss tundra	6	Carex aquatilis-Eriophorum spp./Sphagnum spp. (Wet sedge)	Boggs et al., 2018
H1	*Carex aquatilis, Salix chamissonis, Andromeda polifolia, Sphagnum spp.*	Wetland	Wet tundra	14	501, 502, 503, 504, 507	Sedge, prostrate dwarf-shrub, moss tundra	8	506	Sedge, moss tundra	6	Carex aquatilis–Salix planifolia ssp. pulchra	Jorgenson et al., 2009
											Sphagno-Eriophoretum vaginati (typicum)	Walker et al., 1994
H2	*Carex aquatilis*	Wetland	Wet tundra	14	501, 502, 503, 504, 507	Sedge, prostrate dwarf-shrub, moss tundra	8	506	Sedge, moss tundra	7	Carex aquatilis-Sphagnum (wet sedge)	Boggs et al., 2018
H3	*Eriphorum angustifolium, Carex aquatilis*	Wetland	Wet tundra	14	501, 502, 503, 504, 507	Sedge, moss tundra in fens with flowing water	9	501	Sedge, moss tundra	7	Eriophorum angustifolium-Carex spp. (Wet sedge)	Boggs et al., 2018
											Eriophorum angustifolium-Carex aquatilis	Walker et al., 1994
I	*Leptodictyum riparium*	Pond	Water	15	601, 602, 603, 604	Herbaceous marsh	11	601, 603, 604	Water and herbaceous marsh	8	n/a	n/a

References

Anderson K and Gaston K J 2013 Lightweight unmanned aerial vehicles will revolutionize spatial ecology. Frontiers in Ecology and the Environment, 11 138–146

Antão, L.H., Weigel, B., Strona, G., Hällfors, M., Kaarlejärvi, E., Dallas, T., Opedal, Ø.H., Heliölä, J., Henttonen, H., Huitu, O., Korpimäki, E., Kuussaari, M., Lehikoinen, A., Leinonen, R., Lindén, A., Merilä, P., Pietiäinen, H., Pöyry, J., Salemaa, M., Tonteri, T., Vuorio, K., Ovaskainen, O., Saastamoinen, M., Vanhatalo, J., Roslin, T., Laine, A.-L., 2022. Climate change reshuffles northern species within their niches. Nat. Clim. Chang. 12, 587–592. https://doi.org/10.1038/s41558-022-01381-x

Barrett, R.T.S., Hollister, R.D., Oberbauer, S.F. & Tweedie, C.E. 2015. Arctic plant responses to changing abiotic factors in northernAlaska. AmericanJournal ofBotany 102: 2020–2031.

Berner, L.T., Orndahl, K.M., Rose, M., Tamstorf, M., Arndal, M.F., Alexander, H.D., Humphreys, E.R., Loranty, M.M., Ludwig, S.M., Nyman, J., Juutinen, S., Aurela, M., Happonen, K., Mikola, J., Mack, M.C., Vankoughnett, M.R., Iversen, C.M., Salmon, V.G., Yang, D., Kumar, J., Grogan, P., Danby, R.K., Scott, N.A., Olofsson, J., Siewert, M.B., Deschamps, L., Lévesque, E., Maire, V., Morneault, A., Gauthier, G., Gignac, C., Boudreau, S., Gaspard, A., Kholodov, A., Bret-Harte, M.S., Greaves, H.E., Walker, D., Gregory, F.M., Michelsen, A., Kumpula, T., Villoslada, M., Ylänne, H., Luoto, M., Virtanen, T., Forbes, B.C., Hölzel, N., Epstein, H., Heim, R.J., Bunn, A., Holmes, R.M., Hung, J.K.Y., Natali, S.M., Virkkala, A.-M., Goetz, S.J., 2024. The Arctic Plant Aboveground Biomass Synthesis Dataset. Sci Data 11, 305. https://doi.org/10.1038/s41597-024-03139-w

Bertin, R.I., 2008. Plant Phenology And Distribution In Relation To Recent Climate Change. The Journal of the Torrey Botanical Society 135, 126–146. https://doi.org/10.3159/07-RP-035R.1

Bjorkman, A.D., García Criado, M., Myers-Smith, I.H., Ravolainen, V., Jónsdóttir, I.S., Westergaard, K.B., Lawler, J.P., Aronsson, M., Bennett, B., Gardfjell, H., Heiðmarsson, S., Stewart, L., Normand, S., 2020. Status and trends in Arctic vegetation: Evidence from experimental warming and long-term monitoring. Ambio 49, 678–692. https://doi.org/10.1007/s13280-019-01161-6

Boggs K W, Boucher T V, and McTeague M L 2018 Plant Association Classification for Northern Alaska. Alaska Center for Conservation Science, University of Alaska Anchorage. Anchorage, Alaska. 144 pp

Callaghan, T.V., L.O. Bjo¨rn, Y. Chernov, F.S. Chapin III, T.R. Christensen, B. Huntley, R.A. Ims, M. Johansson, et al. 2004. Effects on the function of Arctic ecosystems in the short- and long-term perspectives. Ambio 33: 448–458.

Cannone N, Sgorbati S, & Guglielmin M 2007 Unexpected impacts of climate change on alpine vegetation Frontiers in Ecology and the Environment 5(7) 360-364

Cannone N, Lewkowicz A. G, and Guglielmin M 2010 Vegetation colonization of permafrost-related landslides, Ellesmere Island, Canadian High Arctic, J. Geophys. Res. 115 G04020

Cannone N. and Pignatti S 2014 Ecological responses of plant species and communities to climate warming: upward shift or range filling processes? Clim. Change 123 201–214

Cannone N & Malfasi F 2024 Climate change triggered synchronous woody plants recruitment in the last two centuries in the treeline ecotone of the Northern Hemisphere Science of the Total Environment 921 170953

Cahoon S M, Sullivan P F & Post E 2016 Carbon and water relations of contrasting Arctic plants: implications for shrub expansion in West Greenland Ecosphere 7(4) e01245

Chapin III F S, Sturm M, Serreze M C, McFadden J P, Key J R, Lloyd A H, & Welker J M 2005 Role of land-surface changes in Arctic summer warming Science 310(5748) 657-660. https://doi.org/10.1126/science.1117368.

Cruzan M B, Weinstein B G, Grasty M R, Kohrn B F, Hendrickson E C, Arredondo T M & Thompson P G 2016 Small unmanned aerial vehicles (micro-UAVs, drones) in plant ecology Applications in plant sciences 4(9) 1600041

DeMarco J, Mack M C, & Bret-Harte M S 2014 Effects of arctic shrub expansion on biophysical vs. biogeochemical drivers of litter decomposition Ecology 95(7) 1861-1875

Dial R J, Scott Smeltz T, Sullivan P F, Rinas C L, Timm K, Geck J E, & Berg E C 2016 Shrubline but not treeline advance matches climate velocity in montane ecosystems of south-central Alaska Global Change Biology 22(5) 1841-1856

Duchesne R R, Chopping M J, Tape K D, Wang Z & Schaaf C L 2018 Changes in tall shrub abundance on the North Slope of Alaska, 2000–2010 Remote sensing of environment 219 221-232

Elmendorf S C, Henry G H, Hollister R D, Björk R G, Boulanger-Lapointe N, Cooper E J & Wipf S 2012 Plot-scale evidence of tundra vegetation change and links to recent summer warming. Nature climate change 2(6) 453-457

Euschirken E S, McGuire A D, Chapin F S, Yi S, and Thompson C C 2009 Changes in vegetation in northern Alaska under scenarios of climate change, 2003–2100: implications for climate feedbacks Ecol. Appl. 19(4) 1022–1043

Forbes, B.C., Fauria, M.M. & Zetterberg, P. 2010. Russian Arctic warming and 'greening' are closely tracked by tundra shrub willows. Global Change Biology 16: 1542–1554.

Fraser R H, Olthof I, Lantz T C, Schmitt C 2016 UAV photogrammetry for mapping vegetation in the low-Arctic Arctic Science 2 79–102

Gamon J A, Huemmrich K F, Stone R S, Tweedie C E 2013 Spatial and temporal variation in primary productivity (NDVI) of coastal Alaskan tundra: decreased vegetation growth following earlier snowmelt Remote Sens. Environ. 129 (15) 144–153.

Greaves H E, Eitel J U H, Vierling L A, Boelman N T, Griffin K L, Magney T S, Prager C M, 2019 20cm resolution mapping of tundra vegetation communities provides an ecological baseline for important research areas in a changing Arctic environment. Environ. Res. Commun. 1 105004

Harris J A, Hollister R D, Botting T F, Tweedie C E, Betway K R, May J L & Fuson T L 2021 Understanding the climate impacts on decadal vegetation change in northern Alaska. Arctic Science 8(3) 878-898

Høye, T.T., Post, E., Meltofte, H., Schmidt, N.M. & Forchhammer, M.C. 2007. Rapid advancement of spring in the High Arctic. Current Biology 17: R449–R451.

Hudson J M & Henry G H R 2009 Increased plant biomass in a High Arctic heath community from 1981 to 2008 Ecology 90(10) 2657-2663

Hulten E 1968 Flora of Alaska and neighboring territories: A manual of the vascular plants. Stanford University Press, Stanford.

Huryn A, Hobbie J 2012 Land of Extremes: A Natural History of the Arctic North Slope of Alaska University of Alaska Press

IPCC 2018: Global warming of 1.5°C. An IPCC Special Report on the impacts of global warming of 1.5°C above pre-industrial levels and related global greenhouse gas emission pathways, in the context of strengthening the global response to the threat of

climate change, sustainable development, and efforts to eradicate poverty [V Masson-Delmotte, P Zhai, H O Pörtner, D Roberts, J Skea, P R Shukla, A Pirani, W Moufouma-Okia, C Péan, R Pidcock, S Connors, J B R Matthews, Y Chen, X Zhou, M I Gomis, E Lonnoy, T Maycock, M Tignor, T Waterfield (eds.)]

Jagerbrand, A.K., Lindblad, K.E.M., Bjork, R.G., Alatalo, J.M. & Molau, U.2006. Bryophyte and lichen diversity under simulated environmental change compared with observed variation in unmanipulated alpine tundra. Biodiversity and Conservation 15: 4453–4475.

Jones, M.H., Bay, C. & Nordenha¨ll, U. 1997. Effects of experimental warming on arctic willows (Salix spp.): a comparison of responses from the Canadian High Arctic, Alaskan Arctic, and Swedish Subarctis. Globa lChange Biology3: 55–60.

Jorgenson M T, J E Roth, P F Miller, M J Macander, M S Duffy, A F Wells, G V Frost, E R Pullman 2009 An Ecological Land Survey and Landcover Map of the Arctic Network Natural Resource Technical Report NPS/ARCN/NRTR- 2009/270 National Park Service Fort Collins Colorado

Kapfer, J., Grytnes, J., 2017. Large climate change, large effect? Vegetation changes over the past century in the European High Arctic. Applied Vegetation Science 20, 204–214. https://doi.org/10.1111/avsc.12280

Lawrence D M & Swenson S C 2011 Permafrost response to increasing Arctic shrub abundance depends on the relative influence of shrubs on local soil cooling versus large-scale climate warming Environmental Research Letters 6(4) 045504

Linderholm, H.W., 2006. Growing season changes in the last century. Agricultural and Forest Meteorology 137, 1–14. https://doi.org/10.1016/j.agrformet.2006.03.006

Loranty M M, Goetz S J & Beck P S 2011 Tundra vegetation effects on pan Arctic albedo Environmental Research Letters 6(2) 024014

Liu, H., Mi, Z., Lin, L., Wang, Y., Zhang, Z., Zhang, F., Wang, H., Liu, L., Zhu, B., Cao, G., Zhao, X., Sanders, N.J., Classen, A.T., Reich, P.B., He, J.-S., 2018. Shifting plant species composition in response to climate change stabilizes grassland primary production. Proc. Natl. Acad. Sci. U.S.A. 115, 4051–4056. https://doi.org/10.1073/pnas.1700299114

Mack M C, Schuur E A G, Bret-Harte M Syndonia Shaver G R, Chapin III F S 2004. Ecosystem carbon storage in arctic tundra reduced by long-term nutrient fertilization Nature 431 (7007) 440–443

Malfasi Francesco & Cannone Nicoletta 2021 Phytosociology of the vegetation communities of the Stelvio Pass area Journal of Maps 17(2) 367 375

Macander M J, Nelson P R, Nawrocki T W, Frost G V, Orndahl K M, Palm E C & Goetz S J 2022 Time-series maps reveal widespread change in plant functional type cover across Arctic and boreal Alaska and Yukon Environmental Research Letters 17(5) 054042

Martin A C, Jeffers E S, Petrokofsky G, Myers-Smith I & Macias-Fauria M 2017 Shrub growth and expansion in the Arctic tundra: an assessment of controlling factors using an evidence-based approach Environmental Research Letters 12(8) 085007

McEwing K R, Fisher J P & Zona D 2015 Environmental and vegetation controls on the spatial variability of CH4 emission from wet-sedge and tussock tundra ecosystems in the Arctic Plant Soil 388 37–52

Moffat N D, Lantz T C, Fraser R H & Olthof I 2016 Recent vegetation change (1980–2013) in the tundra ecosystems of the Tuktoyaktuk Coastlands, NWT, Canada Arctic, Antarctic, and Alpine Research 48(3) 581-597

Myers-Smith I H, Forbes B C, Wilmking M, Hallinger M, Lantz T, Blok D, & Hik D S 2011 Shrub expansion in tundra ecosystems: dynamics, impacts and research priorities Environmental Research Letters 6(4) 045509

Myers-Smith, I.H., and D.S. Hik. 2013. Shrub canopies influence soil temperatures but not nutrient dynamics: An experimental test of tundra snow–shrub interactions. Ecology and Evolution 3: 3683–3700. https://doi.org/10.1002/ece3.710.

Myers-Smith I H, Elmendorf S C, Beck P S, Wilmking M, Hallinger M, Blok D & Vellend M 2015 Climate sensitivity of shrub growth across the tundra biome Nature climate change 5(9) 887-891

Myers-Smith I H & Hik D S 2018 Climate warming as a driver of tundra shrubline advance Journal of Ecology 106(2) 547-560

Naito A T, Cairns D M 2015 Patterns of shrub expansion in Alaskan arctic river corridors suggest phase transition Ecol. Evol. 5 (1) 87–101

Oldeland J, Revermann R, Luther-Mosebach J, Buttschardt T, Lehmann J R K 2021 New tools for old problems comparing drone and field-based assessments of a problematic plant species Environ Monit Assess 193 90

Orndahl, K.M., Berner, L.T., Macander, M.J., Arndal, M.F., Alexander, H.D., Humphreys, E.R., Loranty, M.M., Ludwig, S.M., Nyman, J., Juutinen, S., Aurela, M., Mikola, J., Mack, M.C., Rose, M., Vankoughnett, M.R., Iversen, C.M., Kumar, J., Salmon, V.G., Yang, D., Grogan, P., Danby, R.K., Scott, N.A., Olofsson, J., Siewert, M.B., Deschamps, L., Maire, V., Lévesque, E., Gauthier, G., Boudreau, S., Gaspard, A., Bret-Harte, M.S., Raynolds, M.K., Walker, D.A., Michelsen, A., Kumpula, T., Villoslada, M., Ylänne, H., Luoto, M., Virtanen, T., Greaves, H.E., Forbes, B.C., Heim, R.J., Hölzel, N., Epstein, H., Bunn, A.G., Holmes, R.M., Natali, S.M., Virkkala, A.-M., Goetz, S.J., 2025. Next generation Arctic vegetation maps: Aboveground plant biomass and woody dominance mapped at 30 m resolution across the tundra biome. Remote Sensing of Environment 323, 114717. https://doi.org/10.1016/j.rse.2025.114717

Ovaskainen, O., Skorokhodova, S., Yakovleva, M., Sukhov, A., Kutenkov, A., Kutenkova, N., Shcherbakov, A., Meyke, E.& Delgado, M.D. 2013. Community-level phenological response to climate change. Proceedings of the National Acad emy of Sciences of the United States of America 110: 13434 13439.

Pearson, R.G., S.J. Phillips, M.M. Loranty, P.S.A. Beck, T. Damoulas, S.J. Knight, and S.J. Goetz. 2013. Shifts in Arctic vegetation and associated feedbacks under climate change. 123 Nature Climate Change 3: 673–677. https://doi.org/10.1038/ nclimate1858.

Petrenko, C.L., J. Bradley-Cook, E.M. Lacroix, A.J. Friedland, and R.A. Virginia. 2016. Comparison of carbon and nitrogen storage in mineral soils of graminoid and shrub tundra sites, western Greenland. Arctic Science 2: 165–182. https://doi.org/10.1139/ as-2015-0023.

Raynolds M K, Walker D A & Maier H A 2005 Plant community-level mapping of arctic Alaska based on the Circumpolar Arctic Vegetation Map Phytocoenologia 35(4) 821–848

Richardson, A.D., Keenan, T.F., Migliavacca, M., Ryu, Y., Sonnentag, O., Toomey, M., 2013. Climate change, phenology, and phenological control of vegetation feedbacks to the climate system. Agricultural and Forest Meteorology 169, 156–173. https://doi.org/10.1016/j.agrformet.2012.09.012

Serreze M C and Barry R G 2011 Processes and impacts of Arctic amplification: a research synthesis Global Planet Change 77: 85–96

Shaver, G.R., Bret-Harte, S.M., Jones, M.H., Johnstone, J., Gough,L., Laundre,J. & Chapin, F.S. 2001. Species composition interacts with fertilizer to control long-term change in tundra productivity. Ecology 82: 3163–3181.

Shiklomanov N 2023 Seasonal soil active layer measurements from a Circumpolar Active Layer Monitoring (CALM) grid, U12A Toolik 1 kilometer grid, Alaska, 1995-2020

Sturm M, Racine C & Tape K 2001 Increasing shrub abundance in the Arctic Nature 411(6837) 546-547

Sturm M, Schimel J, Michaelson G, Welker J M, Oberbauer S F, Liston G E & Romanovsky V E 2005 Winter biological processes could help convert arctic tundra to shrubland Bioscience 55(1) 17-26

Tape K E N, Sturm M & Racine C 2006 The evidence for shrub expansion in Northern Alaska and the Pan-Arctic Global change biology 12(4) 686-702

Tape K D, Hallinger M, Welker J M & Ruess R W 2012. Landscape heterogeneity of shrub expansion in Arctic Alaska Ecosystems 15 711-724

ter Braak C J F, Šmilauer P 1998 CANOCO Reference manual and user's guide to CANOCO for windows. Software for Canonical Community Ordination (version 4) Centre for Biometry, Wageningen

Thomson J W W, Brehmer B 1984 American Arctic lichens Columbia University Press 520 pp

Viereck L A, Dyrness C T, Batten A R, Wenzlick K J 1992 The Alaska vegetation classification Gen. Tech. Rep. PNW-GTR-286 Portland OR: U.S. Department of Agriculture Forest Service Pacific Northwest Research Station 278 p

Virkkala, A.-M., Niittynen, P., Kemppinen, J., Marushchak, M.E., Voigt, C., Hensgens, G., Kerttula, J., Happonen, K., Tyystjärvi, V., Biasi, C., Hultman, J., Rinne, J., Luoto, M., 2024. High-resolution spatial patterns and drivers of terrestrial ecosystem carbon dioxide, methane, and nitrous oxide fluxes in the tundra. Biogeosciences 21, 335–355. https://doi.org/10.5194/bg-21-335-2024

Waldo S, Russell E S, Kostyanovsky K, Pressley S N, O'Keeffe P T, Huggins D R 2019. N2O emissions from two agroecosystems: High spatial variability and long pulses observed

using static chambers and the flux-gradient technique Journal of Geophysical Research: Biogeosciences 124, 1887 1904

Walker D A, & Barry N 1991 Toolik Lake permanent vegetation plots: site factors, soil physical and chemical properties, plant species cover, photographs, and soil descriptions Data report 48 Department of Energy R4D Program Institute of Arctic and Alpine Research University of Colorado Boulder

Walker M D, Walker D A and Auerbach N A 1994 Plant communities of a tussock tundra landscape in the Brooks Range Foothills, Alaska, J. Veg. Sci. 5 843–866

Walker D A & Walker M D 1996 Terrain and vegetation of the Imnavait Creek watershed. Landscape function and disturbance in Arctic Tundra Berlin Heidelberg pp 73-108

Walker D A 2000 Hierarchical subdivision of arctic tundra based on vegetation response to climate parent material and topography Global Change Biol. 6 19–34

Walker D A, Raynolds M K, Daniëls F J, Einarsson E, Elvebakk A, Gould W A & Yurtsev B A 2005 The circumpolar Arctic vegetation map Journal of vegetation science 16(3) 267-282

Walker D A, Maier H A 2008 Vegetation in the Vicinity of the Toolik Lake Field Station, Alaska. Biological Papers of the University of Alaska Institute of Arctic Biology No. 28

Walker, D.A., Epstein, H.E., Raynolds, M.K., Kuss, P., Kopecky, M.A., Frost, G.V., Dani€ els, F.J.A., Leibman, M.O., Moskalenko, N.G. (...)& Tichy, L. 2012. Environment, vegetation and greenness (NDVI) along the North 214 America and Eurasia Arctic transects. Environmental Research Letters 7: 015504.

Walker D, Breen A, Druckenmiller L, Wirth L W, Fisher W, Raynolds M K & Zona D 2016 The alaska arctic vegetation archive (ava-ak) Oak Ridge National Laboratory (ORNL) Oak Ridge TN (United States)

Walsh J E & Brettschneider B 2019 Attribution of recent warming in Alaska Polar Science 21 101-109

Wells A F, Swingley C S, Ives S L, McNown R W & Dissing D 2022 Vegetation classification for northwestern Arctic Alaska using an EcoVeg approach: tussock tundra and low and tall willow groups and alliances Vegetation Classification and Survey 3 8 7

CONCLUSIONS

Warming of the climate system has been defined, by the IPCC 2023, as unequivocal and that many of the changes observed, since the 1950s, are unprecedented over decades to millennia.

It is expected that a further increase in global warming would lead to an increase in the intensity and frequency of warming extremes, including heat waves and summer droughts which could exert relevant impacts on ecosystems, especially on vegetation (e.g. Gallinat et al., 2015; IPCC, 2021). These changes are increasing the tree mortality rate, shifting in timing the vegetation phenology, reducing the forests capacity of carbon sequestration, leading to shifts in species distribution and limiting the recovery capacity of forests. Monitoring and understanding these changes are fundamental for future land management and to promote site-specific and forest-specific conservation and adaptation strategies.

The four studies presented in this thesis contribute to better understanding how two biomes (temperate forests and arctic tundra) respond to global warming, focusing on impact of heatwaves and drought on fall phenology and growth, and on methane dynamics.

In a scenario of increasing frequency and severity of heat and drought events, the assessment of the impact of these extreme climatic events on forests through remote sensing analysis, can provide important information on forest sensitivity and resilience even in difficult-to-reach areas.

The analysis on temperate forests demonstrated that the combined heatwaves and droughts of 2022 caused early crown defoliation and reduced productivity, with impacts differing across the elevation gradient. Lowland thermophilus forests were the most affected by the impact of heat and drought, with an advance of leaf senescence up to 40 days but exhibiting the highest resilience. In the forest types at higher elevations and moist conditions we identified a legacy effect in 2023, indicating prolonged stress from the extreme conditions of 2022 and poor resiliency.

Our study on tree growth and wood anatomy confirmed that heat stress significantly reduced radial growth and altered the functional characteristics of wood in several species, especially in early-leafing species such as *Betula pendula* Roth and *Quercus robur* L., demonstrating a species-specific sensitivity to extreme heat and drought. The study also reported changes in the anatomical characteristics of wood, such as a decrease in the ray parenchyma fraction in *Acer pseudoplatanus* L., indicating a decline in carbon storage in the xylem.

These results demonstrate the relevance of phenological timing, wood anatomy, and site conditions in determining tree sensitivity and resilience to extreme events, with implications for species distribution, forest composition, and long-term ecosystem functioning.

In Arctic ecosystems, vegetation change is among the most widespread responses to climate change. Shrub encroachment, primarily driven by *Betula nana* and *Salix pulchra*, is changing the composition of the tundra community, with consequences for the structure and functioning of the ecosystem. The high-resolution phytosociological and physiognomic mapping conducted carried out as part of the “Insubre Polar” project provides an essential baseline for detecting and quantifying transformations occurring in Arctic plant communities.

The composition of the tundra community is shifting due to shrub encroachment, which is mostly caused by Betula nana and Salix pulchra. This has consequences for the structure and operation of the ecosystem. The "Insubre Polar" project's high-resolution phytosociological and physiognomic mapping is a crucial baseline for identifying and measuring continuous changes in Arctic plant communities.

At the same time, the assessment of methane dynamics revealed that vegetation strongly modulates CH_4 fluxes. Tussock tundra was the main source of methane, with peaks during summer and autumn linked to soil water saturation, permafrost degradation high temperature in summer, and freezing soil in autumn induced CH_4 release. In contrast, dry tundra during summer acted as a methane sink, while in autumn is inactive. According to our data, vegetation may have a significant impact on methane fluxes variability, particularly during colder seasons, and our findings suggest that further investigation is needed to understand the effect of vegetation on CH_4 flux variability and to clarify the potential for elevated emissions during cold seasons and their contribution to the annual budget.

In conclusion, these studies demonstrate how extreme climatic events and global warming influence phenology, productivity, structure, dynamics, and carbon fluxes of ecosystems. The study of climate change impacts on different vegetation types in different sites is essential for future land management and for conservation and adaptation strategies site-specific. Understanding how vegetation is changing and what parameters and factors regulate emissions is important for finding mitigation solutions to recent climate change, identifying effective strategies to reduce feedback to the climate system.

Key messages:

- Extreme climatic events alter ecosystem functioning across biomes**,** affecting phenology, productivity, and carbon cycling.
- The vulnerabilities of different vegetation species and communities determine the capacity for resilience and the possible legacy effects, with implications for the future composition of forests and the stability of ecosystems.
- Functional characteristics, phenological timing, and site conditions influence vegetation responses to extreme climate events, in particular droughts and heatwaves, providing useful information for predicting forest vulnerability, for finding the correct mitigation solutions.
- Arctic vegetation plays a central role in regulating methane emissions**,** that has a very high global warming potential and could have positive feedback on climate change.
- High-resolution spatial data are essential for monitoring ecological changes, enabling the detection of small-scale variations in vegetation structure and function, and providing a robust tool to predict ecosystem trends in the context of accelerating global warming.

Future research should quantify the long-term ecological impact of extreme climate events by integrating multi-year monitoring of phenology, growth, and canopy dynamics through combined approaches of dendroecology, ecophysiology, and remote sensing. Long-term monitoring is essential for identifying delayed or cumulative effects that may not emerge over a single growing season, including changes in carbon allocation, alterations in wood formation, and progressive changes in canopy structure. In Arctic ecosystems, expanding continuous measurements of CH_4 flux, particularly during the cold season, will be essential to improve knowledge of annual budgets and explaining the role of vegetation in the regulation of the methane cycle.

References

Gallinat, A.S., Primack, R.B., Wagner, D.L., 2015. Autumn, the neglected season in climate change research. Trends Ecol. Evol. 30, 169–176. https://doi.org/10.1016/j.tree.2015.01.004

IPCC. (2021). Climate change 2021: The physical science basis. In V. Masson- Delmotte, P. Zhai, A. Pirani, S. L. Connors, C. Pean, S. Berger, N. Caud, Y. Chen, L. Goldfarb, M. I. Gomis, M. Huang, K. Leitzell, E. Lonnoy, J. B. R. Matthews, T. K. Maycock, T.

Waterfield, O. Yelekci, R. Yu, & B. Zhou (Eds.), Contribution of Working Group I to the Sixth Assessment Report of the Intergovernmental Panel on Climate Change. Cambridge University Press.

IPCC, 2023: Climate Change 2023: Synthesis Report. Contribution of Working Groups I, II and III to the Sixth Assessment Report of the Intergovernmental Panel on Climate Change [Core Writing Team, H. Lee and J. Romero (eds.)]. IPCC, Geneva, Switzerland, pp. 35-115, doi: 10.59327/IPCC/AR6 9789291691647.